SCOUR IN SEDIMENT MIXTURES UNDER SUBMERGED CIRCULAR VERTICAL JETS

Ph. D. THESIS

by

ANKIT CHAKRAVARTI

DEPARTMENT OF CIVIL ENGINEERING
INDIAN INSTITUTE OF TECHNOLOGY ROORKEE
ROORKEE – 247 667 (INDIA)
JULY, 2014

SCOUR IN SEDIMENT MIXTURES UNDER SUBMERGED CIRCULAR VERTICAL JETS

A THESIS

Submitted in partial fulfilment of the requirements for the award of the degree

of

DOCTOR OF PHILOSOPHY

in

CIVIL ENGINEERING

by

ANKIT CHAKRAVARTI

DEPARTMENT OF CIVIL ENGINEERING
INDIAN INSTITUTE OF TECHNOLOGY ROORKEE
ROORKEE – 247 667 (INDIA)
JULY, 2014

INDIAN INSTITUTE OF TECHNOLOGY ROORKEE ROORKEE

CANDIDATE'S DECLARATION

I hereby certify that the work which is being presented in the thesis entitled **"SCOUR IN SEDIMENT MIXTURES UNDER SUBMERGED CIRCULAR VERTICAL JETS"** in partial fulfilment of the requirements for the award of the degree of Doctor of Philosophy and submitted in the Department of Civil Engineering of the Indian Institute of Technology Roorkee, Roorkee, is an authentic record of my own work carried out during the period from July, 2010 to July, 2014 under the supervision of Dr. Z. Ahmad, Professor, Department of Civil Engineering, Indian Institute of Technology Roorkee, Roorkee and Dr. R. K. Jain, Associate Professor, Department of Civil Engineering, Vishwakarma Government Engineering College Chandkheda, Gandhinagar.

The matter presented in this thesis has not been submitted by me for the award of any other degree of this or any other Institute.

(ANKIT CHAKRAVARTI)

This is to certify that the above statement made by the candidate is correct to the best of our knowledge.

(R. K. JAIN)
Supervisor

(Z. AHMAD)
Supervisor

Date:……………...

The Ph.D. Viva-Voce Examination of **Mr. Ankit Chakravarti,** Research Scholar, has been held on …………………………………………………………………..

Signature of Supervisors **Chairman, SRC** **Signature of External Examiner**

Head of the Department/Chairman, ODC

ABSTRACT

Hydrodynamic imbalance and instability in river system due to natural and anthropogenic causes has become a subject of concern. In rivers and streams, one of the most challenging problems is to minimize and to know the depth of scour due to changes in flow pattern around the hydraulic structures for its stability and economical consideration. The structures built in rivers and channels are subjected to scour around their foundations. If the depth of scour becomes significant, the stability of the foundations is endangered. Scour is a process of lowering of river bed due to removal of bed material in the vicinity of hydraulic structures by erosive action of the flowing water. In some of the structures like ski-jump, free overfall spillway, jet spillway, the water jet penetrates the sediment bed that reaches its deepest level and is deflected in upward directions resulting in a highly turbulent zone. Scour due to turbulent water jets impacts numerous hydraulic engineering projects. Practicing engineers and planners have been confronted with the task of finding a feasible and cost effective solution to protect scour around the structures. The investigator must seek ways to guide and control the process so as to minimize the risk of failure of the hydraulic structures. Therefore, estimation of maximum scour depth is required for the safe and economic design of hydraulic structures and their foundations.

The scour of sand, gravels and other materials, which often occurs downstream of hydraulic structures, is of considerable importance, as excessive scouring process may endanger the stability of the hydraulic structures such as gates, weirs, culverts, spillways and grade-control structures, etc.

There are two types of scour profile geometries, dynamic scour when the jet flow is in operating condition, and static scour which is the final bed scour hole produced, when the jet flow is stopped. Local scour due to jets is affected by variables such as jet velocity, jet height, nozzle size, type of structure and characteristics of the sediment. For given conditions of these variables, the scour depth also varies with time.

Many researchers have performed laboratory experiments on scour processes due to jets. The experimental investigation on scour due to submerged vertical jet in cohesionless sediments was probably first conducted by Rouse (1940). Thereafter, a number of investigations have been carried out to study the response of submerged water jets in various sediment materials, jet velocities, jet heights and diameter of nozzles.

Clark (1962), Sarma (1967), Westrich and Kobus (1973), Rajaratnam and Beltaos (1977), Rajaratnam (1982), Uyumaz (1988), (1988), Breusers and Raudkivi (1991), Aderibigbe and Rajaratam (1996), Aderibigbe and Rajaratam (1996), Donoghue et al. (2001), Mazurek et al. (2002), Ansari (1999), Ansari et al. (2003), Rajaratam and Mazurek (2003, 2005), Adduce and Mele (2004), Yeh et al. (2009), Mazurek et al. (2009), Dehghani et al. (2010), Chakravarti et al. (2013) studied scour due to jet in cohesionless sediment. Some studies in respect to scour and erosion around the hydraulic structures were studied by Li (1987 a&b), Srivastava and Contractor (1992), Chalov (1995), Patel and Ranga Raju (1996), Patel and Ranga Raju (1999), Ansari et al. (2002), Chalov et al. (2004), Sarma (2005), Pagliara et al. (2006), Pagliara (2007), Pagliara et al. (2008), Pagliara and Palermo (2008), Azamathulla et al. (2009), Fukuoka and Osada (2009), Goel (2010), Chahar (2011), Azamathulla and Zakaria (2011), Fukuoka et al. (2013), Dehghani et al. (2013).

The process of scour due to jets in cohesionless sediment has been investigated at length in the literature. While adequate study has not been carried out in the cohesive soil which comes in the river system through surface erosion of upland areas along with cohesionless soil such as sand and gravel.

Review of the literature reveals that only a few studies have been conducted related to scour in cohesive bed under submerged water jets (Raudkivi and Tan, 1982; Hanson, 1991; Hanson and Robinson, 1993; Ansari, 1999; Ansari et al. 2003; Mazurek et al. 2001; Mazurek and Hossain, 2007). The above studies were mainly focused on either clay or clay-sand mixtures. However, no study has been conducted so far on scour under submerged circular vertical jet in cohesive material consisting of clay-gravel and clay-sand-gravel mixtures to the best of our knowledge. Therefore, it is intended to study the effect of presence of cohesion i.e., clay on scour process in clay-gravel and clay-sand-gravel sediment mixtures under submerged jets; as such types of sediment occurs frequently in nature (Kothyari and Jain, 2008; and Jain and Kothyari, 2009).

The main objective of the present study was to comprehend the scour process under submerged circular vertical water jets in cohesionless and cohesive sediment mixtures, and finding out the various scour parameters like maximum static and dynamic scour depths, temporal variation of scour depth and its various length scale parameters related to scour like radius of scour, dune height and volume of scour for safe and economical design of the hydraulic structures, and to ascertain its practical application.

The experiments were carried out at the Hydraulics Laboratory of the Department of Civil Engineering, Indian Institute of Technology Roorkee, India, and were performed on a circular steel tank having diameter 1.25 m and depth 1.25 m, filled with the desired sediment up to a height of 0.80 m, while the water was filled in the remaining 0.45 m height of the tank. The impinging jet was produced by a nozzle fitted at the end of circular supply pipe of diameter 0.0254 m. Suitable arrangement was provided to adjust the height of the jet above the sediment bed. The jet discharge was measured by calibrated Venturimeter fitted in the supply pipe.

Locally available clay that was excavated from a depth of 1.0 m below the bed level of river bed was used. Various tests for determination of sediment properties were conducted as per Code of Practice. The clay material had a median size d_{50} = 0.014 mm, geometric standard deviation, σ_g = 2.1, sand had a median size, d_{50} = 0.24 mm and σ_g = 1.41, while gravel had a median size, d_{50} = 2.7 mm and σ_g = 1.21. The other engineering properties of clay material which were measured are liquid limit, W_L = 43%, plastic limit, W_P = 22%, plasticity index, PI = 21%, maximum dry density $(\gamma_d)_{\max}$ = 16.75 kN/m^3, optimum moisture content, OMC = 19% and relative density = 2.65.

The experiments were conducted with two sizes of nozzle of 12.5 and 8 mm diameter, and two jet heights of 0.15 and 0.30 m from sediment bed level. Two jet velocities of 7.19 and 5.12 m/s for 12.5 mm nozzle and 9.84 and 6.65 m/s for 8 mm nozzle were considered. In case of cohesionless sediment, three different types of sediment bed were prepared i.e., sand, sand-gravel mixture (equal proportion by weight) and gravel. Cohesive sediment mixture was prepared by mixing clay with gravel and sand-gravel. In all, three mixtures i.e., sand-gravel, clay-gravel, and clay-sand-gravel were prepared. In clay-gravel and clay-sand-gravel mixtures, the clay contents was varied in proportion varying from 10% to 60% by weight, while, in clay-sand-gravel mixture, equal proportion of sand and gravel were used.

1. Scour in Cohesionless Sediment and their Mixtures

In all, 24 experimental runs were conducted in cohesionless sediment consisting of sand, sand-gravel mixture and gravel beds. The characteristics of scour under submerged circular vertical jets in cohesionless sediment were found different in each sediment mixture.

Several shapes of scour hole geometries in sand, sand-gravel mixture and gravel beds were noticed. A close investigation of scour bed profiles revealed that the observed static and dynamic scour depths were high in sand bed compared to gravel and sand-gravel mixture. Also, the volume of scour hole, radius of scour hole and dune height were high in sand beds compared to gravel and sand-gravel mixture sediment beds. The size of scour hole was small in case of gravel beds while high in sand beds. In case of sand-gravel mixture, segregation of sand and gravel was noticed - fine material was deposited on the outer boundary of dune, while gravel was in the core of the scour hole.

Temporal variation of the scour was measured and found that initially the rate of scour is high, however, it decreases with passage of time and attain an equilibrium stage – no significance scour takes place after attainment of equilibrium stage. Sediment size plays an important role in the process of scour in cohesionless sediment. The scour depth is inversely proportional to the size of cohesionless sediment. The experimental observations and analysis presented in this investigation established that the types of sediment have significant role on size of scour hole produced by water jets.

The saturation time, T_s is defined as time required from start of the scour to achievement of 99% of the total scour. The variation of T_s is the function of the jet velocity, diameter of nozzle, height of jet and the sediment size. A relationship is proposed for the estimation of saturation time in cohesionless sediment.

Temporal variation of scour depth have been analyzed using the equations proposed by Lui et al., (1961), Sarma, (1967), Islam et al., (1986), Ansari et al., (2003). In order to estimate the temporal variation of scour depth, the value of exponent which appears in equation of temporal variation of scour depth is needed a priori. Analysis of data collected in the present study showed that the value of the exponent is a function of the jet velocity, diameter of nozzle, height of jet and the sediment size.

Various scour parameters like maximum static scour depth, maximum dynamic scour depth, radius of scour hole, height of dune and volume of scour hole have been analyzed using the data collected in the present study and that available in literature in case of cohesionless sediment.

Maximum static scour depth was analyzed with erosion parameter in the case of cohesionless sediment using the present study data and data of previous investigators. It is found that the equation proposed by Adribigbe and Rajaratnam (1996) needs modification for better representation of the present and previous data. New modified equation has been proposed for estimation of maximum static scour depth.

Variation of maximum static and dynamic scour depth is also studied with sediment size, nozzle diameter and jet velocity. It is found that variation of maximum static and maximum dynamic scour depth can well be explained with other dimensionless parameters in place of erosion parameter (E_c).

Variation in radius of scour hole and dune height was analyzed with erosion parameter for data of present study as well as data of previous investigators. However, further analysis of data reveals that radius of scour hole can be accurately calculated using dimensionless parameters comprising jet velocity, diameter of nozzle, height of jet, sediment size in place of erosion parameter. The volume of scour hole was measured for each of the experimental run. It is found that the volume of scour hole is high in sand compared to the sand-grave and gravel. Higher jet velocity produces high scour volume.

The time required for attainment of equilibrium state of scour i.e. saturation time was found to be low in sand beds as compared to sand-gravel mixture and gravel beds. Radius of scour hole, dune height and volume of scour hole increase with increase of nozzle diameter, jet velocity while they decrease with increase of sediment size and jet height. The differences in maximum dynamic and static scour depths were higher in sand compared to gravel and sand-gravel mixtures.

Relationships are proposed for the computation of various scour parameters like maximum static and maximum dynamic scour depths, radius of scour hole, dune height and volume of scour hole in sand, gravel and sand-gravel mixture using data available in the literature and collected in present study. The proposed relationships are able to predict the desired parameters within ± 20 percent error band.

2. Scour in Clay-gravel Cohesive Sediment Mixtures

In all, 40 experimental runs were conducted in cohesive sediment beds consisting of clay-gravel mixtures. The geometrical characteristics of scour hole in case of clay-gravel mixture were found significantly different than that of cohesionless sediment.

The scour geometries were different for various percentages of clay in the mixture. The scour profile for low percentage of clay i.e., 10% was similar to that of cohesionless sediment. A close investigation of the scour profile reveals that scour depth and size of scour hole decreases with the increase of clay percentage in the mixture. The slopes of scour hole were different with various percentage of clay in the mixture. The dynamic scour depth is much higher than the maximum static scour depth for low clay content, however, their difference decreases with increase of clay in the mixture. The dune height was low in case of higher clay percentage in the mixture.

The temporal variation of scour depth in clay-gravel mixtures was studied with various clay percent in the mixture. The depth of scour reduces drastically with the increase of clay percent in gravel. It was also noticed in the experimentation that the rate of scour process also varies with clay percentages.

The influence of cohesion was more apparent with clay percent more than 40% in the mixture. In such cases, the process of scour initiates after 20 to 40 minutes from start of the experiment. It is found that the saturation time (T_s) of scour is function of dimensionless parameters comprising jet velocity, diameter of nozzle, height of jet, sediment size and percentages of clay content (P_c). A new relationship is proposed for the estimation of saturation time in cohesive sediment consisting of clay-gravel mixtures.

For better representation of temporal variation of scour depth, the exponent, m_s of the equation describing the temporal variation of scour, is estimated for each experimental run of the present study. Analysis of computed value of m_s revealed that it is a function of dimensionless parameters comprising jet velocity, diameter of nozzle, height of jet, sediment size and percentages of clay content. A new equation is proposed to compute the value of exponent for clay-gravel cohesive sediment mixtures.

For estimation of various scour parameters**,** the data collected in the present study have been used to formulate relationships for various scour parameters like maximum static scour depth, maximum dynamic scour depth, radius of scour hole; height of dune and volume of scour hole and it was found that dimensionless parameters comprising jet velocity, diameter of nozzle, height of jet, sediment size and percentage of clay content gives better results in place of erosion parameter. New equations have been proposed to estimate the above parameters within ± 20 percent error.

3. Scour in Clay-Sand-Gravel Cohesive Sediment Mixtures

In all, 44 experimental runs were conducted in clay-sand-gravel mixtures. The shapes of scour profiles developed in clay-sand-gravel mixture have irregular geometries with their side slopes ranging from 30^o to 90^o. At lower percentage of clay i.e., up to 20%, large size of scour hole was observed with a significant dune height. Sand and clay were found on the sides of dune whereas gravel was found in the centre of scour hole.

Analysis of temporal variation of scour depth in clay-sand-gravel mixtures reveals that the scour depth decreases with increase of clay percentage. It has been noted that the rate of scour process also varies with clay percentages. The influence of cohesion has been found more significant with clay percent higher than 40% in the mixture. In such cases, the process of scour initiates after 30 to 50 minutes from start of the experiment.

The value of saturation time of scour for each experimental run is estimated and correlated with jet velocity, diameter of nozzle, height of jet, sediment size and the percentages of clay content. A relationship is proposed for the estimation of saturation time in cohesive sediment consisting of clay-sand-gravel mixtures.

In order to estimate the temporal variation of scour depth, the value of exponent in equation of temporal variation of scour depth is to be known a priori. Analysis of present study data revealed that exponent is function of the jet velocity, diameter of nozzle, height of jet, sediment size and the percentages of clay content. Accordingly, a new equation is proposed to compute the value of exponent for clay-sand-gravel cohesive sediment mixtures.

For estimation of various scour parameters**,** the data collected in the present study have been used to formulate relationships for parameters like maximum static scour depth, maximum dynamic scour depth, radius of scour hole; height of dune and volume of scour hole and it was found that dimensionless parameters comprising jet velocity, diameter of nozzle, height of jet, sediment size and percentage of clay content give better results in place of erosion parameter. New equations have been proposed to estimate the above scour parameters within ± 20 percent error.

Acknowledgements

I feel great privileged to express my deep sense of gratitude to **Late Dr. U. C. Kothyari**, Professor, Civil Engineering Department, IIT Roorkee, **Dr. Z. Ahmad**, Professor, Civil Engineering Department, IIT Roorkee and **Dr. R. K. Jain**, Associate Professor & Head Civil Engineering Department, Govt. Engg. College Chandkheda, Gujrat for giving me an opportunity for doing my Ph. D. work under their sincere, intelligent and honest guidance. His painstaking effort is going through the manuscript and giving precious advice and suggestions for its improvement are gratefully acknowledged.

I would like to express my sincere thanks to **Dr. Deepak Kashyap**, Professor and Head, Department of Civil Engineering, IIT Roorkee, **Dr. C.S.P. Ojha, Dr. K.S. Hari Prasad**, Professor, Civil Engineering Department, IIT Roorkee, **Dr. P.K. Sharma,** Associate Professor, Civil Engineering Department, IIT Roorkee and other faculty member of Civil Engineering Department for their advice, concern and good wishes during the present investigation.

I would also like to express my sincere thanks to **Dr. Deepak Khare,** Member SRC, Professor & Head, Water Resources Development and Management Department, IIT Roorkee, and **Dr. M. Perumal**, Professor & Head Department of Hydrology, IIT Roorkee, **Dr. N.K. Goel**, Professor, Department of Hydrology, IIT Roorkee, **Dr. M.K. Jain**, Associate Professor, Department of Hydrology, IIT Roorkee, for their good wishes and moral support during the course of this research work.

Discussions held with **Dr. K.G. Ranga Raju,** (Former Professor, Civil Engineering Department and Deputy Director, IIT Roorkee, **Dr. Subhasish Dey,** Professor and Head, Department of Civil Engineering, IIT Kharagpur. **Dr. B. S. Mazumder,** Professor, Indian Statistical Institute, Calcutta, India, **Dr. S.A. Ansari,** Professor, A.M.U. Aligarh during the progress of this investigation.

I convey with my heartiest feeling, the never ending heartfelt stream of caring and blessings of my respected parents **Late Shri Vishram Chakravarti, Shrimati Sona Devi,** my grandmother **Shrimati Pusha Devi,** my elder brother **Shri Raj Kumar Chakravarti,**

Shri Sajjan Chakravarti, Shri Rajjan Chakravarti, my sister **Shrimati Kala Devi,** my brother in law **Shri Prahlad Prajapati** for their encouragement and moral support. Their foresight and valuable paved the way of a privileged education since my childhood. They are pillars of my strength, motivation and inspiration. I wish to express my appreciation and thanks to my wife, **Sneha Chakravarti** for her good wishes, believe, patience and understanding during present study. Special thank are due to my son **Divyansh**, my nephew & niece **Sidhant, Soniya, Riya, Yash, Priya, Twenkle, Jai, Sanvi** and **Anant** for allowing me to work, moral understanding and support.

I wish to convey my sincere thanks to **Mr. Y.S. Pundir**, **Mr. Vinod**, Lab Incharge Hydraulic Engg. Laboratory, Mr. Pradeep Singh, Lab Incharge Transportation Engg. Mr Raj Sexena, Lab Incharge Geotech. Engg. **Mr. Ratiram, Mr. Ajay Saini, Mr. Gyanendra**, **Mr. Nadeem, Mr. Pramod, Mr. Chotelal** and others is thankfully acknowledged for providing their assistance in laboratory for performing the tests.

I am extremely thankful to **Mr. Ajay Singh Lodhi, Mr. Nilav Karna, Mr. Umesh K. Sing, Mr. Himanshu Sarma, Mr. Ajmal Hussain, Mr. Bhupesh Jain, Mr. Kapil Rohila,** Research Scholar**,** Department of Civil Engineering, IIT Roorkee, who supported me and helped me constantly for the improvement of my research work. I will always cherish the time spend with them during my stay at IIT Roorkee.

I wish to convey thanks to **Mr. Yaswant Mehta, Dr. Ajay Kumar, Dr. Ashish Kumar, Dr. Ramesh Bhaskar, Dr. Sanjeev Kumar, Dr. Ravindra Kale, Mr. Deepak Swami, Ms. Swati Bhave, Mr. Himanshu Arora,** for their support and encouragement during this research.

I would also like to thanks **Mr. Yogesh U. Shah, Mr. Adtya Kumar Anupam Pathak, Mr. Divyesh Patel, Mr. Kamlesh Jangid, Mr. Himansu Panjiar, Mr. Rituraj Sukla, Mr. Ajay Ahirwar, Mr. Arpan Mehar, Mr. Viral, Mr. Anurag, Mr. Ravikant, Mr. Kaushal,** for wonderful company they gave me during my stay in Azad Bhawan IIT Roorkee. They have always given me tremendous moral support and I thank them for their constant support and friendship. And to the last, I am extremely thankful to those people, whose names have been unknowingly left, it really helped me a lot. I would like to thank God for blessing me the company of such nice people around me.

(**ANKIT CHAKRAVARTI**)

Contents

Description		*Page No.*
CANDIDATE'S DECLARATION		
ABSTRACT		i
ACKNOWLEDGEMENTS		vii
CONTENTS		x
LIST OF FIGURES		xv
LIST OF TABLES		xxiii
LIST OF NOTATIONS		xxiv
CHAPTER - 1	**INTRODUCTION**	1
	1.1 GENERAL	1
	1.2 LOCAL SCOUR PROCESS	4
	1.3 JET SCOUR IN COHESIONLESS SEDIMENT	6
	1.4 JET SCOUR IN COHESIVE SEDIMENT	7
	1.5 PROBLEM STATEMENT	9
	1.6 LIMITATIONS	9
	1.7 ORGANISATION OF THE THESIS	10
CHAPTER - 2	**REVIEW OF LITRATURE**	11
	2.1 INTRODUCTION	11
	2.2 SEDIMENT CHARACTERISTICS	12
	2.2.1 Some Aspects of Cohesive and Cohesionless Sediment	12
	2.2.2 Clay Mineralogy	12
	2.2.3 Forces Among the Clay Particles	13
	(i) Attractive Van der Waals forces	13
	(ii) Electric surface force	14
	(iii) Other bonding mechanisms	14
	2.2.4 Shear Strength of Cohesive Sediment	15
	2.3 CIRCULAR JETS	15

	2.4 LOCAL SCOUR DUE TO JETS	16
	2.5 SCOUR BY JET IN COHESIONLESS SEDIMENT	18
	2.6 SCOUR BY JETS IN COHESIVE SEDIMENT	32
	2.7 CONCLUDING REMARKS	53
CHAPTER - 3	**EXPERIMENTAL SET-UP AND PROCEDURE**	55
	3.1 GENERAL	55
	3.2 USED SEDIMENT MATERIALS	55
	3.2.1 Properties of Cohesionless Material	56
	3.2.2 Properties of the Cohesive Material	56
	3.2.3 Initial Stage of Cohesive Material	58
	3.3 EXPERIMENTAL SET UP	61
	3.3.1 Tank	61
	3.3.2 Final Preparation of Sediment Mixtures	63
	3.4 MEASUREMENT OF SCOUR PARAMETERS	65
	3.5 DATA CHARACTERISTICS	66
	3.6 CONCLUDING REMARKS	69
CHAPTER - 4	**ANALYSIS OF DATA, RESULTS AND DISCUSSIONS FOR COHESIONLESS SEDIMENT**	71
	4.1 PRELIMINARY REMARKS	71
	4.2 SALIENT OBSERVATIONS IN COHESION LESS SEDIMENT	71
	4.3 TEMPORAL VARIATION OF SCOUR DEPTH IN COHESIONLESS SEDIMENT	75
	4.3.1 Temporal Variation of Scour Depth with 12.5 mm Nozzle Diameter	75
	(a) Sand bed	75
	(b) Sand-gravel mixtures bed	76
	(c) Gravel bed	77
	4.3.2 Temporal Variation of Scour Depth with 8 mm Nozzle Diameter	78
	(a) Sand bed	78

(b) Sand-gravel mixtures bed 78

(c) Gravel bed 79

4.3.3 Comparison of Temporal Variation of Scour Depth 80

4.3.4 Development of Relationship for Estimation of Scour Depth With Respect to Time 81

4.3.5 Relationship for Saturation Time 81

4.3.5.1 Relationship for the value exponent 86

4.3.5.2 Validation of proposed relationship for estimation of scour depth with time 87

4.4 ESTIMATION OF VARIOUS SCOUR PARAMETERS 88

4.4.1 Maximum Static Scour Depth 88

4.4.2 Maximum Dynamic Scour Depth 92

4.4.3 Radius of Scour Hole 94

4.4.4 Dune Height 96

4.4.5 Volume of Scour Hole 98

4.5 CONCLUDING REMARKS 100

CHAPTER - 5 ANALYSIS OF DATA, RESULTS AND DISCUSSIONS IN COHESIVE SEDIMENT MIXTURES 101

5.1 PRELIMINARY REMARKS 101

5.2 SCOUR IN CLAY-GRAVEL MIXTURES 101

5.2.1 Temporal Variation of Scour Depth in Clay-Gravel Mixtures 104

5.2.1.1 Temporal variation of scour depth in 12.5 mm nozzle diameter 104

5.2.1.2 Relationship for saturation time in clay-gravel mixtures 108

5.2.1.3 Development of relationship for estimation of scour depth with time 109

5.2.1.4 Relationship for the value of exponent 112

5.2.1.5 Validation of Proposed Relationship in Clay-Gravel Mixtures 113

5.2.2 Estimation of Various Scour Parameters in Clay-Gravel Mixtures 114

(a) Maximum static scour depth 114

(b) Maximum dynamic scour depth 116
5.3 SCOUR IN CLAY-SAND-GRAVEL MIXTURES 120
5.3.1 Temporal Variation of Scour Depth in Clay-Sand-Gravel Mixtures 123
5.3.1.1 Temporal Variation of Scour Depth in 12.5 mm Nozzle Diameter 123
5.3.1.2 Relationship for saturation time in clay-sand-gravel mixtures 126
5.3.1.3 Development of relationship for estimation of scour depth with time 127
5.3.1.4 Relationship for the value exponent 131
5.3.1.5 Validation of proposed relationship in clay-sand-gravel mixtures 131
5.3.2 Estimation of Various Parameters in Clay-Sand-Gravel Mixture 133
(a) Maximum static scour depth 133
(b) Maximum dynamic scour depth 135
5.4 CONCLUDING REMARKS 139

CHAPTER - 6 **CONCLUSIONS** 141
6.1 GENERAL 141
6.2 SCOUR DUE TO JETS IN COHESIONLESS SEDIMENT 142
6.3 SCOUR DUE TO JETS IN COHESIVE SEDIMENT 143
6.4 RECOMMENDATIONS FOR FUTURE RESEARCH 144
REFERENCES 147
APPENDICES 155
APPENDIX - A HYDRAULIC AND SEDIMENT PARAMETERS UNDER SUBMERGED CIRCULAR VERTICAL JETS IN SAND BEDS 155

APPENDIX - B HYDRAULIC AND SEDIMENT PARAMETERS UNDER SUBMERGED CIRCULAR VERTICAL JETS IN SAND-GRAVEL MIXTURES BEDS 155

APPENDIX - C HYDRAULIC AND SEDIMENT PARAMETERS UNDER 155

SUBMERGED CIRCULAR VERTICAL JETS IN GRAVEL BEDS

APPENDIX - D HYDRAULIC AND SEDIMENT PARAMETERS UNDER SUBMERGED CIRCULAR VERTICAL JETS IN CLAY-GRAVEL COHESIVE SEDIMENT MIXTURES 156

APPENDIX - E HYDRAULIC AND SEDIMENT PARAMETERS UNDER SUBMERGED CIRCULAR VERTICAL JETS IN CLAY-SAND-GRAVEL COHESIVE SEDIMENT MIXTURES 158

APPENDIX - F TEMPORAL VARIATION OF SCOUR DEPTH UNDER SUBMERGED CIRCULAR VERTICAL JETS IN COHESIONLESS SEDIMENTS 160

APPENDIX - G TEMPORAL VARIATION OF SCOUR DEPTH UNDER SUBMERGED CIRCULAR VERTICAL JETS IN CLAY-GRAVEL COHESIVE SEDIMENT MIXTURES 169

APPENDIX - H TEMPORAL VARIATION OF SCOUR DEPTH UNDER SUBMERGED CIRCULAR VERTICAL JETS IN CLAY-SAND-GRAVEL COHESIVE SEDIMENT MIXTURES 184

List of Figures

Figure No.	Description	Page No.
1.1	River bed material of the Gola River at Haldwani, Uttarakhand, India (Kumar, 2011)	4
1.2	River bed material of the Ganga River at Rishikesh, Uttarakhand, India (Kumar, 2011)	4
1.3	Water release through hydraulic structure of the Krishna River in Srisailam Dam, Andhra Pradesh, India	5
1.4	Water release through hydraulic structure of the Zambezi River in Kariba Dam, Zimbabwe	6
2.1	Fundamental building blocks of clay minerals	13
2.2	Impingement of a jet on a flat plate (George, 1980)	16
2.3	Flow regimes of a vertical impinging jet (Ansari, 1999)	17
2.4	Sediment motion during impingement of jet (Mih and Kabir, 1983)	20
2.5	Depth of gravel motion during impingement of jet (Mih and Kabir, 1983)	21
2.6	Flow regimes of eroded sand beds (Aderibigbe and Rajaratnam, 1996)	23
2.7	Variation of dune height with erosion parameter (Adribigbe and Rajaratnam, 1996)	24
2.8	Variation of radius of scour hole with E_c (Adribigbe and Rajaratnam, 1996)	25
2.9	Variation of maximum scour depth with F_o (Adribigbe and Rajaratnam, 1998)	26
2.10	Variation of scour hole length with F_o (Adribigbe and Rajaratnam, 1998)	26
2.11	Growth of maximum depth of scour with time (Rajaratnam and Mazurek, 2003)	28
2.12	Normalized maximum scour depth versus jet velocity with E_c = 5.28 (Yeh et al. 2009)	30

2.13 Variation of depth of scour versus time (Dehghani et al. 2010) 32

2.14 Scour rate index versus Reynold number for different sediment (Moore and Masch, 1962) 34

2.15 Scour rate index versus Reynold number for different jet diameters (Moore and Masch, 1962) 34

2.16 View of various shapes of scour profiles (Moore and Masch, 1962) 35

2.17 Variation of J_i with moisture contents (Hanson and Robinson, 1993) 38

2.18 Variation of J_i with dry unit weight (Hanson and Robinson, 1993) 38

2.19 Temporal variation of scour depth for sediment A at different applied stress (Hanson, 1993) 39

2.20 Predicted versus measured equilibrium scour depth (Stain et al. 1993) 41

2.21 Ratio of volume of scour hole to the maximum depth of scour (Mazurek el al. 2001) 42

2.22 Dimensionless maximum depth of scour at equilibrium (Mazurek el al. 2001) 43

2.23 Variation of d_{sms}/h_j with erosion parameter, E_c (Ansari et al., 2003) 45

2.24 Comparison of computed $d_{sms})_{cohesion} / d_{sms})_{cohesionless}$ using Eq. (2.48) with observed values (Ansari, 1999) 47

2.25 Comparison of computed $\nabla_{cohesion} / \nabla_{cohesionless}$ using Eq. (2.49) with observed value (Ansari et al. 2003) 47

2.26 Variation of $d_{sms})_{cohesion} / d_{sms})_{cohesionless}$ with w/w_*, $PI > 0$ (Ansari et al. 2003) 48

2.27 Variation of $\nabla_{cohesion} / \nabla_{cohesionless}$ with w/w_*, $PI > 0$ (Ansari et al. 2003) 49

2.28 Maximum depth of scour at equilibrium condition (Mazurek et al. 2003) 50

2.29 Length scale of scour for equilibrium scour hole (Mazurek et al. 2003) 50

2.30 Maximum scour depth in cohesionless and cohesive sediment due to circular impinging jets (Mazurek and Hossain, 2007) 52

2.31 Scour hole radius in cohesionless and cohesive sediment (Mazurek and Hossain, 2007) 52

2.32	Maximum depth of scour in cohesionless and cohesive sediment due to circular wall jets (Mazurek and Hossain, 2007)	53
3.1	Particle size distribution curve for clay, sand and gravel sediment	56
3.2	Photographic view of bed material used (a) clay (b) sand (c) gravel and (d) sand-gravel mixture	57
3.3	Results of X-ray diffraction test for clay	58
3.4	Picture showing (a) dry, (b) semi-solid, (c) plastic and (d) viscous states of cohesive sediment	59
3.5	Relative location of the non-plastic, plastic and viscous states of cohesive sediment (Ansari, 1999)	60
3.6	Variation of dry density with moisture content of clay-gravel mixtures for different clay percent	60
3.7	Variation of dry density in clay-sand-gravel mixtures with moisture content for different clay percent	61
3.8	Experimental set-up	62
3.9	A photographic view of the experimental set-up	62
3.10	Calibration curve of Venturimeter	63
3.11	Prepared cohesive sediment bed before start of the experiment	64
3.12	Measurement of unconfined compressive strength of the sediment sample	65
4.1	View of developed scour hole profiles in sand beds	73
4.2	View of developed scour hole profiles in sand-gravel beds	74
4.3	View of developed scour hole profiles in gravel beds	75
4.4	Temporal variation of scour depth with time for 12.5 mm nozzle in sand bed	76
4.5	Temporal variation of scour depth with time for 12.5 mm nozzle in sand-gravel mixture bed	77
4.6	Temporal variation of scour depth with time for 12.5 mm nozzle in gravel bed	77
4.7	Temporal variation of scour depth with time for 8 mm nozzle in sand bed	78

4.8 Temporal variation of scour depth with time for 8 mm nozzle in gravel bed 79

4.9 Temporal variation of scour depth with time for 8 mm nozzle in sand-gravel bed 79

4.10 Comparison of temporal variation of scour depths in sand, sand-gravel mixture and gravel beds for run no. S2, SG2 and G2 respectively 80

4.11 Comparison of temporal variation of scour depths in sand, sand-gravel mixture and gravel beds for run no. S6, SG6 and G6 respectively 80

4.12 Comparison of observed and computed saturation time in cohesionless sediment 82

4.13 Variation of d_{ss} / d_{dms} with t/T_s in sand bed 83

4.14 Variation of d_{ss} / d_{dms} with t/T_s in sand-gravel mixtures bed 83

4.15 Variation of d_{ss} / d_{dms} with t/T_s in gravel bed 84

4.16 Variation of d_{ss} / d_{dms} with $\sin(\pi t/2T_s)$ in sand bed 84

4.17 Variation of d_{ss} / d_{dms} with $\sin(\pi t/2T_s)$ in sand-gravel mixtures bed 85

4.18 Variation of d_{ss} / d_{dms} with $\sin(\pi t/2T_s)$ in gravel bed 85

4.19 Comparison of observed and computed exponent, m_s value in cohesionless sediment 86

4.20 Comparison of computed scour depth using Eq. (4.5) with observed values in sand beds for run S2 87

4.21 Comparison of computed scour depth using Eq. (4.5) with observed values in gravel beds for run G2 87

4.22 Comparison of computed scour depth using Eq. (4.5) with observed values in sand-gravel mixtures for run SG2 88

4.23 Comparison of observed and computed depth of scour for present and previous data using Eq. (4.8) 89

4.24 Comparison of observed and computed depth of scour for present and previous data using Eq. (4.9) 90

4.25 Variation of d_{sms} / h_j with erosion parameter E_c in cohesionless sediment 91

4.26	Comparison of observed and computed maximum depth of scour using proposed relationship using Eq. (4.10)	91
4.27	Comparison of observed and computed maximum static scour depth (d_{sms}) using Eq. (4.11)	92
4.28	Comparison of observed and computed maximum dynamic scour depth (d_{dms}) using Eq. (4.12)	93
4.29	Variation of ratio of maximum dynamic and maximum static scour depths with erosion parameter	94
4.30	Variation of radius of scour hole, (r) with erosion parameter (E_c)	95
4.31	Comparison of observed and computed radius of scour hole using Eq. (4.13)	95
4.32	Comparison of observed and computed radius of scour hole using Eq. (4.14)	96
4.33	Variation in volume of scour hole with erosion parameter, E_c	97
4.34	Comparison of observed and computed dune height using Eq. (4.15)	97
4.35	Comparison of observed and computed dune height (Δ) in cohesionless sediment	98
4.36	Variation in volume of scour hole with erosion parameter, E_c	99
4.37	Comparison of observed and computed volume of scour hole using Eq. (4.17)	99
4.38	Comparison of observed and computed volume of scour hole using Eq. (4.18)	100
5.1	Scour bed profiles under submerged vertical jets in different clay percent in clay-gravel mixture bed	104
5.2	Temporal variation of scour depth in clay-gravel mixtures using 12.5 mm nozzle for d_o = 12.5 mm, h_j = 0.30 m, u_o = 7.19 m/s	105
5.3	Temporal variation of scour depth in clay-gravel mixtures using 12.5 mm nozzle for d_o = 12.5 mm, h_j = 0.15 m, u_o = 5.12 m/s	106
5.4	Variation of scour depth with time in 10% clay in clay-gravel mixture	107
5.5	Variation of scour depth with time in 20% clay in clay-gravel mixture	107
5.6	Comparison of observed and computed saturation time using Eq. (5.4)	109

5.7 Variation of d_{ss}/d_{dms} with t/T_s for 10 % clay with gravel 110

5.8 Variation of d_{ss}/d_{dms} with t/T_s for 20 % clay with gravel 110

5.9 Variation of d_{ss}/d_{dms} with $\sin(\pi t/2T_s)$ for 10 % clay mixture 111

5.10 Variation of d_{ss}/d_{dms} with $\sin(\pi t/2T_s)$ for 20 % clay in mixture 111

5.11 Comparison of observed and computed exponent (m_s) values using Eq. (5.5) in clay-gravel mixture 112

5.12 Validation of proposed relationship in scour depth with time in 10% clay in mixture 113

5.13 Validation of proposed relationship in scour depth with time for 20% clay in mixture 113

5.14 Validation of proposed relationship in scour depth with time in 30% clay in mixture 114

5.15 Variation of static scour depth with erosion parameter for different clay percentage in clay-gravel mixture 115

5.16 Comparison of observed and computed maximum static scour depth using Eq. (5.6) 115

5.17 Comparison of observed and computed maximum static scour depth using Eq. (5.7) 116

5.18 Comparison of observed and computed maximum dynamic scour depth 117

5.19 Ratio of maximum dynamic and maximum static scour depths for different clay percentage in mixture 117

5.20 Comparison of observed and computed radius of scour hole 118

5.21 Comparison of observed and computed volume of scour hole 119

5.22 Comparison of observed and computed dune height 119

5.23 Scour bed profiles under submerged vertical jets in different clay percent in the mixture 123

5.24 Comparison of temporal variation of scour depth in clay-sand-gravel mixtures for d_0 = 12.5 mm, h_j = 0.30 m, u_o = 7.19 m/s 124

5.25 Comparison of temporal variation of scour depth in clay-sand-gravel mixtures for d_0 = 12.5 mm, h_j = 0.15 m, u_o = 7.19 m/s 124

5.26	Variation of scour depth with time in 10% clay in mixture	126
5.27	Variation of scour depth with time in 20% clay in mixture	126
5.28	Saturation time (T_s) for clay gravel sediment in observed and computed conditions	127
5.29	Variation of d_{ss}/d_{dms} with t/T_s for 30 % clay in clay-sand-gravel mixtures	128
5.30	Variation of d_{ss}/d_{dms} with t/T_s for 40 % clay in clay-sand-gravel mixtures	129
5.31	Variation of d_{ss}/d_{dms} with $\sin(\pi t/2T_s)$ for 30 % clay in clay-sand-gravel mixtures	130
5.32	Variation of d_{ss}/d_{dms} with $\sin(\pi t/2T_s)$ for 40 % clay in clay-sand-gravel mixture	130
5.33	Comparison of observed and computed value of exponent in clay-sand-gravel mixtures	131
5.34	Comparison of observed and computed saturation time (T_s) in clay-sand-gravel mixture having 10% clay	132
5.35	Comparison of observed and computed saturation time, T_s for clay-sand-gravel mixture having 20% clay	132
5.36	Comparison of observed and computed saturation time (T_s) for clay-sand-gravel mixture having 30% clay	133
5.37	Variation of static scour depth, d_{sms} with erosion parameter, E_c in different clay percent in clay-sand-gravel mixture	134
5.38	Comparison of observed and computed maximum static scour depth using Eq. (5.14)	134
5.39	Comparison of observed and computed maximum static scour depth using Eq. (5.15) in clay-sand-gravel mixtures	135
5.40	Comparison of observed and computed maximum dynamic scour depth using Eq. (5.16) in clay-sand-gravel mixture	136
5.41	Ratio of maximum dynamic and maximum static scour depths for different clay percentage in mixture	137
5.42	Comparison of observed and computed radius of scour hole using Eq. (5.17) in clay-sand-gravel mixture	138

5.43 Comparison of observed and computed height of dune using Eq. (5.18) in clay-sand-gravel mixtures 138

5.44 Comparison of observed and computed volume of scour hole using Eq. (5.19) in clay-sand-gravel mixture 139

List of Tables

Table No.	*Description*	*Page No.*
2.1	Physical Properties of the sediment used by Hanson (1993)	37
2.2	Summary of the sediment properties used by Hanson (1993)	39
2.3	Characteristics of cohesive sediments used by Ansari et al. (2003)	44
2.4	Range of data on scour under submerged vertical jet in cohesionless sediment by Ansari et al. (2003)	44
3.1	Range of the data (present and previous investigations) on scour under submerged circular vertical jet in cohesionless sediment	66
3.2	Range of the data for present investigation in cohesionless sediments	67
3.3	Range of data on scour under submerged circular vertical impinging jets in cohesive sediments consisting of clay-gravel mixtures	68
3.4	Range of data on scour under submerged circular vertical impinging jets in cohesive sediments consisting of clay-sand-gravel mixtures	68

List of Notations

Symbol	Description	Dimension
A^o	Angstrom	L
Al	Aluminium	-
b_o	Thickness of nozzle	L
$b_{m\infty}$	Half width of scour profile	L
C	Coefficient	-
Ca	Calcium	-
C_f	Friction coefficient	-
Cr	Chromium	-
C_d	Diffusion coefficient	-
C_*	Dimensionless clay content defined as $P_c C_u /(\gamma_s - \gamma_w) d_a$	-
Cu	Copper	-
C_u	Cohesion	$ML^{-1}T^{-2}$
d	Scour depth	L
D	Culvert diameter	L
D_*	dimensionless grain size of the sediment	-
d_a	Arithmetic mean size of cohesive sediment mixture	L
d_o	Nozzle diameter	L
d_{ss}	Instantaneous scour depth	L
d_{sms}	Maximum static depth of scour	L
d_{dms}	Maximum dynamic depth of scour	L
$\bar{d}_{sms}$	Average maximum scour depth at equilibrium	L
d_{50}	The particle size such at which 50% is finer by weight	L
d_{95}	The particle size such at which 95% is finer by weight	L
E_c	Erosion parameter $= u_o (d_o / h_j) / \sqrt{(g d_{50} \Delta\rho_s / \rho_f)}$; where $d_o / h_j > 8.3$	-
Fe	Iron	-
F_o	Densimetric Froude number defined as $F_o = u_o /(\sqrt{g d_{50} \Delta\rho_s / \rho_f})$	-
g	Acceleration due to gravity	LT^{-2}
h	Flow depth	L

h_j	Jet height from original bed level	L
J_i	Jet scour index	-
K_e	Erodibility coefficient	-
K_c	A constant	-
K_o	A constant	-
K_s	Scour rate index	-
K	Potassium	-
L	Length of apron	L
m, m_s	Exponent	-
Mg	Magnesium	-
Na	Sodium	-
Ni	Nickel	-
O	Oxygen	-
OH	Hydroxide	-
OMC	Optimum moisture content	-
P	Pressure	MLT^{-2}
P_c	Clay content	-
P_s	Stagnation pressure	MLT^{-2}
PI	Plasticity index	-
q	Discharge	L^3T^{-1}
r	Radius of scour hole	L
r_d	Distance from jet centre line	L
r_∞	Maximum radial of scour hole	L
R_e	Reynold Number (= $u_o d_o/v$)	-
S	Ratio of jet velocity to carriage speed (= u_o/u_s)	-
S_d	Submerged water depth on the tank	L
Si	Silica	-
T_c	Saturation time	L
t	Instantaneous time	L
t_1	Characteristics time	L
u_*	Shear velocity	LT^{-1}
u_{*cs}	Shear velocity corresponding to incipient motion of the sediment in the approach flow	LT^{-1}

u_o	Jet velocity	LT^{-1}
u_s	Ship velocity	LT^{-1}
v_s	Carriage speed	LT^{-1}
W	Antecedent moisture content	-
W_*	Antecedent moisture content require to saturate the soil sample	-
W_L	Liquid limit (%)	-
W_P	Plastic limit (%)	-
X	Cohesive sediment erosion value $(=\rho_f u_o^2 (d_o / h_j)^2$	-
X_c	Critical value of X below which mass erosion is not observed	-
X_o	Scour hole length	L
$\overline{X}_{m\infty}$	Average distance from nozzle of the maximum scour depth at equilibrium	L
$\overline{X}_{o\infty}$	Average Scour hole length	L
UCS	Unconfined compressive strength of cohesive sediment bed	$ML^{-1}T^{-2}$

GREEK NOTATIONS

φ	Jet angle	-
α	Scanning angle	-
γ	Bulk density of sediment	$ML^{-2}T^{-2}$
γ_d	Dry density of sediment	$ML^{-2}T^{-2}$
$(\gamma_d)_{\max}$	Maximum dry density of cohesive sediment	$ML^{-2}T^{-2}$
γ_f	Specific weight of fluid	$ML^{-2}T^{-2}$
γ_s	Specific weight of sediment	$ML^{-2}T^{-2}$
γ_w	Specific weight of water	$ML^{-2}T^{-2}$
$\Delta\gamma_s$	Difference in specific weight of sediment and water	$ML^{-2}T^{-2}$
$\Delta\rho_s / \rho_f$	Relative density difference defined as $(\rho_s - \rho_f)/\rho_f$	-
ρ_f	Mass density of fluid	ML^{-3}
ρ_s	Mass density of sediment	ML^{-3}
θ	Scanning angle of inclination for the diffractogram	-
ν	Kinematic viscosity of fluid	L^2T^{-1}
σ	Applied stress	$ML^{-1}T^{-2}$

σ_g	Geometric standard deviation	-
σ_n	Normal stress	$ML^{-1}T^{-2}$
τ	Average shear stress on the bed	$ML^{-1}T^{-2}$
τ_{cc}	Critical shear strength of cohesive sediment	$ML^{-1}T^{-2}$
τ_{om}	Maximum shear stress	$ML^{-1}T^{-2}$
μ	Dynamic viscosity	$M L^{-1}T^{-1}$
∇	Volume of scour hole	L^3
Δ	Dune height	L
τ_{sh}	Shear strength of the sediment	$ML^{-1}T^{-2}$
ε	Erosion or detachment rate in volume per unit area per unit time	LT^{-1}
λ	Parameter describing hydraulic properties of jet (= $\rho_s u_o^2$)	-
λ_c	Critical value of λ below which no significant scour occurs	-
ω_f	Fall velocity	LT^{-1}
ϕ_β	Entrainment effect	-
ϕ_c	Angle of repose or internal friction for cohesive sediment	-
ϕ_*	Dimensionless angle of internal friction for cohesive sediment mixture defined as $\frac{P_c \tan\phi_c + (1-P_c)\tan\phi_{sh}}{\tan\phi_{sh}}$	-

ABBREVIATIONS USED

A.S.C.	American soil classification system
A.S.T.M.	American society of testing and material
CEC	Cation exchange capacity
CD	Characteristics dimensions i.e. d_{sms}/d_o, w/d_o, etc.
CL	Clay with low plasticity
CH	Inorganic clays of high plasticity
C	Clay
G	Gravel
S	Sand

SG	Sand-gravel
CG	Clay-gravel
CSG	Clay-sand-gravel
IS	Indian Standard
XRD	X-ray diffraction
OH	Hydroxyl group formed by Oxygen and Hydrogen atoms
PI	Plasticity Index
U.S.C.	Unified soil classification system
O.M.C.	Optimum moisture content
GSD	Geometric standard deviation
WDJR	Weakly deflected jet regimes
SDJR	Strongly deflected jet regimes

CHAPTER 1

INTRODUCTION

1.1 GENERAL

Hydrodynamic imbalance and instability in river system due to natural and anthropogenic causes has become a subject of concern. In rivers, one of the most challenging problems is to know the depth of scour around the hydraulic structures for its stability like bridge scour, abutment scour, scour around spur dikes, scour due to jets etc. The hydraulic structures are subjected to scour around their foundations due to erosive action of the flowing water. If the depth of scour becomes significant, the stability of the foundations is endangered. Therefore, estimation of maximum scour depth due to water jets is required for the safe and economic design of hydraulic structures and their foundations e.g. gates, culverts, weirs, spillways and grade control structures etc. The present study is undertaken to investigate the process of scour due to jets at various scales and parameters. This has revived the interest in advancing our understanding of the scour process. Scour due to water jets is a complex phenomenon resulting from the strong interaction of the three dimensional turbulent flow fields downstream of the hydraulic structures and the erodible bed sediments. This phenomenon becomes further complex when scour due to jet takes place in the cohesive sediment.

Scour due to submerged water jets occurs downstream of hydraulic structures like free overfall spillway, trajectory bucket type energy dissipater etc. In such cases, water jet emerges out from the structures and impinges into water downstream and subsequently scours the river bed. The jet behaves as free before impinging into water and the flow characteristics of the jet like angle of attack, size of jet, velocity, discharge etc. are governed by the dimensions of the structures and water level upstream of the structures. After impinging into the water, the jet behaves as submerged water jet which causes the scour around the hydraulic structures. Thus, estimation of various parameters of scour like maximum scour depth, volume of scour, radius of scour, dune height under submerged jet is essential for the design of protection measures downstream of the structures.

The depth of scour due to water jets downstream of the hydraulic structures is significantly affected by inter-dependent variables, such as velocity, jet height, nozzle size and sediment characteristics. For given conditions of these variables, the scour depth also varies with time. These facts are addressed through an experimental study to comprehend objective use of relations and putting them in practice. The foundations of hydraulic structures shall be placed at higher depth below the river bed (up to 50 m) in case of large rivers like the Ganga and the Brahmputra in India (Kothyari, 2007). Thus considerable amount of money can be saved in the construction of hydraulic structure if the depth of scour could be realistically estimated at the design stage.

The scour process due to water jets depends upon various factors and also it varies with the type of hydraulic structures. The local scour in the vicinity of the hydraulic structures due to submerged water jet poses an immense problem in designing the foundation of these hydraulic structures. The water jet penetrates into the sediment bed and deflected in the upward direction resulting in a highly turbulent zone. The factors influencing the development of scour are complex and vary according to the type of structure, flowing water and sediment bed. There are two types of scour profile geometries: dynamic scour when the jet flow is in operating condition, and static scour which is the final bed scour hole produced, when the jet flow is stopped.

Many researchers have performed laboratory experiments on scour processes due to jets. The experimental investigation on scour due to submerged vertical jet in cohesionless sediments was first conducted by Rouse (1940). Thereafter, a number of investigations have been carried out to study the response of submerged water jets for various sediment materials, jet velocities, jet heights and diameter of nozzles under different types of water jets like horizontal water jets, vertical water jets, inclined water jets in submerged and non-submerged conditions. Experience has shown that scouring can progressively undermine the foundations of hydraulic structures because full protection against scour process is generally prohibitively expensive. Therefore, designer must seek ways to control and guide the scour process so as to minimize the risk of failure of the hydraulic structures.

Scour due to turbulent jets impacts numerous hydraulic engineering projects. Turbulent jets are typically associated with engineered hydraulic features, including stationary structures such as spillways, outlet works, and grade control structures, and with mobile sources such as propeller wash and nozzle discharges. Natural occurrences of turbulent water jets are more limited, but can be found where water flows over and around natural stream obstructions.

Sediment is transported when the combination of drag and lift forces overcome the gravitational forces and surrounding river bed sediment particle interactions. While lower pressures in a scour hole promote sediment transport, the primary mechanism of sediment transport is the high shear stress created by a flow along the river or stream sediment beds. Significant localized sediment bed degradation may occur when shear stresses along the bed are abnormally high, such as in a high water flow conditions. Reservoir spillways and grade control structures can alter the natural water flow regime of a stream, leading to increased scouring process of the river or stream sediment bed material downstream. Outlet pipes from sources such as factories and water treatment facilities also create scour, especially if they are located near the channel bed.

The scour process under submerged water jets was conducted mainly for uniform cohesionless sediment i.e. sand, gravel. However, in nature the river and stream beds are mostly composed of mixtures of a clay, sand and gravel.

The methods available for the estimation of maximum scour depth under submerged water jets are applicable mainly in steady flow. But water flows in the stream beds at high flood situation is unsteady and the water discharge changes in it at a faster rate. Therefore, the time variations of maximum depth of scour are also most important aspects for the estimation of maximum depth of scour in unsteady flows (Kothyari et al., 1992 a & b)

This research shall relate theoretical relationships in fluid mechanics to experimental observations and also enhance the knowledge of the scour process due to submerged vertical jets for the scientific community. While the application of the data collection methods utilized in this research was limited to a controlled laboratory setting. This research developed physically based relationships that advanced the current state of knowledge on jet scour process. The results obtained in this investigation can be applied to several engineering scenarios. The hydraulic structures such as spillways, outlet works, vertical gate, weirs, culverts and grade control structures produce water jets and their behavior correlates to this research. Spillways and submerged culverts discharging into downstream beds exhibit similar behavior. Also, bridges under high food condition, ice or debris dams, and bottom-release hydraulic structures can all produce accelerated flow along the stream bed, therefore, the foundations of these structures are susceptible to bed scour due to jets.

Figure 1.1 depicts the stream bed and banks consisting of cohesive sediment mixture in the Gola river near Haldwani, Uttarakhand in Shiwaliks of Indian Himalayas. The hydraulic structure constructed on this river failed by excessive scouring of river bed during floods in monsoon season of 2008. Similarly Fig. 1.2 depicts the presence of clay with cohesionless sediments in the bed material of the river Ganga at Rishikesh, India.

Fig. 1.1 River bed material of the Gola River at Haldwani, Uttarakhand, India (Kumar, 2011)

Fig. 1.2 River bed material of the Ganga River at Rishikesh, Uttarakhand, India (Kumar, 2011)

1.2 LOCAL SCOUR PROCESS

Local scour can be defined as degradation of river banks and or stream bed that is localized to a specific area due to a sudden change in the parameters associated with the river flow i.e. change in geometry, slope, flow, or placement of a structure, etc. The local scour process of a hydraulic structure is complex in nature because of abrupt or sudden changes of the flow characteristics over the erodible bed. It is important to monitor local scour in order to minimize adverse effects on infrastructure and on the surrounding natural environment. The local scour process downstream of hydraulic structures due to submerged water jet poses an immense problem in designing the foundation and the stability of these structures. The scour process starts downstream of hydraulic structures through which a jet is issued when the bed shear stress induced by vertical jet exceeds the critical bed shear stress for the initiation of bed particles. Studies on scour due to water jets are mainly focused on the analysis of submerged circular vertical impinging jet in cohesionless soils. The process of scour due to jets founded in cohesionless uniform and non-uniform sediments are reasonably well understood at present. However, the land surfaces and river bed materials frequently consist of mixture of cohesive as well as cohesionless sediments like mixtures of sand, gravel and clay etc. (Jain and Kothyari, 2009a&b). Soil in upland catchment areas is one of the examples of this type of sediment (Kothyari and Jain, 2008). One of the practical examples of scour due to water jets downstream of the bucket type energy dissipater is shown in Fig. 1.3.

Fig. 1.3 Water release through hydraulic structure of the Krishna River in Srisailam Dam, Andhra Pradesh, India

The 128 meter high Kariba Dam is one of Africa's biggest dams as shown in Fig. 1.4. Millions of people live downstream of it in the Zambezi River Basin. Operated by the Zambezi River Authority on behalf of Zimbabwe and Zambia, it has been a cause for concern on a number of safety issues. Most recently, at a meeting of dam operators in July 2012, engineers from the Zambezi River Authority (ZRA) revealed that the plunge pool jet scour below the Kariba Dam has deepened beyond expectation. It has now eroded to a depth of more than 90 m into the rock substrate. The plunge pool jet scour is the area where the water is released after going through the dam's spillways. The main concern is not the depth of the plunge pool jet, but that it has been eroding towards the dam wall, with the likely possibility of undercutting the foundation of the 128 m high wall. This is of great concern, as an unstable foundation can lead to dam failure, a potentially catastrophic event for the hundreds of thousand people living downstream of the Kariba Dam.

Fig. 1.4 Water release through hydraulic structure of the Zambezi River in Kariba Dam, Zimbabwe

1.3 JET SCOUR IN COHESIONLESS SEDIMENT

In case of cohesionless sediment the resistance to scour the bed material is provided mainly by submerged weight of the sediment. However in case of cohesive sediment, the electro-chemical forces and inter-particle net attractive forces affect the resistance against scour. The process of scour in gravels, sand or different types of sediment, which are mostly found downstream of hydraulic structures are importance aspects because an excessive scour may damage the stable hydraulic structures such as gates, weirs, culverts, spillways and grade control structures etc. So that the evaluation of accurate maximum scour depth is very useful for economical stable hydraulic structures. The significant fundamental works and the problem of sediment bed response due to submerged water jets in cohesionless sediment have been investigated by a number of researchers such as Doddiah et al. (1953), Sarma (1967), Westrich and Kobus (1973), Altinbilek and Okyay (1973), Rajaratnam and Beltaos (1977), Rajaratnam (1982), Aderibigbe and Rajaratnam (1996), Rajaratnam and Mazurek (2003, 2005, 2006). Functional relationships were proposed by the above researchers for the estimation of the equilibrium depth of scour. They also studied shear stress distribution due to different jet flow and bed conditions.

Westrich and Kobus (1973) studied the phenomenon of jet scour through experiments on a uniform sand bed with vertical submerged jet having different mean velocity, two types of nozzle diameter and two type of jet height. Rajaratnam (1982) studied erosion by planer, two-dimensional jets, primarily in the context of scour at hydraulic structures. Raudkivi (1990) suggested that the erosion resistance of a cohesionless material depends primarily on the particle buoyant weight, shape, and packing. Ansari (1999), Donoghue et al. (2001), Ansari et al. (2003), Mazurek and Hossain (2007) also studied the temporal variation of scour depth in cohesionless sediments. Ansari et al. (2003) conducted laboratory based research work on the topic of scour due to vertical submerged circular water jets in both cohesive as well as cohesionless sediment material and identified the difference of scour hole profiles between these two sediment materials. Aderibigbe and Rajaratnam (1996) conducted a laboratory experiment on the erosion of loose beds by submerged circular impinging vertical jets by using sand as a loose sediment beds. They investigated the variation of maximum depth of scour with impinging distance and found two major jet flow regimes i.e., strongly deflected and weekly deflected jet flow regimes. Donoghue et al. (2001) conducted experiment in cohesionless sediment to investigate the response of sand beds due to submerged circular vertical water jet. The experimental data was generated by larger diameter of jet, fine sediment and small jet impingement height from original bed level.

Rajaratnam and Mazurek (2003) presents the laboratory based experimental study on the scour in cohesionless sediment beds due to water jets having low tail water depth. The laboratory work conducted by Yeh et al. (2009) showed that the scour hole lengths at the equilibrium conditions can be estimated using developed relationships proposed by Aderibigbe and Rajaratnam (1996).

1.4 JET SCOUR IN COHESIVE SEDIMENT

The sediment particles with size smaller than 0.06 mm normally behave as cohesive sediment and the material exhibits cohesion effects, studied by Kuti and Yen (1976). Cohesive sediment is composed mainly of clay material in which the clay particles have strong inter-particle forces due to their surface ionic attraction between each other. The cohesive sediment consists of organic and inorganic mineral (Hayter, 1983). The organic minerals may exist as plant and animal detritus and bacteria. The inorganic mineral mainly consists of Illite, Kaolinite and Montmorillonite. The area per unit volume of cohesive particles is large because of that the physico-surface chemical forces become much more important as to particle weight of the sediment.

Cohesive sediments have different characteristics as compared to the cohesionless material. The topic of scour by jets has also been studied for cohesive materials mainly consisted of either pure clays or clay-sand mixtures (Ansari et al. 2003, Mazurek et al., 2001, 2003). To be the best of our knowledge, no studies have been reported so far in the literature on scour of cohesive material consisted of clay-sand-gravel mixtures**.** Recently, Jain (2008), Kothyari and Jain (2008), Jain and Kothyari (2009a & 2010) have reported the results from an experimental study on erosion and transport of clay-sand-gravel mixtures by channel flows. The study done by Ansari et al. (2003), Mazurek et al. (2001, 2003) needs to be extended to jet scour in cohesive materials mainly consisting of clay-sand-gravel mixtures as such type of sediment river bed material frequently occur in nature.

The laboratory study under submerged water jets in case of cohesive sediment materials have not been studied extensively. Mazurek et al. (2001) conduct experiments on the topic of scour in case of cohesive sediment materials due to turbulent water jets to predict maximum scour depth in cohesive bed condition. Lambermont and Lebon (1978), Raudkivi and Tan (1984), Rajaratnam and mazurek (2005), Hanson (1991, 1992), Hanson and Robinson (1993) studied erodibility of various forms of cohesive materials consisting of clay-sand mixtures. Abt and Ruff (1982) carried out studies for determination of culvert scour in cohesive sediments. Mazurek et al. (2003) Mazurek and Hossain (2007) also study scour by jet in cohesive soil (consisting of clay-sand) and cohesionless soils under submerged circular vertical impinging jets flow conditions.

In the present study, it is intended to investigate the effect of presence of cohesive material such as clay on the process of scour due to submerged circular vertical jets in cohesive sediments such as clay with gravel and with sand-gravel mixture.

1.5 PROBLEM STATEMENT

The process of scour due to jets in cohesionless sediment has been investigated at length in the literature. However, such study has not been studied adequately in the cohesive soil which comes in the river system through surface erosion of upland areas along with cohesionless soil such as silt, sand and gravel. So, it is intended to study the effect of presence of cohesion i.e., clay in jet scour process by using clay-gravel and clay-sand-gravel sediment mixtures; as such types of sediment occurs frequently in nature (Kothyari and Jain, 2008 and Jain and Kothyari, 2009). The present study is being taken up keeping in mind the above gaps in the knowledge.

The specific objectives of the present investigation are as follows:

1. To study the process of scour under submerged circular vertical jets in cohesionless sediment consisting of sand, sand-gravel mixture and gravel.
2. To study the process of scour under submerged circular vertical jets in cohesive sediment consisting of clay-gravel and clay-sand-gravel sediment mixtures.
3. To identify parameters influencing the scour process in cohesionless and cohesive sediment.
4. To study the temporal variation of scour due to submerged circular vertical impinging jets in cohesionless and cohesive sediment mixtures.
5. To develop relationships for the computation of temporal variation of scour depth, maximum static and dynamic scour depths, height of dune, radius and volume of scour hole in cohesionless and cohesive sediment mixtures.

1.6 LIMITATIONS

In the present investigation, sand, gravel and sand-gravel mixture was used to estimate depth of scour in cohesionless sediment. In case of cohesive materials, the mixture of clay-gravel and clay-sand-gravel were prepared by mixing clay in varying percentage of 10 to 60 % by weight. For the study of scour in cohesive and cohesionless sediment under submerged circular vertical jet, nozzles of constant diameter of 8 and 12.5 mm were used. These nozzles had exit velocities 6.65 and 9.84 m/s in case of 8 mm nozzle diameter and 5.12 and 7.19 m/s in case of 12.5 mm nozzle diameter. Experiments were performed under jet heights of 0.15 and 0.30 m from the initial bed level. The present study is limited to scour due to submerged circular vertical water jets in sand-gravel, clay-gravel and clay-sand-gravel sediment mixture. The study is limited to one type of clay, however in the field; clay having different characteristics may be anticipated. All the cohesive sediment bed is prepared near to optimum moisture content. The proposed relationships in the present investigation are valid for clay percent (P_c) varying from 0 to 60%, ratio of sediment size to height of jet varying from 0.00727 to 0.0162, ratio of size of jet to height of jet varying from 0.0267 to 0.0834 and Froude Number (Fr) varying from 2.984 to 8.11.

1.7 ORGANIZATION OF THE THESIS

The present thesis is organized into the six chapters. Chapter-1 gives the basic introduction of the scour process due to jets in cohesive and cohesionless sediments, problems and objectives of the present investigations. Chapter-2 provides a brief literature review on the characteristics and behavior of sediment on scour process under submerged water jets. It also includes a brief discussion of many factors that affects the scour process of the cohesive and cohesionless sediments and how these are related to clay particle behavior. This chapter also provides a discussion on various scour process of cohesionless and cohesive sediments by many investigators. Chapter-3 gives the laboratory based experimental setup details and procedure. In the Chapter-4, analysis of the data and the discussion of results, development of dimensionless parameters for estimation of depth of scour, temporal variation of scour depth, radius of scour hole, dune height and volume of scour hole were carried out in case of cohesionless sediment and their mixtures. Chapter-5 presents the analysis of the data, discussion of results and aforesaid scour parameters in case of cohesive sediment mixtures. Chapter-6 summarizes the major conclusions from the present study and identifies some of the future research needs.

CHAPTER 2

REVIEW OF LITRATURE

2.1 INTRODUCTION

This chapter presents a critical review of the investigations on scour due to submerged water jets. A vast amount of literature exists on the topic of scour under submerged water jets in cohesionless and cohesive sediment, however, less attention have been focused on the mixture of sediment i.e., sand-gravel, clay-gravel and clay-sand-gravel mixtures. Various aspects of scour process, role of different parameters on equilibrium scour depth, dimensional analysis, variation of scour depth with respect to time, scour hole profiles and equations for scour depth estimation are discussed herein. Scour processes have been studied from time to time by many scientists and researchers. They have mainly focused on scour in the cohesionless sediments. However the main objectives of the present laboratory research work is to study the scour due to submerged circular vertical water jets in cohesionless and cohesive sediment mixtures. Therefore, review of literatures related to scour in the cohesionless and cohesive sediments is presented in details in this chapter.

Scour near hydraulic structures is an important problem and has been studied by many investigators in order to identify the variables that govern these phenomena. Scour due to jets is controlled by many factors; firstly, a jet can be two-dimensional or three-dimensional. Secondly, the angle at which the jet impinges on the sediment bed strongly affects the scouring process. Thirdly, the composition of the bed also controls the process of scour. Beds consisted of cohesive sediment exhibit different scouring characteristics in comparison to the cohesive sediment bed.

The sediments which have no cohesion mean that the clay is not present in the material i.e. cohesionless sediment. The dynamic scour depth in the cohesionless sediment is much greater compared to the static scour depth. However, the difference between these becomes small in case of cohesive sediment. A large number of laboratory experiments have been carried out over past five decades on this topic. They are mostly focused on the development of relationships for estimation of equilibrium or maximum scour depth under different jets flow conditions for cohesionless sediment. Only, few studies have been conducted on the estimation of maximum scour depth or equilibrium scour depth due to submerged jets impinging on cohesive sediment bed.

2.2 SEDIMENT CHARACTERISTICS

2.2.1Some Aspects of Cohesive and Cohesionless sediment

Cohesive sediments are composed mainly of clay material in which the clay particles have strong inter-particles forces due to their surface ionic attraction between each other. As the clay sediment size reduces, its surface area per unit volume increases and their inter particle forces dominate the behavior of the sediment. There is no clear boundary in between the cohesionless and cohesive materials in this respect. In general, the finer size of the sediment particles is more cohesive in nature. The sediment size smaller than two microns is normally termed as cohesive sediment. If the sediment size is greater than 0.06 mm then the sediment normally behave as cohesionless sediment (Ansari et al. 2003). The cohesive sediment consists of organic minerals and inorganic mineral (Hayter, 1983). The organic minerals may exist as plant and animal detritus and bacteria. The inorganic minerals mainly consist of Illite, Kaolinite and Montmorillonite.

2.2.2 Clay Mineralogy

Clay minerals that induce cohesion in sediment are mostly silicates of aluminum or iron and magnesium. These are very small in size approximately less than two microns. These are electrochemically active particles and can be seen only by using an electron microscope. With these minerals, there are two fundamental building blocks for crystalline clay mineral structure. One is silica units which has four oxygen atoms that form the tips of a tetrahedron and enclose a silicon atom as shown in Fig. 2.1(a), producing a unit approximately 4.6 A^o high (Angstrom unit A^o equals to 10^{-10} m). The other unit is one in which an aluminum (*Al*) or magnesium (*Mg*) and sometimes Iron (*Fe*), Nickel (*Ni*), Chromium (*Cr*) or Lithium (*Li*) atom is enclosed by six hydroxyls having the configuration of an octahedron which is about 5.05 A^o high as shown in Fig. 2.1 (b) (Bowles, 1984). Tetrahedra are combined in a sheet structure in such a manner that oxygen in the base of tetrahedra is in a common plane and each oxygen belongs to two tetrahedra. The octahedral units combine into a sheet structure (Grim, 1962). Some of the most common clay minerals are Illite, Kaolinite and Montmorillonite (Ansari, 1999)

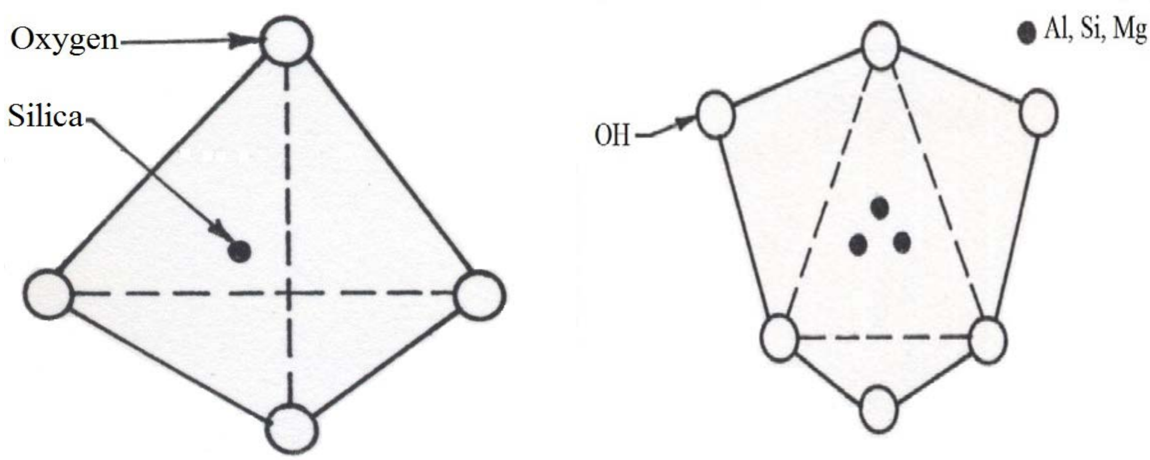

(a) Silica Tetrahedral Unit (b) Octahedral Unit

Fig. 2.1 Fundamental building blocks of clay minerals

2.2.3 Forces Among the Clay Particles

Different types of forces act among clay particles which are responsible for difference in behavior between cohesionless material i.e., sand, gravel, and sand-gravel mixture and cohesive material which invariably contains clay materials. These forces are as follows;

(i) Attractive Van der Waals forces

(ii) Electric surface forces

(iii) Other bonding mechanisms

(i) Attractive Van der Waals forces

Van der Waals forces have inter molecular force of attraction among the clay particles. These are the secondary valence forces, which are electro-chemical in nature and are independent with the quality of water. Van der Waals forces also define the chemical character of many organic compounds. They are generated by the mutual influence of the motion of electrons atoms and always attractive in nature with each other (Ansari, 1999). For two atoms, the Van der Waals attractive force is inversely proportional to the seventh power of the distance, where as for two spherical particles; the same force is inversely proportional to the third power of the distance between the surfaces as suggested by Bowles (1984).

(ii) Electric surface forces

In contrast to the Van der Waals forces, which are formed within the mass of the matter, there are a number of other forces like attractive and repulsive forces generated by electric charges on the surface of the particles. Isomorphous substitution and preferential ion adsorption on the particle surface are the causes of surface electric charges (Ansari, 1999). The existence of positive and negative electric charges on clay particles is important in relation to flocculation and, in general, to the mechanical behavior of clay deposits.

(iii) Other bonding mechanisms

The cohesive sediment is composed of smaller particles which have larger specific area. Because, the surface physico-chemical forces become more significant as compare to particle weight. In addition, the two forces discussed above, particles can be bonded together by the following bonding mechanisms (Bowles, 1984)

(a) Hydrogen bond

(b) Cation bond

(c) Chemical cementation among the particles by various compounds

(d) The double layer forces, and

(e) Particle interaction forces

It has also been known for a long time that all undisturbed clays lose part of their strength when disturbed or remolded. In fact, certain clays, even at a slight disturbance, lose so much of their strength that they essentially liquefy. Such clays are known as ‘quick’. Certain Norwegian clay deposits are examples of quick clay (Ansari, 1999).

2.2.4 Shear Strength of Cohesive Sediment

The sediment with particle size greater than 0.06 mm in diameter generally behaves as cohesionless sediment. However, when the sand, gravel and sand-gravel sediment is mixed with clay in various proportions, the resulting mixture exhibits some amount of cohesion. Cohesive materials are composed of small particles and of large specific area (i.e. area per unit volume of particle). The surface physico-chemical forces become more significant than the particle weight of the sediment. These physico-chemical forces are not yet fully understood at present and these are found to vary with water environment and time (Partheniades, 1971). For such materials, the shear strength τ_{sh} is given by the following equation;

$$\tau_{sh} = C_u + \sigma_n \tan\phi_c \tag{2.1}$$

Where C_u is cohesion, σ_n is normal stress and ϕ_c is the angle of repose. It is to be mentioned that the parameters of cohesion C_u and ϕ_c are strongly depend on the drainage conditions, rate of application of shear force, the type of shear test, pre-consolidation pressure and degree of saturation of the sediment (Ansari, 1999). The magnitude of C_u is also controlled by the inter particle forces which depend upon the percentage of clay contents, quality and quantity of the clay materials.

2.3 CIRCULAR JETS

The behavior of a plunging jet into a water cushion is similar to a submerged water jets. Several experiments have been presented for submerged circular water jets striking on the sediment beds or flat bed as shown in Fig. 2.2. These laboratory experiments have water cushion above the sediment bed. The maximum induced pressure is equivalent to the stagnation pressure of the jet. A region around the center of the jet will have pressures equal to the stagnation pressure, which can be defined by the following equation:

$$P_s = u_o^2 / 2g \tag{2.2}$$

Where P_s is the stagnation pressure, u_o is the jet velocity; g is the acceleration due to gravity. However, the velocities will decay more rapidly than the submerged jet and the excess pressures will decrease more rapidly (George, 1980).

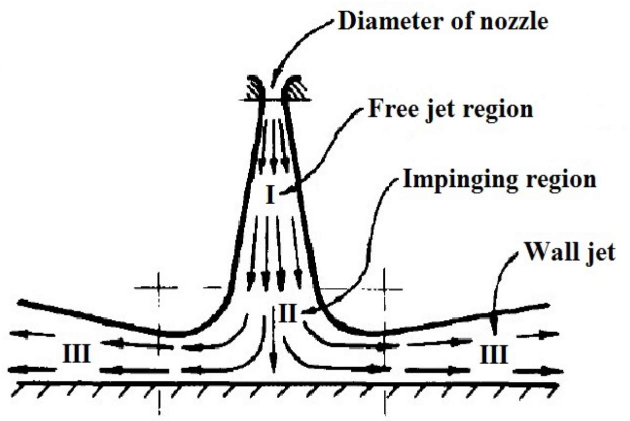

Fig. 2.2 Impingement of a jet on a flat plate (George, 1980)

2.4 LOCAL SCOUR DUE TO JETS

The local scour process in the presence of sand, gravel, and other materials, which are often occurs near the hydraulic structures, is of considerable importance, as excessive scouring process may damage the stability of the hydraulic structures such as gates, weirs, culverts, spillways and grade control structures etc. The local scour near the hydraulic structures due to submerged water jet poses an immense problem in designing the foundation and the stability of such types of structures. The local scour process near a hydraulic structure is complex in nature because of remarkable changes of the flow characteristics over the erodible bed. In the case of submerged vertical circular water jet, the main characteristics of flow regions are as follows (Ansari, 1999)

1. Potential core flow regions
2. Free jet flow regions
3. Impinging jet flow regions
4. Wall jet flow regions

The above flow regimes for impinging jet are shown in Fig. 2.3 and discussed below in details:

1. Potential core flow regions - A region where velocity over the jet area is almost uniform is called potential core region. This region is just below the nozzle exit and along the central portion of the jet. The jet diameter decreases rapidly downstream sides due to shear stress between the jet and the surrounding fluids.
2. Free jet flow regions – The free jet flow region follows the potential core transition and it is characterized by linear increase in width and a Gaussian

velocity distribution. The Free jet flow regions have a near field region where the potential core has not yet experienced turbulent mixing with the quiescent fluids.

3. Impinging jet flow regions – The impinging jet regions are the region just near the bed surface, an impinging occur in which the water flow is deflected from the axial into the radial motion during the water flow through impinging jets.
4. The wall jet region – The deflected water flow continues as wall jet in the regions containing two different shear zones - a boundary layer near the wall jet region and a free shear zone. The impinging of a circular vertical submerged water jets on loose bed i.e. cohesionless sediment beds leads to strong local scouring effects.

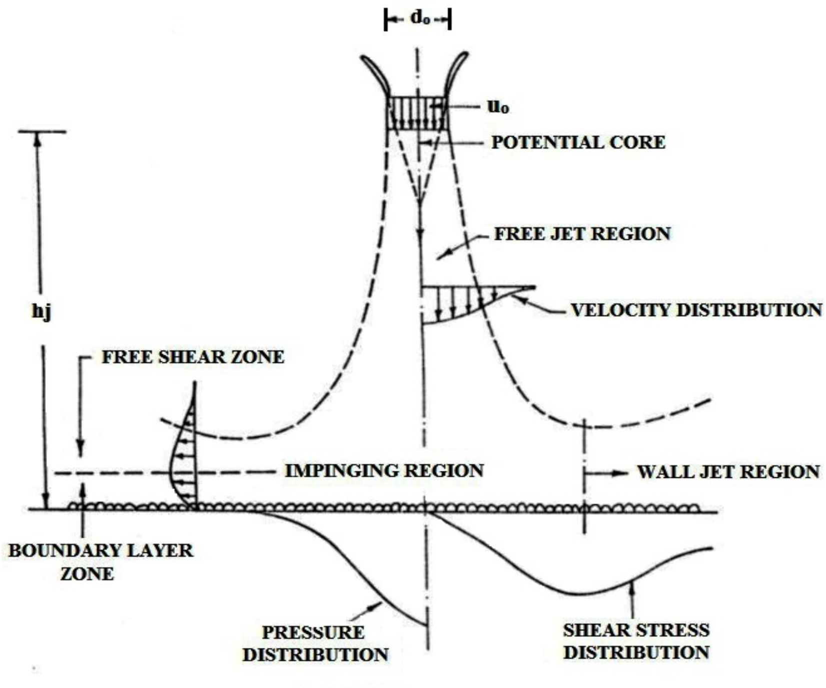

Fig. 2.3 Flow regimes of a vertical impinging jet (Ansari, 1999)

Probably, Rouse (1940) was first to conduct experimental study in the laboratory to study scour in uniform fine sand due to submerged vertical water jet. He found that the scour depth in non-cohesive sediment bed i.e. sand bed varies linearly with the logarithm of impinging time. He also observed that the jet impingement height from the initial bed level is the characteristic length of scoured sand bed profiles. He proposed a functional relationship between two non dimensional parameters like the ratio of depth of scour to jet impingement height, and the ratio of velocity of jet to the fall velocity of sand. Since, a number of investigation have been carried out to investigate the response of channel bed under impinging jet a review of some of the important research contributions are presented herein.

2.5 SCOUR BY JET IN COHESIONLESS SEDIMENT

Westrich and Kobus (1973) conducted experiment on a uniform sand bed having sediment size, (d_{50}) equal to 1.5 mm with a vertical submerged water jet by taking jet velocity in the range of 0.7 to 3.7 m/s and nozzle diameter ranging from 20 to 40 mm. The nozzle height was varied from 0 to 0.82 m from the channel bed level. They reported two types of scour holes depending upon the value of K_0 define as:

$$K_0 = (u_m / \omega_f)^2 \tag{2.3}$$

In which, K_0 is the erosion coefficient, u_m is the maximum velocity estimated at the sand bed surface and ω_f is the fall velocity of the sediment. Also, influence of the jet height on the volume of scour hole was studied. They found that for given jet parameters, the scour hole volume first increases with jet height and then remain constant before decreasing again.

Francis and Mccreath (1979) conducted laboratory study on bed load transport of sediment due to submerged jets. The laboratory work was conducted in Perspex-sided tank having dimension of 10 cm wide and 72 cm deep and 120 cm long. Every end of the working section was fixed to bigger tank in which the weirs were fixed to keep constant water level. Four sizes of sand were used for the preparation of sediment bed having, d_{50} of 1.08, 0.72, 3.41 and 0.88 mm. The laboratory study was performed under the sediment beds for three different heights of jet i.e., 50.8, 41.6, and 30 cm. The erosion process has analogy with transport of sediment rates in streams. They found that the transport rate of the sediment is a function of stream power as suggested by Laursen E.M (1958) and Bagnold, (1966).

Rajaratnam (1981) conducted laboratory based experimental work on erosion under plane turbulent wall jets. The experiments were performed in three series – in first series scour of non-cohesive materials by plane turbulent air jets was conducted by taking one nozzle having thickness, d_o = 2.41 mm. The nozzle jet velocity was measured by a pressure tap attached in the plenum chamber. The cohesionless sediment material i.e., sand were used having sediment size 1.2 mm and bed thickness 102 mm in a rectangular flume. The flume was 156 mm wide, 330 mm high and 183 mm long. He followed the experimental procedure given by i.e. Rajaratnam and Beltaos (1977) and Rajaratnam and Berry (1977).

In the second series, polystyrene particles under air jets were studied. Total seven equilibrium tests were conducted with air jets having thickness of nozzle 5 mm and the size of sand equal to 1.4 mm and the specific gravity of sand equal to 1.04. The laboratory experiments were conducted similar to the experiment performed for sand beds.

In third experimental series, total 14 equilibrium laboratory experiments were conducted on erosion of sand beds by submerged water jets in a rectangular test flume have dimension, 5.5 m long, 0.66 m deep and 0.31 m wide. The flume contained a cohesionless sediment bed having 0.23 m thickness and 0.38 m water depth in the flume was maintained to generate a deeply submerged flow in horizontal water by a tailgate. They found that the maximum depth of scour in the form of height of jet is a function of $F_o / \sqrt{h_j / 2b_o}$ where F_o is densimetric Froude number, h_j is jet impingement height and b_o is the thickness of the jets. The densimetric Froude number parameter was defined as;

$$F_o = \frac{u_o}{\sqrt{gd_{50} \frac{\Delta\rho_s}{\rho_f}}} \tag{2.4}$$

Where, $\frac{\Delta\rho_s}{\rho_f}$ is the relative density defined by $\left(\frac{\rho_s - \rho_f}{\rho_f} \right)$, ρ_s is mass density of bed materials, ρ_f is the mass density of water.

Rajaratnam (1982) carried out experiment on a round jet having nozzle diameter equal to 9.8 mm, impinging on two types of sand beds with sediment size d_{50} equals to 1.2 mm and 2.38 mm, respectively. He proposed the following functional relationship for maximum static scour depth;

$$\frac{d_{sms}}{h_j} = f\left(\frac{F_o}{h_j / d_o} \right) \tag{2.5}$$

Where, d_{sms} is the maximum static scour depth.

Mih and Kabir (1983) studied impinging of water jets on non-uniform sediment streambed through experimental work and theoretical analysis. The tests were conducted in a 1.2 m wide, 1.5 m deep and 9 m long flume with white sand (0.3 mm size) and gravel bed. Jet diameters were 0.5 and 25 mm while jet angles were 45°, 60° and 90°. The jet velocities were 6 m/s and 21 m/s and the heights of jet were varied from 0 to 53 cm from the original bed level. Figure 2.4 indicates the motion of sediment during the impingement of jet. In the initial stage of impingement, the jet penetrated the bed and set nearby bed materials in motion. After jet penetrated to its deepest range, it was deflected upward around its center line to form vertical circulation carrying bed materials. From the center line of the vertical jet, the circulation slowly spreads outward the scour hole of radius. In the downward flow of the jet core, the smaller sediment particles had a high velocity than larger sediment particles because the drag force per unit mass on the smaller particles is larger.

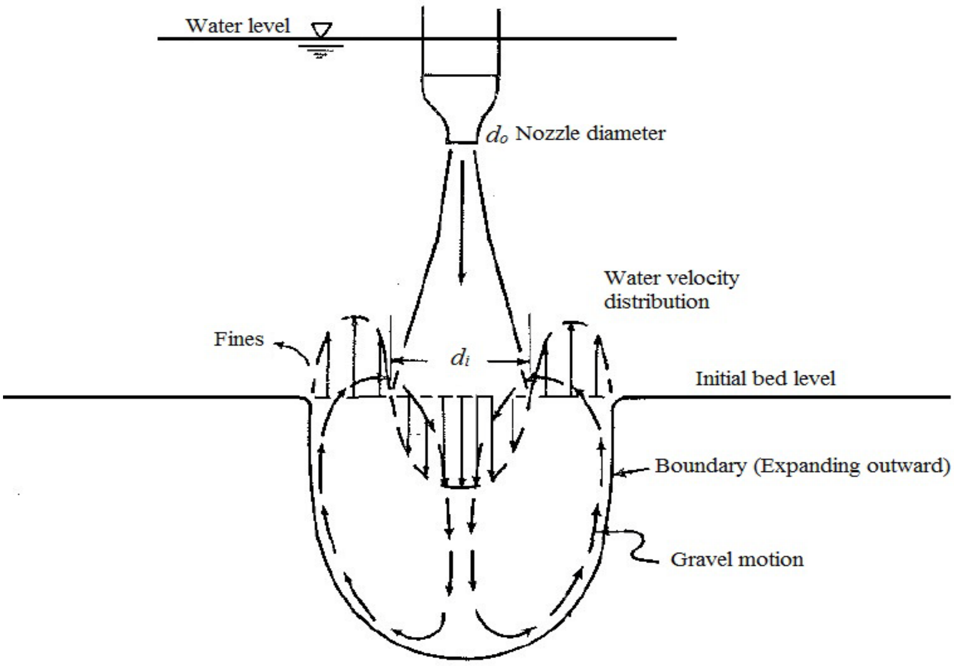

Fig. 2.4 Sediment motion during impingement of jet (Mih and Kabir, 1983)

When the stationary sediment bed was raised, the stagnation pressure on the stationary boundary increased. Finally, about four minute of jetting, a steady state condition was reached. Only the bigger sediment particles remained in the minimum circulative motion near the impingement point by virtue of which the dissipation of energy prevented deep penetration of jet known as armor action. Fig. 2.5 shows the change of depth of sediment motion during impingement of jet.

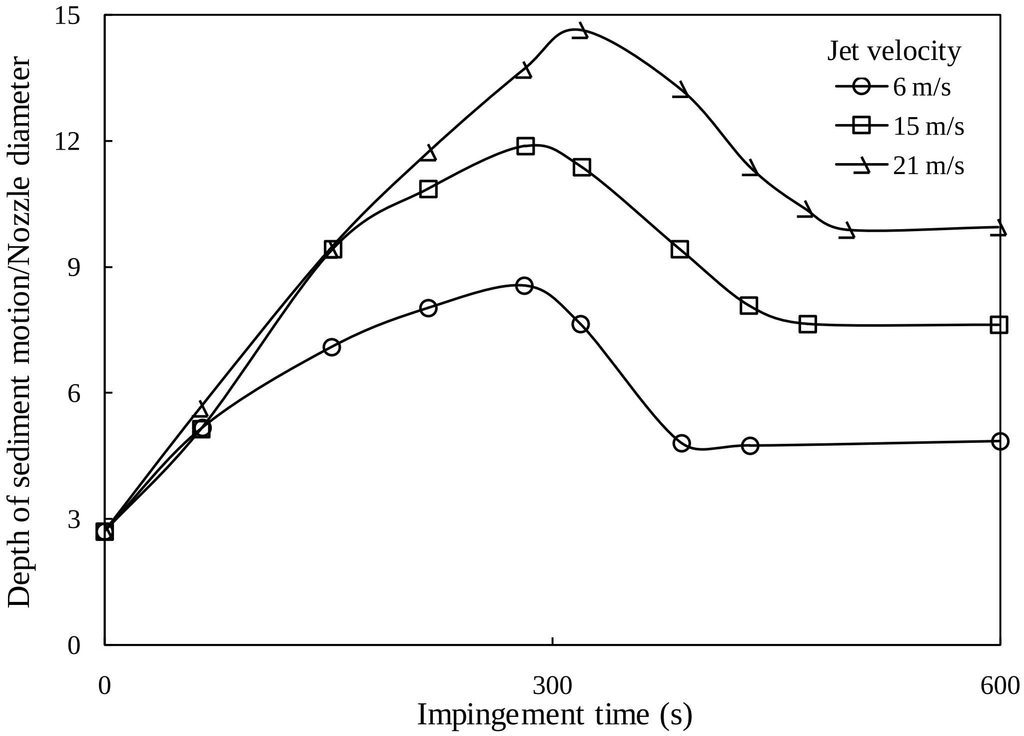

Fig. 2.5 Depth of sediment motion during impingement of jet (Mih and Kabir, 1983)

Uyumaz (1988) studied on scour in cohesionless sediment downstream of vertical gate through laboratory experiment. He performed experiment in a flume of 0.60 m wide, 11.5 m long and 0.85 m deep with a concrete bottom. The vertical gate height was about 0.30 m and the loose gate was placed at the end of the flume. The extent of scour approached asymptotically and after some time the scour reaches in equilibrium condition. It was found that final scour depth was less when there is simultaneous water discharge over and under the gate.

Breusers and Raudkivi (1991) fitted the following equation to the data of Rajaratnam (1982) for the estimation of maximum static scour depth:

$$\frac{d_{sms}}{d_0} = 0.3 \frac{u_0}{\sqrt{\Delta \rho_s g d_{50}}} \tag{2.5}$$

Breusers and Raudkivi (1991) re-plotted the original data of Westrich and Kobus (1973), Clarke (1962), and Rajaratuam (1982) in respect of maximum scour depth and proposed the following equations:

$$\frac{d_{sms}}{d_o} = 0.75 \left(\frac{u_o}{u_{*cs}} \right); \text{ for } \left(\frac{u_o}{u_{*cs}} \right) < 100 \tag{2.7}$$

$$\frac{d_{sms}}{d_o} = 0.035\left(\frac{u_o}{u_{*cs}}\right); \text{ for } \left(\frac{u_o}{u_{*cs}}\right)^{2/3} > 100 \tag{2.8}$$

Where u_{*cs} = Critical shear velocity of the cohesionless sediments.

Aderibigbe and Rajaratam (1996) conducted laboratory experiments on an octagonal plastic box having 0.6 m height and 0.235 m side length. The impinging jet was centrally located and always submerged and fixed to the bottom of a 150 mm diameter. The impinging jet height (h_j) was varied 4-523 mm. The diameter of jet were taken as 4, 8, 12 and 19 mm, particles size of cohesionless materials were taken as 0.88 and 2.42 mm and jet velocities were varied from 2.65 to 4.45 m/s. Total 67 experimental runs were conducted for the duration of 6 to 50 hours to reach in the equilibrium state. They examined the asymptotic scoured depths of sand bed for erosion parameter, $E_C < 5$ under above condition and also examined the scoured bed profiles in equilibrium conditions. The erosion parameter was defined as below:

$$E_c = u_o\left(\frac{d_o}{h_j}\right) / \sqrt{(g d_{50} \Delta\rho_s / \rho_f)} \text{ ; When } \frac{d_o}{h_j} > 8.3 \tag{2.9}$$

They analyzed the following parameters:

1. Effects of impinging jet distance

They analyzed the previous studies in respect of effect of impinging jet distance on maximum scour depth. Westrich and Kobus (1973) observed two peaks in the variation of the equilibrium scour volume with impinging jet distance. Doddiah et al. (1953) conducted the experiment using hollow and solid circular jets found that there exists a critical impinging jet distance at which an increase or decrease in impinging distance cause a decrease in maximum static depth of scour when other variables remain constant. The variations of static and dynamic depth of scour with jet height were studied for two sets of experiment and found that there exists a critical impinging jet distance at which static depth of scour is high.

2. Similarity of scoured bed profiles

The equilibrium scour profiles for similarity in the maximum static scour depth versus radial distance were analyzed. The value of erosion parameter ranges in between 0.14-3.52. The ratio of radius of scour to maximum static depth of scour with erosion parameter is about 1.7 for erosion parameter greater than 0.35 and for erosion parameter smaller than this value, it rapidly increases with decreasing erosion parameter. They concluded that the side slope of the scour profile was very sensitive to erosion parameter when the latter was less than 0.35.

3. Flow regimes characteristics

They classified the regimes of flow as weekly deflected jet regimes (WDJR) and strongly deflected jet regimes (SDJR) in equilibrium condition. These two regimes of flow are associated by narrow transition regimes. The strongly deflected jet regime is divided as SDJR-I and SDJR-II according to the value of erosion parameter E_c. The SDJR flow regimes found at value of erosion parameter E_c greater than 0.35. WDJR is divided into WDJR-I and the WDJR-II. In these flow regimes, the flow occurs at the range of erosion parameter $E_c < 0.35$ and the dynamic and static scour profiles were same. They suggested the following flow patterns and profiles of the eroded sand bed as shown in Fig. 2.6 a-d.

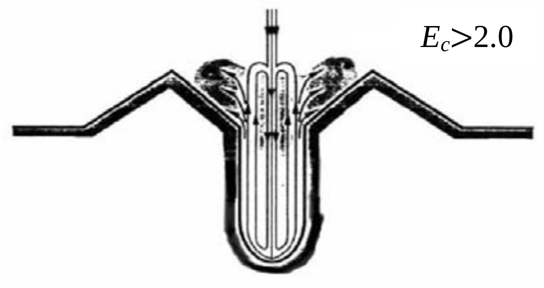

(a) Strongly deflected jet regime I

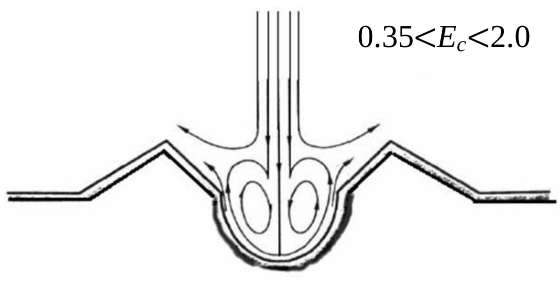

(b) Strongly deflected jet regime II

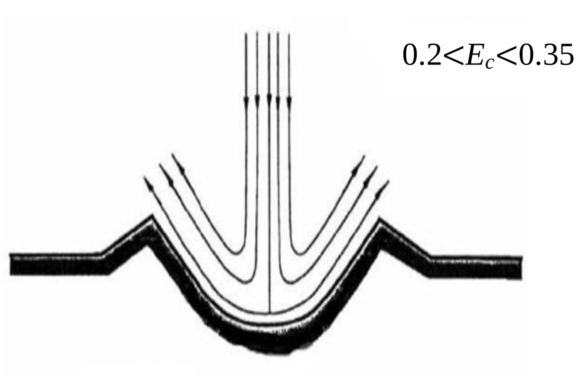

(c) Weakly deflected jet regime I

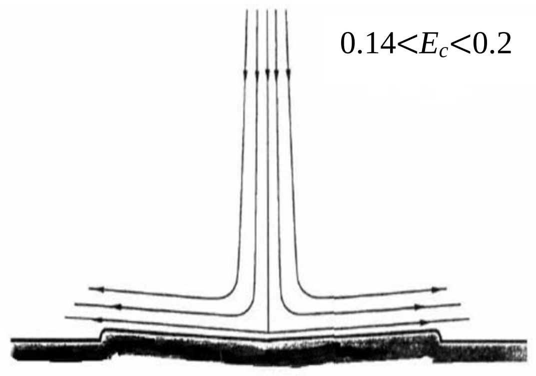

(d) Weakly deflected jet regime II

Fig. 2.6 Flow regimes of eroded sand beds (Aderibigbe and Rajaratnam, 1996)

4. Equilibrium depth of scour

They developed an equation for maximum static scour depth using data from previous studies:

$$\frac{d_{sms}}{h_j} = 1.26E_c^{0.11} - 1 \tag{2.11}$$

Eq. (2.11) is valid only for the ratio of impinging jet height to jet diameter greater than 8.3 as noticed by Rajaratnam and Beltaos (1977). They analyzed the data for other length scale parameters of scour bed profile and proposed the following equations to calculate maximum dynamic depth of scour, radius of scour hole and dune height:

$$\frac{d_{dms}}{h_j} = 7.32E_c\left(\frac{d_o}{h_j}\right)^m - 1 \quad \text{where} \quad m = 1.53E_c^{0.22} - 1 \tag{2.12}$$

$$\frac{r}{h_j} = 0.22 + 0.2E_c \ \text{ for } 0.5 < E_c < 5 \tag{2.13}$$

$$\frac{\Delta}{h_j} = C + 0.044E_c \tag{2.14}$$

Where d_{dms} is the maximum dynamic depth of scour, m is the exponent, r is the radius of scour hole, and Δ is the dune height and C is a coefficient. The value of C is equal to 0.077 and -0.02 for upper and lower limit, respectively. The variation of dune height and radius of scour hole with erosion parameter are shown in Figs. 2.7 and 2.8, respectively.

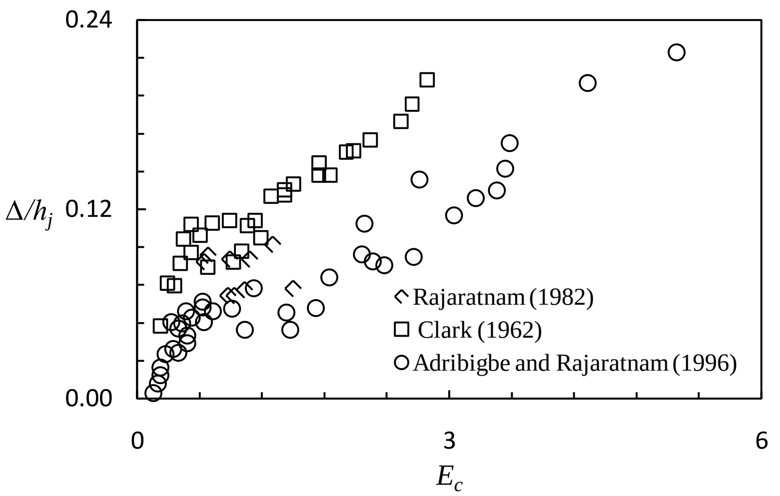

Fig. 2.7 Variation of dune height with erosion parameter (Adribigbe and Rajaratnam, 1996)

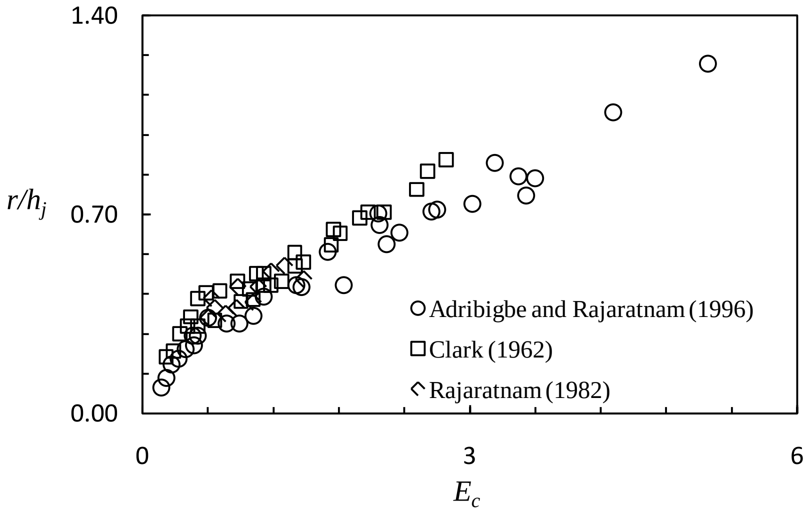

Fig. 2.8 Variation of radius of scour hole with E_c (Adribigbe and Rajaratnam, 1996)

Adribigbe and Rajaratnam (1998) carried out experimental investigation on the effect of sediment gradation on erosion by plane turbulent wall jets. Three different types of cohesionless sediment were used for the study. The cohesionless sediment have d_{50} = 6.75, 1.62, and 1.32 mm, while the geometric standard deviations (GSD), σ_g = 2.02, 3.13, and 1.32. The Reduction in scour profiles in presence of sediment gradation on the bed was studied in terms of densimetric Froude number. They concluded that the non-uniform sediment has a significant effect on the size of the scour profiles generated by submerged wall jet. Fig. 2.9 shows the variation of equilibrium dynamic maximum depth of scour with F_o. The variation of relative scour hole length with F_o is shown in Fig. 2.10.They observed that the scour hole length was significantly shorter for the graded material.

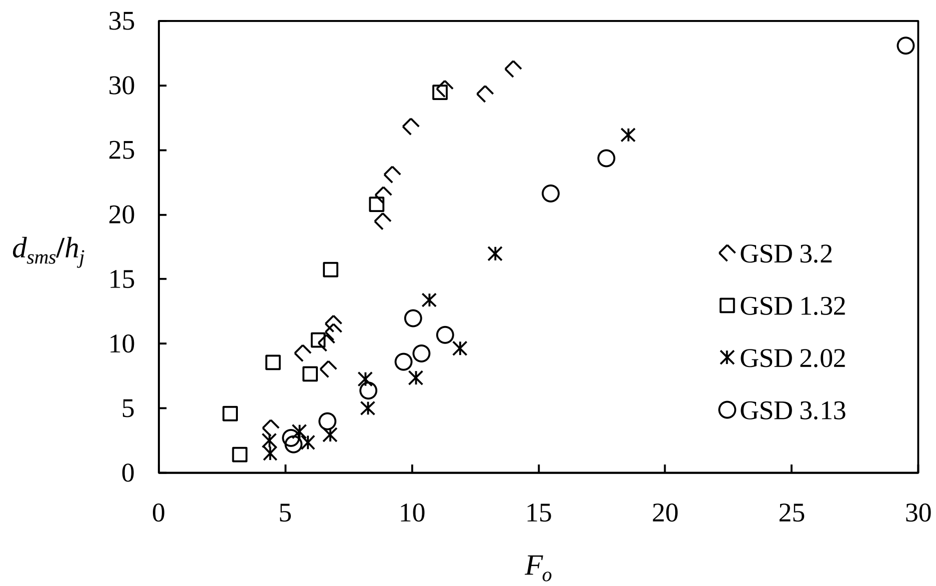

Fig. 2.9 Variation of maximum scour depth with F_o (Adribigbe and Rajaratnam, 1998)

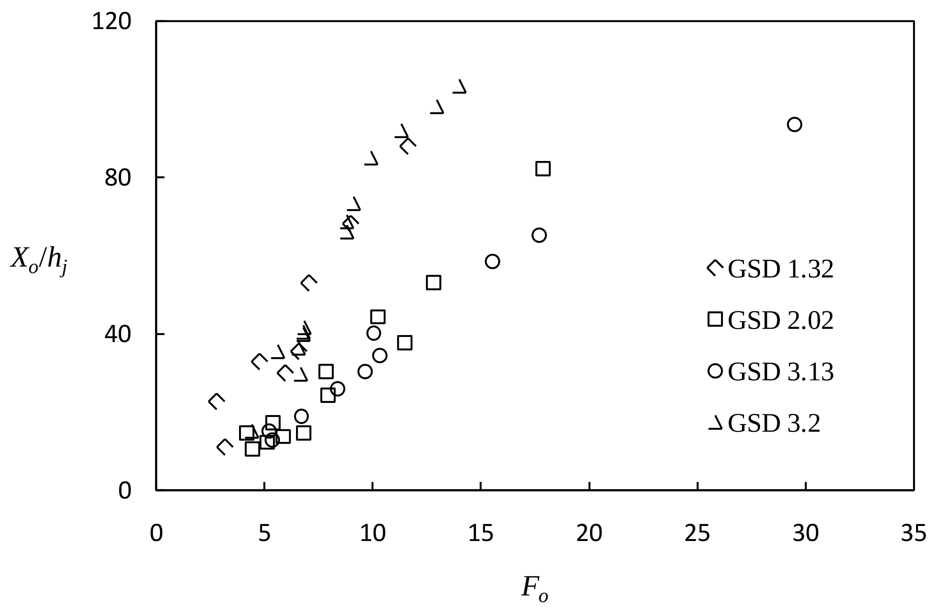

Fig. 2.10 Variation of scour hole length with F_o (Adribigbe and Rajaratnam, 1998)

The sediment size for better correlation for the scour depth was found as d_{95} compared to d_{50}.

Donoghue et al. (2001) conducted experiment in cohesionless sediment to study the response of sand beds under submerged circular vertical water jet. The experimental data was generated using larger diameter of jet having dimensions of 1.5 m wide, 3 m long and 1.7 m high. The steel tank was filled with cohesionless sediment from the bottom up a height of 0.7 m and the depth of water was filled up to 0.85 m.

Total 66 laboratory experiments were conducted having two different types of cohesionless sediment having sediment size, d_{50} equal to 0.3 and 0.13 mm. They took four sizes of nozzle having diameter of 13, 30, 40 and 50 mm and the velocity of jet was kept equal to 5.9 m/s. Two jet heights were taken by making the ratio of height of jet to the nozzle diameter ranging between 5 to 13. The erosion parameter was ranging as $1.7 \leq E_c \leq 14.9$ to indicate that all the laboratory work was well for strongly deflected jet regimes as suggested by Adribigbe and Rajaratnam (1996). Previous laboratory work indicates a dependence of scour hole on erosion parameter or densimetric Froude number, however, this study indicate a strong dependence on the ratio of diameter of jet to size of sediment as well. They proposed empirical equations for the estimation of dynamic scour depth and scour hole diameter. These equations were applied for highly scouring jets with the ratio of jet momentum flux to the submerged weight of sediment up to 10^9.

Mazurek et al. (2002) studied the experimental investigation on jet scour under turbulent sand jet in water. They conducted ten experimental runs in a tank having dimension of 1.25 m long, 1.25 m wide, and 1.17 m deep. A flexi glass tank having diameter of 100 mm and 330 mm long added with cone type hopper at the bottom and filled with non-cohesive sediment was used. Four sizes of cohesionless sediment ranging from 0.17 to 1.47 mm and their standard deviation ranging from 1.18 to 1.25 were used. Since, the standard deviation was less than 1.35; therefore it was considered as uniform sediment as suggested by Breusers and Raudkivi (1991). Three types of nozzles having jet diameter 8, 12.7 and 25.4 mm was added at the bottom of hopper. The Reynolds number R of the sand jets varied from 40 to 300. It was investigated that the linear growth rate of scour under sand jets increases with the densimetric Froude number parameter. The growth rate of the scour under sand jet was 0.19 which was about 20% higher than that of turbulent water jets with Reynolds number larger than 10,000.

Rajaratnam and Mazurek (2003) conducted laboratory based experimental study on scour in non-cohesive sediment under turbulent water jets having minimum tail water depth. Total 18 experimental run were conducted for submerged and un-submerged impinging turbulent water jets in an octagonal tank having 0.61 m height and 0.572 m width, using three different types of cohesionless sediment having sizes equal to 1.0, 1.15 and 2.38 mm. Two types of nozzle having nozzle diameter of 9.8 mm and 12.7 mm were used in the experiment. The observation were taken for maximum static and dynamic depth of scour, scour hole radius. They observed that the depth of scour in dynamic condition is three times of scour depth in static state at equilibrium conditions. From the experimental investigation the scour of cohesionless sediment by un-submerged water jets, they concluded that there are two different types of scour i.e., dynamic and static scour.

They found that the maximum depth of scour linearly increases with logarithm of time for a major part of the scour and reaches at equilibrium conditions. Fig. 2.11 shows the variation of maximum static depth of scour with respect to time. The equilibrium value of scour depth and the scour radius are the functions of densimetric Froude number. The depth of scour in dynamic conditions was observed to be about three times of the static scour at equilibrium state. They also concluded that the maximum scour produced by an un-submerged water jet is less than that for a submerged jet in case when:

$$F_o /(h_j / d_o) < 2.1 \tag{2.15}$$

The radius of scour hole for the un-submerged jet is less than that produced by a submerged jet

$$\text{Where } F_o /(h_j / d_o) < 1 \tag{2.16}$$

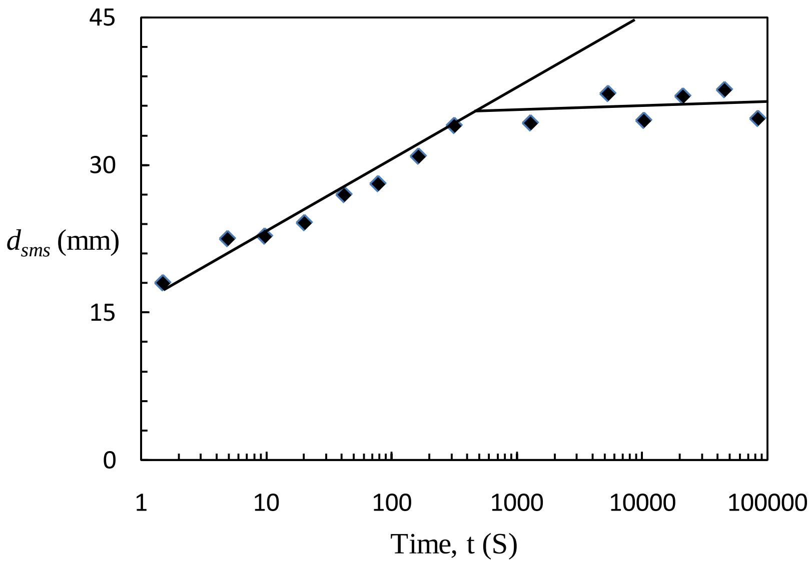

Fig. 2.11 Growth of maximum depth of scour with time (Rajaratnam and Mazurek, 2003)

Adduce and Mele (2004) conducted laboratory based experimental study for erosion by turbulent jets to investigate erosion process downstream of a sill followed by a rigid apron in clear water conditions. Total nine experiments were conducted in tilting flume which has rectangular cross section of 0.8 m wide, 1 m high and 17 m long. The experimental run were conducted in a 0.8 m wide, 0.3 m high, 3 meter length sediment working section fixed at 7 m downstream of the inlet flume and was created raising artificially the flume sediment bed. The uniform sand of size equal to 0.72 mm having density of 2650 kg/m^3 were taken to fill the working section to it mobile bed. The same sediment was also used upstream and downstream of the test section to make sediment bed with homogeneous roughness.

All the experimental runs were conducted for clear water condition and the water discharge were regulated constant for total time required for the experiment. Scour hole profile was recorded by using a camera connected to a digital videocassette recorder. The temporal variation of scour depth was taken using image analysis techniques. The dimensionless scour hole profiles showed geometrical similarity for all experimental runs if the maximum depth of scour shall be taken as length scale of the vertical gate and horizontal distances.

Rajaratnam and Mazurek (2005) conducted study on a circular air jet impinging on smooth walls having jet nozzle diameter of 6.4 and 12.7 mm and impinging on wall having roughness 15.18, 8.23 and 1.73 mm in a cylindrical plenum, with air regulated by a compressed air arrangement. The nozzle velocity varies 45-90 m/s. Reynolds number $R_e = (u_0 d_o)/\nu)$ was in the range of 79000-26000, height of jet were varied from 310 to 152 mm. The ratio of h_j/d_o was 12–26. The stagnation pressure (p_s) and the maximum shear stress (τ_{om}) can be estimated by the following equations

$$p_s = C \; \frac{\rho_s u_o^2 / 2}{\left(h_j / d_o\right)} \qquad (2.17)$$

$$\tau_{om} = 0.16 \frac{\rho_s u_o^2}{\left(h_j / d_o\right)} \qquad (2.18)$$

Where, C is a dimensionless coefficient that was found to be 50, 48 and 60.4 by Beltaos and Rajaratnam (1974), Hrycak et al. (1970), Poreh and Cermack (1959) respectively.

Yeh et al. (2009) presents the experiments on sand beds scour due to moving vertical circular jet to investigate the topographic deformation. Seven experimental run were conducted in which the first two runs have stationary jets. Remaining five experiments were conducted by moving jet by varying carriage speeds. The size of the laboratory tank was 3.66 m wide, 45.72 m long and 3.05 m deep. The horizontal plate and the jet exit were located at 0.76 m above the sand bed. Sand has d_{50} equal to 0.258 mm and the geometric standard deviation (σ_g) equal to 1.71. The sand bed topography was measured by the use of laser profiler to estimate the changes on the sand bed. Figure 2.12 shows the variation in maximum normalized scour depth versus jet to ship velocity ratio with E_c = 5.28.

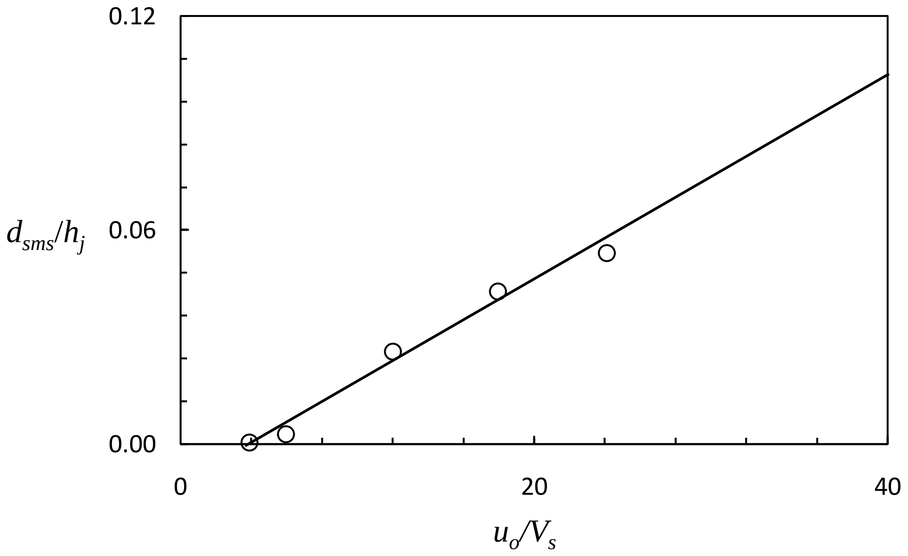

Fig. 2.12 Normalized maximum scour depth versus jet velocity with E_c = 5.28 (Yeh et al. 2009)

The modified Adribigbe and Rajaratnam (1996) prediction equations for estimation of equilibrium depth of scour (d_{sms}), radius of scour hole (r), and height of dune (Δ) are as follows;

$$\frac{d_{sms}}{h_j} = 0.64E_c^{0.11} - 1 \tag{2.19}$$

$$\frac{r}{h_j} = 0.78(1.46E_c^{0.15} - 1) \text{ For } E_c \le 0.5 \tag{2.20}$$

$$\frac{r}{h_j} = 0.78(0.22 + 0.20E_c) \text{ For } 0.5 < E_c < 5 \tag{2.21}$$

$$\frac{\Delta}{h_j} = 0.52(-0.02 + 0.044E_c) \tag{2.22}$$

These modified equations can be used to evaluate the length of scour profile when h_j/d_o is about 6. The formulae were proposed to know the length scales, radius of scour hole and the dune height. The jet velocity in horizontal direction was varied to know the effect on the scour hole profile geometry. The depth of scour hole in equilibrium condition was estimated with the modification of formulae proposed by Aderibigbe and Rajaratnam (1996).

Mazurek et al. (2009) presented the laboratory study on submergence effects of jet behavior and scour of plane wall jets in cohesionless material. The laboratory works show two different studies on how submergence or tail water depth affects the scour process under plane wall jets in cohesionless material. In case of first experiment, the effects of submergence on the flow regime, development of temporal scour, and the profile of scour holes at equilibrium condition were determined. In case of second experiment, the characteristics of flow jet in scour holes created by varying submergence condition were studied. The tail water was ranging from 25–508 mm for first set of experiment which provided a range of submergence equal to 1 to 20. The velocity of jet at nozzle was varying from 0.26 to1.13 m/s. The Froude numbers at the nozzle was 0.52 to 2.27 and Reynolds numbers at the nozzle varied 6600 to 28570. The cohesionless sediment as sand was taken having sediment size of 2.08 mm and geometric standard deviation 1.33.

Second stages of experiments were conducted to know the flow in a scour profile at equilibrium condition. Three different types of flow regimes of jet behavior were seen by varying submergence condition. Such profiles were similar to those described by Johnston (1990), i.e., a bed jet regime, a surface jet regime and a bed surface jet regime. Scour holes created for a jet in the surface jet regime were longer and shallower than those created by the bed jet. It is also seen that the bed jet regime shows a similar behavior to a wall jet on a smooth bed, while the surface jet regime shows a jet behavior similar to a free jump.

Dehghani et al. (2010) conducted experimental investigation on local scour under the jet flow downstream of rectangular sharp crested weirs. The laboratory experiments were performed in a laboratory flume having dimensions of 0.12m width, 3.7m long and 0.17m depth with bed slope of 0.0001. The sediment bed material was composed of cohesionless uniform sediment having a diameter of 1.5 mm and a geometric standard deviation equal to 1.3. Both the side walls in the working section of the flume were made of glass. Total

23 experimental runs were performed by taking different discharges and the height of weirs. The cohesionless sediment i.e., sand was placed on the channel bed in 8 cm thickness. The experiments were performed using clear water condition and were continued until equilibrium condition was reached. All the measurements were taken to observe the scour hole profiles by using a simple point gauge. Figure 2.13 shows the variation of maximum depth of scour with respect to time. They found that the maximum depth of scour reaches in equilibrium condition almost in 60 minutes from the start of the experiment.

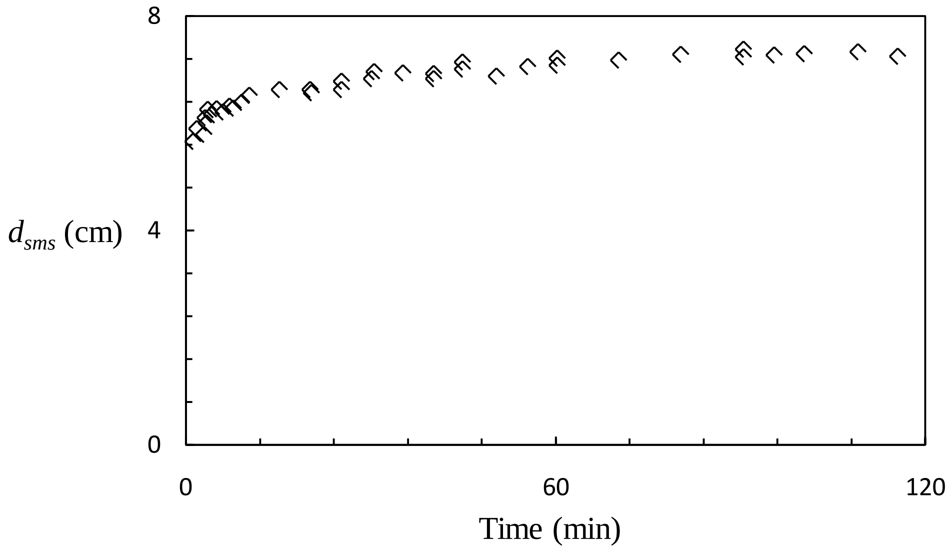

Fig. 2.13 Variation of depth of scour versus time (Dehghani et al. 2010)

It was observed that the extent of scour profiles mainly depends on the flow characteristics, sediment bed material composition and geometry of the structure. It was found that increase in the height of weir increases maximum scour depth for a specific Froude number. They also found that the scouring process has an oscillatory manner to reach in equilibrium state.

2.6 SCOUR BY JETS IN COHESIVE SEDIMENT

All the studies related to scour due to submerged vertical jets in cohesive sediments are laboratory based and they have been concerned with determination of their scour resistance of cohesive sediment in natural and remolded conditions.

Dunn (1959) used a submerged water jet to determine the tractive resistance of cohesive sediments. In his experiment, the surface of a cohesive soil sample was subjected to the erosive action of a water jet. The head of water on a nozzle placed vertically above the sample was increased until an initial erosion of the sample took place. It was observed that initial scour occurred at a short distance away from the center line of the jet. The location of this initial scour was unaffected by changes in either the head on the nozzle or in the elevation of the nozzle above the sediment. The magnitude of the tractive force causing scour was measured by replacing the soil sample by a steel plate coated with clay sediment and having a shear plate at the position of the initial scour. The critical shear stress was then related to the shear strength of the soil as determined from a vane test, the mean grain size, and the plastic limit.

Smerdon and Beasley (1959) applied the tractive force theory for the stability of open channels in cohesive soils. They conducted the laboratory based experimental study on sediment material which was placed on bottom of flume. Water was allowed to flow through the flume and over the sample until bed failure was observed. The sediment bed was considered to have failed when the tractive force was large enough to cause movement of the sediment. For the sediment tested, the critical tractive force was correlated to soil properties viz; plasticity index, dispersion ratio, mean particle size, and percentage of clay.

Moore and Masch (1962) performed laboratory study on submerged vertical impinging jet to estimate relative scour resistance of remolded and natural sediments. In these tests, the rate of scour was taken by measuring the loss of sample weight. The set-up was designed to take direct observation of a uniform shear stress. They mainly studied the time variation of depth of scour. The laboratory experiments were conducted in two different types of sediment by mixing the montmorillonite clay, Taylor marl, and medium sand. The cohesive sediment mixtures were prepared for laboratory experiment by taking 60 percent clay and 40 percent sand. For one type of specimen, the sediment was added to the desired consistency and placed in layers by hand in a three inch diameter mold. The scour rate index was defined using the slope of the curves. The variation in scour rate index, K_s with Reynolds number, R_e is shown in Fig. 2.14 for different types of sediment samples. Three unsymmetrical scour hole profiles were obtained in cohesive sediments as shown in Fig. 2.15. The view of various shapes of scour profiles is shown in Fig. 2.16. It indicates that for the value of h_j/d_o less than 7, the scour was deep and localized. At the higher h_j/d_o values, the scour profile was wider and shallower covering a more portion of the sediment sample.

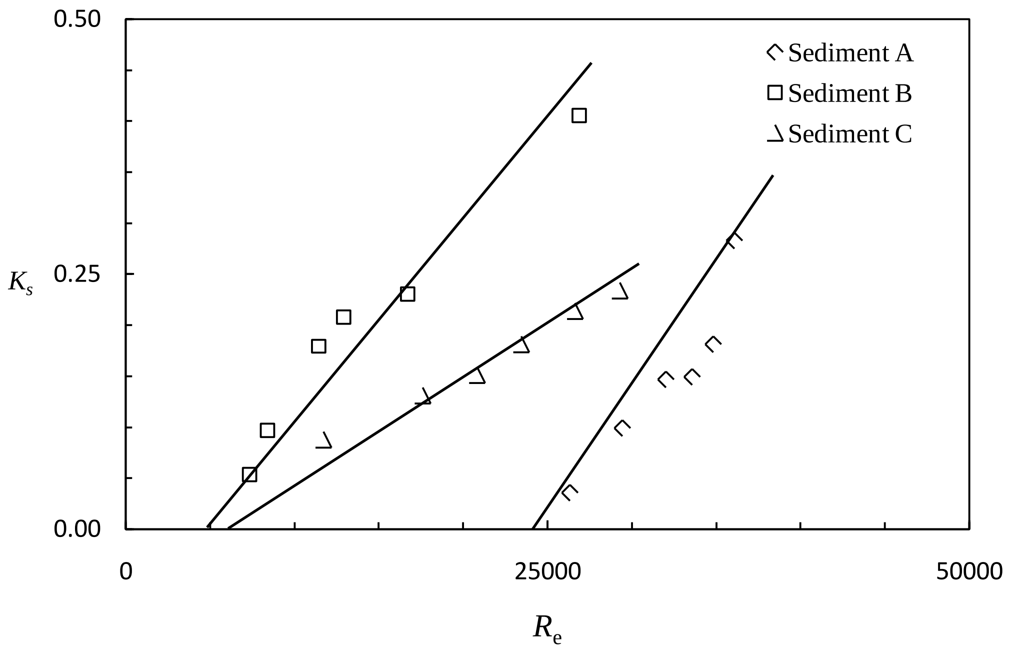

Fig. 2.14 Scour rate index versus Reynolds number for different sediment (Moore and Masch, 1962)

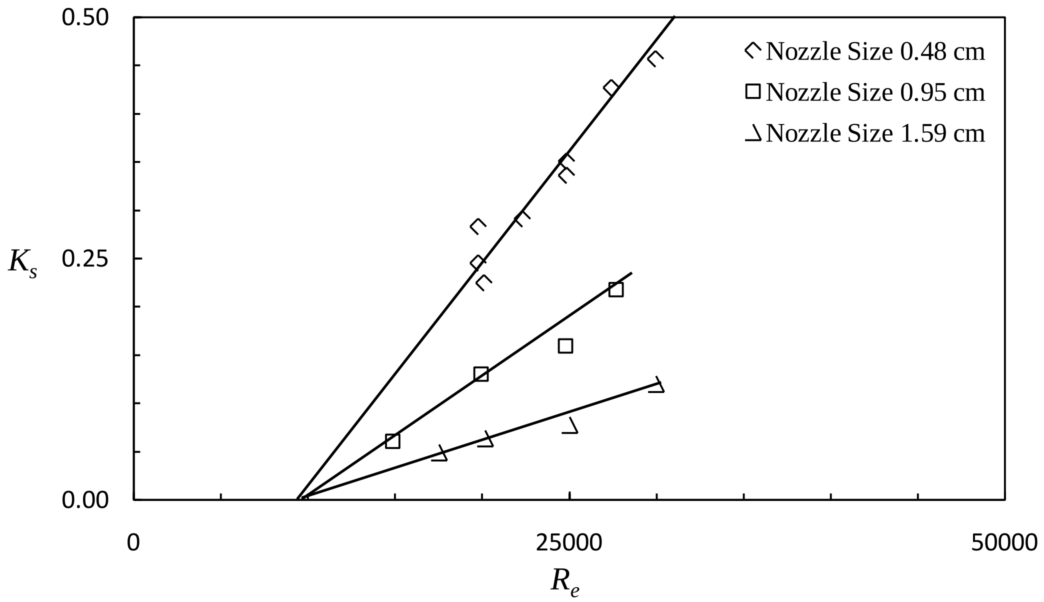

Fig. 2.15 Scour rate index versus Reynolds number for different jet diameters (Moore and Masch, 1962)

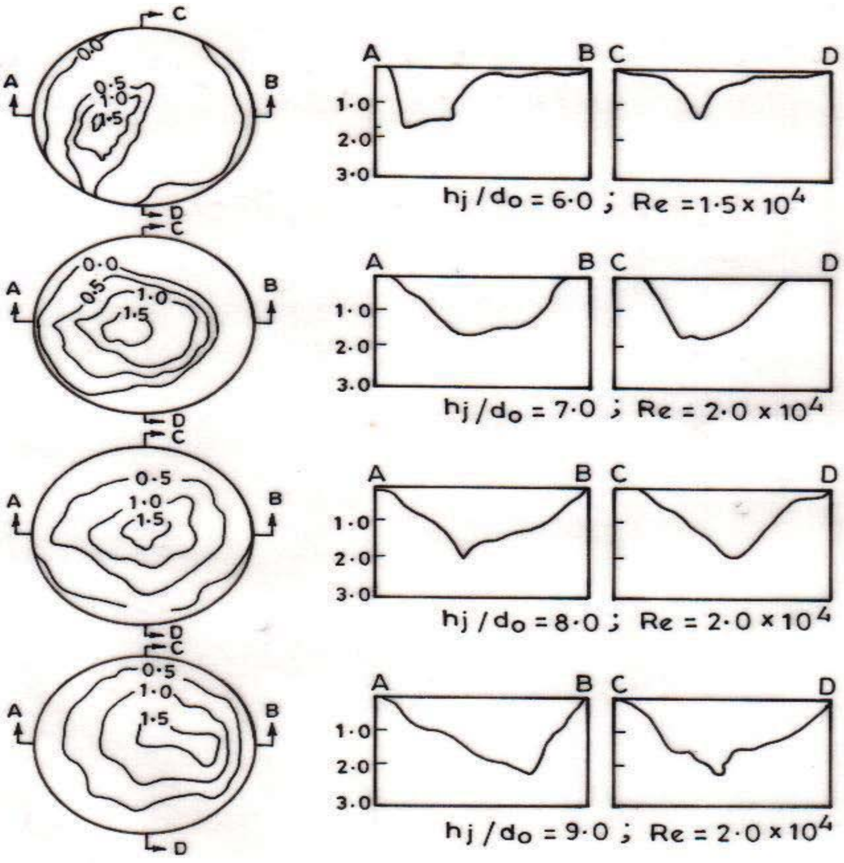

Fig. 2.16 View of various shapes of scour profiles (Moore and Masch, 1962)

Lambermont and Lebon (1978) studied erosion of cohesive sediment under a turbulent water flow to find out sediment density distribution of bed in initial time. The boundary conditions in between the water flow interface were observed through laboratory experiment. It was noticed that the physical chemical composition at the top of the sediment bed was related to the bed shear stress at the time of scouring process. The solution of stationary scour flux under a constant shear stress was estimated and found that it depends upon the properties of the sediment beds and the shear stress induced by turbulent flow.

Abt and ruff (1982) performed laboratory experiment to evaluate culvert scour in cohesive sediment. Total 12 experiments were conducted in a flume of dimension 30.5 m length, 6.1 m width and 2.4 m depth. Four experiments were conducted using circular culverts having outside diameter 10.65, 14 and 18 inches. The cohesive sediment was derived from residual, Colorado expansive clay mixed with graded sand comprising a tan - green, sandy clay classified as sandy clay (SC) soil type in accordance with the Unified

Soil Classification System. Three culvert having 0.273 m, 0.356 m, and 0.457 m diameter were used with discharge varying from 0.54 to 8.24 mm. The tail water elevation was maintained in between (0.45 $\pm$0.05) m above the culvert. Cohesive sediment was consisted of 58% sand, 27% clay and 1% organic matter and has a liquid limit is equal to 34, plastic limit 19 and plasticity index 15.

They formulate a series of equations to calculate the scour hole dimensions at any finite time less than or equal to 1000 minute. The maximum values of scour depth (d_{sms}), scour width (W_{sms}), length of scour hole (L_{sms}) and volume of scour (∇) were found to vary with culvert diameter, culvert outlet velocity (u_0), critical shear stress which is expressed as;

$$CD = V_1\left(\frac{\rho_f u_o^2}{\tau_c}\right)^{V_2} \tag{2.23}$$

CD is the desired scour hole characteristics dimension which can be expressed as $\frac{d_{sms}}{d_o}, \frac{W_{sms}}{d_o}, \frac{L_{sms}}{d_o}\ and\ \frac{\nabla}{d_o^3}$; where V_1 is the regression coefficient and V_2 is the slope of the linearized plots. The temporal variation of scour hole characteristics was expressed as;

$$CD = V_1\left(\frac{\rho_f u_o^2}{\tau_c}\right)^{V_2}\left(\frac{t}{T_s}\right)^{V_3} \tag{2.24}$$

Where, V_3 is the regression coefficient, t is the instantaneous time, T_s is the total time required in equilibrium condition.

Hanson (1991) proposed a jet scour index (J_i) to characterize scour characteristics of cohesive sediment channel bed. The jet scour index was formulated as;

$$J_i = \frac{d_{sms}/t}{u_o(t/t_1)^{-0.931}} \tag{2.25}$$

Where, t_1 is the characteristics time. A vertical submerged round jet of nozzle diameter of 13 mm was used at a jet height of 0.22 m. The experiments were performed over a range of jet velocities from 1.66 m/s to 7.31 m/s. Four types of cohesive sediments namely A, B, *C* and *D* was selected for the study. Their characteristics are summarized as shown in Table 2.1

Table 2.1 Physical properties of the sediment used by Hanson (1991)

Physical Properties	Sediment A	Sediment B	Sediment C	Sediment D
Liquid limit	21	37	26	-
Plastic Limit	14	19	20	NP
Plasticity Index	17	18	6	0
U.S.C.	4	CL	48	SM
A.S.C.	CL-ML	Clay-loam	loam	Sandy-loam
U.S.C.	Unified Soil Classification			
A.S.C.	American Soil Classification			

Hanson (1991) also defined the erodibility coefficient, K_e for cohesive sediment in terms of the excess shear stress as formulated below

$$K_e = \frac{K_s}{(\tau - \tau_c)} \tag{2.26}$$

Where K_s is the erosion rate in volume per unit area per unit time. The relationship between the jet scour index J_i, and the erodibility coefficient K_e was expressed as:

$$K_e = 0.003e^{385J_i} \tag{2.27}$$

The results of the laboratory testing were used to quantify the changes in J_i due to changes in bulk density and moisture content. Increases in compaction moisture content were observed to result in increased resistance to scour.

Hanson (1992) studied the effect of bulk density and moisture content on the jet index defined by Eq. (2.32). The results of the laboratory test were performed to quantify the changes in J_i due to changes in bulk density and moisture content. Increases in bulk moisture content were observed to result in increased resistance to scour. Increase in density at constant moisture content was also observed to result in increased resistance to scour.

Hanson and Robinson (1993) conducted submerged jet scour experiments in cohesive bed compacted by dynamic and static load methods over a range of dry unit weights and moisture contents to determine the influence of density and moisture content on scour process. The sediments selected for this test exhibited a liquid limit of 23%, a plastic limit of 12% to 16% and a plasticity index of 7% to 12%. The soil was CL or CL-ML as classified by the Unified Soil Classification System. The sediment material consisted of 34% sand, 39% silt, and 27% clay. Scour characteristics were represented by jet scour index parameter that decreased as the moisture content increased for a constant dry unit weight before the saturation stage while it increased for saturated and above saturated stages of the samples as shown in Fig. 2.17. The jet scour index also decreases with dry unit weight for constant moisture content as shown in Fig. 2.18.

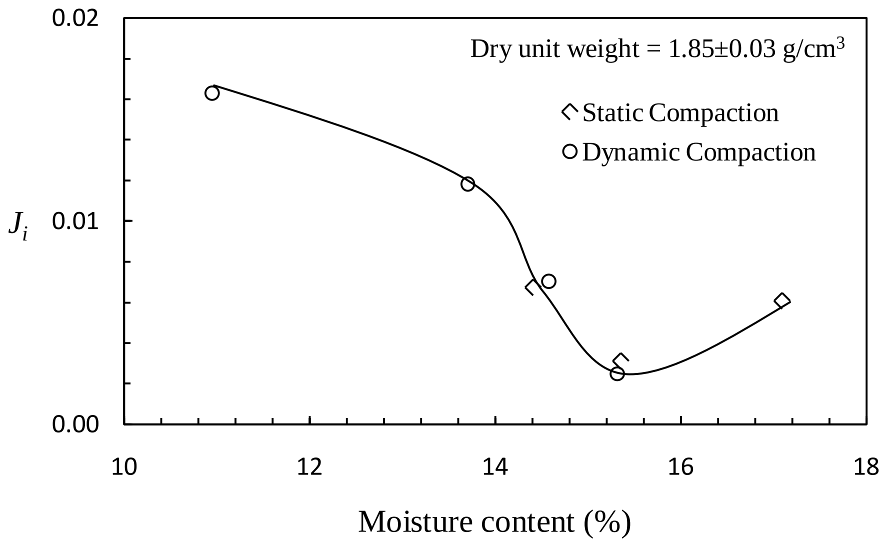

Fig. 2.17 Variation of J_i with moisture contents (Hanson and Robinson, 1993)

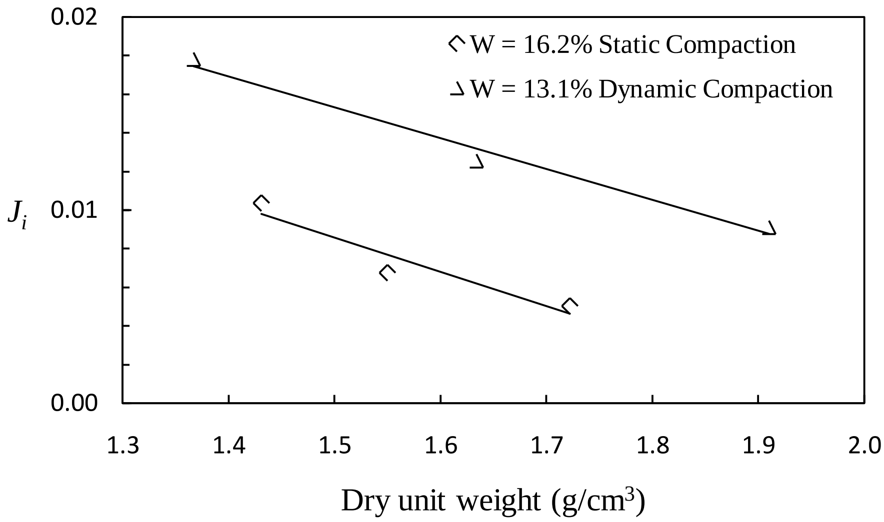

Fig. 2.18 Variation of J_i with dry unit weight (Hanson and Robinson, 1993)

Hanson (1993) studied the effect of consolidation on jet scour index in saturated and unsaturated conditions using a large consolidometer. The sediments were consolidated over a range of 19 to 306 kPa. Three sediments A, B and C having characteristics as per Table 2.2 were tested using a submerged jet. Temporal variation of jet scour as obtained under different consolidation stresses is shown in Fig. 2.19.

Table 2.2 Summary of properties sediment used by Hanson (1993)

Physical Properties	Sediment A	Sediment B	Sediment C
Liquid limit	23	37	26
Plastic Limit	14	19	20
Plasticity Index	9	18	6
% Sand > 0.05 mm	34	37	48
% Silt > 0.002 mm	39	36	33
% Clay <0.002 mm	27	27	19
U.S.C.	CL	CL	CL-ML
A.S.C.	Clay Loam	Clay Loam	Loam

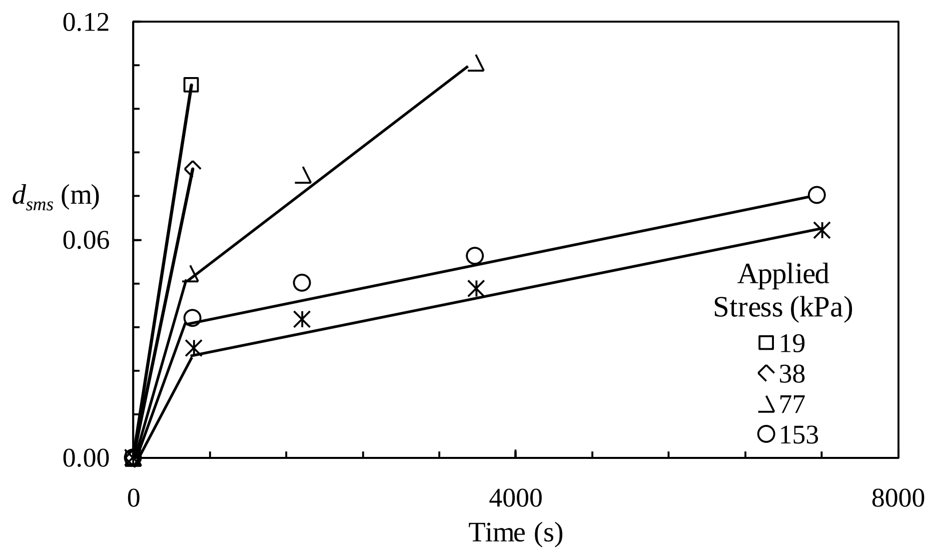

Fig. 2.19 Temporal variation of scour depth for sediment A at different applied stress (Hanson, 1993)

Stein et al. (1993) performed the laboratory works on mechanics of scour due to jets downstream of a headcut. An impinging water jets, similar to that which may also occur downstream below a natural headcut, was created by a free overfall at the end of 100 cm long Plexiglas plate set within a 10.4 cm wide by 200 cm long and 33 cm Plexiglas flume. The flume was set at 3.7 percent slope for all the experiments.

Three different types of sediment i.e., coarse sand having sediment size, d_{50} equals to 1.5 mm, fine sand, d_{50} equals to 0.15 mm and cohesive soils, d_{50} equals to 0.045 mm were used for preparation of sediment beds. Eight experimental run were conducted in coarse sand, 6 run in fine sand and 10 run in cohesive sediment. They used the concept of jet diffusion in the scour hole and the critical shear stress for sediment detachment. They analytically derived the following equation for equilibrium scour depth downstream of a two-dimensional nappe. The depth of tail water was small as compared the scour depth.

$$d_{sms} = \frac{C_d^2 C_f \rho_f u_o^2 b_o}{\tau_c} \sin\varphi \tag{2.28}$$

Where C_d = diffusion coefficient and C_f = friction coefficient, b_o = thickness of jet and φ is the jet angle at tailwater impingement and τ_c is the critical shear stress for cohesive or cohesionless material. The value of C_f is given by:

$$C_f = 0.0275(q/v)^{-0.25} \tag{2.29}$$

Where q is the discharge intensity and v is the kinematic viscosity of fluid.

The validity of the Eq. (2.8) was tested using experimental data collected by conducting 8 runs on coarse sand with mean diameter of 1.5 mm, 6 runs on a fine sand and 10 runs on cohesive sediments. The computed depth of scour in equilibrium state was compared with observed scour depth as given in Fig. 2.20 that shows all the computed maximum scour depth were within 20% of the observed scour depth. They also studied the temporal variation of scour depth both for cohesive and non-cohesive sediment and proposed the following equation:

$$\frac{\partial d_{sms}}{\partial t} = K_c(\tau - \tau_c)^m \tag{2.30}$$

Where, the values of constant K_c were much smaller for cohesive materials than for cohesionless materials. While the exponent m for cohesionless material was 1.5 and it is unity for the cohesive material and τ is the average shear stress on the bed.

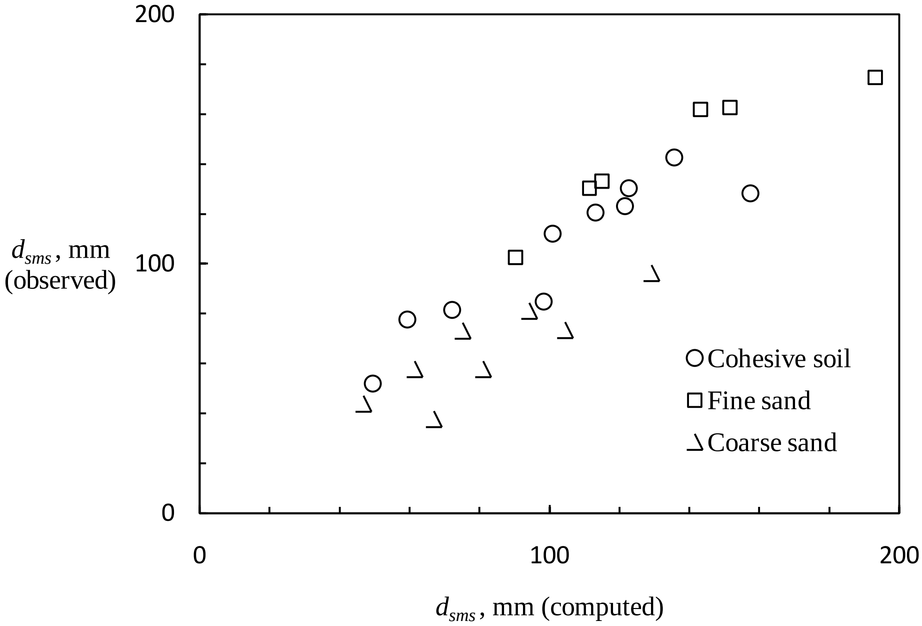

Fig. 2.20 Predicted versus measured equilibrium scour depth (Stain et al. 1993)

Mazurek et al. (2001) the laboratory experiments were performed in scour due to submerged circular jets in cohesive sediment. The experiments were conducted in an octagonal tank having dimensions of 572 mm width and 610 mm height and filled with water so that the jet and the sample were under submerged condition. In a cylindrical plenum, having dimensions of 830 mm long, 120 mm diameter, a pumping tab water jet was created and the nozzle was fixed at 90 degree above the sediment bed. Two types of nozzle i.e. 4 and 8 mm in diameter and two different jet velocities of 4.97 and 25.9 m/s were used. The cohesive sediment sample of size 244 mm long, 175 mm wide and 85 mm high was fixed on a platform on octagonal tank. The cohesive sediment was consisting of 53% silt, 40% clay and 7% fine sediment and had vane shear strength of around 20 kPa. The sediments had liquid limit = 36%, plastic limit = 18%. The dry density of cohesive sediment was 1540 kg/m^3.

They correlated maximum depth of scour, volume of scour hole and the centre line depth of scour with parameter $(X - X_c)/X_c$, where X is the cohesive sediment erosion parameter for impinging jets and expressed as $\rho u_o^2 (d_o / h_j)^2$ and X_c are the critical value of X below which the mass erosion is not observed. Assuming a smooth variation of the geometrical properties of the scour holes with $(X - X_c)/X_c$ as plotted in Fig. 2.21, the change in scour hole regime form weakly deflected (WD) to strongly deflected (SD) occurs at about $(X - X_c)/X_c \cong 1.55$. The variation in maximum depth of scour is also shown in Fig. 2.22. The results show that the scour hole dimensions were well correlated with $(X - X_c)/X_c$ which can be given by the following equation;

$$\frac{\sqrt[3]{\nabla}}{h_j} = 0.37 \left\{ \frac{X - X_c}{X_c} \right\}^{0.51} \tag{2.31}$$

$$\frac{d_{sms}}{h_j} = 0.19 \left\{ \frac{X - X_c}{X_c} \right\}^{0.74} \tag{2.32}$$

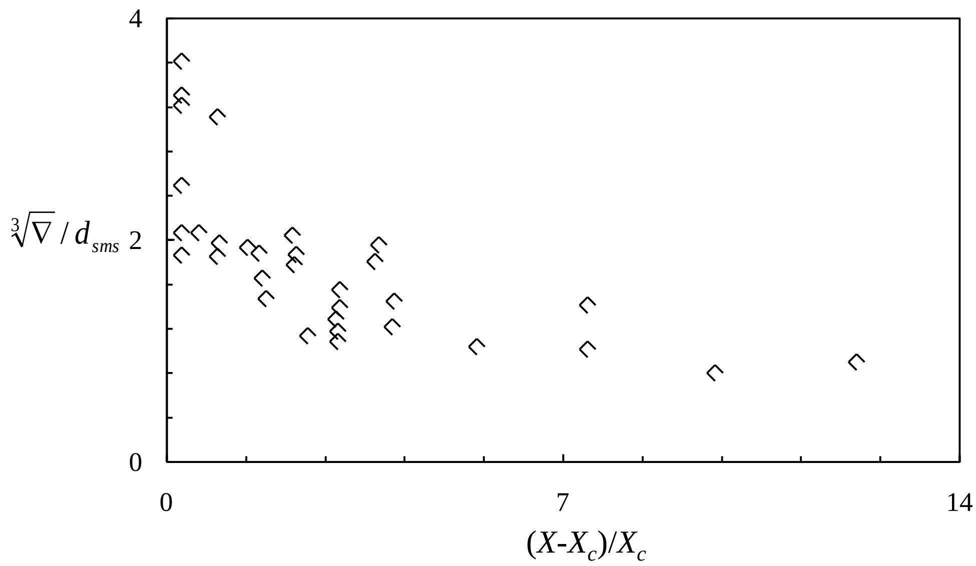

Fig. 2.21 Ratio of volume of scour hole to the maximum depth of scour (Mazurek el al. 2001)

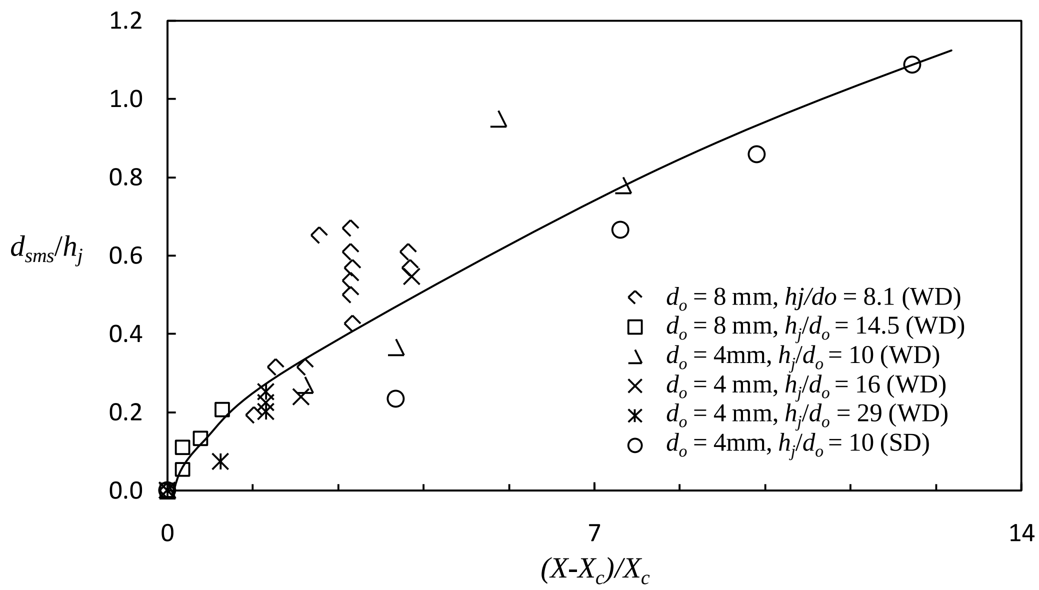

Fig. 2.22 Dimensionless maximum depth of scour at equilibrium (Mazurek el al. 2001)

They found that the scour hole profile increases linearly with the logarithmic time, except at the times close to start of the experiment.

Ansari et al. (2003) conducted laboratory experiment on scour in both cohesive and cohesionless sediment material due to submerged circular vertical jets. They also studied the difference of scour hole profiles in cohesive and cohesionless sediment. Total 15 experiments were performed in cohesionless sediment and 74 experiments were performed in cohesive sediment. The experiments were conducted in a steel tank having

1.25 m diameter of tank and 1.25 m depth. The sediment was filled in the tank at the desired height of 0.60 m. Discharge was measured with the help of venturimeter fitted in the inlet pipe. In the case of cohesive sediment, nozzle diameter was equal to 12.5 mm, jet velocities were 1.7 and 2 m/s, jet heights were 0.15 and 0.20 m. While in case of cohesionless sediment, nozzle diameters were 8 and 12.5 mm, jet heights were 0.15 and 0.30 m and jet velocities were1.3 and 5.75 m/s.

The cohesionless sediment has sediment size of 0.27 mm and geometrical standard deviation 1.48. The specific gravity of the cohesionless sediment was 2.65. The cohesive sediment has sediment size of 0.0053 mm and geometrical standard deviation was 2.1. They also compiled the previous experimental data under submerged vertical jets in cohesive and cohesionless sediment. They found that more than 70% of the scour observed in first 30 minutes from the start of the test run in case of cohesionless sediment. Tables 2.3 and 2.4 show the characteristics of cohesive sediments and range of data on scour under submerged vertical jet in cohesionless sediment used by Ansari et al. (2003), respectively.

Table 2.3 Characteristics of cohesive sediments used by Ansari et al. (2003)

Clay Content (%)	Liquid limit	Plastic limit	Plasticity index
10	-	-	Non Plastic
20	-	-	Non Plastic
30	18	14	4
40	22	15	7
50	25	16	9
60	31	18	13

Table 2.4 Range of data on scour under submerged vertical jet in cohesionless sediment used by Ansari et al. (2003)

Investigators	Median size, d_{50} (mm)	Jet diameter, d_0 (mm)	Jet velocity, u_o (m/s)	Jet height, h_j (m)
Sarma (1967)	0.53 - 0.75	8.26-16.5	0.66-2.83	0.24
Westrich and Kobus (1973)	1.5	20 - 40	0.7 - 3.7	0 - 0.82
Rajaratnam (1982)	1.2 - 2.38	9.8	2.99 - 4.6	0.14 - 0.28
Aderibigbe and Rajaratnam (1996)	0.88 - 2.42	4 - 12	2.65 - 4.45	0.004 - 0.523

Ansari et al. (2003)	0.27	8 - 12.5	1.3 - 5.75	0.15 - 0.30

They expressed the temporal variation of maximum scour depth under submerged vertical circular jets in cohesive and cohesionless sediment as

$$\frac{d_{ss}}{d_{sms}} = \left[\sin\left(\frac{\pi t}{2T_s}\right)\right]^{m_s} \tag{2.33}$$

Where, d_{ss} is the instantaneous scour depth below the bed level. The relationship proposed by Adribigbe and Rajaratnam (1996) between maximum scour depths with E_c is shown in Fig. 2.23 and can be expressed as;

$$\frac{d_{sms}}{h_j} = 0.26(E_c)^{0.11} - 1 \tag{2.34}$$

Ansari et al. (2003) modified the Eq. (2.34) to describe better relationship between the two parameters as plotted in Fig. 2.23 and expressed as;

$$\frac{d_{sms}}{h_j} = 0.3(E_c)^{0.15} - 1 \tag{2.35}$$

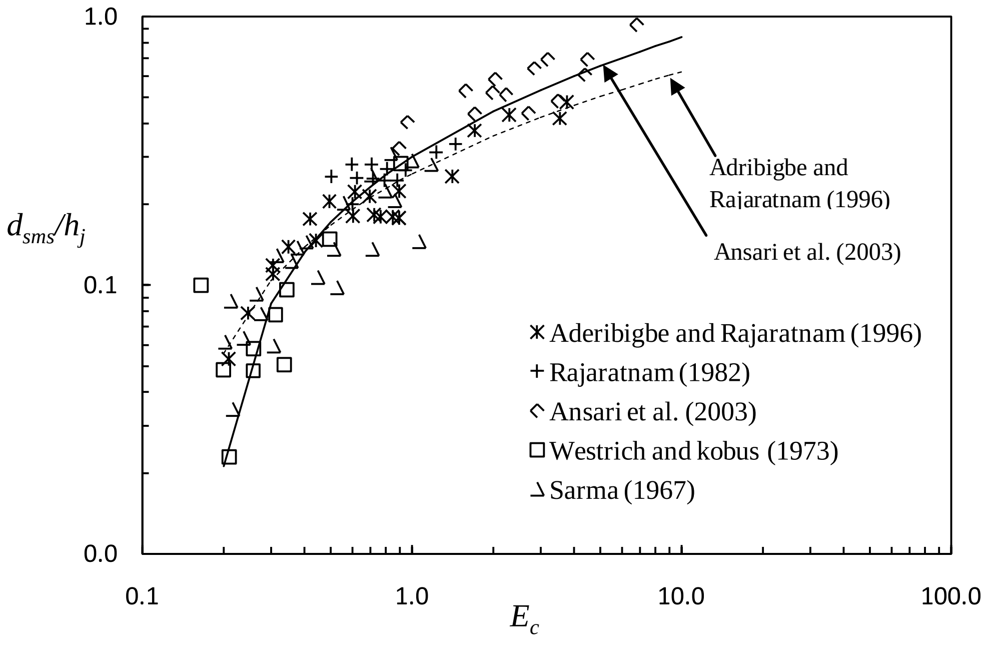

Fig. 2.23 Variation of d_{sms}/h_j with erosion parameter, E_c (Ansari et al., 2003)

For cohesive sediment, the scour rate and the profile of scour were observed to change with antecedent moisture content (*AMC*), percentage of clay, dry unit weight as also observed by Hanson and Robinson (1993) and Hanson (1991).

They proposed the following equations to compute depth of scour d_{sms} and volume of scour, ∇ in case of non-plastic sediment (for plasticity index, $PI < 0$)

$$\frac{d_{sms})_{cohesion}}{d_{sms})_{cohesionless}} = 0.38\left(\frac{C_*}{\phi_*}\right)^{0.3}\left(\frac{W}{W_*}\right)^{0.11}\left(\frac{\gamma_d}{\gamma_w}\right)^{2} \tag{2.36}$$

and

$$\frac{\nabla_{cohesion}}{\nabla_{cohesionless}} = 0.21\left(\frac{C_*}{\phi_*}\right)^{0.15}\left(\frac{W}{W_*}\right)^{0.1}\left(\frac{\gamma_d}{\gamma_w}\right)^{3} \tag{2.37}$$

Where C_* is the dimensionless clay content which can be expressed as;

$$C_* = \frac{P_c.C_u}{(\gamma_s - \gamma_f)d_a} \tag{2.38}$$

ϕ_* is dimensionless angle of internal friction which can be given by the following equations;

$$\phi_* = \frac{P_c \tan\phi_{cohesion} + (1 - P_c)\tan\phi_{cohesionless}}{\tan\phi_{cohesionless}} \tag{2.39}$$

Where P_c = percentage of clay content, W = Antecedent moisture content in percent, W_* = antecedent moisture content require to saturate the clay sample (W_* = W for sediment having Plasticity Index greater than zero.), γ_d = dry unit weight of the sediment, γ_w = wet unit weight of sediment, γ_s = specific weight of sediment, γ_f = specific weight of fluid, d_a = arithmetic mean size of the sediment mixtures, C_u = cohesion, $\phi_{cohesion}$ = angle of internal friction for cohesive sediment and $\phi_{cohesonless}$ = angle of internal friction for cohesionless sediment. They computed depth of scour and volume of scour using proposed Eqs. (2.48) and (2.49) and compared with the observed values. They found that the computed results are within ± 20 % of the observed values as depicted Figs. 2.24 and 2.25.

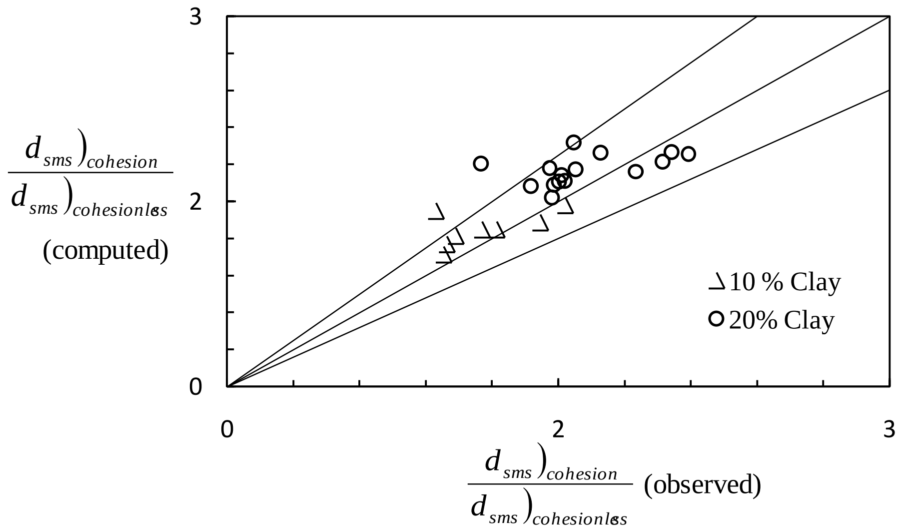

Fig. 2.24 Comparison of computed $d_{sms})_{cohesion} / d_{sms})_{cohesionless}$ using Eq. (2.48) with observed values (Ansari, 1999)

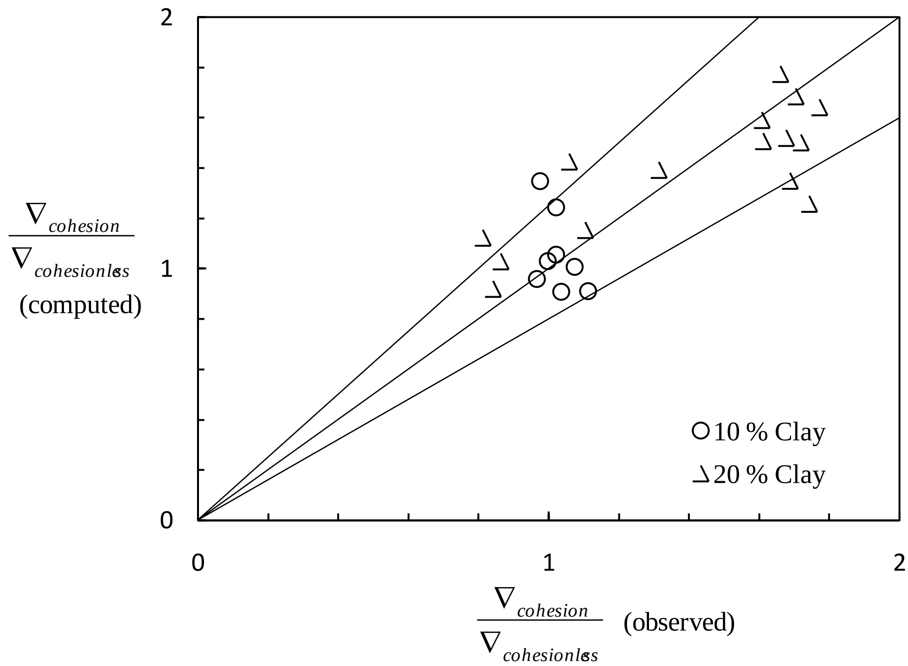

Fig 2.25 Comparison of computed $\nabla_{sms})_{cohesion} / \nabla_{sms})_{cohesionless}$ using Eq. (2.49) with observed value (Ansari et al. 2003)

In case of non-cohesive sediment, the dynamic depth of scour was higher compared to static depth of scour, however, differences in such scours was low in case of cohesive sediment. For plastic sediments, when the plasticity index was greater than zero, the proposed equation between $d_{sms})_{cohesion} / d_{sms})_{cohesionless}$ and W/W_* are;

$$\frac{d_{sms})_{cohesion}}{d_{sms})_{cohesionless}} \approx 1.5 \pm 0.3 \quad (2.40)$$

$$\frac{\nabla_{cohesion}}{\nabla_{cohesionless}} = 1.11\left(\frac{W}{W_*}\right)^{-0.37} \quad (2.41)$$

It is therefore understandable that the ratio $d_{sms})_{cohesion}/d_{sms})_{cohesionless}$ is always greater than unity in case of plastic sediment. The depth of scour was observed to increase with increase in C_*/ϕ_* for non-plastic materials. Also, the maximum scour depth increases slightly with an increase in W/W_* as shown in Fig. 2.26. The volume of scour hole reduces slightly with increase in W/W_* as shown in Fig. 2.27.

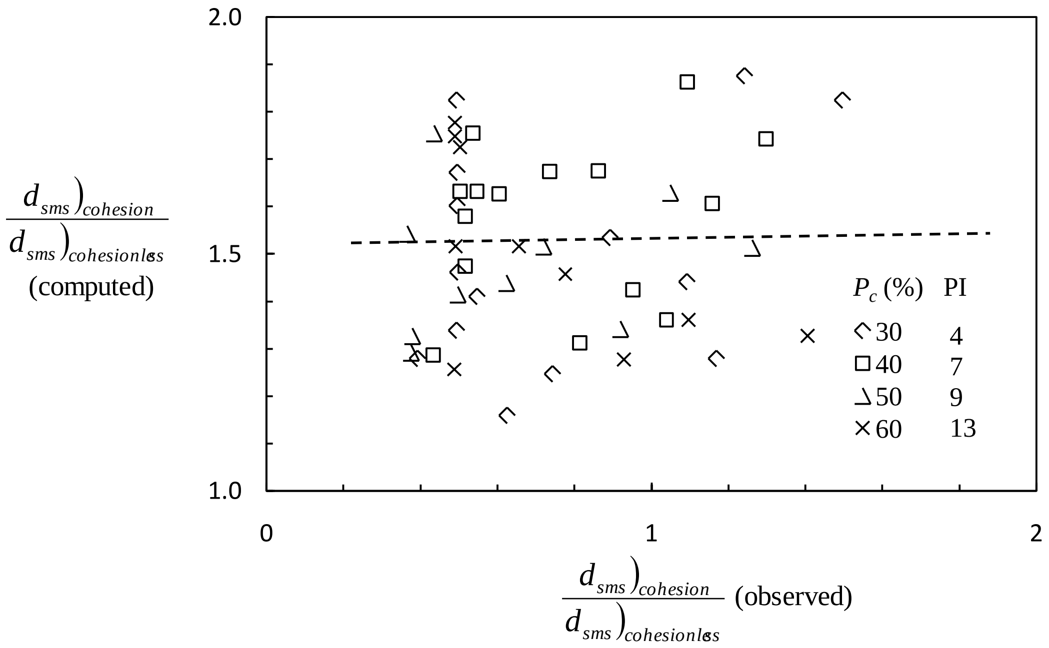

Fig. 2.26 Variation of $d_{sms})_{cohesion}/d_{sms})_{cohesionless}$ with w/w_*, $PI > 0$ (Ansari et al. 2003)

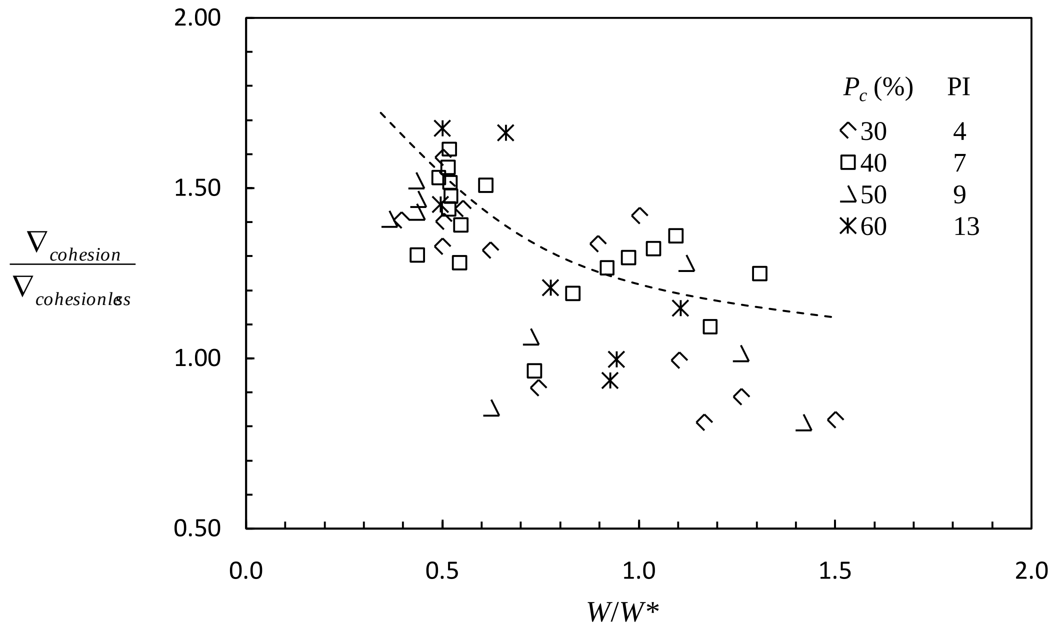

Fig. 2.27 Variation of $\nabla_{sms})_{cohesion} / \nabla_{sms})_{cohesionless}$ with w/w_*, $PI > 0$ (Ansari et al. 2003)

Mazurek et al. (2003) performed laboratory work on erosion under submerged plane wall jets in cohesive materials. They used to create scour in 32 types of clay samples of similar properties. The samples contained 40% clay, 53% silt and 7% fine sand and have liquid limit = 36 %, plastic limit = 18 % and vane shear strength of 20 kN/m^2. The dry density of sediment was 1540 kg/m^3. A rectangular plenum having dimensions of 144 mm wide, 100 mm high and 670 mm long with a nozzle of 144 mm width to generate a jet that issued into a flume of 4.1 m length and 150 mm width with a constant submergence water depth of 350 mm. The experiments were conducted by using flows from two different type of thickness of nozzle i.e. 2.33 and 5.10 mm by varying the water flow rates from 1.63 to 5.40 liters per second. The jet velocity was varied from 4.86 to13.56 m/s. The effect of hydraulic variables on the process of scour generated by wall jet was determined. The scour hole dimension was related to $(\lambda - \lambda_c)/\lambda_c$ as shown in Figs. 2.28 and 2.29. Where λ is the parameter describing the hydraulic properties of the jet and is equal to $\rho_f u_o^2$, here ρ_f is the mass density of eroding fluid, λ_c is the critical value of λ below which no significant erosion occurs. They proposed the following relationships for estimation of maximum depth of scour, location of higher scour depth and the scour length profiles at equilibrium condition;

$$\frac{\overline{d_{sms}}}{b_o} = 3.78\left(\frac{\lambda - \lambda_c}{\lambda_c}\right) \qquad 2.42)$$

$$\frac{\overline{X}_{m\infty}}{b_o} = 3.84\left(\frac{\lambda - \lambda_c}{\lambda_c}\right) \quad (2.43)$$

$$\frac{\overline{X}_{o\infty}}{b_o} = 27.0\left(\frac{\lambda - \lambda_c}{\lambda_c}\right) \quad (2.44)$$

Where $\overline{d_{sms}}$ is the average depth of scour in cohesive sediment, $\overline{X}_{m\infty}$ is the average distance from the nozzle of the maximum scour depth at equilibrium, $\overline{X}_{o\infty}$ is the average length of scour hole at asymptotic condition, b_o is the thickness of nozzle.

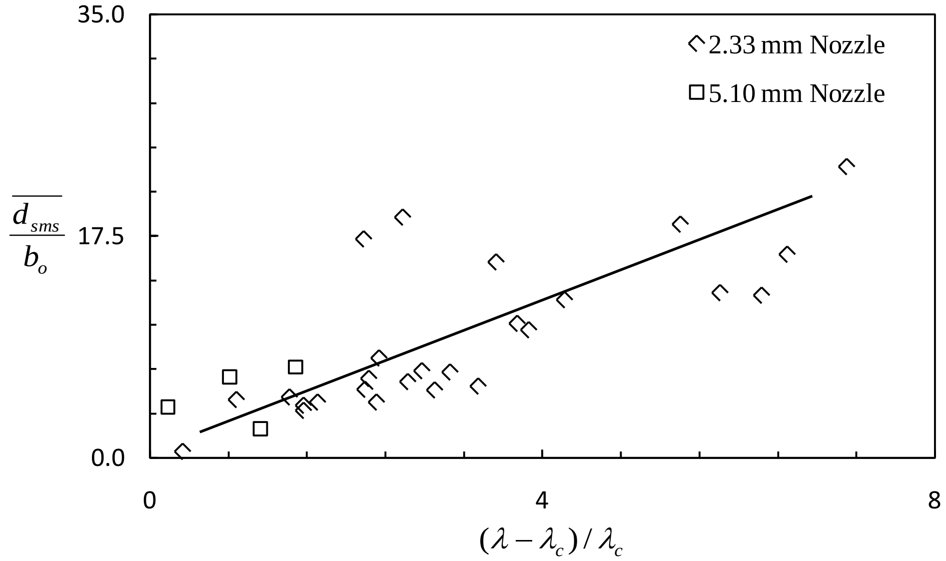

Fig. 2.28 Maximum depth of scour at equilibrium condition (Mazurek et al. 2003)

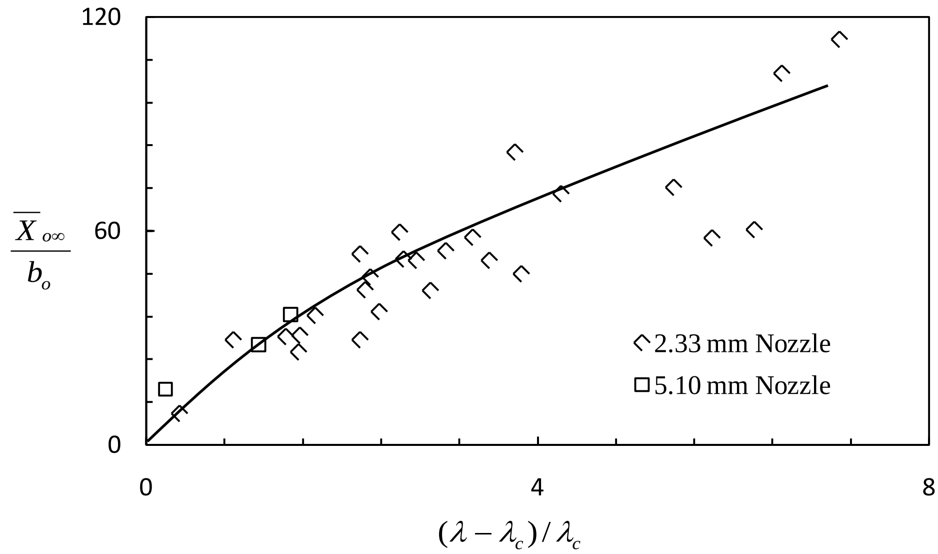

Fig. 2.29 Length scale of scour for equilibrium scour hole (Mazurek et al. 2003)

Mazurek and Hossain (2007) studied scour in cohesive as well as non-cohesive sediment due to impinging water jets and wall jets. For the analysis of cohesionless sediment, the data from Rajaratnam (1982) and Aderibigbe and Rajaratnam (1996) were used while for cohesive sediment, the data of Mazurek (2001) were used. The dimension of scour profile at equilibrium conditions depends up on the ratio of the relative impingement (h_j/d_o) to the densimetric Froude number. Aderibigbe and Rajaratnam (1996) developed an equation for dimensionless scour profile using the maximum scour depth d_{sms}, as the scale for the scour depth (d_s), and the half width of scour hole b as the scale for the radial distance from the jet r_d, where the half width b is the radial distance r where is d_s equal to $d_{sms}/2$.The proposed equation is as follows;

$$\frac{d_s}{d_{sms}} = \exp\left[-0.693\left(\frac{r_d}{b}\right)^2\right] \qquad (2.45)$$

For cohesive sediment, Mazurek (2001) found the dimensions of scour profile at equilibrium condition are function of parameter $(X - X_c)/X_c$, where X = cohesive sediment erosion value for water jets and is equal to $\rho_f u_o^2 (d_o / h_j)^2$ and X_c is the critical value of X below in which the mass erosion is not observed. The value of X is related to the maximum shear stress τ_{om} on the bed at the start of scour. The bed shear stress can be obtained from the following equation of Beltaos and Rajaratnam (1974) with the assumption that the sediment bed is smooth, which is a reasonable assumption for cohesive sediment.

$$\tau_{om} = 0.16\rho_f u_o^2 \left(\frac{d_o}{h_j}\right)^2 = 0.16X \qquad (2.46)$$

The parameter X can be related to the maximum shear stress on the bed at the start of erosion, τ_{om}. For the estimation of τ_{om} cohesionless sediment, the above formulation for bed shear stress was modified by Rajaratnam and Mazurek (2005) and presented as;

$$\frac{\tau_{om}}{\rho_f u_0^2}\left(\frac{h_j}{d_o}\right)^2 = -37.6\left(\frac{k_s}{h_j}\right)^2 + 0.505\left(\frac{k_s}{h_j}\right) + 0.72 \qquad (2.47)$$

Where, k_s is the roughness of the cohesionless sediment bed. The value of k_s shall be approximated equal to two times of the sediment size as suggested by Yalin (1977).

Mazurek and Hossain (2007) reanalyzed the data of Mazurek (2001) and found that the soil is eroded mostly by mass erosion in the form of lump and chunk of about 2 to 140 mm in size. In Figs. 2.30 and 2.31, the maximum scour depth, d_{sms}/h_j and radius of scour hole, r/h_j were plotted with $\left(\tau_{om} - \tau_c / \tau_c\right)$, They found that the maximum depth of scour and radius of scour hole in cohesive sediment appear to be larger than cohesionless sediment.

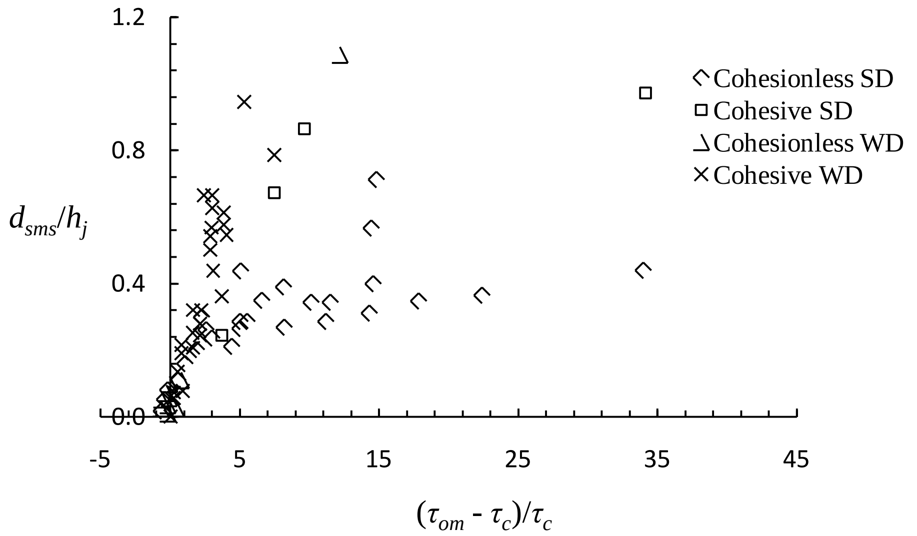

Fig. 2.30 Maximum scour depth in cohesionless and cohesive sediment due to circular impinging jets, for strongly deflected jet regime, SD; and weakly deflected jet regime, WD (Mazurek and Hossain, 2007)

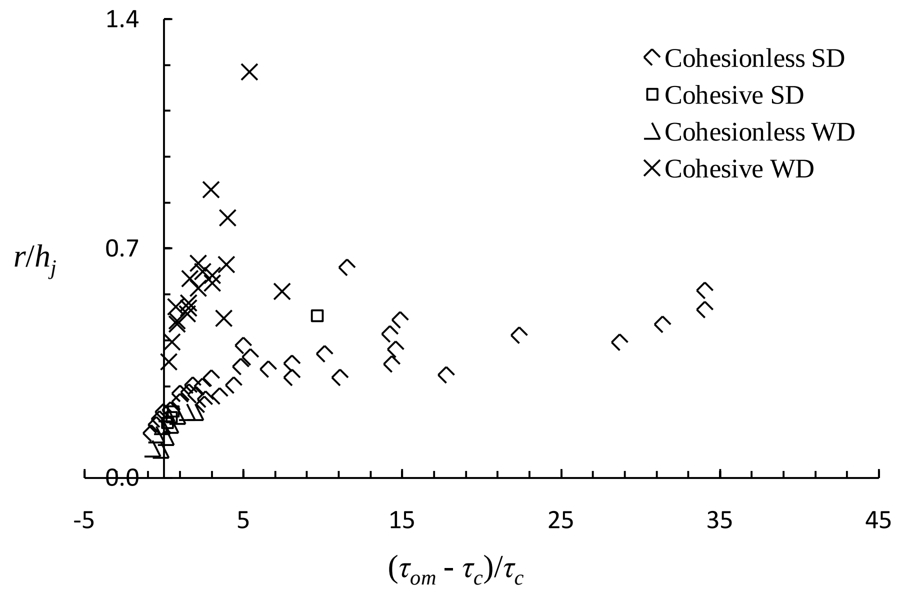

Fig. 2.31 Scour hole radius in cohesionless and cohesive sediment (Mazurek and Hossain, 2007)

Figure 2.32 shows a comparison for maximum scour depth due to circular wall jets in cohesive and non-cohesive sediment and found that the maximum scour depth and its location were similar in both the sediment; however, the length of scour profile was high in cohesive and fine sediment because of lack of dune generation.

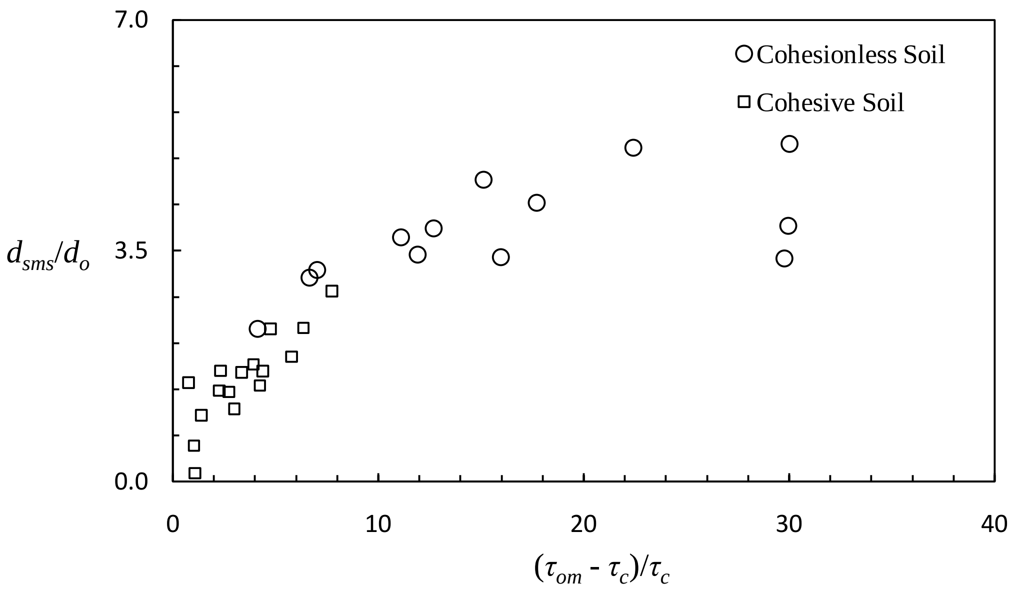

Fig. 2.32 Maximum depth of scour in cohesionless and cohesive sediment due to circular wall jets (Mazurek and Hossain, 2007)

2.7 CONCLUDING REMARKS

Based on the comprehensive review of literature, it is noted that numerous studies have been carried out on scour in cohesionless sediment under submerged water jets. However, less attention has been focused in case of cohesive sediment. Various equations have been developed using the laboratory and field data for the estimation of various scour parameters like maximum scour depth, scour hole profile, radius of scour hole, dune height etc. In the nature, the river bed material is consisted of cohesionless and cohesive sediment mixtures such as clay-gravel mixture, clay-sand-gravel mixture etc. Little information is available on the process of scour in such bed materials mixture occurring under the submerged jet. Some investigations have been conducted on jet scour in cohesive sediments. However, these investigations are based on limited amount of data covering a narrow range of variables on jet configurations, physical properties of cohesive sediments etc. However, a general expression is not available, so far, that can be used for determination of the scour depth its various length scale parameters due to submerged circular vertical water jet in cohesive sediments mixtures such as clay-gravel and clay-sand-gravel. The present study, therefore, aims at filling the above stated gaps in the knowledge.

CHAPTER 3

EXPERIMENTAL SET-UP AND PROCEDURE

3.1 GENERAL

This chapter describes the laboratory experiments conducted under submerged circular vertical jets for different configurations of the bed material, different jet velocities, height of jet and nozzle size. The experimental setup, test conditions and data collection procedures are also elaborated and illustrated in this chapter. The observations made during the experimental runs along with equipments and instruments used are described. The tested ranges of hydraulic variables are listed at the end of the chapter. The experiments were conducted in the Hydraulics Engineering Laboratory of Civil Engineering Department at Indian Institute of Technology, Roorkee, India. For studying the hydraulics of submerged jet scour in the cohesionless and cohesive sediments, a circular steel tank was used.

Cohesionless sediment such as fine sand, gravel and sand-gravel mixtures were taken as the base bed material. The cohesive material i.e. clay was mixed in different proportions to prepare sediment mixtures of different clay percentage.

A wide range of field conditions was simulated by varying the antecedent moisture content of the cohesive sediment mixtures. The experimental works were also performed to estimate different engineering properties of cohesionless and cohesive sediment for fine sand, gravel, sand-gravel mixtures, clay- gravel and clay-sand-gravel sediment mixtures.

3.2 USED SEDIMENT MATERIALS

Cohesionless sediments consisting of fine sand, gravel and sand-gravel mixture (each in equal proportion by weight) were used as the base sediment. Clay was added in various proportions varying from 10 to 60% to the base sediment to make the cohesive sediment mixtures. A wide range of field conditions were simulated by varying the antecedent conditions of cohesive sediment mixtures. The experiments were also conducted to obtain various engineering properties of clay, sand, gravel and their mixtures, these are described here.

3.2.1 Properties of Cohesionless Material

Experiments were performed on the sediment bed consisting of fine sand, gravel and sand-gravel mixtures (equal proportions by weight). The particle size distributions of the used sediment were carried out as per Indian Standard Code practices (IS 1948-1970) for sand, gravel are shown in Fig. 3.1. The sizes (d_{50}) of sand and gravel were 0.24 m and 2.7 mm while geometric standard deviations σ_g were 1.41 and 1.21 respectively. The mean size of the sand-gravel mixture was taken weighted arithmetic mean of sizes of sand and gravel. The computed mean size of the sand-gravel was d_a =1.47 mm. The relative density of the sediment was equal to 2.65.

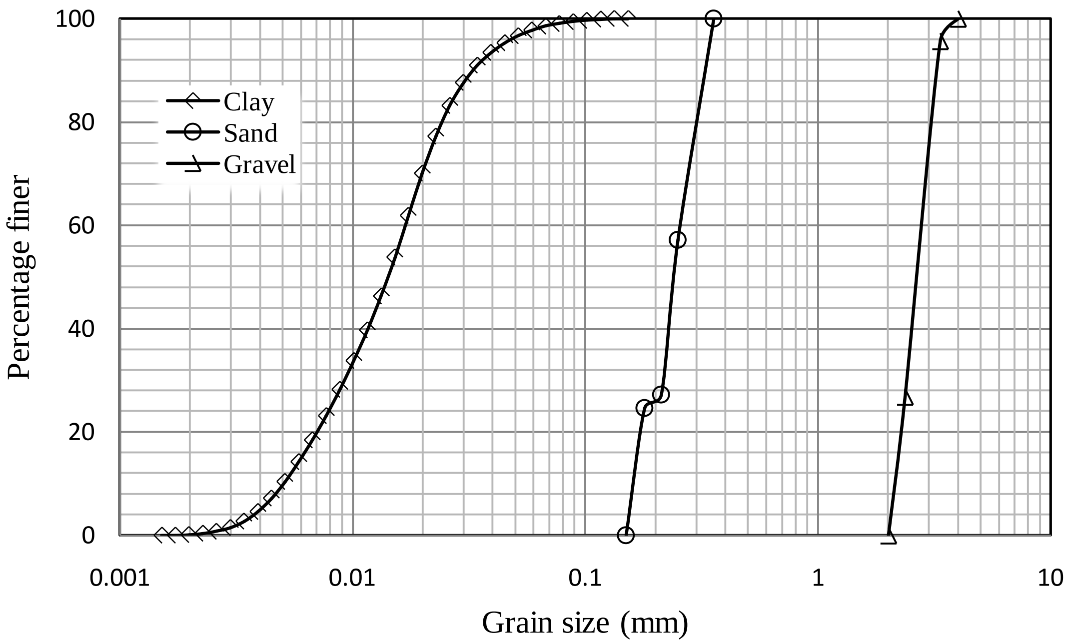

Fig. 3.1 Particle size distribution curve for clay, sand and gravel sediment

3.2.2 Properties of the Cohesive Material

Locally available clay that was excavated from a depth of 1.0 m below the bed level of river bed was used. Various laboratory tests were conducted for determination of clay properties as per Indian Standard Code of Practice (IS-1498, 1970) to obtain engineering properties of the clay such as plasticity index, P.I., plastic limit, W_P, liquid limit, W_L, optimum moisture content, OMC, maximum dry density, bulk density, and void ratio. The specific gravity of clay sediment was determined according to Indian Standard

Code practice (IS-1498, 1970). A laser particle size analyzer was used for obtaining particle size distribution of clay. The obtained particle size distribution is shown in Fig.3.1. The unconfined compressive shear strength of cohesive mixtures was measured as per IS-2720-X, 1991). The bulk density of sediment was measured by Core Cutter method as per IS-2720-XXIX, 1975)

The cohesive sediment i.e. clay has median size (d_{50}) = 0.014 mm, geometric standard deviation (σ_g) = 2.1, liquid limit (W_L) = 43%, plastic limit (W_P) = 22% and plasticity index (P.I.) = 21% optimum moisture content (OMC) = 19%, maximum dry density (γ_d) = 16.75 kN/m^3, cohesion at optimum moisture content (OMC) C_u = 49.23 kN/m^2, angle of internal friction at OMC, $\emptyset_c$ = 30.7^o, and the relative density of clay = 2.60. Figure 3.2 show the photographic view of bed material used for the present investigations i.e. clay, sand, gravel and sand-gravel mixtures, respectively.

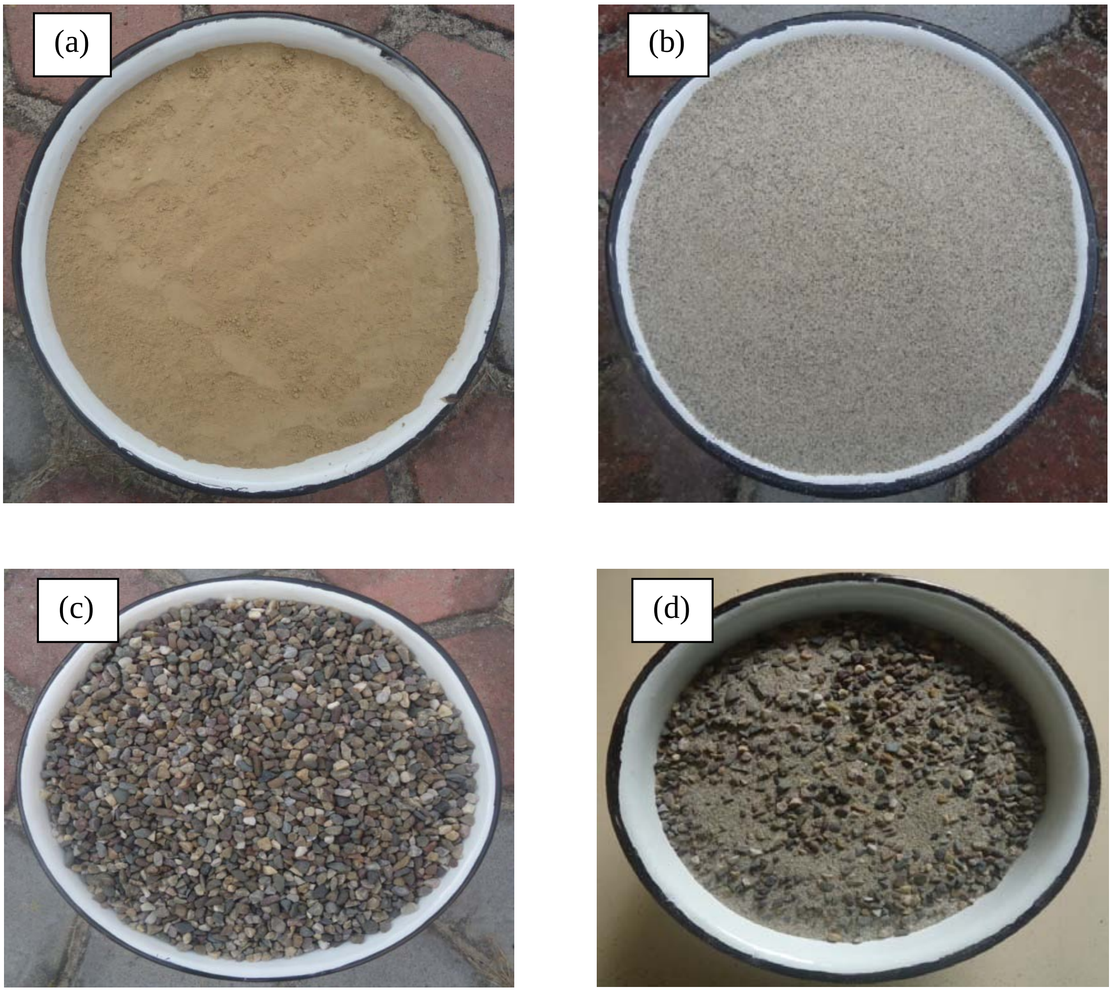

Fig. 3.2 Photographic view of bed material used (a) clay (b) sand (c) gravel and (d) sand-gravel mixture

The X-ray diffraction (XRD) test was conducted to determine the composition of various minerals present in the clay. The results of the XRD test are shown in Fig. 3.3. The analysis of sample yielded minerals; Illite, Kaolinite and Montmorillonite.

The specified openings for X-ray diffraction (X.R.D.) test are summarized below:

Radiation	*K* (Potassium)
Target	*Cu* (Copper)
Filter	*Ni* (Nickel)
Scanning angle	3^{o} to 30^{o} of 2θ
Current	20 mA
Voltage	35KV
Range	2 KC/S
Chart speed	1 cm per minute
Goniometric speed	1^{o} of 2θ/ minute

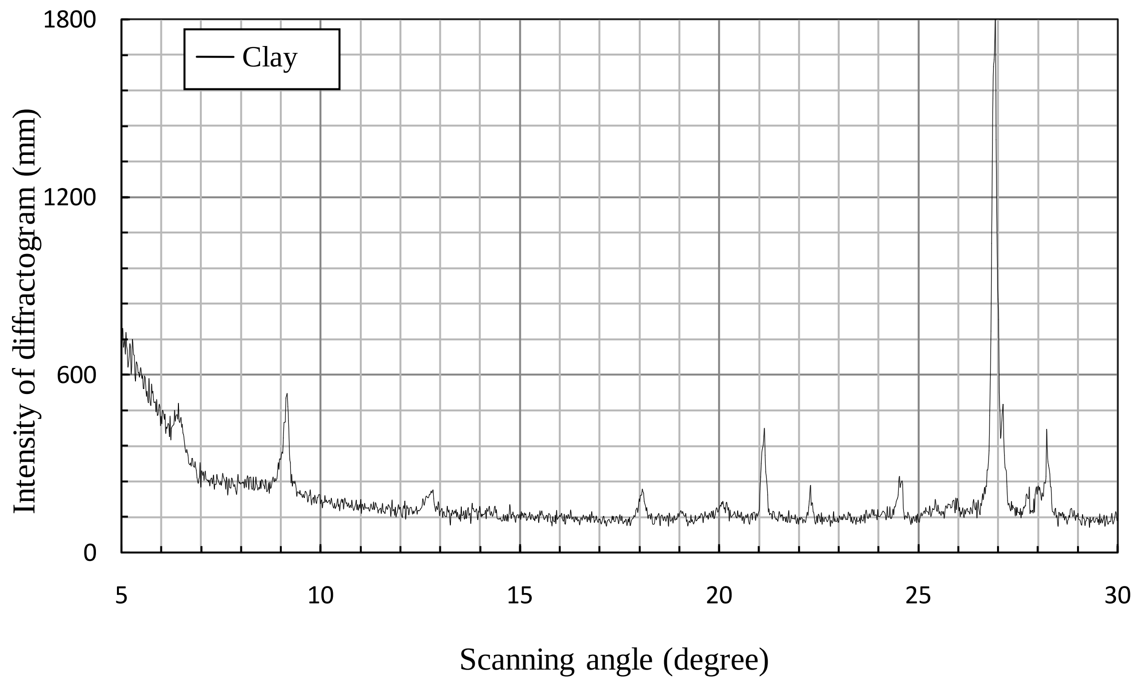

Fig. 3.3 Results of X-ray diffraction test for clay

3.2.3 Initial Stage of Cohesive Material

The cohesive sediment mixtures were prepared by adding clay with gravel and clay with sand-gravel in different proportions ranging from 10% to 60% by weight. The amount of moisture content in the sediment has its great influence on the physical properties (Ansari et al. 2002). Depending upon the moisture content present, the cohesive sediments change their stages i.e. dry, liquid, plastic and non-plastic (semi-solid) as shown in Figs. 3.4. The relative locations of plastic and non-plastic and viscous states of cohesive sediment are shown in Fig. 3.5.

In the present investigation, the tests were conducted under highest possible range of antecedent moisture content so as to represent their different stages as anticipated in field conditions. The cohesive sediments were tested at various moisture contents ranging from very soft soil with less value of cohesion to hard soil with a high value of cohesion.

Fig. 3.4 Picture showing (a) dry, (b) semi-solid, (c) plastic and (d) viscous states of cohesive sediment

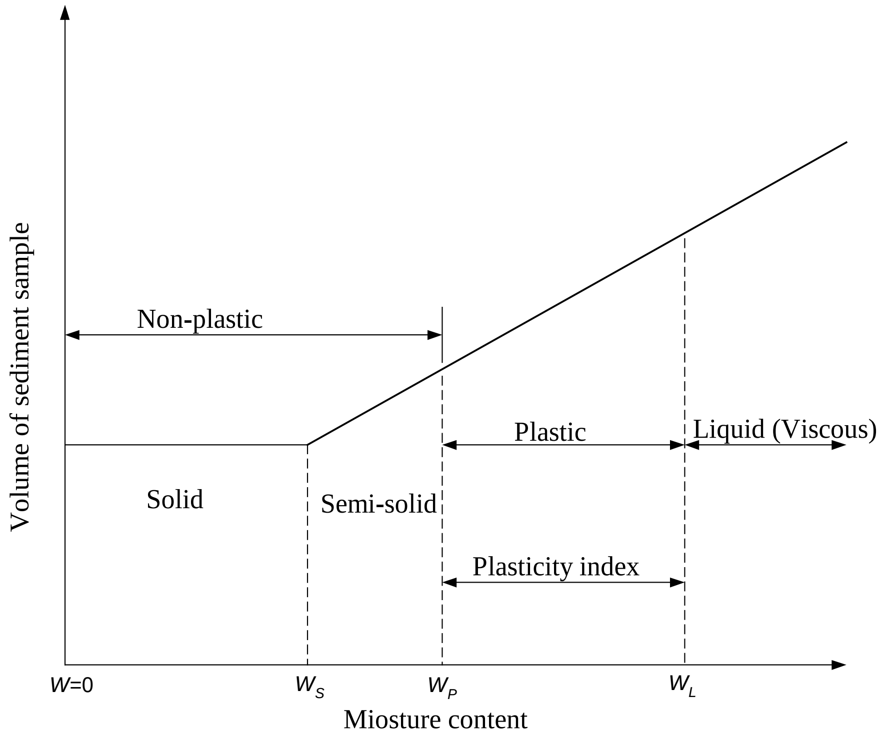

Fig. 3.5 Relative location of the non-plastic, plastic and viscous states of cohesive sediment (Ansari, 1999)

Maximum dry density and moisture contents as obtained using the standard Proctor compaction test for various clay-gravel mixtures and clay-sand-gravel mixtures are shown in Fig. 3.6 and Fig. 3.7, respectively.

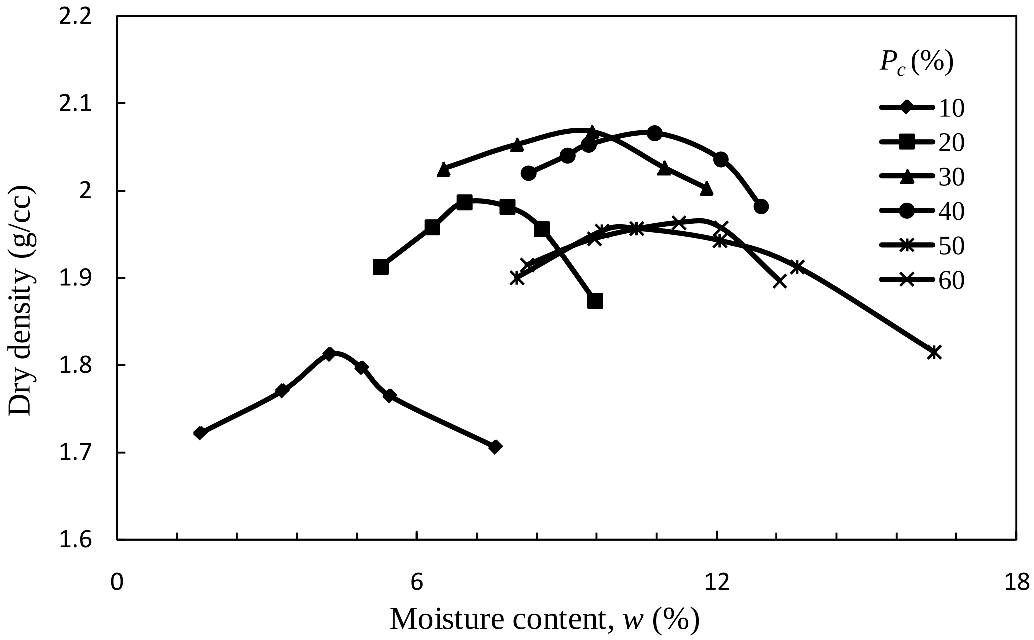

Fig. 3.6 Variation of dry density with moisture content of clay-gravel mixtures for different clay percent

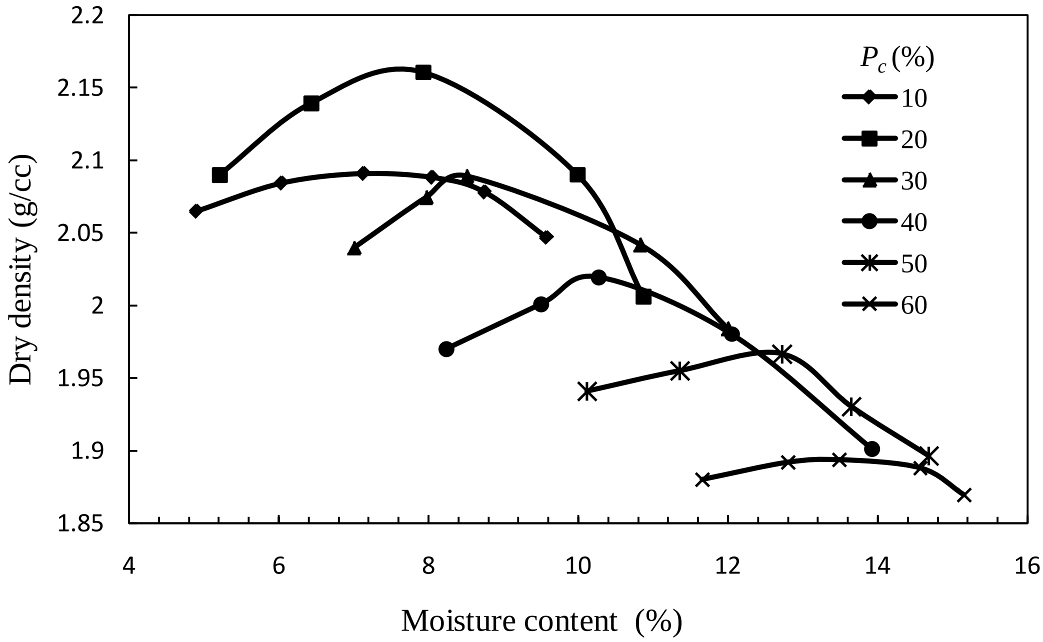

Fig. 3.7 Variation of dry density clay-sand-gravel mixtures with moisture content for different clay percent

3.3 EXPERIMENTAL SET UP

3.3.1 Tank

A circular steel tank having diameter 1.25 m and depth 1.25 m, filled with the desired sediment up to a height of 0.80 m was used for the experiments on scour due to submerged circular vertical jets. It was ensured that the diameter of the tank is sufficiently large enough so that its size would have no influence on scour process. The impinging jet was produced by a nozzle fitted at the end of circular supply pipe of diameter 0.0254 m. Suitable arrangement was provided to adjust the height of the jet above the sediment bed. For each experimental run, the tank was filled by the desired sediment up to the height of 0.80 m, while the water was filled in the remaining 0.45 m height of the tank. The jet discharge was measured with volumetric measurement by calibrated Venturimeter fitted in the supply pipe. The jet was aligned vertically downward through plumb bob. The experimental set-up for jet scour study is shown in Fig. 3.8, while a photographic view of the experimental set-up is shown in Fig 3.9.

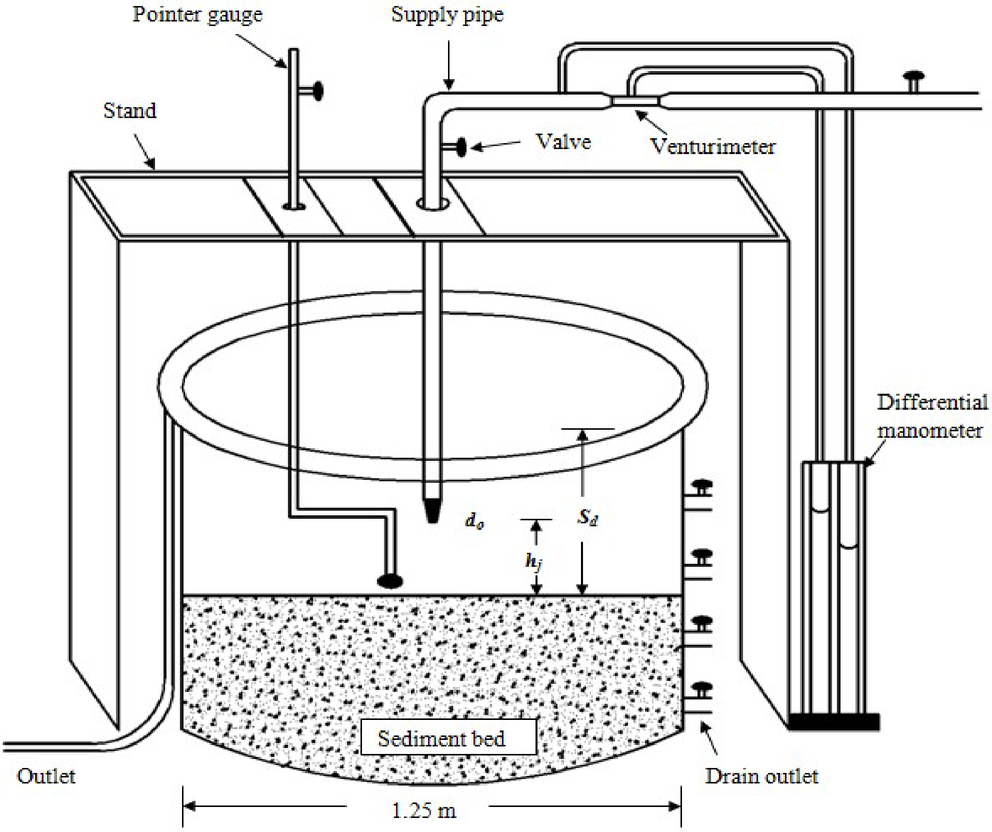

Fig. 3.8 Experimental set-up

Fig. 3.9 A photographic view of the experimental set-up

The laboratory experiments were conducted with two types of nozzle i.e. 12.5 and 8 mm diameter, at two jet heights i.e. 0.15 and 0.30 m from sediment bed level. Two jet velocities i.e. 7.19 and 5.12 m/s for 12.5 mm nozzle and 9.84 and 6.65 m/s for 8 mm nozzle were set in the experimentation. In case of cohesionless sediment, three different types of sediment bed ware prepared i.e., fine sand, gravel and sand-gravel mixtures (in equal proportion by weight). Cohesive sediment mixture was prepared by mixing clay with gravel and with sand-gravel. In all, three mixtures i.e., sand-gravel, clay-gravel, and clay-sand-gravel were prepared. In clay-gravel and clay-sand-gravel mixtures, the clay contents was varied in proportion varying from 10% to 60% by weight, however, in clay-sand-gravel mixture, equal proportion of sand and gravel were used. The calibration curve for Venturimeter is shown in Fig. 3.10.

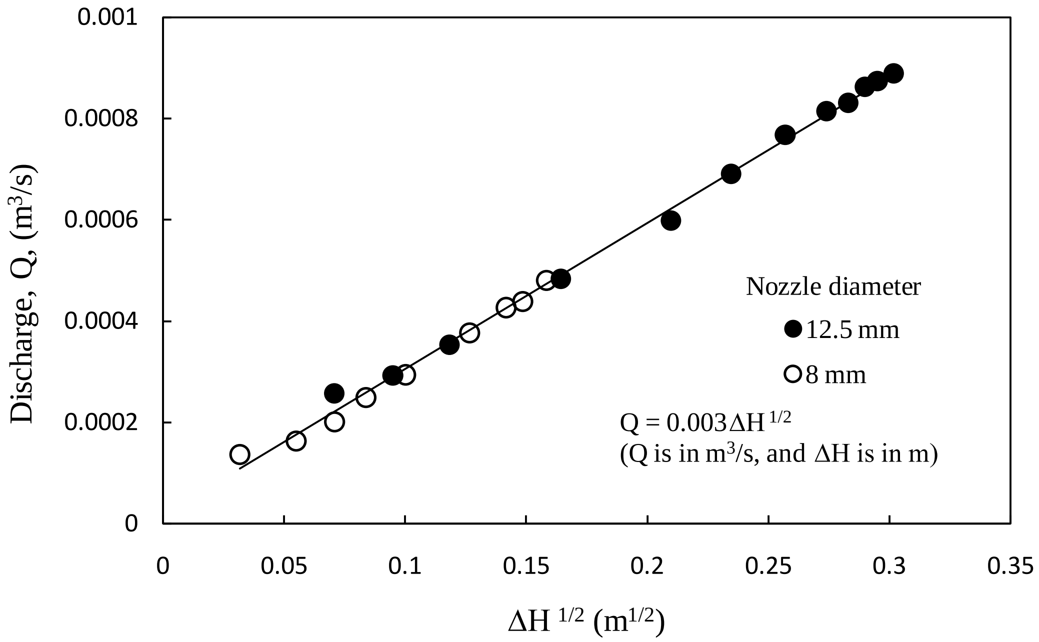

Fig. 3.10 Calibration curve of Venturimeter

3.3.2 Final Preparation of Sediment Mixtures

The sun-dried powdered clay, sand and gravel were used for the preparation of the sediment mixture. Accurately weighed clay powder, sand and gravel were mixed thoroughly with water. The mixed sediments were covered with polythene and left for 24 hours for uniform distribution of the moisture. The sediment was mixed thoroughly again before placing it into the test section. The cohesive sediment mixture was filled in the test section and compacted by a dynamic compaction method while the cohesionless sediment mixtures were not compacted. The dynamic compaction method has been successfully used for cohesive sediments by other investigator like Kothyari and Jain (2008) and Jain and Kothyari (2009). The dynamic compaction method was used for cohesive sediment mixtures of hard, semi-solid and plastic consistencies. In the present study, the sediment was compacted in test section in three layers each of thickness 0.265 m. Each layer was compacted with a hand tamper of weight 8 kg. Sufficient numbers of blows were applied throughout the test section to obtain desired density. The hand tamper was allowed to drop freely under gravity from a height of about 0.30 m to ensure the bonding between the different layers. The top surface of each compacted layer was roughened before laying the next layer over it. The test was slightly over-filled with sediment. Later, extra material was trimmed off using a sharp edged large knife. The bulk density of compacted sediment and antecedent moisture content was measured at three different locations to ensure the uniformity of compaction and placement. The observed value of moisture content and density were found equal at all the locations for the experimental runs being reported herein. The prepared bed was saturated for 24 hours before the start of experiments. Figure 3.11 depicts a freshly laid sediment bed. The value of dry density and antecedent moisture content reported in this study are taken at the time of compaction.

Fig. 3.11 Prepared cohesive sediment bed before start of the experiment

The compacted bed samples were taken and analyzed for the bulk unit weight of sediment by using standard core cutter method as per Indian Standard Code (IS-2720-XXIX, 1975). The value of dry density was computed by using the observed value of bulk density and measured antecedent moisture content. The void ratio was obtained from the computed value of dry density of cohesive sediments.

The unconfined compressive strength of cohesive sediments was measured using laboratory based unconfined compression test apparatus. Cylindrical specimens were extracted from the compacted bed and tested in unconfined compression apparatus as per Indian Standard Code (IS-2720-X, 1991). Figure 3.12 shows the measurement of unconfined compressive strength of the sediment sample.

Fig. 3.12 Measurement of unconfined compressive strength of the sediment sample

3.4 MEASUREMENT OF SCOUR PARAMETERS

For initial measurement of the prepared sediment bed level before the start of the experiment was measured with the help of simple pointer gauge having a least count of 0.1 mm whereas the scoured bed profile i.e. maximum static, maximum dynamic scour depth, temporal variation of the scour depth from initial condition and other various length scale parameters like radius of scour hole, dune height etc. were measured by using the another pointer gauge having a flat bottom which also have the least count of 0.1 mm. The volume of scour hole was measured by water replacement method i.e. volume of water required to fill the scour hole completely under no seepage condition.

In all, 24 experimental runs were conducted in cohesionless sediment i.e., sand, gravel and sand-gravel mixture to study the temporal variation of scour depth in static and dynamic conditions. Various scour parameters like radius of scour, volume of scour and dune height have also been measured. Total 84 experiments were conducted for cohesive sediment consisting of clay-gravel and clay-sand-gravel mixtures. The characteristics of scour under submerged circular vertical jets in cohesive sediments were found different than the scour profile formed in cohesionless sediment and measured its various scour parameters in similar manner as in cohesionless sediment.

3.5 DATA CHARACTERISTICS

The experimental data collected in the present investigation are listed in the Appendix under the major hydraulic parameters. The Appendix- A, B & C gives the hydraulic and sediment parameters under submerged circular vertical jets in sand, sand-gravel mixture and gravel bed. For cohesive sediment mixtures, the hydraulic and sediment parameters under submerged circular vertical jets in clay-gravel and clay-sand-gravel mixtures are given in Appendix – D and E respectively. The data on temporal variation of scour depth under submerged circular vertical jets in cohesionless sediment consisting of sand, sand-gravel mixture and gravel beds are given in Appendix – F. In case of cohesive sediment mixtures, the data on temporal variation of scour depth under submerged circular vertical jets in clay-gravel and clay-sand-gravel mixtures are given in Appendix – G and H respectively. Table 3.1 gives the range of collected data for present and previous investigation on scour under submerged circular vertical jet in cohesionless sediment. Table 3.2 gives the range of data for scour due to jet in cohesionless sediments. The ranges of the data for present investigation in clay-gravel and clay-sand-gravel mixture are given in Table 3.3 and 3.4 respectively.

Table 3.1 Range of the data (present and previous investigations) on scour under submerged circular vertical jet in cohesionless sediment

Investigators	Median size, d_{50} (mm)	Jet diameter, d_0 (mm)	Jet velocity, u_o (m/s)	Jet height, h_j (m)
Sarma (1967)	0.53 - 0.75	8.26-16.5	0.66-2.83	0.24
Westrich and Kobus (1973)	1.5	20 - 40	0.7 - 3.7	0 - 0.82
Rajaratnam (1982)	1.2 - 2.38	9.8	2.99 - 4.6	0.14 - 0.28
Aderibigbe and Rajaratnam (1996)	0.88 - 2.42	4 - 12	2.65 - 4.45	0.004 - 0.523
Ansari et al. (2003)	0.27	8 - 12.5	1.3 - 5.75	0.15 - 0.30
Present study	0.24 - 2.7	8 - 12.5	5.12 - 9.84	0.15- 0.30

Table 3.2 Range of the data for present investigation in cohesionless sediments

d_o (mm)	h_j (m)	u_o (m/s)	d_a (mm)	d_{dms} (m)	d_{sms} (m)	r (m)	Δ (m)	∇ (lit)
8-12.5	0.15-0.30	5.12-9.84	0.24-2.7	0.107-0.36	0.045-0.14	0.175-0.785	0.007-0.047	1.60-28

For documentation, the experimental runs of clay-gravel sediment mixtures were designated like C10G1, C10G2 etc. Here first character C presents the clay sediment, second digit 10 represents the clay percent, third character G stands for gravel and fourth digit 1 stands for experiment number. Similarly the experimental runs of clay-sand-gravel mixtures were designated as C10SG1, C10SG2 etc. Here SG stands for sand-gravel, while meaning of other characters remain same.

Table 3.3 Range of data on scour under submerged circular vertical impinging jets in cohesive sediments consisting of clay-gravel mixtures

P_c (%)	d_o (mm)	h_j (m)	u_o (m/s)	d_a (mm)	W (%)	γ kN/m^3	γ_d kN/m^3	e	d_{dms} (m)	d_{sms} (m)	r (m)	Δ (m)	∇ (lit)	UCS (kN/m^2)
10-60	8-12.5	0.15-0.30	5.12-9.84	0.00109-0.00243	3.63-16.98	16.92-20.66	16.14-18.01	0.444-0.612	0.039-0.239	0.042-0.134	0.045-0.20	0.0045-0.0175	0.11-6.5	3.46-41.60

Table 3.4 Range of data on scour under submerged circular vertical impinging jets in cohesive sediments consisting of clay-sand-gravel mixtures

P_c (%)	d_o (mm)	h_j (m)	u_o (m/s)	d_a (mm)	W (%)	γ kN/m^3	γ_d kN/m^3	e	d_{dms} (m)	d_{sms} (m)	r (m)	Δ (m)	∇ (lit)	UCS (kN/m^2)
10-60	8-12.5	0.15-0.30	5.12-9.84	0.00060-0.00132	4.09-16.36	18.63-22.40	17.65-19.27	0.348-0.472	0.018-0.267	0.018-0.177	0.038-0.275	0.00035-0.021	0.09-12	7.75-61.63

3.6 CONCLUDING REMARKS

The experimental dataset for jet scour study under various configurations of sediment bed material, jet velocities, jet height and size were collected in the present experimental works. Experiments were performed with jet diameters 12.5 and 8 mm; jet heights 0.15 and 0.30 m, jet velocities 7.19 and 5.12 m/s for 12.5 mm diameter nozzle and 9.84 and 6.65 m/s for 8 mm diameter nozzle. Various laboratory tests were performed for obtaining engineering properties of used sediment i.e., clay, sand and gravel. A test was conducted for identification of minerals present in the clay sample. Depending upon the moisture content present in cohesive sediment, their engineering properties were measured. The experimental setup, discharge measurement device, calibration of Venturimeter, procedure for preparation of the sediment bed under different clay percent with gravel and with sand-gravel mixtures, method of compaction, description on unconfined compressive strength test of the sediment material and measurement of scour parameters are described in this chapter. The collected data are systematically tabulated for analysis of data in the respect of maximum static and maximum dynamic scour depth, temporal variation of scour depth, dune height, scour radius and volume of scour hole in the next chapter.

CHAPTER 4

ANALYSIS OF DATA, RESULTS AND DISCUSSIONS FOR COHESIONLESS SEDIMENT

4.1 PRELIMINARY REMARKS

This chapter elaborates the analysis of data recorded in the experiments conducted to study scour in cohesionless sediment under submerged circular vertical water jets. First, the laboratory tests were conducted to know the sediment properties also the salient observations during the experimentation are discussed. Then, the characteristics of scour, different shapes of scour bed profiles are discussed in detail. The comparisons of temporal variation of scour depth in cohesionless sediment i.e. sand, sand-gravel mixture and gravel have been made. The results found from analysis of the experimental data due to jets in cohesionless are presented to address temporal variation of scour depth, maximum static scour depth, and maximum dynamic scour depth. Further, the chapter explicated the existing relationships prescribed for scour under submerged circular vertical impinging jets in cohesionless sediment along with associated variables using the experimental dataset of the present investigation. Based on the functional relationship, new equations are proposed for the estimation of maximum static and maximum dynamic scour depth and the same are validated. Analysis of data have been carried out in respect of volume of scour hole, radius of scour hole, height of dune and new relationship to estimate the above scour parameters have been proposed.

4.2 SALIENT OBSERVATIONS IN COHESIONLESS SEDIMENT

Three different types of cohesionless sediment beds were prepared to understand the behavior of the scour phenomenon due to vertical impinging water jets. In this experimental study, the observations of temporal variation of scour depth, maximum dynamic and maximum static depth of scour were measured with the help of point gauge. It should be noted that, all the experiments were conducted until the equilibrium condition was attained. The static and dynamic scour hole profiles produced by water jets were axissymmetric, i.e., measurement of bed level along one diagonal was sufficient to define the complete scour hole geometry. When the scour process reaches equilibrium condition, the scour bed profiles appear on the sediment beds after turning the jet off. The radius of scour hole, volume of scour hole, height of dune were measured for all types of cohesionless sediment i.e. sand, sand-gravel mixtures and gravel.

The characteristics of scour due to submerged circular vertical water jets in three different types of cohesionless sediments were found to be different from each other. The depth of scour, volume of scour, radius of scour hole and the dune height were found different for each sediment bed conditions. Photographic views of experimental scour hole profiles of sand, sand-gravel mixture and gravel are shown in Figs. 4.1 to 4.3, respectively, as illustration. Figs. 4.1a-d show various shapes of scour hole profile for sand beds while Figs.4.2a-d show the same for sand-gravel beds and Figs. 4.3a-d show various shapes of scour hole profile for gravel beds.

A close investigation of scour bed profiles reveals that the observed static and dynamic scour depth was maximum in the case of sand beds as compared to gravel and sand-gravel beds. However, sand-gravel mixtures also produced high dynamic scour depth in few experimental runs and it was observed that both the static and dynamic scour depth are minimum in gravel beds due to heavy weight of the gravel resulting in less movement of the sediment particle under submerged circular vertical jets.

The volume of scour hole, radius of scour hole, dune height were observed maximum in sand beds as compared to gravel and sand-gravel mixture sediment beds. However, it was minimum in gravel beds. This is due to light weight of sand particle compared to the gravel particle. Therefore, it can be concluded that the sediment size have significant effect on scour depth and size of scour hole produced by water jets. It was also seen that the high nozzle size, low jet height and high jet velocity produces maximum dynamic depth of scour.

The size of scour hole, dune height was observed maximum in case of sand beds which produce maximum size of scour hole as evident from Figs. 4.1a-d. The static scour depth (when the jet flow was stopped) was found minimum in case of gravel beds as compared to sand and sand-gravel mixtures beds because after stopping the jet, gravel deposited on scour hole fall inside it due to its weight. Also the shapes of scour hole profiles was observed smallest in case of gravel beds and found maximum in sand beds. In case of sand-gravel mixture, fine material i.e. sand observed to be deposited on the outer boundary of dune. However, gravel observed to be deposited inside portion of dune which signifies segregation of finer material from coarser one due to submerged jet action as evident from Figs. 4.2a-d.

Run no. S1, d_o = 12.5 mm,
u_o = 7.19 m/s, h_j = 0.30 m, d_{50} = 0.24 mm

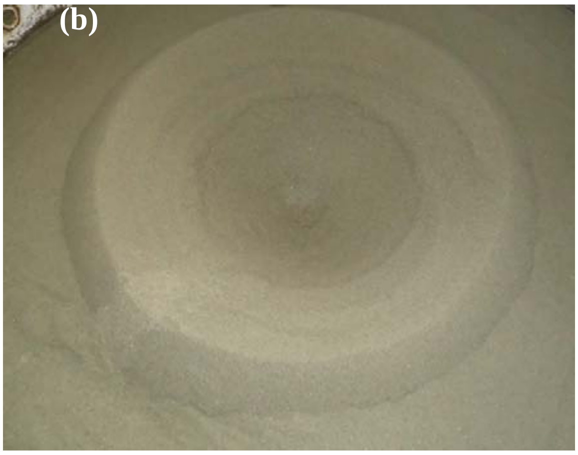

Run no. S2, d_o = 12.5 mm,
u_o = 7.19 m/s, h_j = 0.15 m, d_{50} = 0.24 mm

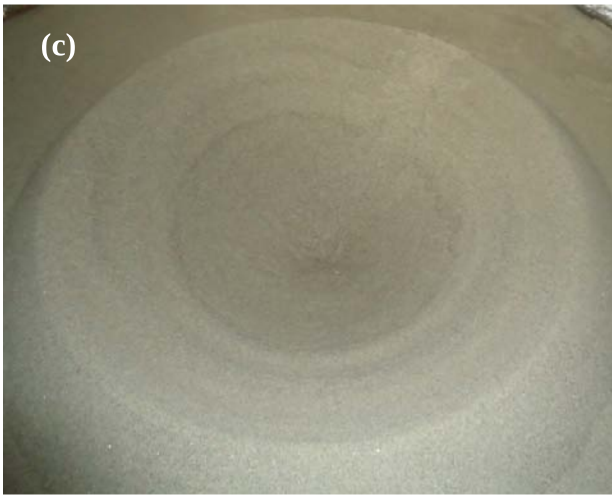

Run no. S5, d_o = 8 mm,
u_o = 9.84 m/s, h_j = 0.30 m, d_{50} = 0.24 mm

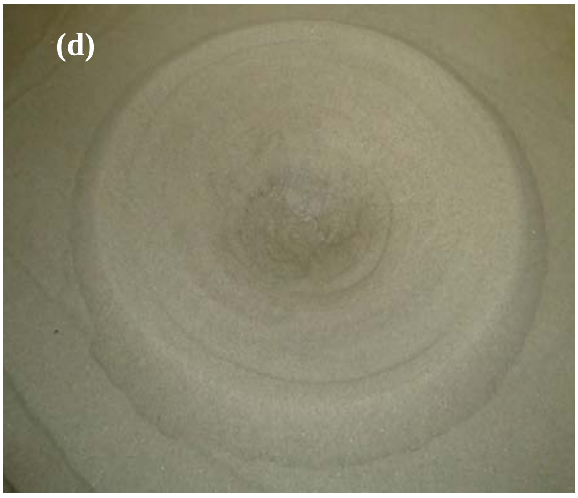

Run no. S6, d_o = 8 mm,
u_o = 9.84 m/s, h_j = 0.15 m, d_{50} = 0.24 mm

Fig. 4.1 View of developed scour hole profiles in sand beds

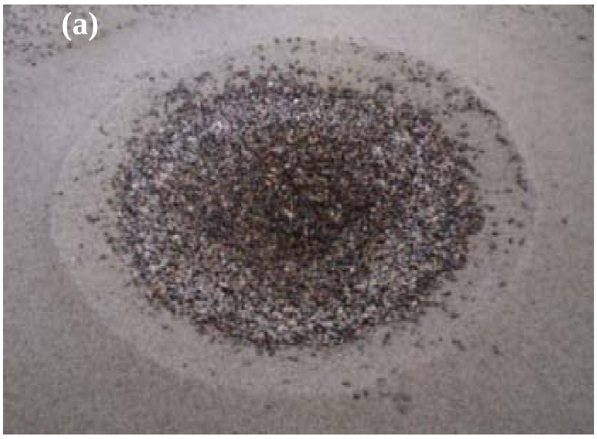

Run no. SG1, d_o = 12.5 mm,
u_o = 7.19 m/s, h_j = 0.30 m, d_a = 1.47 mm

Run no. SG2, d_o = 12.5 mm,
u_o = 7.19 m/s, h_j = 0.15 m, d_a = 1.47 mm

Run no. SG5, d_o = 8 mm,
u_o = 9.84 m/s, h_j = 0.30 m, d_a = 1.47 mm

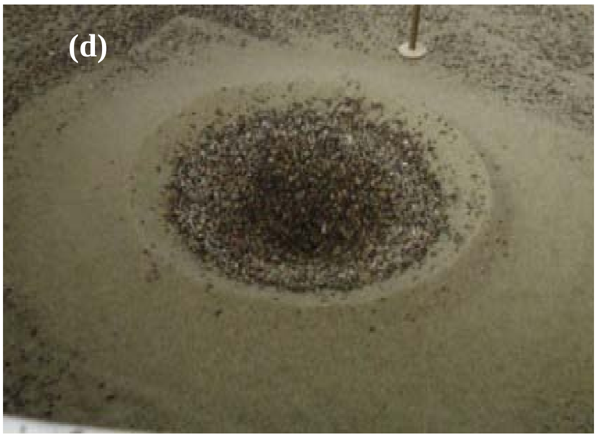

Run no. SG6, d_o = 8 mm,
u_o = 9.84 m/s, h_j = 0.15 m, d_a = 1.47 mm

Fig. 4.2 View of developed scour hole profiles in sand-gravel beds

Run no. G1, d_o = 12.5mm,
u_o = 7.19 m/s, h_j = 0.30 m, d_{50} = 2.7 mm

Run no. G2, d_o = 12.5mm,
u_o = 7.19 m/s, h_j = 0.15 m, d_{50} = 2.7 mm

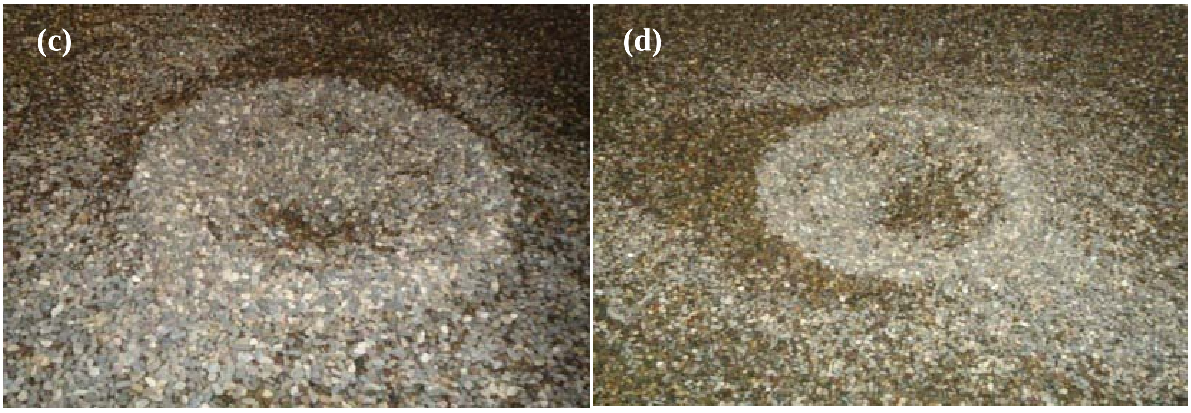

Run no. G5, d_o = 8 mm, u_o = 9.84 m/s, h_j = 0.30 m, d_{50} = 2.7 mm

Run no. G6, d_o = 8 mm, u_o = 9.84 m/s, h_j = 0.15 m, d_{50} = 2.7 mm

Fig. 4.3 View of developed scour hole profiles in gravel beds

4.3 TEMPORAL VARIATION OF SCOUR DEPTH IN COHESIONLESS SEDIMENT

4.3.1 Temporal Variation of Scour Depth with 12.5 mm Nozzle Diameter

(a) Sand bed

The experiment were conducted under submerged circular vertical impinging water jets in sand beds to know the temporal variation of scour depth. Fig. 4.4 presents the temporal variation of scour depth with time for 12.5 mm nozzle in sand bed for selected runs, as illustration. It was found that the 99 percent of scour is completed in 40 minutes from start of the experiment. The maximum dynamic scour depths were found for low jet height and high jet velocity. The static scour depth was observed minimum for above conditions this is may be due to jet off condition, all the sediment particle get settled on the scoured bed profiles. For higher jet height, the dynamic depth of scour was observed minimum as compared to above conditions and static scour depth was found maximum due to impact of jet velocity and jet height.

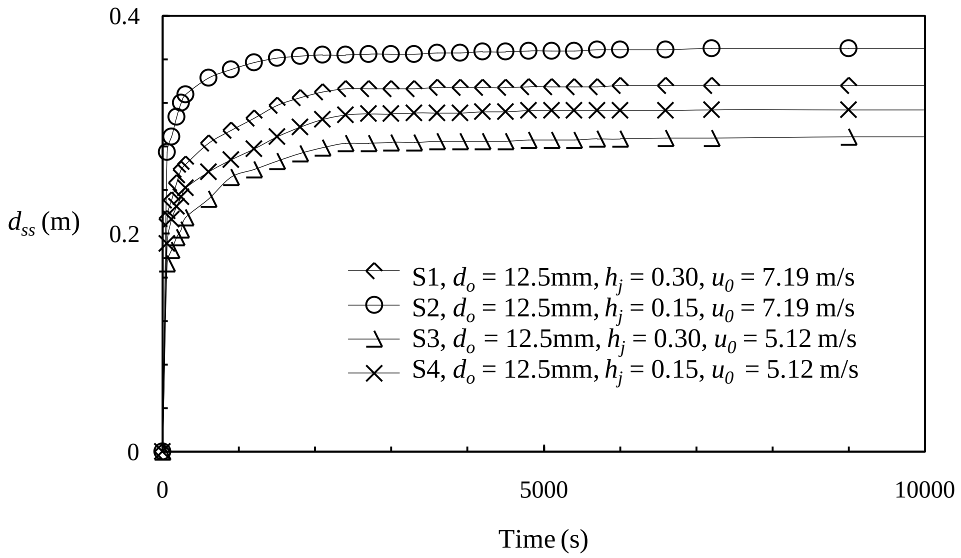

Fig. 4.4 Temporal variation of scour depth with time for 12.5 mm nozzle in sand bed

(b) Sand-gravel mixtures bed

The temporal variation of scour depth in sand gravel sediment mixtures bed for the nozzle size 12.5 mm shows that the 99 percent of scour is completed in 55 minutes from start of the experiment. Fig. 4.5 presents the temporal variation of scour depth with time for 12.5 mm nozzle in sand-gravel mixture beds. It was found that the sand-gravel mixture bed have higher dynamic and static scour depth as compared to gravel bed but lower compare to sand bed. For higher jet height, the dynamic depth of scour was observed low while static scour depth high. This could be due to separation of sediment by virtue of turbulence as the turbulence is more for higher jet height and vice versa. The temporal variation of scour depth revealed that more than 70 % of the scour depth occurred in first 30 min from the start of the experiment, a feature that was also noticed earlier by Clarke (1962), Rajaratnam (1982) and Ansari et al. (2003).

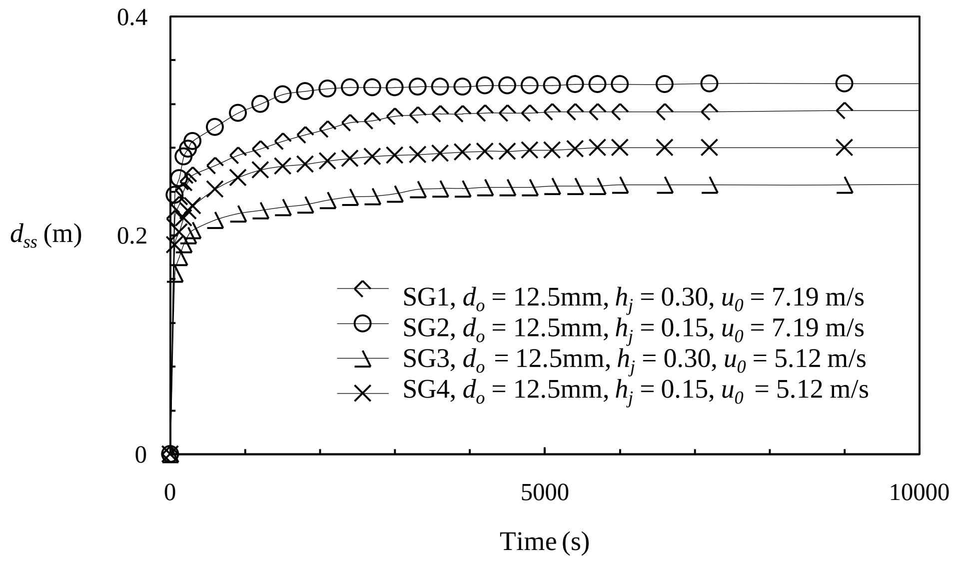

Fig. 4.5 Temporal variation of scour depth with time for 12.5 mm nozzle in sand-gravel mixtures bed

(c) Gravel bed

The temporal variation of scour depth in gravel bed for 12.5 mm nozzle size revealed that the 99 percent of scour is completed in 65 minutes from start of the experiment. Fig. 4.6 presents the temporal variation of scour depth with time for 12.5 mm nozzle in gravel bed for selected runs, as illustration. It may be noticed that the gravel bed take longer time to reach in equilibrium conditions compared to sand beds. Dynamic and static scour depths are low in gravel beds compared to sand beds. This reveals that the sediment size have significant role in scouring process under submerged circular vertical jets.

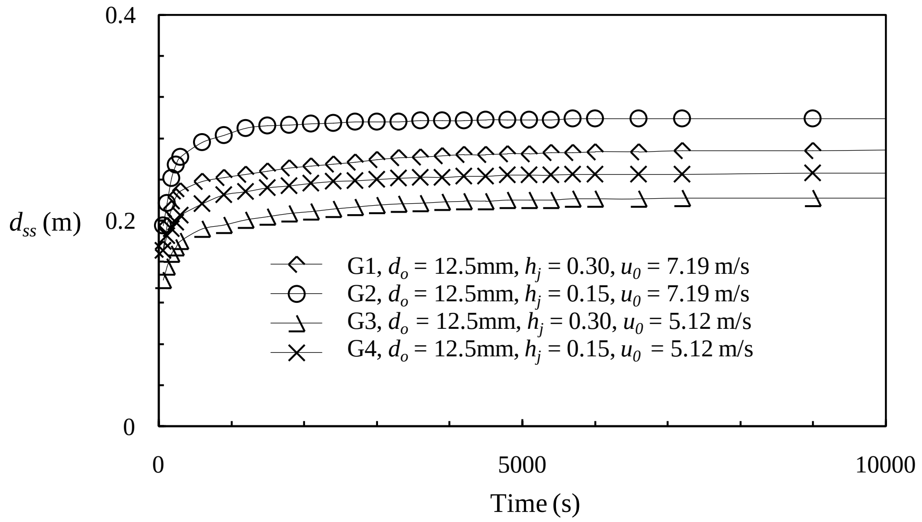

Fig. 4.6 Temporal variation of scour depth with time for 12.5 mm nozzle in gravel bed

4.3.2 Temporal Variation of Scour Depth with 8 mm Nozzle Diameter

(a) Sand bed

The temporal variation of scour depth under submerged circular vertical jets in sand bed were conducted using 8 mm nozzle size and found that 99 percent of scour is completed in 45 minutes from start of the experiment that is almost similar to 12.5 mm nozzle. Fig. 4.7 presents the temporal variation of scour depth with time for 8 mm nozzle in sand bed. The measured maximum static and dynamic scour depths for 8 mm diameter nozzle are different than the 12.5 mm diameter. The dynamic depth of scour under 8 mm nozzle diameter was found higher compared to 12.5 mm nozzle diameter for other parameters constant.

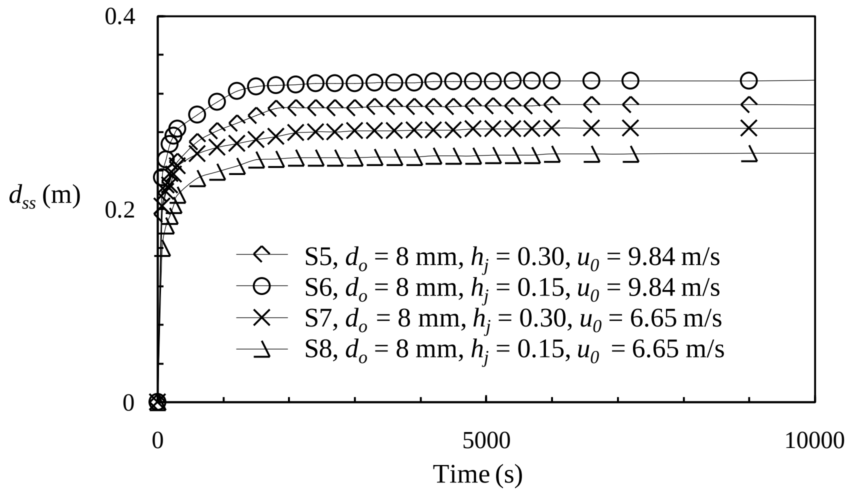

Fig. 4.7 Temporal variation of scour depth with time for 8 mm nozzle in sand bed

(b) Sand-gravel mixtures bed

The temporal variation of scour depth in sand-gravel mixtures bed using 8 mm nozzle size revealed that the 99 percent of scour is completed in 55 minutes from start of the experiment which is almost similar to 12.5 mm nozzle. Fig. 4.8 presents the temporal variation of scour depth with time for 8 mm nozzle in sand-gravel mixture. It was found that the sand-gravel mixture bed have high dynamic and static scour depths as compared to gravel bed but low compare to sand bed. For higher jet height, the dynamic depth of scour was observed low and static scour depth was found more because of separation of sediment due to turbulence as the turbulence is more for higher jet height and vice versa.

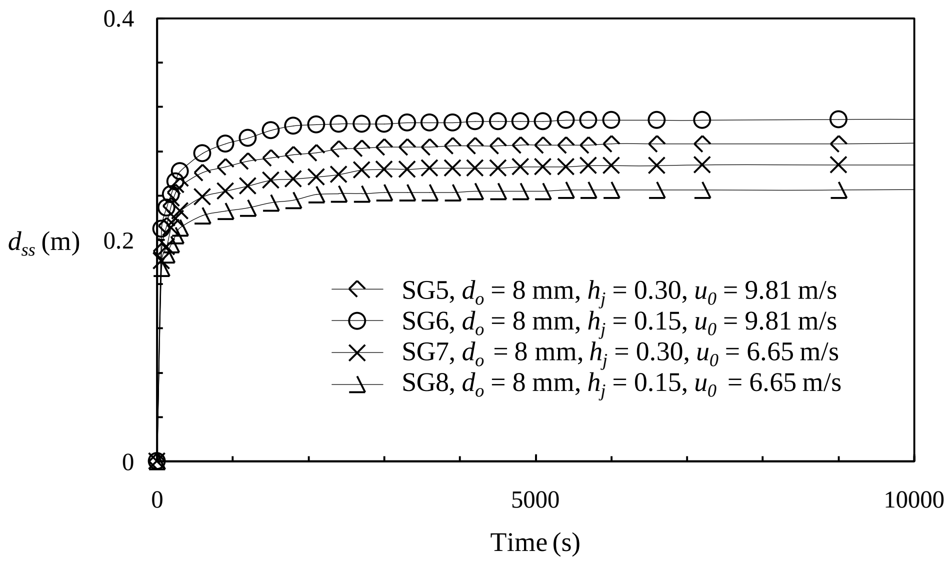

Fig. 4.8 Temporal variation of scour depth with time for 8 mm nozzle in sand-gravel bed

(c) Gravel bed

The temporal variation of scour depth in gravel bed for 8 mm nozzle size reveals that the 99 percent of scour is completed in 70 minutes from start of the experiment. Fig. 4.9 presents the temporal variation of scour depth with time for 8 mm nozzle in gravel bed. It may be noticed that the gravel bed take longer time to reach in equilibrium condition compared to sand and sand-gravel mixture. Low dynamic and static depth of scours as compared to sand and sand-gravel mixture beds were found due to heavy weight of the gravel particles.

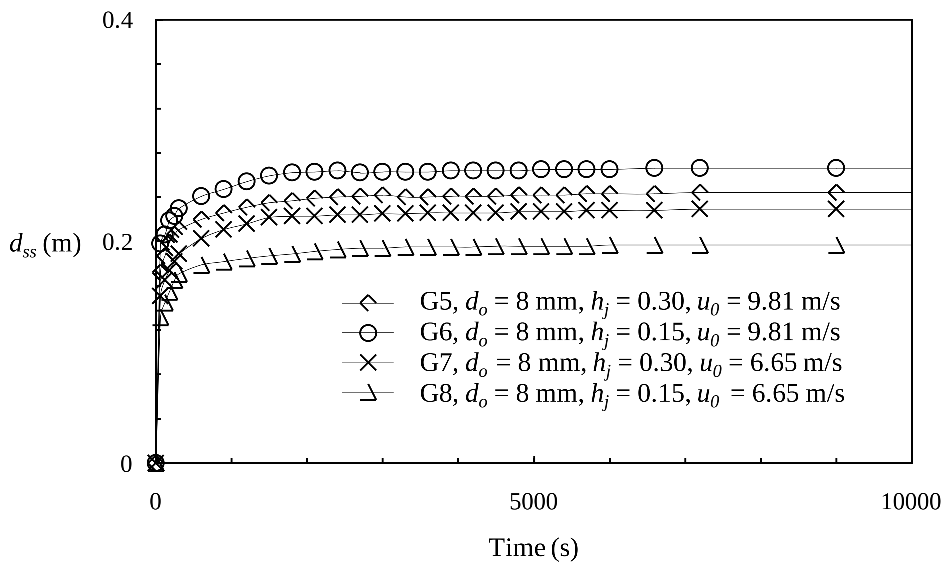

Fig. 4.9 Temporal variation of scour depth with time for 8 mm nozzle in gravel bed

4.3.3 Comparison of Temporal Variation of Scour Depth

Figures 4.10 to 4.11 show comparison of temporal variation of scour depth in three different types of cohesionless sediment i.e. fine sand, sand-gravel mixture and gravel for two hydraulic conditions, as illustration. It is apparent from these figures that maximum depth of scour occurs in sand bed followed by sand-gravel mixture and gravel. Minimum scour was found in gravel beds which reveals that the sediment size play significant role in scouring process.

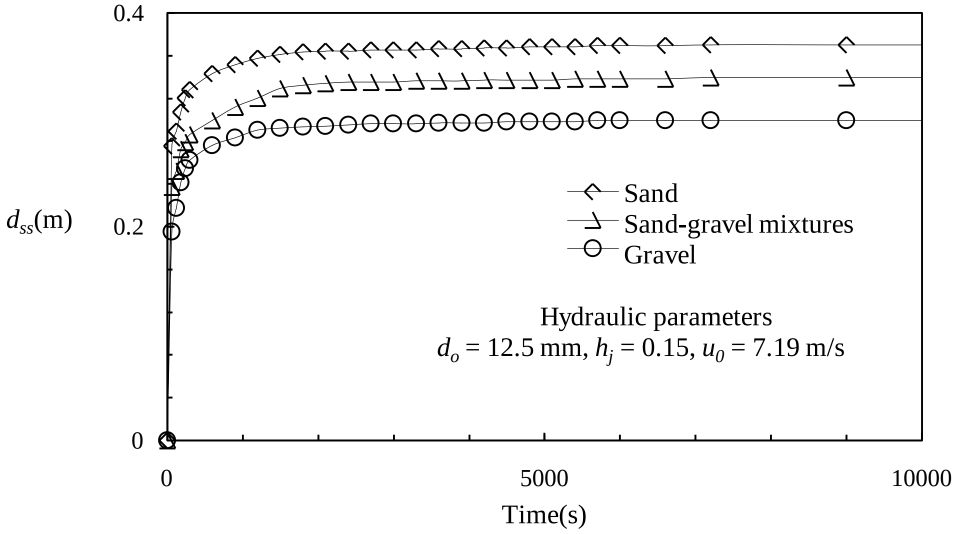

Fig. 4.10 Comparison of temporal variation of scour depths in sand, sand-gravel mixture and gravel beds for run no. S2, SG2 and G2

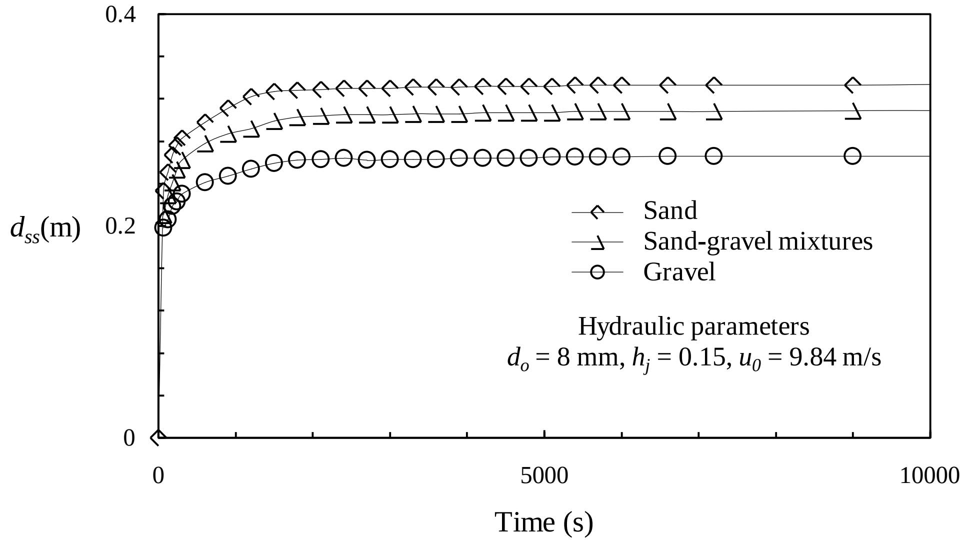

Fig. 4.11 Comparison of temporal variation of scour depths in sand, sand-gravel mixture and gravel beds for run no. S6, SG6 and G6

4.3.4 Development of Relationship for Estimation of Scour Depth With Respect to Time

Moore and Mach (1962) and Hanson (1990) have suggested that the dimensional analysis can be an important tool for development of equation for various scour parameters. The temporal evaluation of the maximum depth of scour in cohesionless sediment i.e. sand, sand-gravel mixtures and gravel, under submerged circular vertical impinging water jets have been analyzed herein using dimensional analysis.

The probable parameters affecting various aspects of scour process are;

$$u_o, d_o, d_{50}, d_a, h_j, g, t, T_s \tag{4.1}$$

For an example, maximum static scour depth is function of the following variables which may be written as;

$$d_{sms} = f\left(u_o, d_o, d_{50}, d_a, h_j, g\right) \tag{4.2}$$

Considering the parameter h_j, u_o as repeating variables, and the above functional form may be converted into dimensionless form as;

$$\left(\frac{d_{sms}}{h_j}\right) = f\left(\frac{d_o}{h_j}, \frac{d_a}{h_j}, \frac{d_{50}}{h_j}, \frac{u_o}{\sqrt{gh_j}}\right) \tag{4.3}$$

Same procedure has been adopted to develop functional relationship for other scour parameters, however, in case of cohesive sediment mixture, P_c has been included.

4.3.5 Relationship for Saturation Time

The saturation time, T_s is defined as time required from start of the scour process to achieve 99% of the total scour. The effect of various dimensionless parameters on T_s has been analyzed and it is found that d_a/h_j, d_o/h_j and $u_o/\sqrt{gh_j}$ are the main parameters that affects the T_s value. A relationship (Eq. 4.4) is proposed for the estimation of saturation time in cohesionless sediment consisting of sand, sand-gravel mixture and gravel.

$$T_s/(h_j / u_o) = 1500(d_a / h_j)^{0.223}(d_o / h_j)^{-0.014}(u_o / \sqrt{gh_j})^{0.647} \quad (R^2=0.93) \tag{4.4}$$

Equation (4.4) was tested for the data collected in present study for cohesionless sediment.

It is found that Eq. (4.4) predicts saturation time within error bend of ± 10 % as shown in Fig. 4.12.

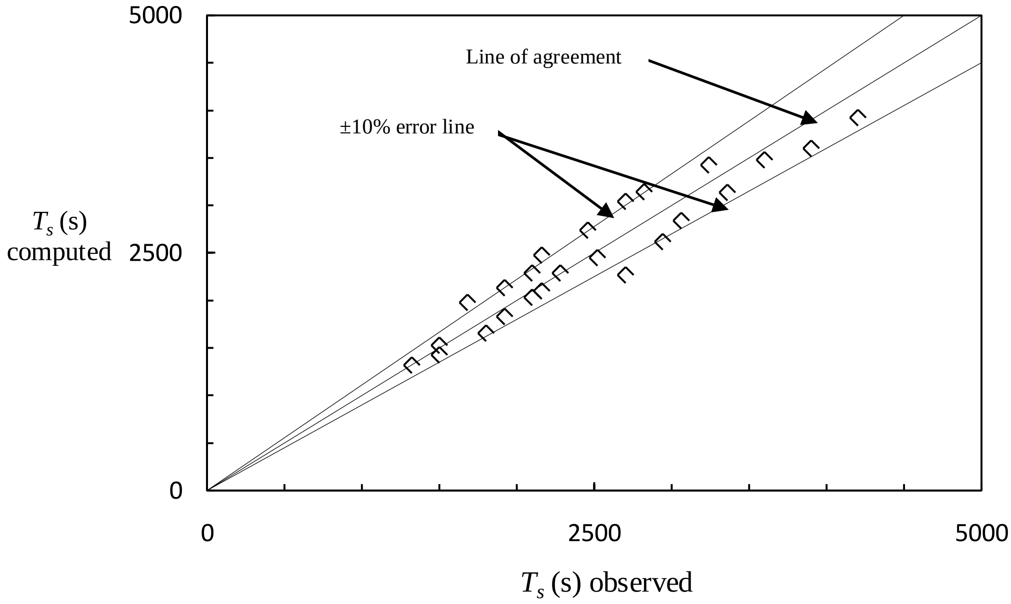

Fig. 4.12 Comparison of observed and computed saturation time in cohesionless sediment

It may be mentioned here that various other functional forms of the relations viz. exponential, power, logarithmic etc. were also attempted for describing the temporal variation of scour depth under submerged circular vertical impinging water jets. The variation in saturation time was also studied with other hydraulic parameters such as $d_a/h_j, u_o/\sqrt{gd_o}$ or $d_o/h_j, u_o/\sqrt{gd_a}$ however, the best results obtained are reported herein.

To develop a relationship for estimation of temporal variation of scour depth, relevant data are plotted in dimensionless scour depth d_{ss}/d_{dms} with dimensionless time t/T_s as shown in Figs. 4.13, 4.14 and 4.15 for sand, sand-gravel mixture and gravel, respectively (here d_{dms} = dynamic maximum scour depth at equilibrium).

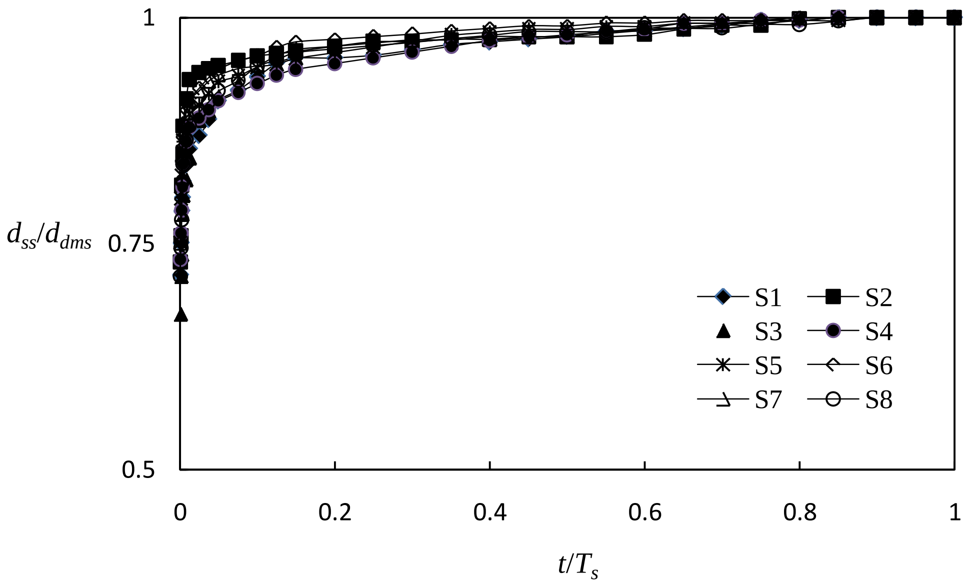

Fig. 4.13 Variation of d_{ss}/d_{dms} with t/T_s in sand bed

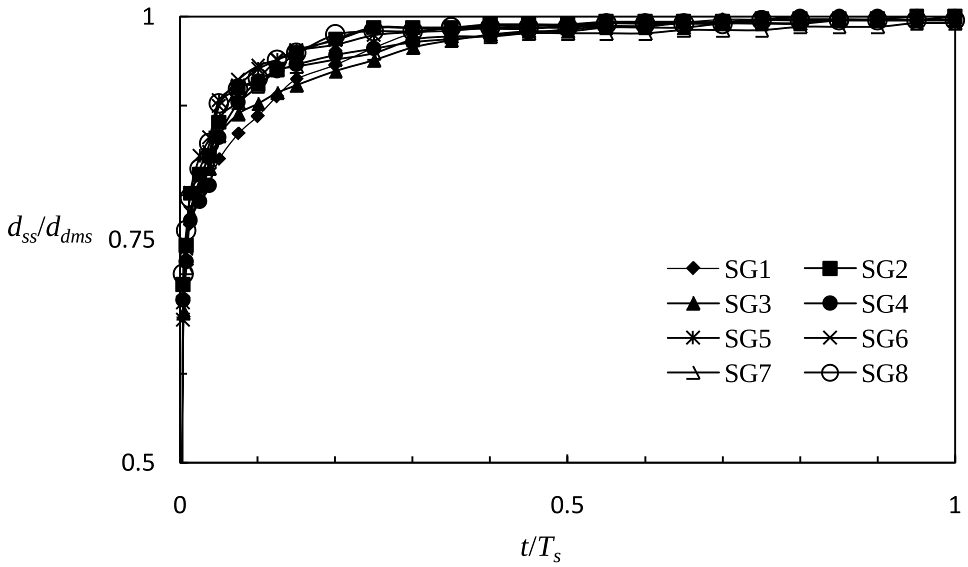

Fig. 4.14 Variation of d_{ss}/d_{dms} with t/T_s in sand-gravel mixtures bed

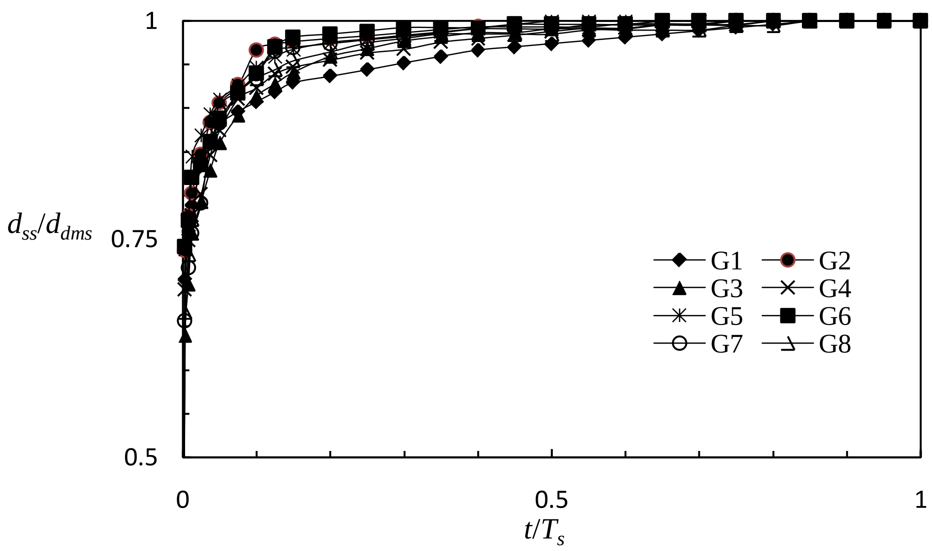

Fig. 4.15 Variation of d_{ss}/d_{dms} with t/T_s in gravel bed

Form the above figures, it is found that the temporal variation of scour depth follows a sin curve for better indication of the variation in between these two parameters. Therefore, Figs. 4.13 to 4.15 are re-plotted for dimensionless scour depth d_{ss}/d_{dms} with dimensionless time $\sin(\pi t/2T_s)$ in Figs. 4.16, 4.17 and 4.18 for sand, sand-gravel mixtures and gravel respectively.

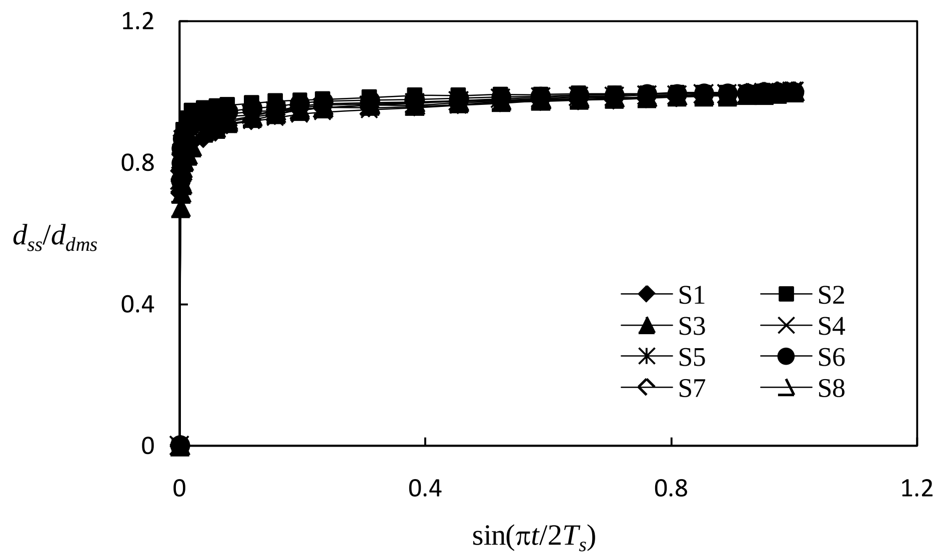

Fig. 4.16 Variation of d_{ss}/d_{dms} with $\sin(\pi t/2T_s)$ in sand bed

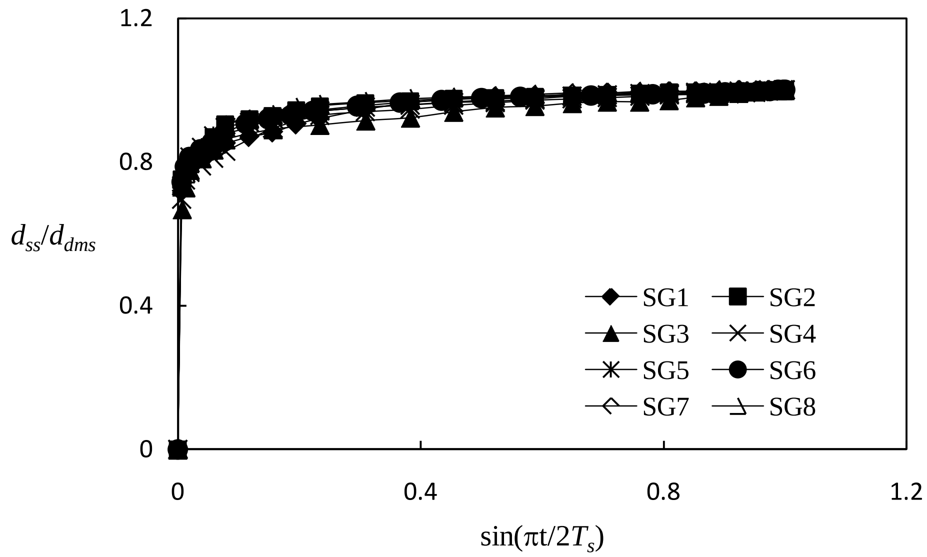

Fig. 4.17 Variation of d_{ss}/d_{dms} with $\sin(\pi t/2T_s)$ in sand-gravel bed

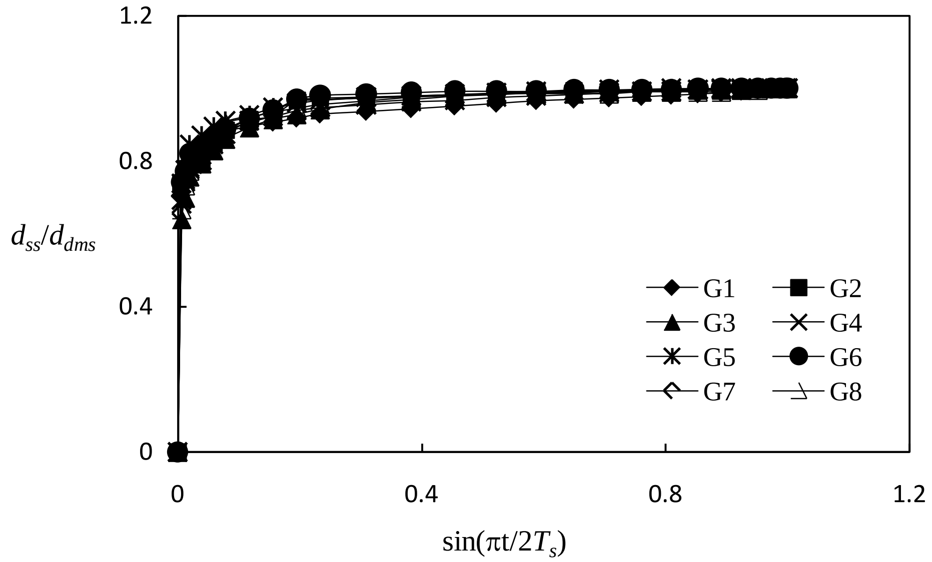

Fig. 4.18 Variation of d_{ss}/d_{dms} with $\sin(\pi t/2T_s)$ in gravel bed

Various investigators (Lui et al., 1961, Sarma, 1967, Islam et al., 1986, Ansari et. al. 2003) have suggested empirical relationships for temporal variation of scour depth in cohesionless sediments. Figs. 4.16 to 4.18 reveal that the following functional relationship satisfactorily described the temporal variation of maximum scour depth under submerged circular vertical impinging water jets in cohesionless sediment consisting of sand, sand-gravel mixture and gravel;

$$\frac{d_{ss}}{d_{dms}} = \left[\sin\left(\frac{\pi t}{2T_s}\right)\right]^{m_s} \qquad (4.5)$$

Kumar (1996) also noticed that the temporal variation of scour depth around bridge piers in cohesionless sediment to follow the above mentioned equation.

4.3.5.1 Relationship for the value exponent

In order to estimate the temporal variation of scour depth, the value of exponent (m_s) which appears in the equation for temporal variation of scour depth (Eq. 4.5) is needed a priori. The effect of various dimensionless parameters on m_s has been analyzed and it is found that d_a/h_j, d_o/h_j and $u_o/\sqrt{gh_j}$ are the main parameters that affects the m_s value. The following equation is proposed to compute the value of exponent using presently collected data.

$$m_s = 0.064\left(\frac{d_a}{h_j}\right)^{0.158}\left(\frac{d_o}{h_j}\right)^{-0.153}\left(\frac{u_o}{\sqrt{gh_j}}\right)^{-0.090} \qquad (R^2 = 0.98) \qquad (4.6)$$

The suitability of the proposed relationship was analyzed in observed and computed conditions and it was found that Eq. (4.6) predicts the value of m_s within error band of ± 10 % as shown in Fig. 4.19.

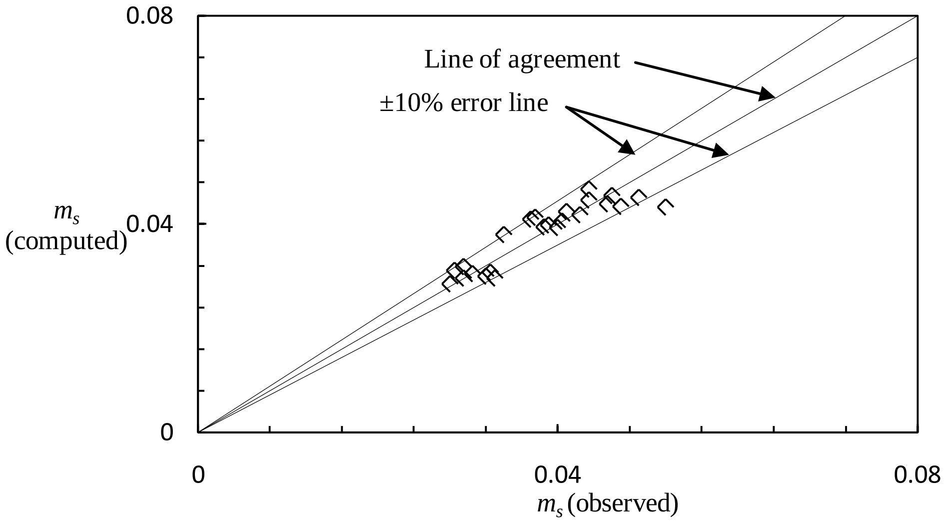

Fig. 4.19 Comparison of observed and computed exponent, m_s value in cohesionless sediment

The variation of m_s was also studied with other dimensionless groups viz; $d_a/h_j, u_o/\sqrt{gd_o}$ or $d_o/h_j, u_o/\sqrt{gd_a}$, however, a weak correlation was observed with these variables.

4.3.5.2 Validation of the proposed relationship for estimation of scour depth with time

The proposed Eqs. (4.4), (4.5) and (4.6) for estimation of scour depth with time were validated using data of cohesionless sediment i.e. sand, sand-gravel mixtures and gravel as shown in Figs. 4.20, 4.21 and 4.22, as illustration. It is apparent that computation of temporal scour depth using Eq. (4.5) is quite satisfactory.

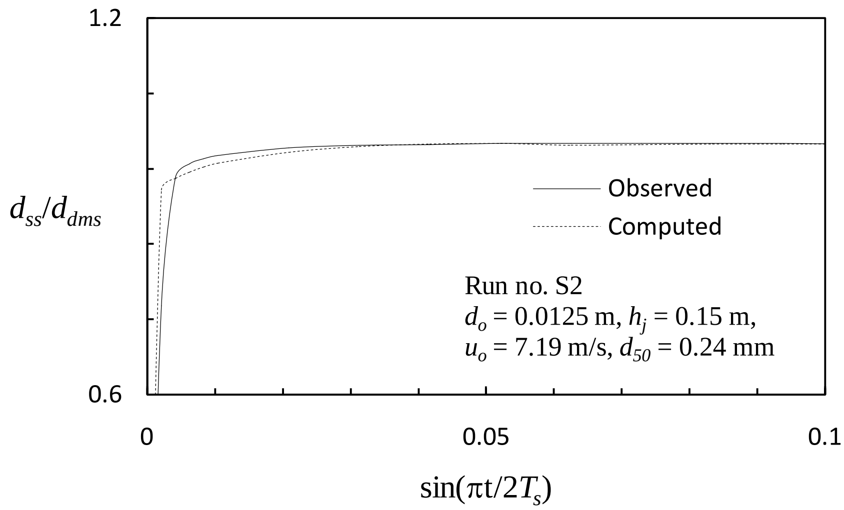

Fig. 4.20 Comparison of computed scour depth using Eq. (4.5) with observed values in sand beds for run S2

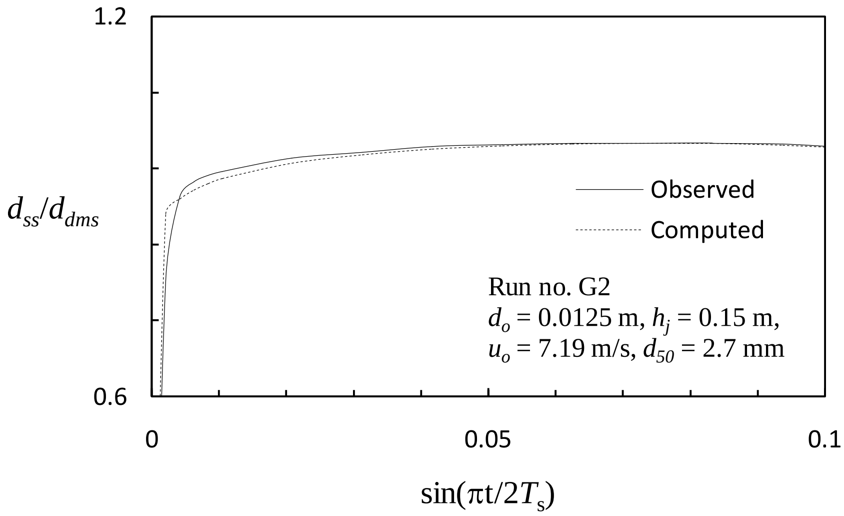

Fig. 4.21 Comparison of computed scour depth using Eq. (4.5) with observed values in gravel beds for run G2

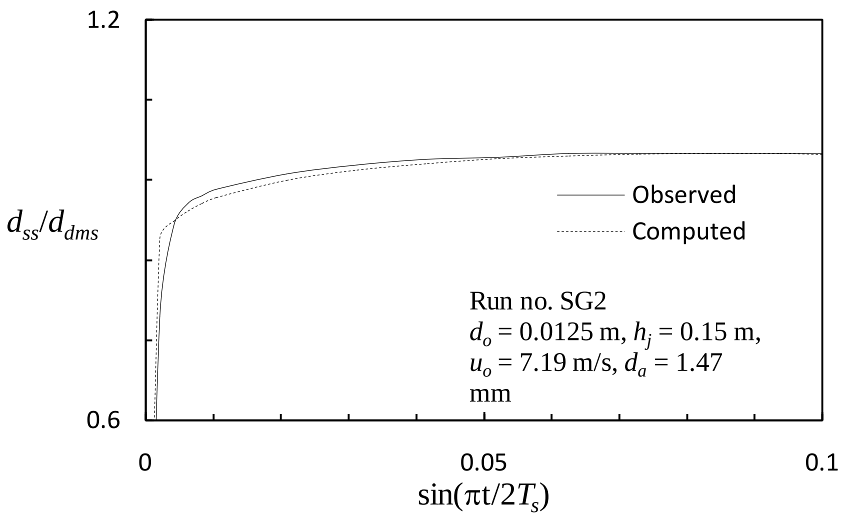

Fig. 4.22 Comparison of computed scour depth using Eq. (4.5) with observed values in sand-gravel mixtures for run SG2

4.4 ESTIMATION OF VARIOUS SCOUR PARAMETERS

Equations for various scour parameters like maximum static scour depth, maximum dynamic scour depth, radius of scour hole, height of dune and volume of scour hole have been proposed using the data collected in the present study and that available in literature.

4.4.1 Maximum Static Scour Depth

Sarma (1967), Westrich and Kobus (1973) and Rajaratnam (1982), Aderibigbe and Rajaratnam (1996) and Ansari et al. (2003) identified non-dimensional parameter (E_c). It was used to describe the process of estimation of maximum static scour depth and can be expressed by the following equation;

$$E_c = u_o\left(\frac{d_o}{h_j}\right)/\sqrt{\left(\frac{g d_{50}\Delta\rho_s}{\rho_f}\right)} \tag{4.7}$$

Involving the E_c, Aderibigbe and Rajaratnam (1996) proposed the following equation for static maximum scour depth;

$$\frac{d_{sms}}{h_j} = 1.26(E_c)^{0.11} - 1.0 \tag{4.8}$$

The accuracy of the Eq. (4.8) in estimation of maximum static scour depth was checked using data of present study and those collected from the literature. It is to be noted that wide range of data have been used herein compared to earlier studies. It was found that the Eq. (4.8) predicts the d_{sms} within ± 30 percent error as shown in Fig. 4.23.

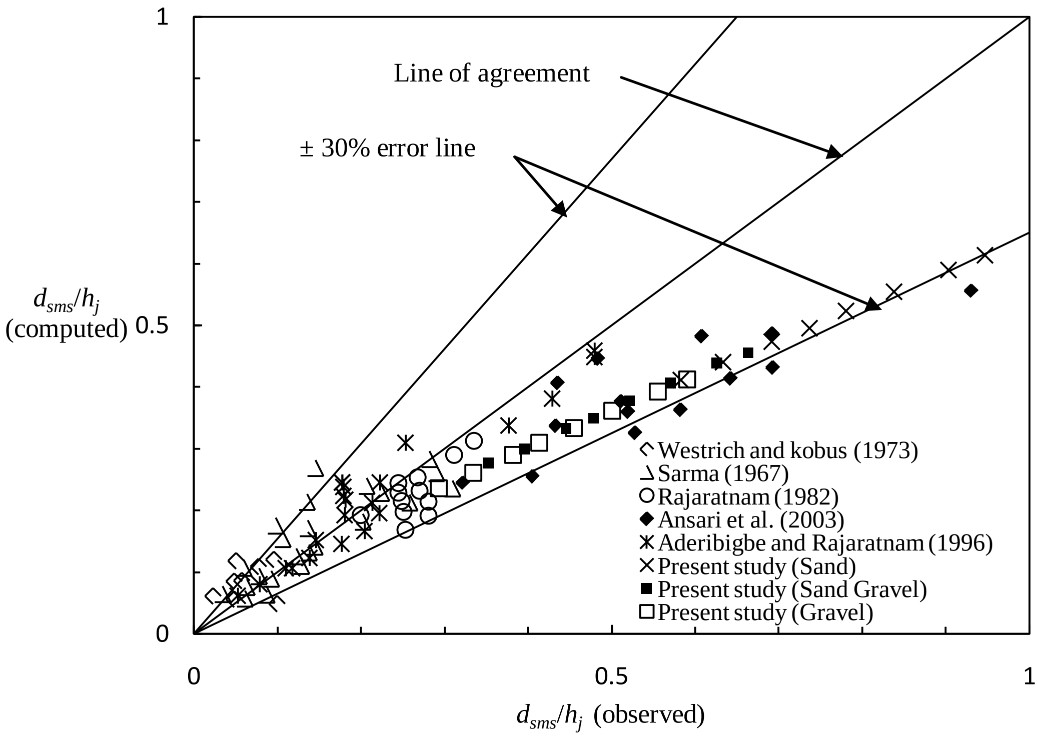

Fig. 4.23 Comparison of observed and computed depth of scour for present and previous data using Eq. (4.8)

Ansari et al. (2003) modified Eq. (4.8) and proposed the following equation for estimation of maximum static scour depth;

$$\frac{d_{sms}}{h_j} = 1.30(E_c)^{0.15} - 1.0 \tag{4.9}$$

Equation (4.9) was tested with presently collected data and those collected by previous investigation and it was found that the equation predicts the d_{sms} within ± 25 percent error line as shown in Fig. 4.24.

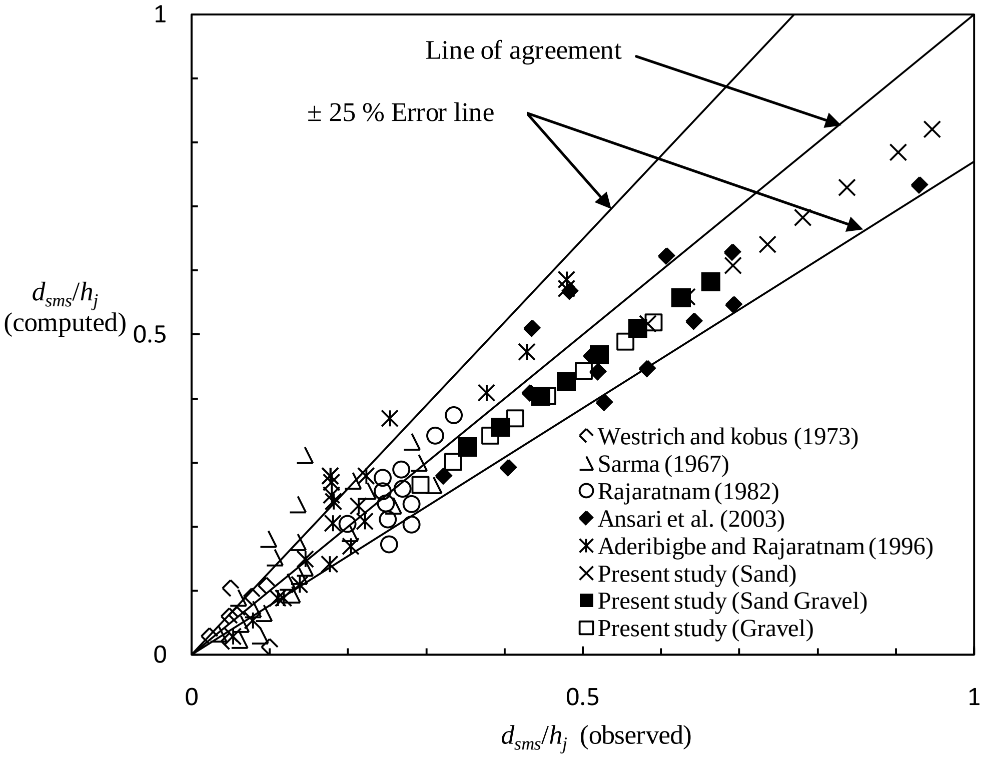

Fig. 4.24 Comparison of observed and computed depth of scour for present and previous data using Eq. (4.9)

Variation of dimensionless maximum static scour depth with E_c is shown in Fig. 4.25 for all the available data which reveals that the static scour increases with increase of erosion parameter. A close study of Fig. 4.25 indicates that Aderibigbe and Rajaratnam (1996) equation does not follow the trend of data particularly for higher value of E_c. Thus modification in Eq. (4.8) is required for better description of the relationship between the two parameters under submerged circular vertical water jets in case of cohesionless sediment. The following equation is proposed for maximum static scour depth using the available data;

$$\frac{d_{sms}}{h_j} = 1.33(E_c)^{0.17} - 1.0 \tag{4.10}$$

The plots of given data between the two variable E_c and d_{sms}/h_j represents the variation in a better way in present investigation in comparison to the relationship proposed by previous investigators.

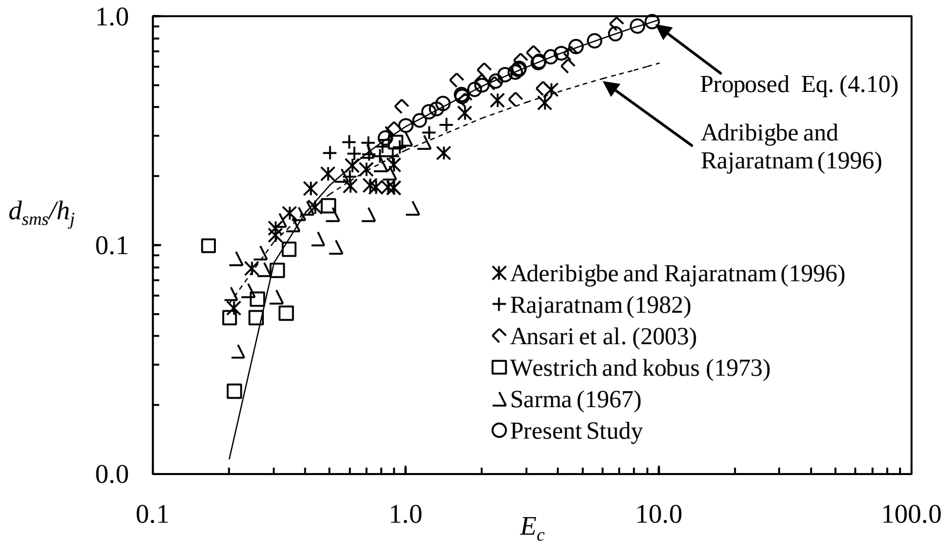

Fig. 4.25 Variation of d_{sms} / h_j with erosion parameter E_c in cohesionless sediment

Eq. (4.10) was also used to compute the maximum scour depth for the whole data collected (present and previous study data). The comparison of computed scour depth with observed scour depth yielded that present equation is able to produce the results with maximum error $\pm 20\%$ for all data as shown in Fig. 4.26. This plot shows that results estimated by the present proposed relationship produced minimum error as compared to the data estimated by previous relationships.

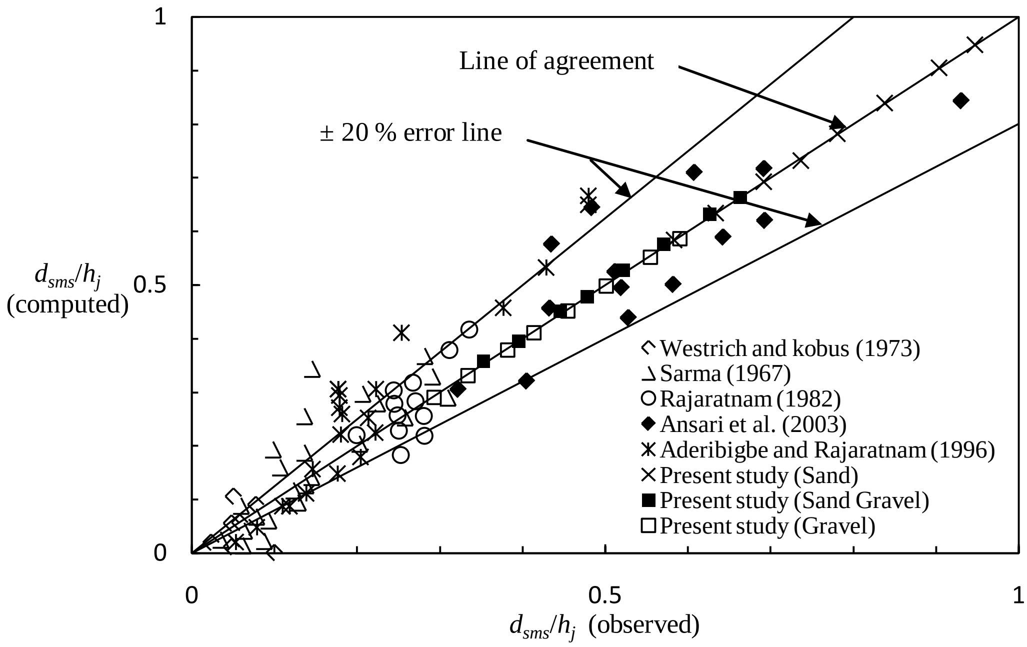

Fig. 4.26 Comparison of observed and computed maximum depth of scour using proposed relationship (Eq. 10)

Further, the data of maximum static scour depth (d_{sms}/h_j) were also studied with sediment size, nozzle diameter and jet velocity. It is found that variation of maximum static scour depth can be well explained with these parameters in place of erosion parameter (E_c). Analysis of data reveals that the static scour depth increases with decrease of sediment size and increase of nozzle diameter and jet velocity. Further, the data were analyzed using multiple regression analysis. At outset, Eq. (4.11) is proposed by using available data which predicts the maximum scour depth with ± 10 percent error band as shown in Fig. 4.27. The proposed relationship for maximum static scour depth is as follows;

$$d_{sms}/h_j = 0.23\left(\frac{d_a}{h_j}\right)^{-0.221}\left(\frac{d_o}{h_j}\right)^{0.516}\left(\frac{u_o}{\sqrt{gh_j}}\right)^{0.52578} \quad (R^2=0.92) \tag{4.11}$$

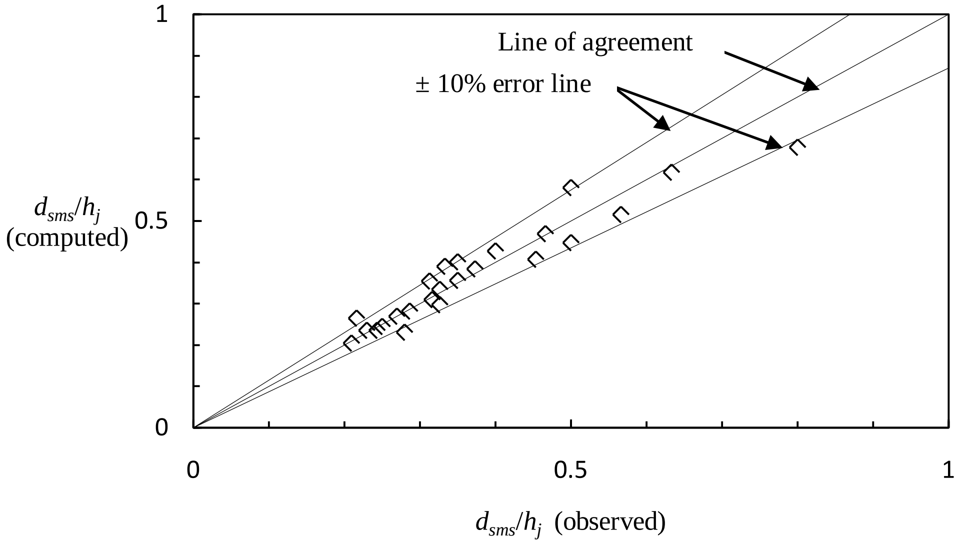

Fig. 4.27 Comparison of observed and computed maximum static scour depth (d_{sms}) using Eq. (4.11)

4.4.2 Maximum Dynamic Scour Depth

It is found from analysis of data that the dynamic scour depth increases with decrease of sediment size and increase of nozzle diameter and jet velocity. The variation of maximum dynamic scour depth is studied with the similar parameters as that of maximum static scour depth and the data were analyzed using multiple regression analysis. Eq. (4.12) is proposed using multiple regression analysis.

$$d_{dms}/h_j = 2.69\left(\frac{d_a}{h_j}\right)^{-0.096}\left(\frac{d_o}{h_j}\right)^{0.765}\left(\frac{u_o}{\sqrt{gh_j}}\right)^{0.69} \qquad (R^2 = 0.97) \qquad (4.12)$$

Equation (4.12) predicts the maximum dynamic scour depth within ± 10 percent as shown in Fig. 4.28.

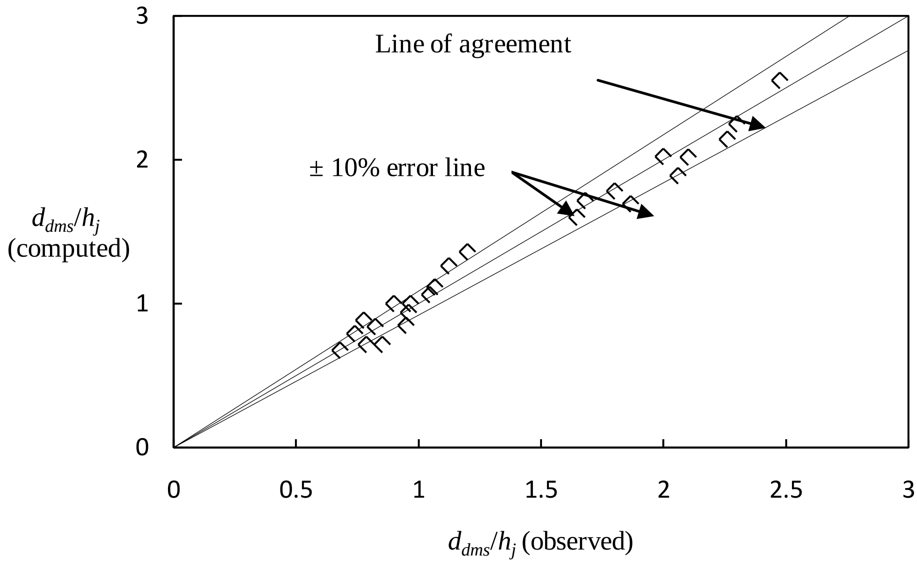

Fig. 4.28 Comparison of observed and computed maximum dynamic scour depth (d_{dms}) using Eq. (4.12)

Ratio of maximum dynamic and maximum static depths of scour were also analyzed as shown in Fig. 4.29 and found that this ratio increases with E_c for sand, sand-gravel mixture and gravel beds. However, increasing trend is slow in the sand compared to sand-gravel mixture and gravel. This is to be noticed that the gravel beds have almost similar pattern as observed in sand-gravel sediment mixtures. This may be due to fact that after saturation time only gravel particles remain in the scoured hole due to its high particle weight compared sand. Being small in size and light weight, the sand particles move away from the scour bed. In the view of this, the sand-gravel sediment beds behave like a gravel beds after saturation time.

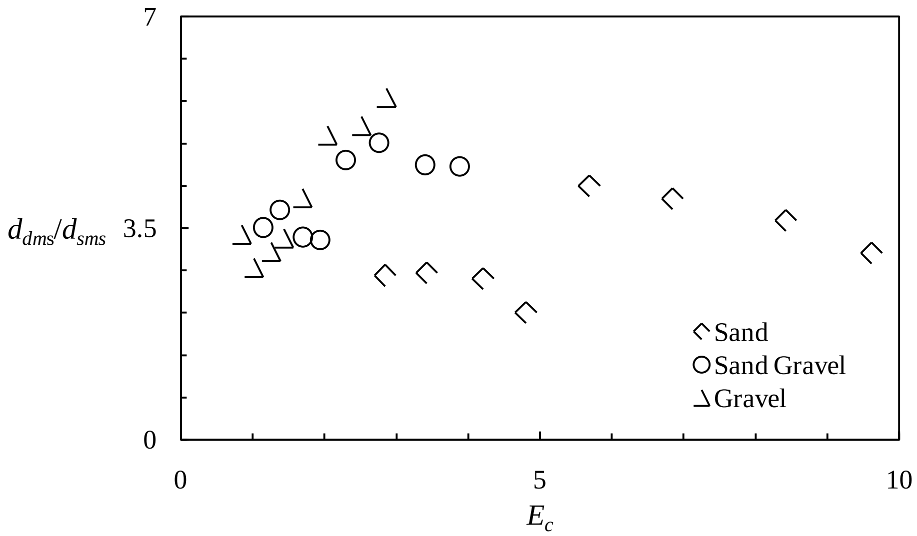

Fig. 4.29 Variation of ratio of maximum dynamic and maximum static scour depths with erosion parameter

4.4.3 Radius of Scour Hole

The variation in radius of scour hole with erosion parameter for data of previous investigators such as Clark (1962), Rajaratnam (1982), Aderibigbe and Rajaratnam (1996) and those collected in the present investigation in cohesionless sediment consisting of sand, sand-gravel mixture and gravel were analyzed.

The variation of radius of scour hole with the value of erosion parameter is shown in Fig. 4.30 which reveals that the radius of scour hole has increasing trend with erosion parameter for the data collected in the present study. This is consistent with the data collected by previous investigators. Eq. (4.13) is evolved to estimate the radius of scour hole which is able to compute the radius of scour hole within ± 20 % error band, which is shown in Fig. 4.31. This can be described by the following equations

$$r / h_j = 0.239(E_c) + 0.262 \qquad (R^2 = 0.95) \qquad (4.13)$$

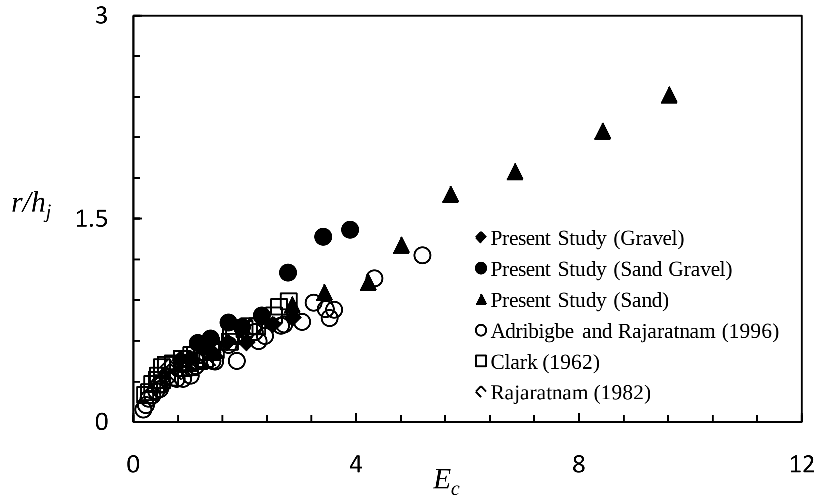

Fig. 4.30 Variation of radius of scour hole (r) with erosion parameter (E_c)

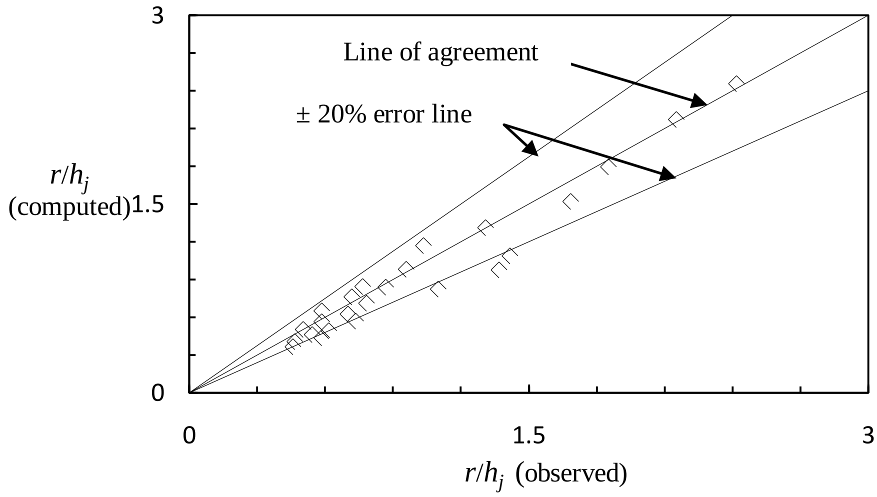

Fig. 4.31 Comparison of observed and computed radius of scour hole using Eq. (4.13)

Further analysis of data in this respect reveals that radius of scour hole can be accurately calculated using dimensionless parameters d_a / h_j, d_o / h_j and $u_o / \sqrt{gh_j}$ in place of erosion parameter. It is found that the radius of scour hole increases with decrease of sediment size and with increase of nozzle diameter and jet velocity. Eq. (4.14) is evolved to estimate the radius of scour hole in cohesionless sediment consisting of sand, sand-gravel mixture and gravel which able to compute the radius of scour hole within ± 15 % error band as shown in Fig. 4.32.

$$r / h_j = 0.323\left(\frac{d_a}{h_j}\right)^{-0.348}\left(\frac{d_o}{h_j}\right)^{0.640}\left(\frac{u_o}{\sqrt{gh_j}}\right)^{0.707} \quad (R^2 = 0.89) \qquad (4.14)$$

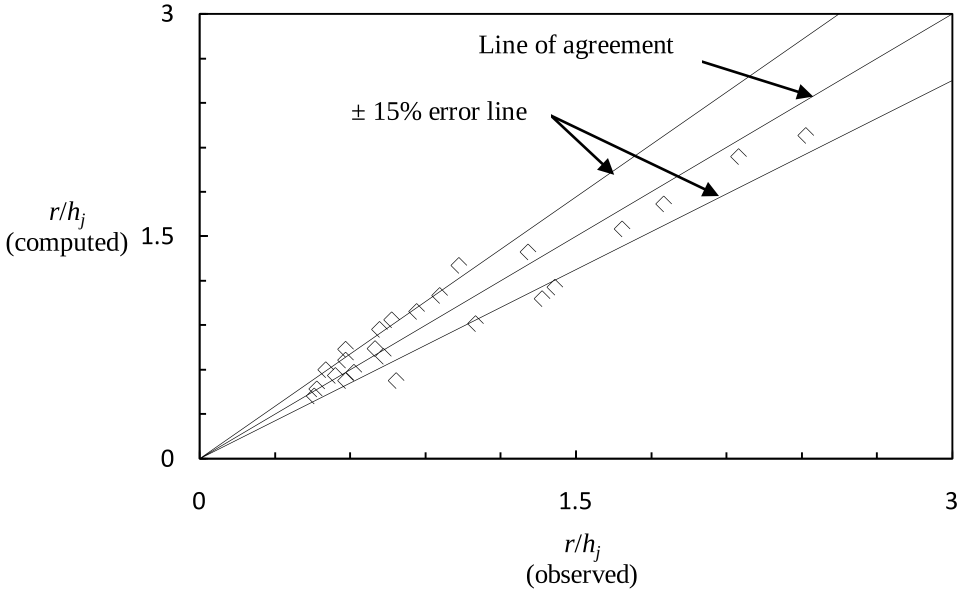

Fig. 4.32 Comparison of observed and computed radius of scour hole using Eq. (4.14)

4.4.4 Dune Height

The variation of dune height was also studied with erosion parameter for data of present study as well as data of previous investigators as shown in Fig. 4.33. It is found that the dune height show increasing trend with erosion parameter for the data collected in the present and previous investigators. It is worthy to mention here that the wide range of erosion parameter is studied in case of present study.

In Fig. 4.33, it may be noticed that the Clark (1962) data deviate from the rest of all previous and present data beyond the erosion parameter, E_c = 3 and, therefore, the Clark's data is not used for fitting the equation. The evaluation of Clark's depth of scour against the time data represents that his laboratory works were not conducted for enough time to reach in equilibrium state (Aderibigbe and Rajaratnam, 1996). The variation of dune height is able to compute the radius of scour hole within ± 20 % error band as shown in Fig. 4.34, which can be described as

$$\Delta / h_j = 0.032(E_c) + 0.009 \qquad (R^2=0.85) \qquad (4.15)$$

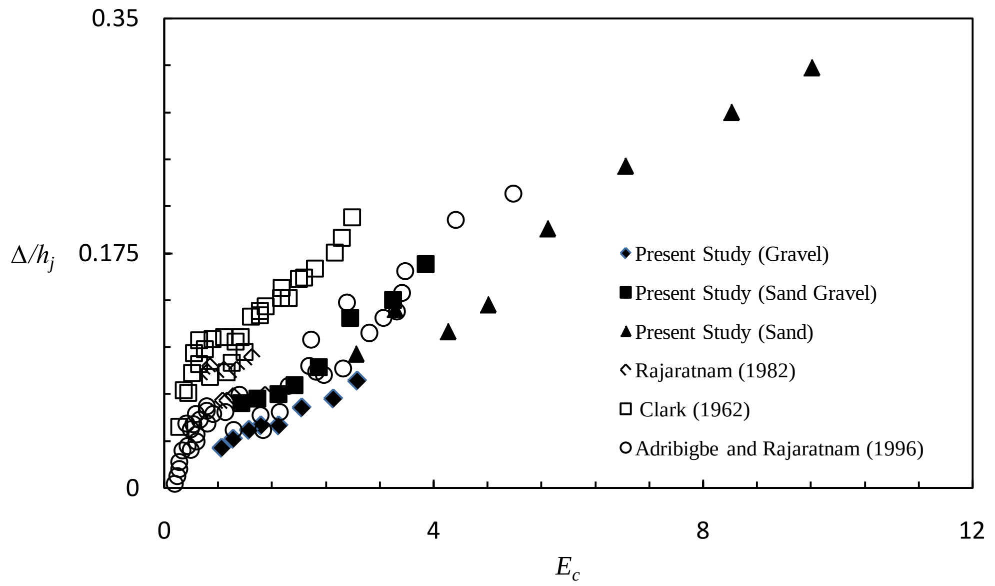

Fig 4.33 Variation of height of dune, Δ with erosion parameter, E_c

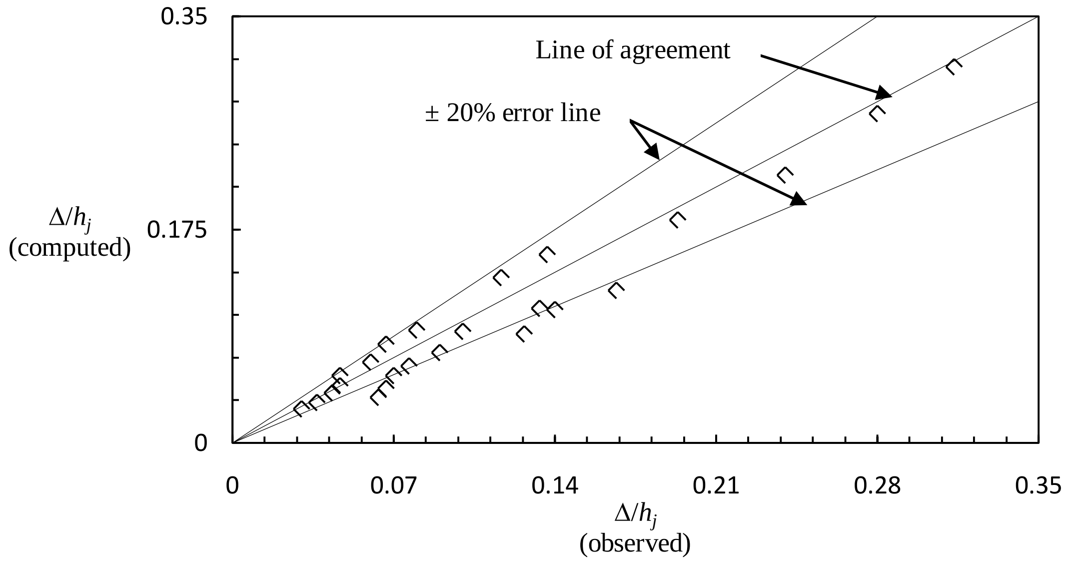

Fig. 4.34 Comparison of observed and computed dune height using Eq. (4.15)

However, further analysis reveals that the dune height can be better related to the dimensionless parameters d_a / h_j , d_o / h_j and $u_o / \sqrt{gh_j}$ in place of erosion parameter. Analysis of data reveals that the dune height increases with decrease of sediment size and increase with nozzle diameter and jet velocity. Therefore, Eq. (4.16) is proposed that can predict dune height with ± 15 % error as shown in Fig. 4.35.

$$\Delta / h_j = 0.034 \left(\frac{d_a}{h_j} \right)^{-0.471} \left(\frac{d_o}{h_j} \right)^{0.861} \left(\frac{u_o}{\sqrt{g h_j}} \right)^{0.725} \qquad (R^2 = 0.87) \qquad (4.16)$$

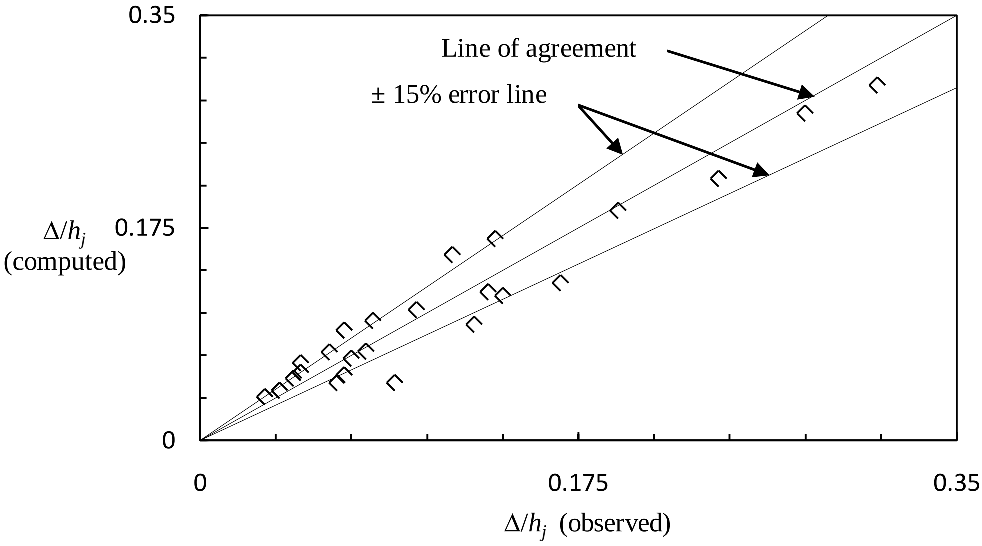

Fig. 4.35 Comparison of observed and computed dune height (Δ) in cohesionless sediment

4.4.5 Volume of Scour Hole

The volume of scour hole was measured for each experimental run. The variation of volume of scour hole with erosion parameter is shown in Fig. 4.36. The variation of volume of scour hole with respect to the erosion parameter reveals that the volume of scour increases linearly with increase of erosion parameter. It may be noticed that the sand bed have maximum volume of scour as compared to gravel and the sand-gravel mixtures. Low volume of scour was observed in gravel beds. Higher jet velocity produces high scour volume.

Equation (4.17) is proposed to estimate volume of scour hole with erosion parameter that can predict volume of scour within ± 25 % error as shown in Fig. 4.37.

$$\frac{\nabla}{h_j^3} = 0.743(E_c) - 1.012 \qquad (R^2 = 0.86) \qquad (4.17)$$

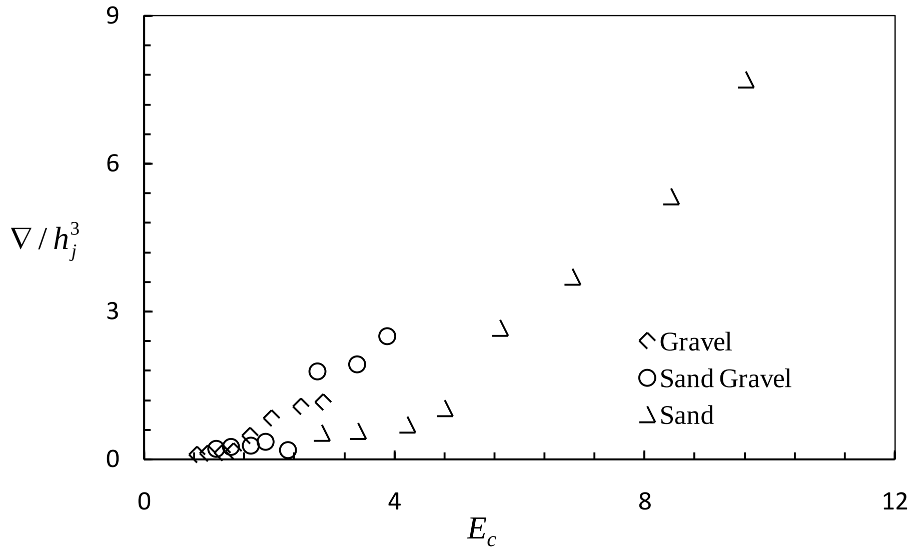

Fig. 4.36 Variation in volume of scour hole with erosion parameter, E_c

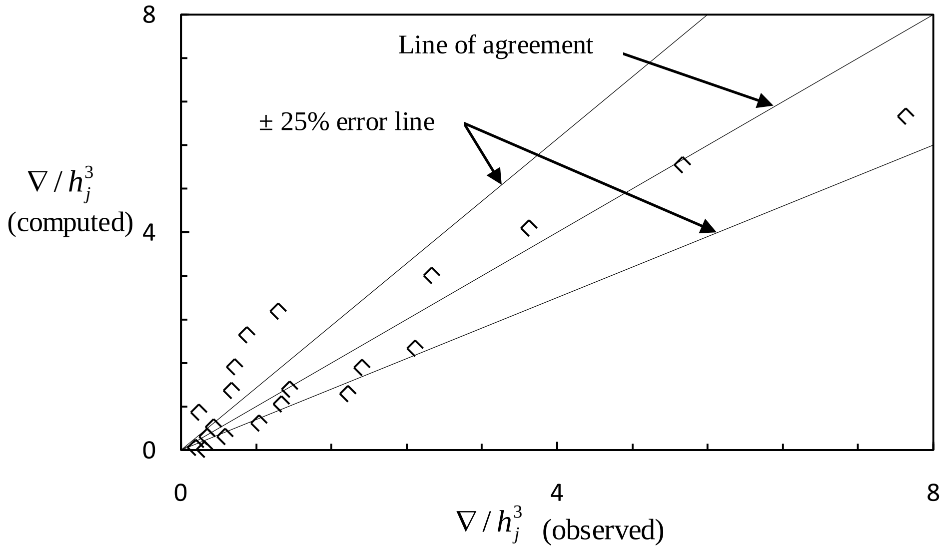

Fig. 4.37 Comparison of observed and computed volume of scour hole using Eq. (4.17)

Further analysis of the data reveal that volume of scour hole can be better related to the dimensionless parameters d_a / h_j , d_o / h_j and $u_o / \sqrt{gh_j}$ in place of erosion parameter. Analysis of data reveals that volume of scour increases with nozzle diameter and jet velocity and reduces with sediment size. Eq. (4.18) is evolved to estimate the volume of scour hole using the data collected in the present study.. It was found the proposed relationship is able to predict dune height with ± 15 percent error as shown in Fig. 4.38.

$$\nabla / h_j^3 = 0.9617\left(\frac{d_a}{h_j}\right)^{-0.649}\left(\frac{d_o}{h_j}\right)^{2.21}\left(\frac{u_o}{\sqrt{gh_j}}\right)^{1.88} \qquad (R^2 = 0.96) \qquad (4.18)$$

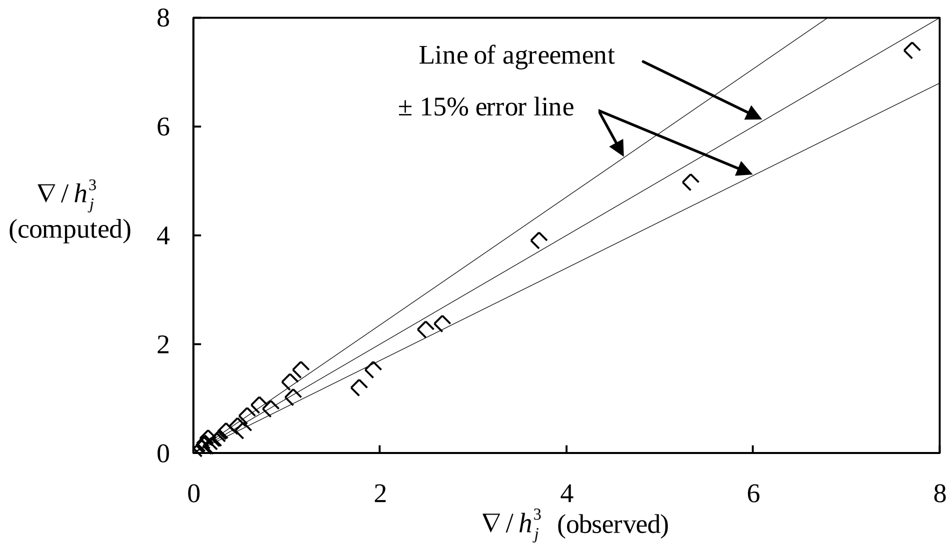

Fig. 4.38 Comparison of observed and computed volume of scour hole using Eq. (4.18)

The variation of radius of scour hole, dune height and volume of scour hole were also studied with other hydraulic parameters. However, the best results obtained are reported herein.

4.5 CONCLUDING REMARKS

The experimental data collected under submerged circular vertical impinging water jets in various configurations of the bed material have been analyzed in this chapter. The effect of various parameters related to scour were investigated for cohesionless sediment and their mixture i.e. sand, sand-gravel mixture and gravel under various permutations and combinations of the test conditions. Analysis regarding the temporal variation of scour depth in cohesionless sediment has been presented using the data obtained in the present research work and the data available from previous investigators. The existing equations developed by previous investigators were used for the computation of temporal variation of scour depth and a new equation for computation of scour depth with time has been proposed. Using experimental data working relationships are established for computation of maximum static and maximum dynamic scour depth. The relationships are also proposed for other length scale scour parameters like radius of scour hole, dune height and volume of scour hole have been quantified.

CHAPTER 5

ANALYSIS OF DATA, RESULTS AND DISCUSSIONS IN COHESIVE SEDIMENT MIXTURES

5.1 PRELIMINARY REMARKS

This chapter elaborates the analysis of data recorded in the experiments conducted for scour in cohesive sediment mixtures under submerged circular vertical water jets. First, the laboratory tests were conducted to determine the engineering properties of the cohesive sediment mixtures like unconfined compressive strength, moisture content, dry density, bulk density, void ratio etc. Also the procedure for preparation of sediment bed and the salient observations during the experimentation have been discussed. The characteristics of scour in respect of shapes of scour bed profiles are discussed in detail. Temporal variations of scour depth in cohesive sediment mixture have also been analyzed. The maximum static scour depth and maximum dynamic scour depth are compared. This chapter explicates the existing relationships prescribed for scour depth computation under submerged circular vertical impinging jets in cohesive sediment mixtures. Based on the functional relationship, new equations are proposed for the estimation of maximum static and maximum dynamic scour depth. In addition, the temporal variation of scour depth, volume of scour hole, radius of scour hole, height of dune are analyzed and new relationships have been developed to estimate the above scour parameters in clay-gravel and clay-sand-gravel mixtures.

5.2 SCOUR IN CLAY-GRAVEL MIXTURES

The process of scour under submerged circular vertical impinging water jets in clay-gravel cohesive sediment beds is discussed here. The cohesive sediment beds of clay-gravel were prepared by varying clay percentages from 10% to 60% by weight with gravel. Initially, the laboratory tests were conducted to determine the engineering properties of the clay-gravel mixtures like unconfined compressive strength, moisture content, dry density, bulk density and void ratio. The observations were taken for temporal variation of dynamic scour depth, maximum static scour depth, volume of scour hole, dune height and radius of scour hole.

The characteristics of scour due to submerged circular vertical jets in clay-gravel cohesive sediment mixtures were found different than the cohesionless sediments. The behavior of the scour phenomenon i.e., scour hole profiles, maximum dynamic and static scour depth, volume of scour, radius of scour hole and the dune height were found to vary with clay percentage in the mixtures.

The photographic view of scour bed profiles in clay-gravel mixtures is shown in Figs. 5.1a-f, which shows various shapes of scour bed profiles in different clay percent with gravel.

The characteristics of scour due to submerged circular vertical water jets in 10 % clay with gravel was seen almost to have similar behavior as in gravel beds. There was little or no influence of cohesion in these particular sediment mixtures on scour parameters. The extent of scour hole profiles at low jet height was found to be minimum and the clay was found deposited at the periphery of the dune. The scour depth was found maximum in dynamic condition as compared to static condition. This is due to fact that when the water jet is being stopped the moving sediment particles get settled on the scoured bed. The volume of scour hole, radius of scour hole, height of dune was observed and found almost similar to that were observed in gravel beds. It was also seen that large nozzle size produces high depth of scour at low jet height and high jet velocity.

In case of 20 % clay with gravel mixture, the cohesion influence was observed on static and dynamic depth of scour (Fig. 1b). The volume of scour hole, radius of scour hole, height of dune have different behavior to that observed in cohesionless sediment consisting of gravel.

The difference between static and dynamic depth of scour decreases with increase in percentage of clay (greater than 30 %) in clay-gravel mixture (Fig. 1c). The deposition of clay sediment was seen at the ridge of boundary of scour hole.

With further increase of clay percentage in sediment bed (greater than 40 %), the scour holes had almost vertical profile (Fig. 1d). The slope of the sides of the scour holes was found to be almost 90^{o} in most cases. The scour of these sediment mixtures was found to occur in the form of lumps of varying shapes and sizes. However, in few experimental runs the scour hole had irregular shapes and geometry. The formation of dune was seen very small and the sediment deposited far away from the scour hole profiles in the form of lumps and chunks.

A close investigation of scour bed profiles revealed that the dynamic scour depth was observed maximum up to 30 % clay in clay-gravel mixture (Fig. 1d). A large difference in the value of static and dynamic scour depths was found in clay-gravel mixture having higher percentage of gravel. However, with clay percentage greater than 30 % in clay-gravel mixture, the static and dynamic scour depth appear almost same due to high clay percentage. As the clay percent increases, influence of cohesion in the sediment mixture also increases.

In the case of 50 % clay with gravel, the formation of dune was not observed and also negligible difference in the static and dynamic depth of scours was found (Fig.1e). The scour was not observed at high jet height within the range of jet velocities maintained in the experiment. The scour was observed only at low jet height for both the nozzle sizes. The volume of scour hole, radius of scour hole and height of dune reduces with increase of clay content in the mixture.

The scour hole profiles were found almost similar in case of 60 % clay gravel as noticed in 50 % clay (Fig.1f) the scour was observed only at low jet height for both the nozzle sizes. The volume and radius of scour hole reduce with increase of clay percentage. At 60% clay in the mixture no noticeable dune was observed. The dynamic depth of scour was higher than the static depth of scour. Unconfined compressive strength (UCS) of the mixture was higher for higher percentage of clay; however, void ratio was low for higher percentage of clay.

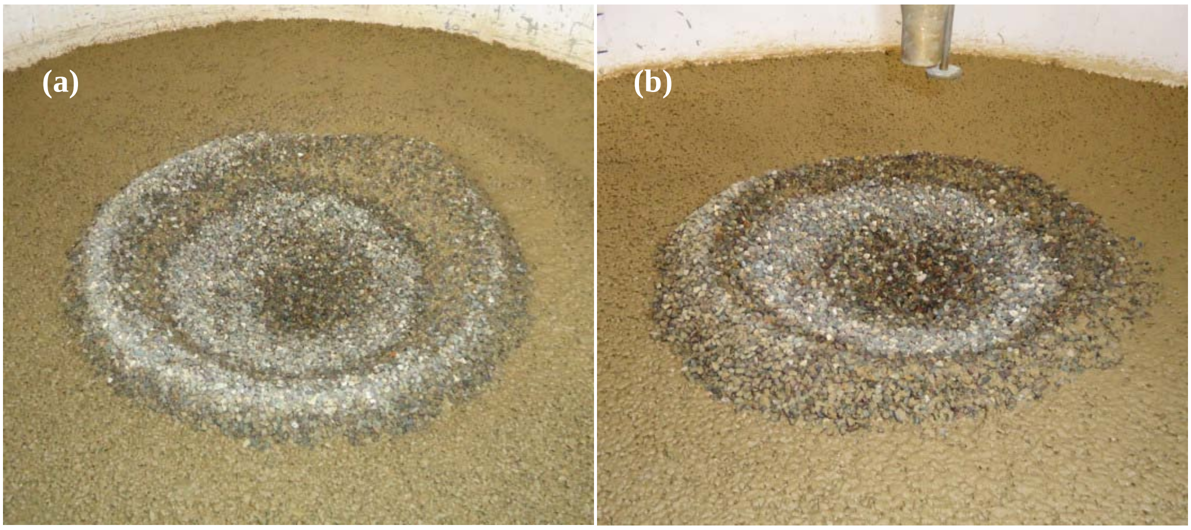

Run no. C10G2, d_o = 12.5mm, h_j = 0.15 m, u_o = 7.19 m/s, d_a = 0.00243 m, P_c = 10%

Run no. C20G2, d_o = 12.5mm, h_j = 0.15 m, u_o = 7.19 m/s, d_a = 0.00216 m, P_c = 20%

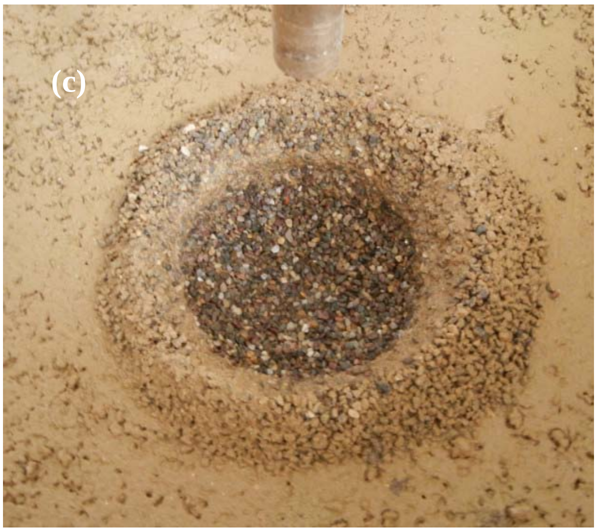

Run no. C30G2, d_o = 12.5mm, h_j = 0.15 m, u_o = 7.19 m/s, d_a = 0.00189 m, P_c = 30%

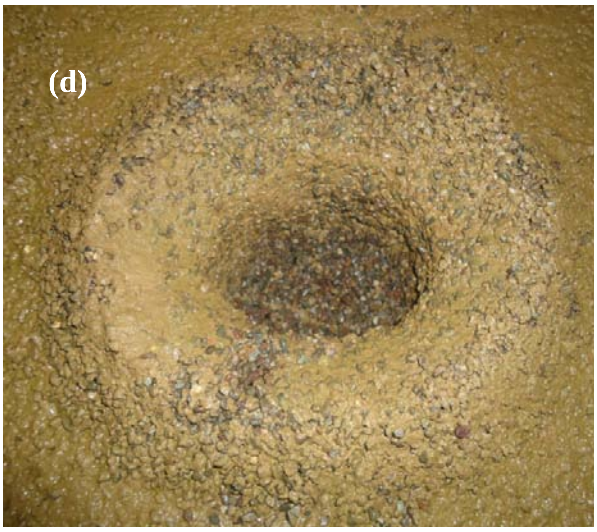

Run no. C40G2, d_o = 12.5mm, h_j = 0.15 m, u_o = 7.19 m/s, d_a = 0.00163 m, P_c = 40%

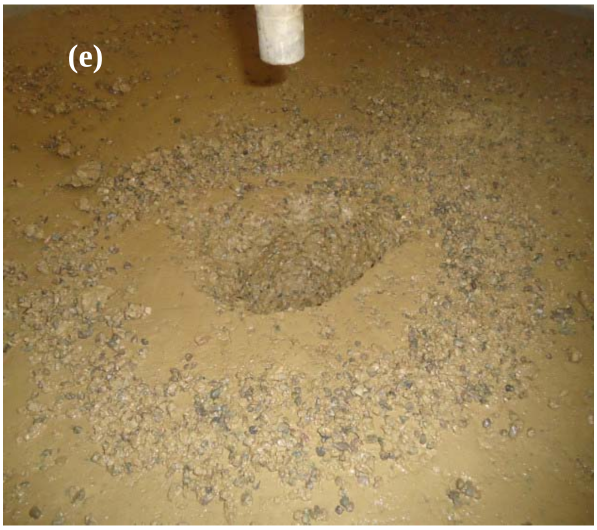

Run no. C50G2, d_o = 12.5mm, h_j = 0.15 m, u_o = 7.19 m/s, d_a = 0.00136 m, P_c = 50%

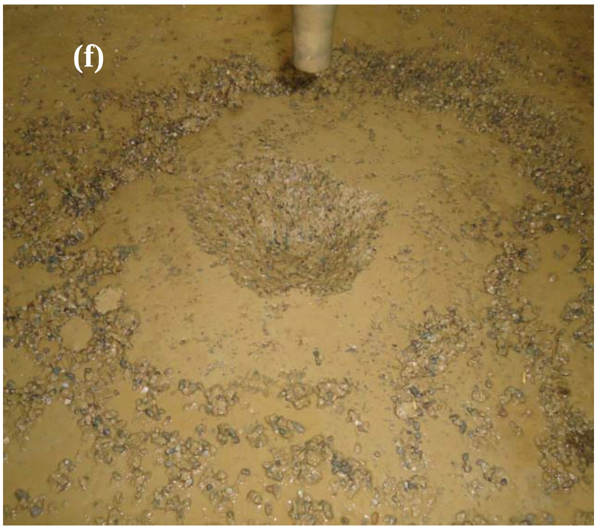

Run no. C60G2, d_o = 12.5mm, h_j = 0.15 m, u_o = 7.19 m/s, d_a = 0.00109 m, P_c = 60%

Fig. 5.1 Scour bed profiles under submerged vertical jets in different clay percent in clay-gravel mixture bed (here the notation C10G2, stands for C = clay, 10 = 10 % clay in the mixture, G = gravel and 2 = run number in clay-gravel mixture and similarly other notations have the nominal meaning)

5.2.1 Temporal Variation of Scour Depth in Clay-Gravel Mixtures

5.2.1.1 Temporal variation of scour depth with 12.5 mm nozzle diameter

The experiments were conducted under submerged circular vertical impinging water jets in clay-gravel mixtures. Temporal variation of scour depth with respect to time were plotted to study the behavior of scour in clay-gravel sediment mixtures in proportion of clay with gravel varying from 10% to 60% using 12.5 mm nozzle diameter.

Figures 5.2 and 5.3 show the temporal variation of scour depth in clay-gravel mixtures with different clay percentages, as illustration. Both these figures clearly reveal that scour depth increases with passage of time and maximum scour depth reduces with increase of clay percentage. Negligible scour was observed for higher percentage of clay with gravel viz. 50 and 60 percent in the mixture for d_0 = 12.5 mm, h_j = 0.30 m, u_o = 7.19 m/s. Therefore, Fig. 5.2 shows temporal variation of scour depth up to 40 % clay in the mixture. However, for d_0 = 12.5 mm, h_j = 0.15 m, and u_o = 5.12 m/s scour occurred up to 60 % clay in the clay-gravel mixture. The influence of cohesion was more apparent with clay percent more than 40% in the mixture. In such cases, the process of scour initiated after 20 to 40 minutes from start of the experimental run.

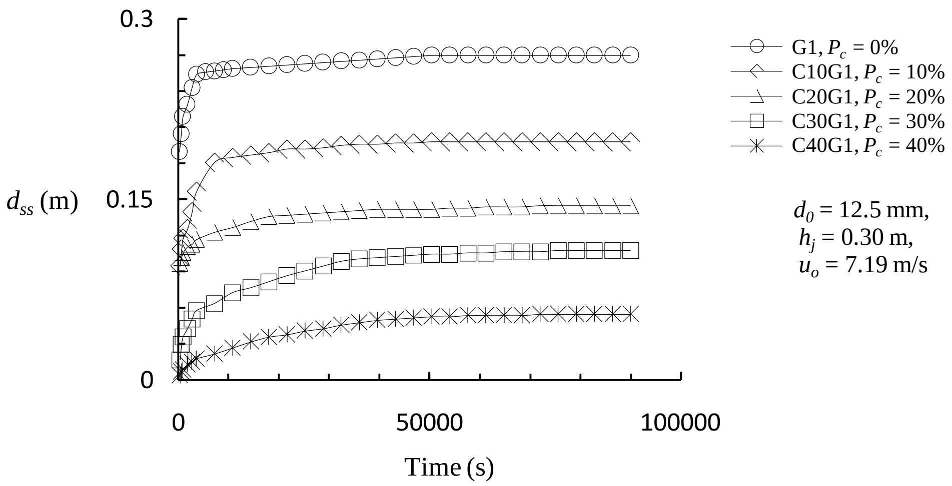

Fig. 5.2 Temporal variation of scour depth in clay-gravel mixtures using 12.5 mm nozzle for d_0 = 12.5 mm, h_j = 0.30 m, and u_o = 7.19 m/s

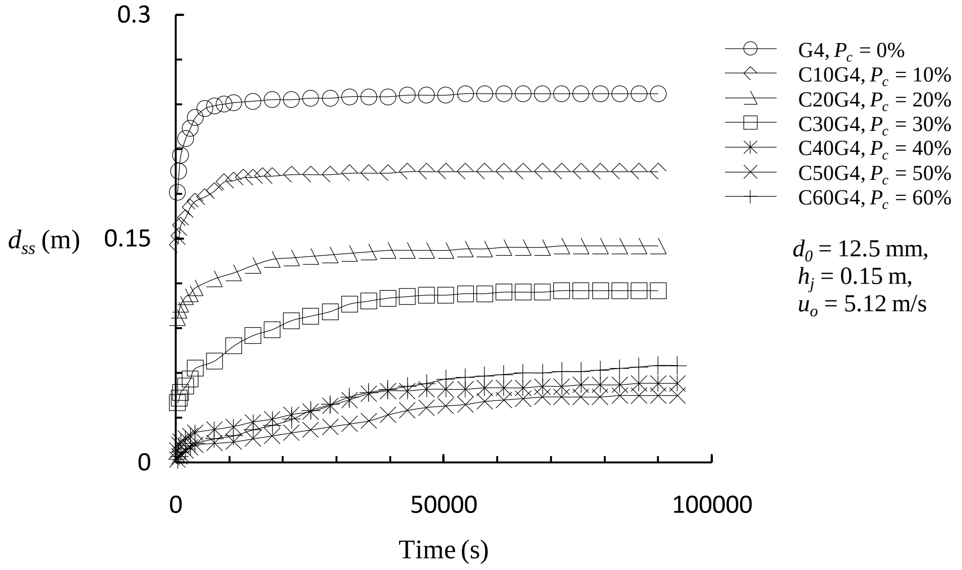

Fig. 5.3 Temporal variation of scour depth in clay-gravel mixtures using 12.5 mm nozzle d_0 = 12.5 mm, h_j = 0.15 m, and u_o = 5.12 m/s

For higher jet height and low jet velocity, the dynamic scour depth was observed low as compared to lower jet height and high jet velocity. The static scour depth was observed low for lower jet height and lower jet velocity. This may be due to jet off condition in which all the moving sediment particles get settled on the scour hole. The difference in static and dynamic scour depth is not significant up to 30% clay in the clay-gravel mixture. Low clay percentage in the mixture possesses less cohesion influence and due to this, the attraction between the particles is less.

Almost similar pattern has been observed for temporal variation of scour depth in clay-gravel mixtures using 8 mm nozzle diameter. However, significant differences have been observed in static and dynamic scour depths. The temporal variation of scour depth in this case is not shown here due to similar pattern as noticed using 12.5 mm nozzle diameter.

Figures 5.4 and 5.5 show temporal variation of scour depth for 10% and 20% clay in the mixture as illustration for different flow and jet parameters. The behavior of temporal variation of scour depth in 10 % clay in the mixture, the scour depth was almost similar to that observed in gravel bed due to negligible effect of cohesion of clay. However, in case of 20 % clay in the mixture, the cohesion starts influencing, which results in reduction of scour depth. The time taken to reach in equilibrium state increases with increase in clay percent.

Similarly, variation of scour depth with time was also studied in case of 30%, 40%, 50% and 60% clay in present in clay-gravel cohesive sediment mixtures. But these figures are not shown here due to space limitations.

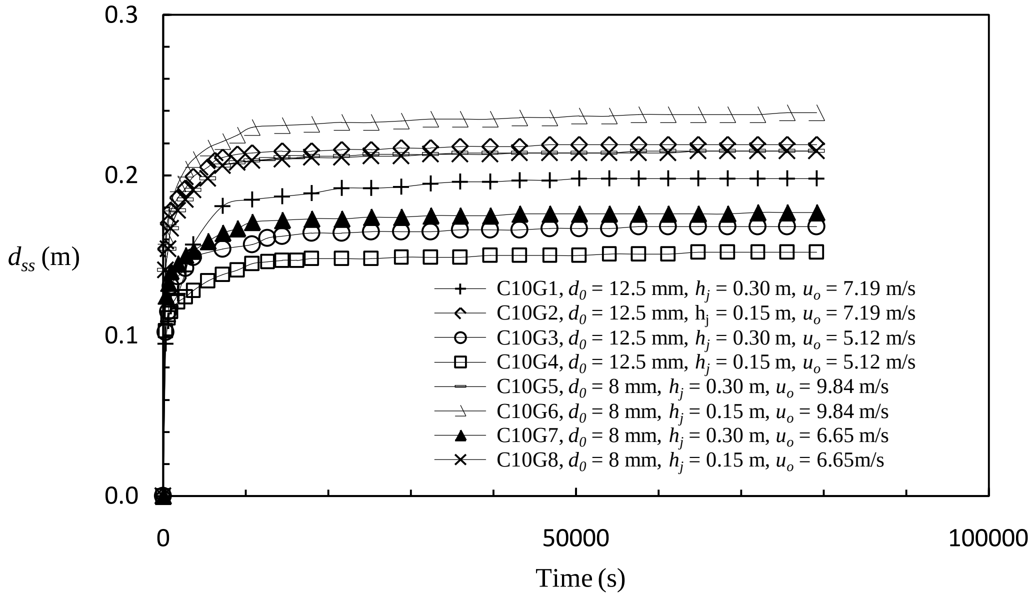

Fig. 5.4 Variation of scour depth with time in 10% clay in clay-gravel mixture

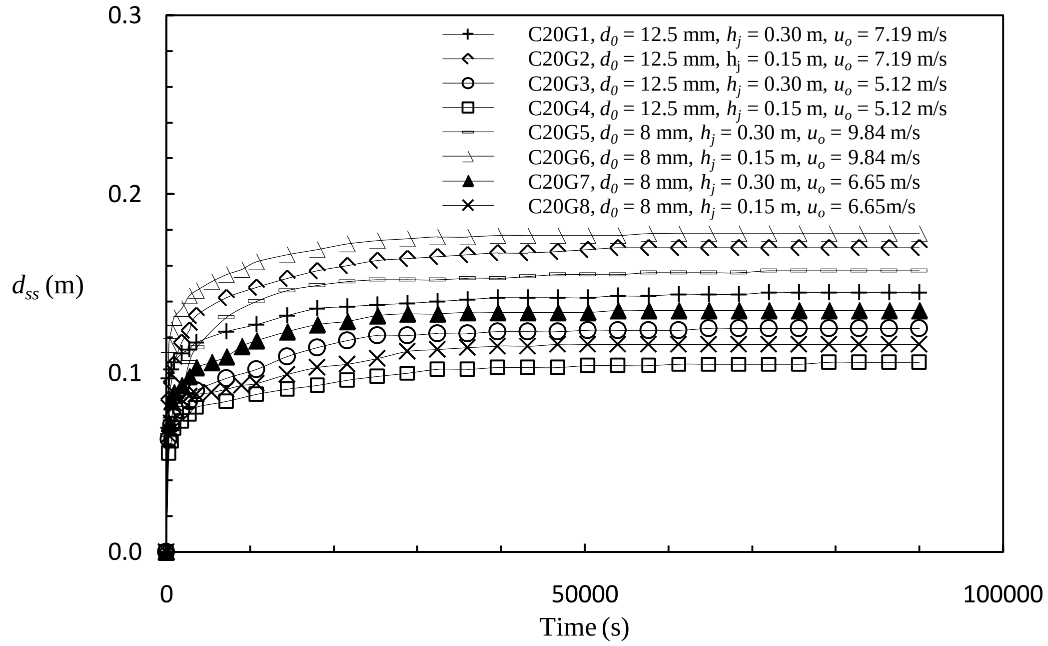

Fig. 5.5 Variation of scour depth with time in 20% clay in clay-gravel mixture

5.2.1.2 Relationship for saturation time of scour in clay-gravel mixtures

The saturation time, T_s is defined as time required from start of the scour process to achieve 99% of the total scour. The value of T_s is the function of the jet velocity, diameter of nozzle, height of jet and the sediment size and percentage of clay content in the mixtures. The functional relationship may be written as;

$$T_s = f\left(u_o, d_o, d_{50}, d_a, h_j, g, P_c\right) \tag{5.1}$$

Considering h_j and u_o as repeating variables, the functional form may be written in terms of the following dimensionless form;

$$\left(\frac{T_s}{h_j / u_0}\right) = f\left(\frac{d_o}{h_j}, \frac{d_a}{h_j}, \frac{d_{50}}{h_j}, \frac{u_o}{\sqrt{g h_j}}, P_c\right) \tag{5.2}$$

Analysis of the data collected in the present study reveals that dimensionless parameter d_{50}/h_j has little effect on saturation time. Thus Eq. (5.2) may be written as;

$$\left(\frac{T_s}{h_j / u_0}\right) = f\left(\frac{d_o}{h_j}, \frac{d_a}{h_j}, \frac{u_o}{\sqrt{g h_j}}, P_c\right) \tag{5.3}$$

The following relationship is proposed for the estimation of saturation time which appears in the equation for temporal variation of scour depth in clay-gravel cohesive sediment mixtures invoking the least square method;

$$\frac{T_s}{(h_j / u_o)} = 4.91\left(\frac{d_a}{h_j}\right)^{0.291}\left(\frac{d_o}{h_j}\right)^{0.04}\left(\frac{u_o}{\sqrt{g h_j}}\right)^{0.814}\left(P_c\right)^{1.29} \quad (R^2 = 0.96) \tag{5.4}$$

Equation (5.4) was tested for the data collected in present study for clay-gravel cohesive sediment mixtures. It is found that Eq. (5.4) predicts saturation time within error band of ± 10 % as shown in Fig. 5.6.

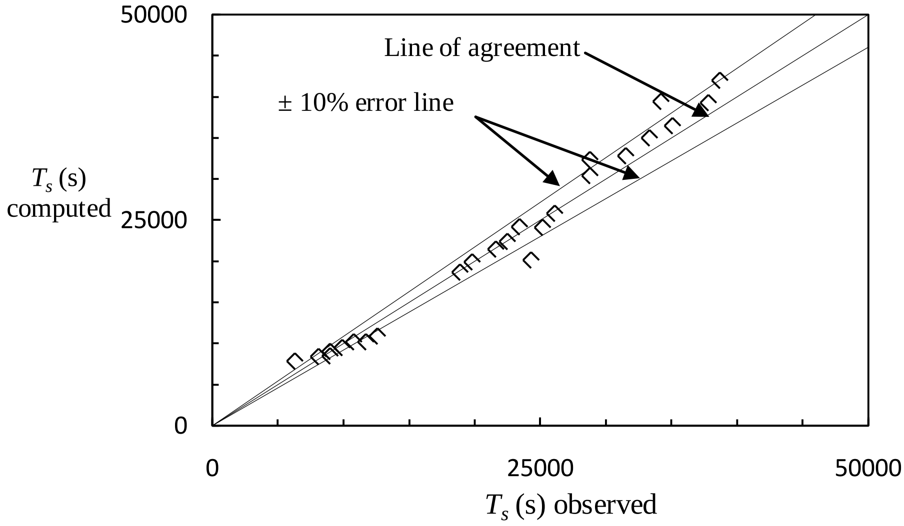

Fig. 5.6 Comparison of observed and computed saturation time using Eq. (5.4)

It may be mentioned here that various other functional forms of the relations viz. exponential, power, logarithmic etc. were also attempted for describing the temporal variation of scour depth under submerged circular vertical impinging water jets. The variation in saturation time was also studied with other hydraulic parameters such as $d_a/h_j, u_o/\sqrt{gd_o}$ or $d_o/h_j, u_o/\sqrt{gd_a}$ with P_c, however, it was found that their correlation was not satisfactory; therefore, the best results are reported herein.

5.2.1.3 Development of relationship for estimation of scour depth with time

To develop a relationship for estimation of temporal variation of scour depth, data have been analyzed in dimensionless form to show the variation of instantaneous depth of scour below the original bed level with respect to time.

The temporal variation of scour depth was first plotted as dimensionless scour depth d_{ss}/d_{dms} with dimensionless time t/T_s as shown in Figs. 5.7 and 5.8 for 10 and 20 % clay in the mixture (where d_{ss} = instantaneous scour depth at time t in cohesive sediment, T_s = saturation time, d_{dms} = dynamic maximum scour depth at equilibrium in clay-gravel mixture).

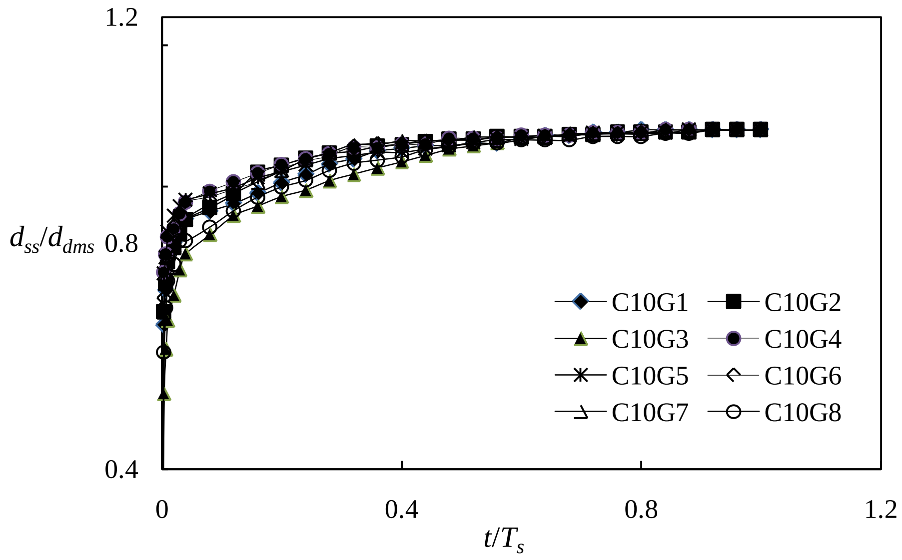

Fig. 5.7 Variation of d_{ss}/d_{dms} with t/T_s for 10 % clay with gravel

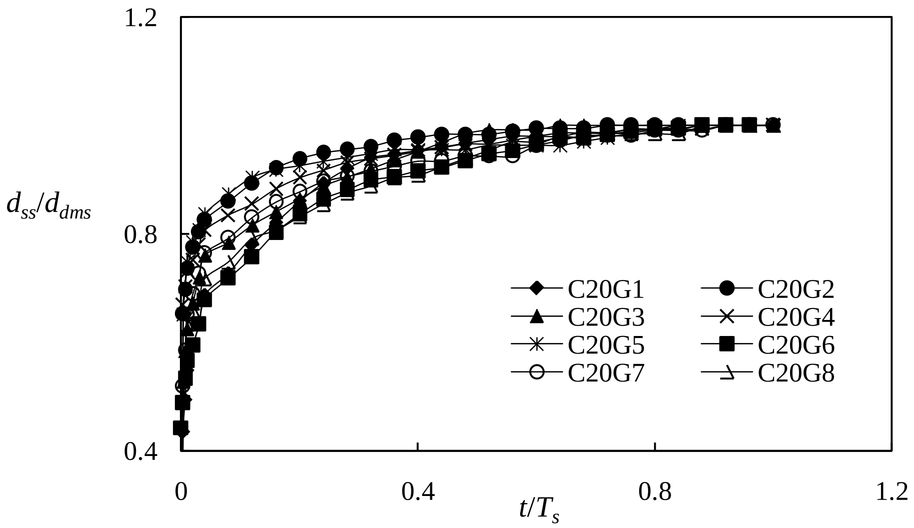

Fig. 5.8 Variation of d_{ss}/d_{dms} with t/T_s for 20 % clay with gravel

Form the above figures, it is found that the temporal variation of scour depth follows a sin curve for better indication of the variation in these two parameters. Therefore, again the temporal variations of scour depth were analyzed using sin function.

Figures 5.7 to 5.8 are re-plotted in dimensionless scour depth d_{ss}/d_{dms} with dimensionless time $\sin(\pi t/2T_s)$ for better representation of the variation between the two parameters. These are shown in Figs. 5.9 and 5.10 for 10 and 20% clay in the mixture, as illustration.

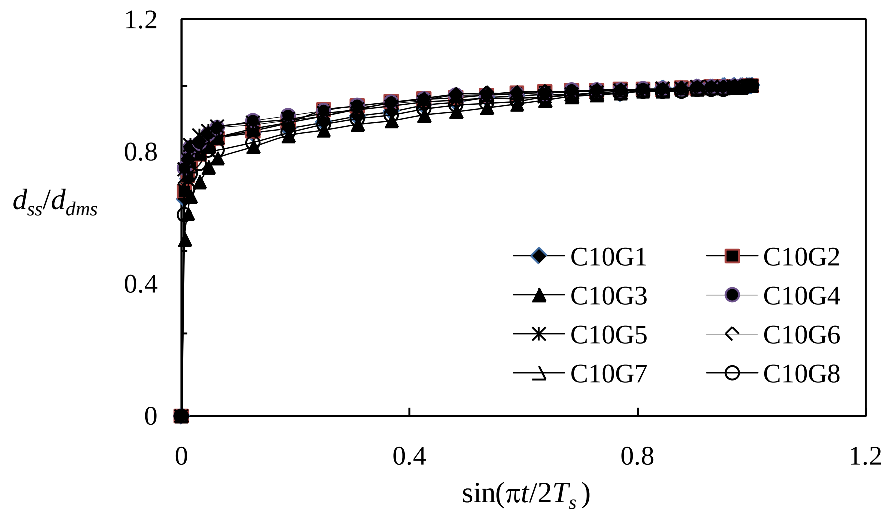

Fig. 5.9 Variation of d_{ss}/d_{dms} with $\sin(\pi t/2T_s)$ for 10 % clay in mixture

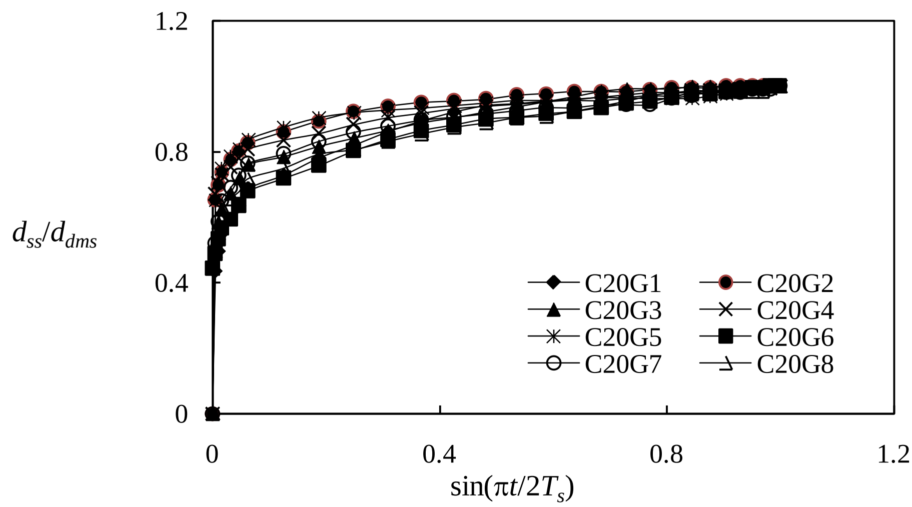

Fig. 5.10 Variation of d_{ss}/d_{dms} with $\sin(\pi t/2T_s)$ for 20 % clay in mixture

Many investigators, Hanson (1991), Hanson and Robinson (1993) Ansari (1999) and Ansari et al. 2003) have suggested the following relationship for the temporal variation of scour depth in cohesionless as well cohesive sediment.

$$\frac{d_{ss}}{d_{dms}} = \left[\sin\left(\frac{\pi t}{2T_s}\right)\right]^{m_s} \tag{4.5}$$

Analysis of the present study data as plotted in Figs 5.9 and 5.10 also reinforce that the Eq. (4.5) satisfactorily describes the temporal variation of maximum scour depth under submerged circular vertical impinging water jets in case of cohesive mixtures.

5.2.1.4 Relationship for the exponent

In order to estimate the temporal variation of scour depth, the value of exponent which appears in the equation for temporal variation of scour depth is needed a priori. The value of exponent, m_s is estimated for each experimental run in the present study. Analysis of computed value of m_s reveals that it is a function of dimensionless parameters d_a/h_j, d_o/h_j, $u_o/\sqrt{gh_j}$ and percentages of clay content, P_c. It is found that the value of exponent increases with increases of sediment size, nozzle diameter, jet velocity and clay percent. Following the dimensional analysis carried out for time of saturation, Eq. (5.5) is proposed to compute the value of exponent for clay-gravel cohesive sediment mixtures.

$$m_s = 0.002\left(\frac{d_a}{h_j}\right)^{0.013}\left(\frac{d_o}{h_j}\right)^{0.049}\left(\frac{u_o}{\sqrt{gh_j}}\right)^{0.181}(P_c)^{1.47} \qquad (R^2 = 0.92) \qquad (5.5)$$

The suitability of the proposed relationship is analyzed in the respect of observed and computed conditions and it is found that Eq. (5.5) predicts the value of m_s within error band of ± 15 % as shown in Fig. 5.11.

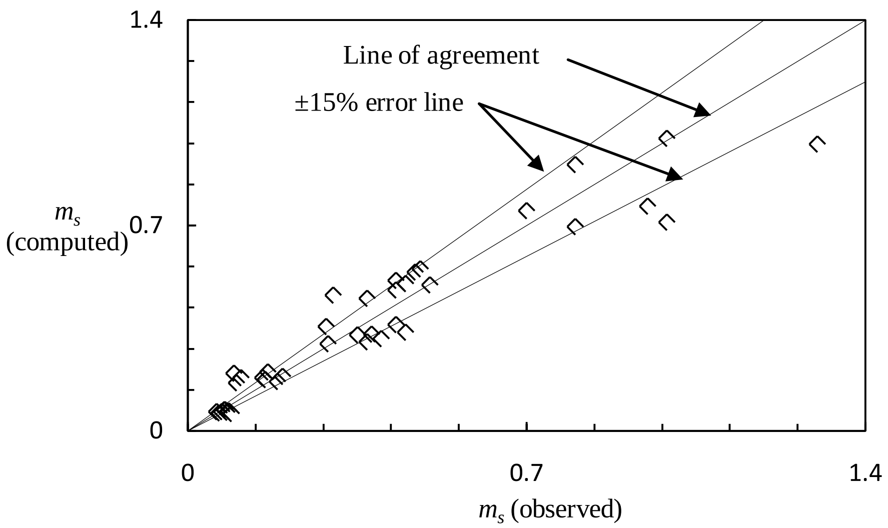

Fig. 5.11 Comparison of observed and computed exponent (m_s) values using Eq. (5.5) in clay-gravel mixture

The variation of m_s was also studied with other dimensionless groups viz; $d_a/h_j, u_o/\sqrt{gd_o}$ and $d_o/h_j, u_o/\sqrt{gd_a}$ and P_c, however, a weak correlation was observed with these variables.

5.1.2.5 Validation of proposed relationship in clay-gravel mixtures

The proposed Eqs. (4.5), (5.4) and (5.5) for estimation of scour depth with time have been validated using data of clay-gravel mixtures collected in the present study. Figs. 5.12, 5.13 and 5.14 shows the validation of the proposed relationship to compute scour depth with respect to time for clay percentage 10, 20 and 30 %, respectively. It is apparent that computation of temporal variation of scour depth using Eq. (4.5) is quite satisfactory for clay-gravel cohesive sediment mixtures.

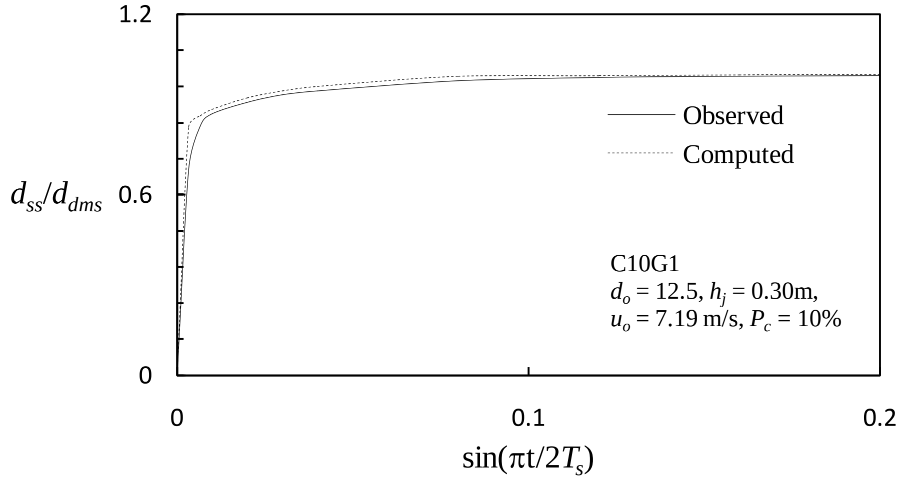

Fig. 5.12 Validation of proposed relationship in scour depth with time for 10% clay in mixture

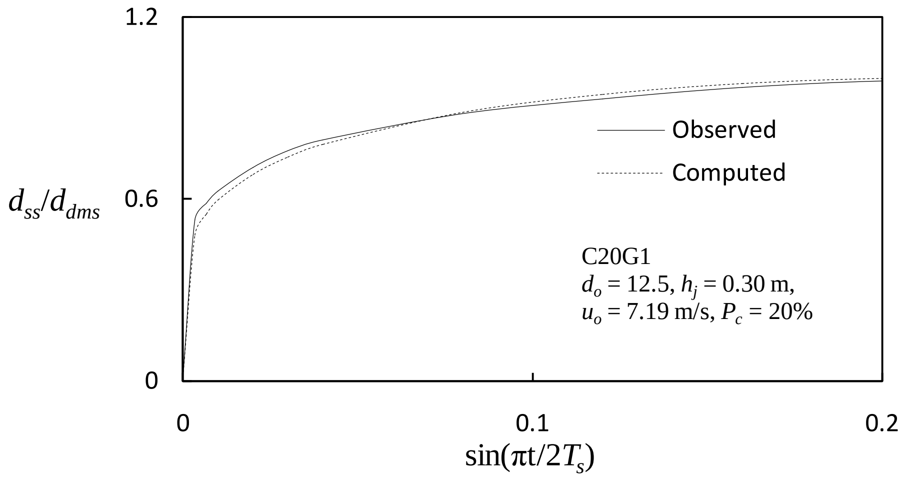

Fig. 5.13 Validation of proposed relationship in scour depth with time for 20% clay in mixture

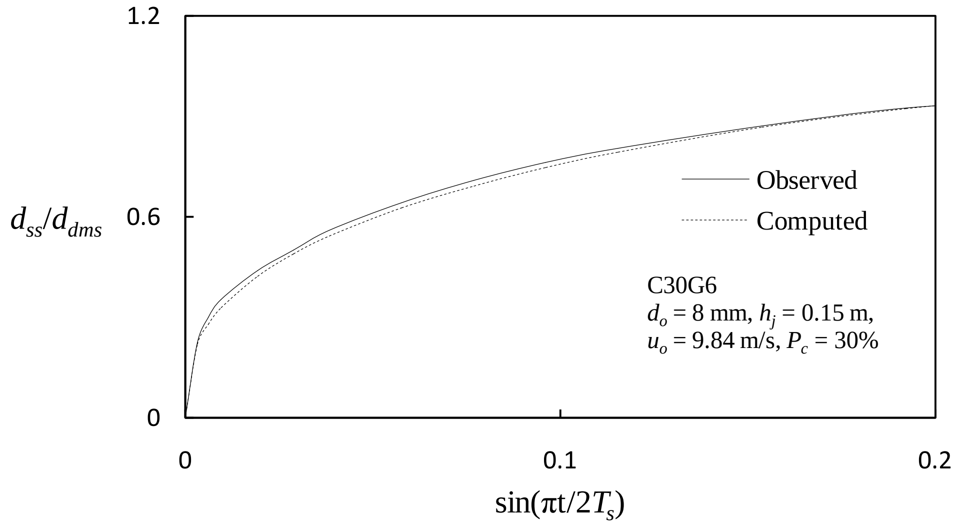

Fig. 5.14 Validation of proposed relationship in scour depth with time for 30% clay in mixture

A similar comparison was also obtained in case of 40%, 50% and 60 % clay in clay- gravel cohesive sediment mixtures. These figures are not shown here due to space limitation.

5.2.2 Estimation of Various Scour Parameters in Clay-Gravel Mixtures

The data collected in the present study have been used to formulate relationships for various scour parameters like maximum static scour depth, maximum dynamic scour depth, radius of scour hole; height of dune and volume of scour hole. It should be noted that no data other than present study was available in the literature related to scour in clay-gravel mixtures.

(a) Maximum static scour depth

Sarma (1967), Westrich and Kobus (1973) and Rajaratnam (1982), Aderibigbe and Rajaratnam (1996) and Ansari et al. (2003) identified non-dimensional parameter (E_c) as given in Eq. (4.7) as a representative parameter for scour. It is used herein to describe the process of estimation of maximum static scour depth in clay-gravel mixture.

Maximum static scour depth is analyzed with erosion parameter for various percentages of clay content, P_c i.e. 10 to 60% with gravel as shown in Fig. 5.15. It is apparent that the depth of scour reduces with increase in clay percentage in the mixture which indicates that the depth of scour is a function of clay content and erosion parameter.

The following equation is proposed to estimate the maximum static scour depth in clay-gravel mixtures

$$\frac{d_{sms}}{h_j} = 0.836(P_c)^{-0.469}(E_c)^{1.394} \qquad (R^2 = 0.81) \qquad (5.6)$$

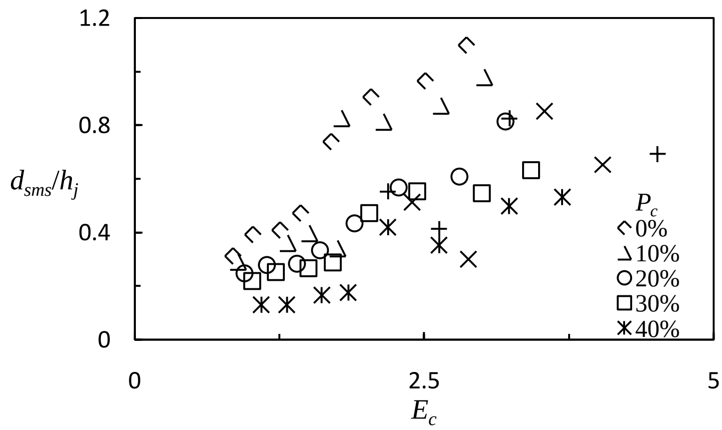

Fig. 5.15 Variation of static scour depth with erosion parameter for different clay percentage in clay-gravel mixture

It was found that the Eq. (5.6) predicts the maximum static scour depth within ± 30 percent error band as shown in Fig. 5.16.

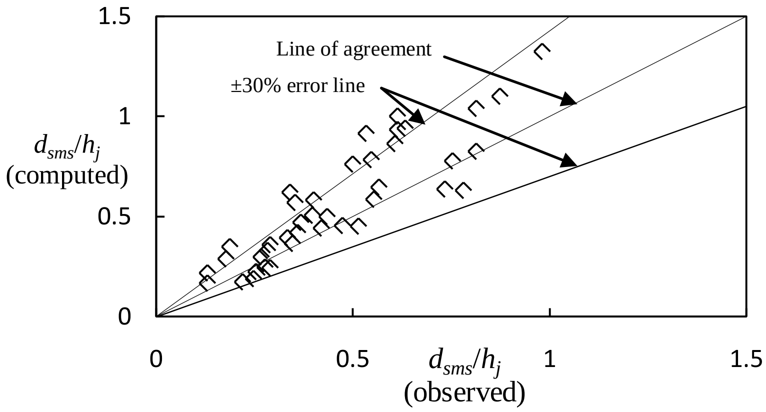

Fig. 5.16 Comparison of observed and computed maximum static scour depth using Eq. (5.6)

Further, the maximum static scour depth is also analyzed with sediment size, nozzle diameter, jet velocity, and clay percentages. The variation of maximum static scour depth can be well explained with dimensionless parameters d_a / h_j, d_o / h_j, $u_o / \sqrt{gh_j}$ and clay content, P_c instead of erosion parameter. Analysis of data reveals that the static scour depth increases with increase of sediment size, nozzle diameter and jet velocity and decreases with clay percent. Equation (5.7) is proposed to estimate the maximum static scour depth in clay-gravel sediment mixtures.

$$d_{sms}/h_j = 3.87\left(\frac{d_a}{h_j}\right)^{0.081}\left(\frac{d_o}{h_j}\right)^{0.756}\left(\frac{u_o}{\sqrt{gh_j}}\right)^{0.886}(P_c)^{-0.3204} \quad (R^2=0.87) \quad (5.7)$$

The proposed relationship have been analyzed for computation of maximum static scour depth to check the suitability of the equation which predicts the scour depth ± 20% error band as shown in Fig. 5.17. Increase in scour depth with increase in sediment size is due to segregation of bed material.

In the case of segregation of the bed material, the fine particles i.e. clay washed away from scour hole in the form of suspension and only gravels stay in the scour hole due to its heavy weight. In that case, the scour is mainly in gravel. However, in the analysis of data of cohesive sediment i.e. clay-gravel mixture, weighted arithmetic mean has been taken into account, which is smaller than the size of the boulder. Since in the calculation smaller size is being used, however, the maximum scour is mainly governed by gravel size, therefore, positive exponent of d_a/h_j has been obtained in Eq. (5.7).

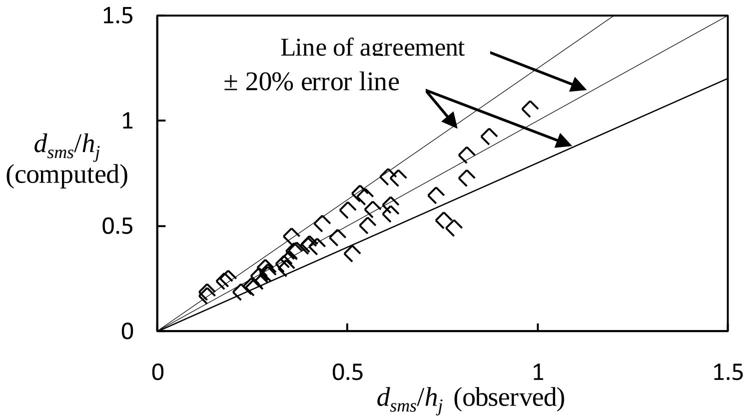

Fig. 5.17 Comparison of observed and computed maximum static scour depth using Eq. (5.7)

(b) Maximum dynamic scour depth

The variation of maximum dynamic scour depth is studied with the similar parameters as studied for maximum static scour depth. It is found that the dynamic scour depth increases with increase of sediment size, nozzle diameter and jet velocity, and decreases with increase of clay percent. A new relationship (Eq. 5.8) is proposed to estimate the maximum dynamic scour depth in clay-gravel cohesive sediment mixtures.

$$d_{dms}/h_j = 30.65\left(\frac{d_a}{h_j}\right)^{0.407}\left(\frac{d_o}{h_j}\right)^{0.599}\left(\frac{u_o}{\sqrt{gh_j}}\right)^{0.824}\left(P_c\right)^{-0..509} \quad (R^2=0.92) \quad (5.8)$$

The proposed relationship predicts the dynamic scour depth with ± 15% error band as shown in Fig. 5.18. As mentioned earlier, positive exponent of d_a/h_j is due to segregation of bed material.

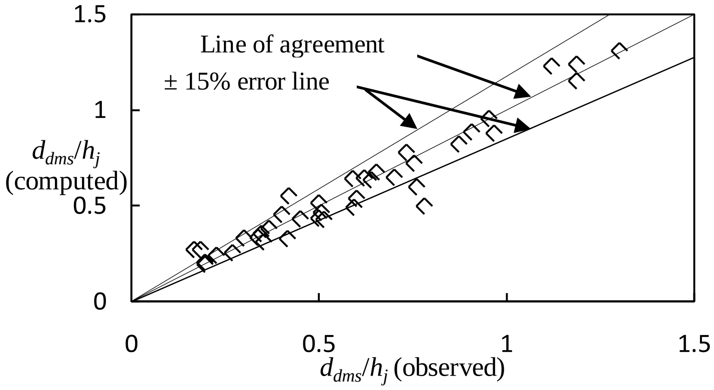

Fig. 5.18 Comparison of observed and computed maximum dynamic scour depth

It is to be mentioned that no data other than collected in the present study were available for comparison. Since, no study has been conducted for the jet scour in cohesive sediment consisting of clay-gravel mixtures to the best of knowledge of the writer.

Figure 5.19 presents the variation of ratio of maximum dynamic and maximum static scour depth with different percentages of clay content in the clay-gravel mixture. It is evident from Fig. 5.19 that the difference between the maximum dynamic and maximum static scour depth decreases with the increase in clay percentage in the mixture. At higher percentage of clay viz P_c > 40%, both maximum dynamic and maximum static scour depth appears to be almost same.

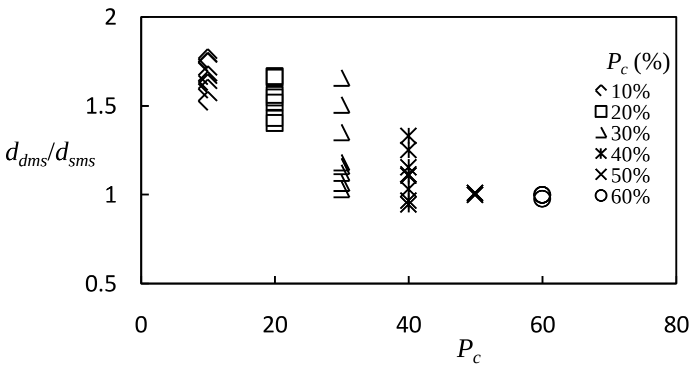

Fig. 5.19 Ratio of maximum dynamic and maximum static scour depths for different clay percentage in mixture

The variation of radius of scour hole, dune height, and volume of scour hole for presently collected data has been studied with various sediment and hydraulic parameters. After careful analysis it is found that these quantities are function of dimensionless parameters d_a/h_j, d_o/h_j, $u_o/\sqrt{gh_j}$ and percentages of clay content, P_c. Analysis of data reveals that the radius of scour, dune height and volume of scour increases with sediment size, nozzle diameter and jet velocity, and decreases with clay percent. Following relationships have been developed using the data collected in the present study to predict radius of scour hole, dune height, and volume of scour hole in clay-gravel mixtures.

$$r/h_j = 58.03\left(\frac{d_a}{h_j}\right)^{0.516}\left(\frac{d_o}{h_j}\right)^{0.446}\left(\frac{u_o}{\sqrt{gh_j}}\right)^{0.321}(P_c)^{-0.511} \quad (R^2=0.87) \qquad (5.9)$$

$$\Delta/h_j = 1.826\left(\frac{d_a}{h_j}\right)^{0.2214}\left(\frac{d_o}{h_j}\right)^{0.6534}\left(\frac{u_o}{\sqrt{gh_j}}\right)^{0.0.624}(P_c)^{-0.514} \quad (R^2 = 0.91) \qquad (5.10)$$

$$\nabla/h_j^3 = 1.67\times10^7\left(\frac{d_a}{h_j}\right)^{2.21}\left(\frac{d_o}{h_j}\right)^{0.725}\left(\frac{u_o}{\sqrt{gh_j}}\right)^{0.675}(P_c)^{0.082} \quad (R^2 = 0.97) \qquad (5.11)$$

It is to be noted that positive exponent of d_a/h_j is due to segregation of bed material during scour of bed. It is found that the Eqs. 5.9 to 5.11 predict radius of scour hole with ± 20 % error band, volume of scour hole with ± 15 % error band and dune height with ± 15 % error band as shown in Figs. 5.20, 5.21 and 5.22 respectively.

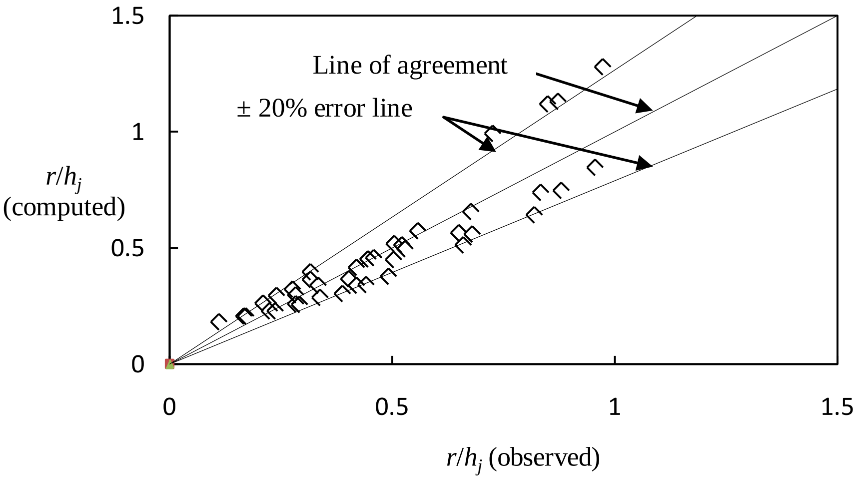

Fig. 5.20 Comparison of observed and computed radius of scour hole

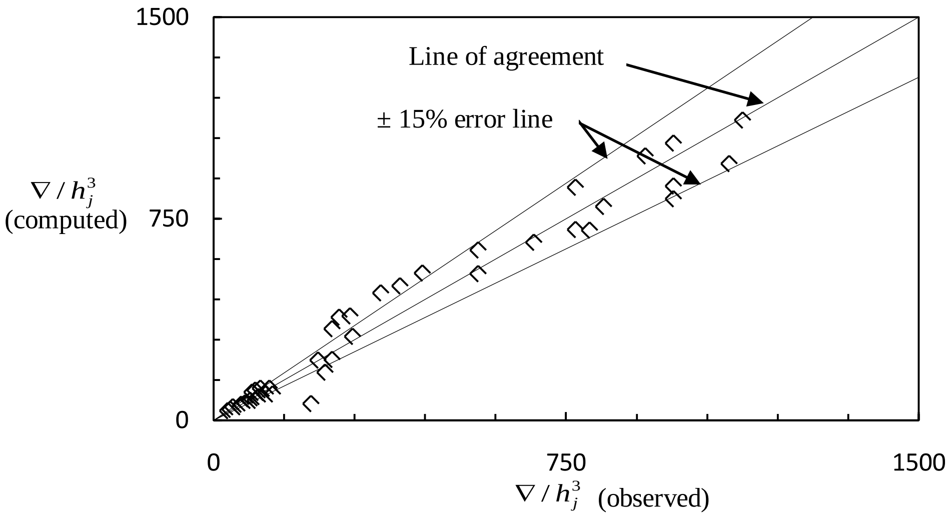

Fig. 5.21 Comparison of observed and computed volume of scour hole

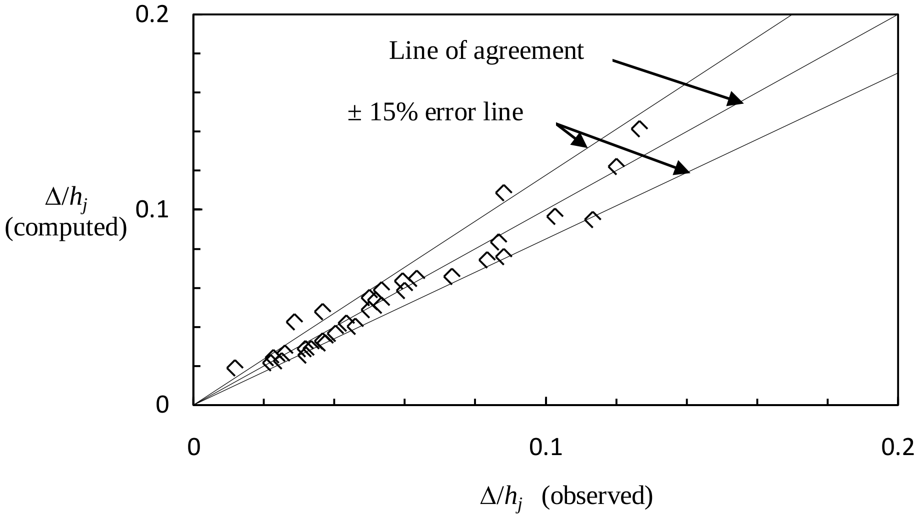

Fig. 5.22 Comparison of observed and computed dune height

The variation in maximum dynamic scour depth, radius of scour hole, dune height, and volume of scour hole was studied with erosion parameter but their correlation was not satisfactory. The variation of dynamic scour depth, radius of scour hole, dune height, and volume of scour hole was also studied with unconfined compressive strength, dry density, and antecedent moisture content. However, it was found that percentage of clay parameter is more coherent to be used in formulation of relationships for various parameters under submerged circular vertical impinging water jets in cohesive sediment consisting of clay-gravel mixture.

5.3 SCOUR IN CLAY-SAND-GRAVEL MIXTURES

The process of scour under submerged circular vertical impinging water jets in clay-sand-gravel cohesive sediment beds is discussed here. The cohesive sediment beds were prepared by varying clay percentages from 10% to 60 % by weight with sand-gravel. Initially the laboratory tests were conducted to know the engineering properties of the clay-gravel mixtures such as, unconfined compressive strength, moisture content, dry density, bulk density, void ratio etc. The observations were taken for temporal variation of maximum dynamic scour depth, maximum static scour depth, volume of scour hole, dune height and radius of scour hole.

The characteristics of scour due to submerged circular vertical jets in clay-sand-gravel cohesive sediment mixtures were found to be much different than cohesionless sediment. The difference between maximum static and dynamic scour depths was found less in clay-sand-gravel mixtures compared to cohesionless sediment. The behavior of the scour phenomenon varies with clay percentage in the mixtures. The depth of scour, volume of scour, radius of scour hole and the dune height were found different for each sediment bed conditions.

The photographic views of scour bed profiles in clay-sand-gravel mixtures are shown in Figs. 5.23(a-f) for varying clay percent in clay-sand-gravel mixture

The characteristics of scour due to submerged circular vertical water jets were firstly analyzed with sediment bed having 10 percent clay with sand-gravel. The scour process was found to have almost similar behavior as noticed in sand-gravel mixtures (Fig. 5.23a). In these sediment mixtures, there was a little or practically no influence of cohesion on scour due to low clay percent. The formation of dune height was seen approximately similar to that observed in sand-gravel beds. The scour depth was found maximum in dynamic condition compared to static condition. It may be due to fact that when the water jet was stopped. The moving sediment particles get settled on the scoured bed. The volume of scour hole, radius of scour hole, height of dune was observed and found almost similar to that observed in sand-gravel beds. It was also seen that large size nozzle produces maximum depth of scour at low jet height and high jet velocity.

In case of 20 % clay with sand-gravel mixtures, the cohesion effect was observed on static and dynamic scour depths i.e., the difference between these was low (Fig. 5.23b). The volume of scour hole, radius of scour hole, height of dune reduce with the increase of clay content in the mixtures. The size and extent of scour hole profiles at low jet height was found to be less as compared to high jet height due to impact of submerged jet action. Clay was found to be deposited at the periphery of the dune.

With the further increase of clay percent in sediment mixtures i.e. greater than 30 %, in the mixtures, the difference between static and dynamic scour depth decreases (Fig. 5.23c). The volume of scour hole, radius of scour hole and dune height also reduces.

The scour hole in the mixture having clay content 40% with sand-gravel is shown in Fig. 5.23 (d). The face of the scour hole profiles were found almost vertical similar to cylindrical shapes. In few experimental runs, the scour hole profiles had irregular shapes and geometry. The formation of small dune was seen in the experiment. The sediment was deposited far away in the form of lumps and chunks in various size and shapes.

A close investigation of the observed scour bed profiles revealed that the dynamic scour depth is maximum up to 40% clay in the mixture. There has been much difference in static and dynamic scour depths. However, in case of clay content greater than 40% with sand-gravel mixtures, the static and dynamic scour depth appears almost same due to more clay percent. As the clay percent increases, influence of cohesion in the mixture also increases.

It was found from the photographs of the scour profile that the thick dune was observed up to 30% clay in sand-gravel mixtures and much difference was seen in the value of static and dynamic scour depth due to higher sand-gravel percentage in the mixtures. However, with clay percentage greater than 30% in the mixture, the static and dynamic scour depths appear almost same due to more cohesion influences at higher clay percent. As the clay percent increases, the influence of cohesion of the sediment mixture also increases due to attraction between the individual particles.

The formation of dune was not observed in 50 % clay with sand-gravel mixtures (Fig. 5.23e). The maximum static and maximum dynamic scour depth were found almost equal. The scour was not seen at high jet height with both the jet velocities. The scour was observed only at low jet height for both the nozzle size. For higher jet velocity and low jet height, the dune formation was noticed in few experimental runs. The slope of the scour profile was almost vertical.

The scour under submerged circular vertical impinging water jets in 60 percent clay in the mixtures were seen approximately similar to that noticed in 50 percent clay content in the sand-gravel mixtures (Fig. 5.23f). The scour was not seen at high jet height with both jet velocities in 50 and 60% clay in the sediment mixtures. The scour was observed only at low jet height for both nozzle sizes. The formation of dune was not observed. Also static and dynamic depth of scour was seen similar for these sediment mixtures. When the percentages of clay content increases in the mixtures moisture content, unconfined compressive strength also increases with decreases in void ratio.

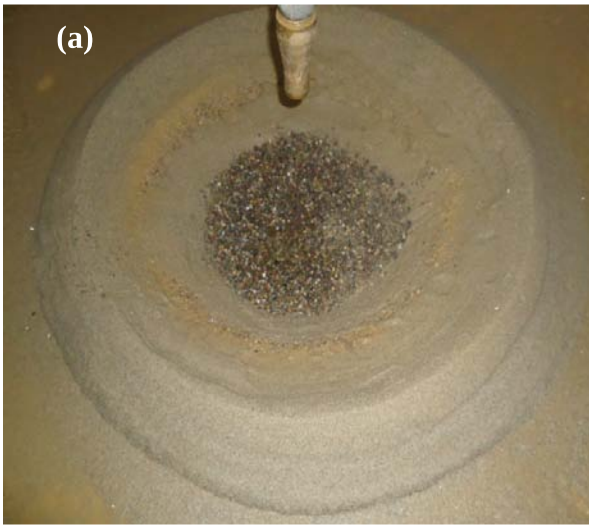

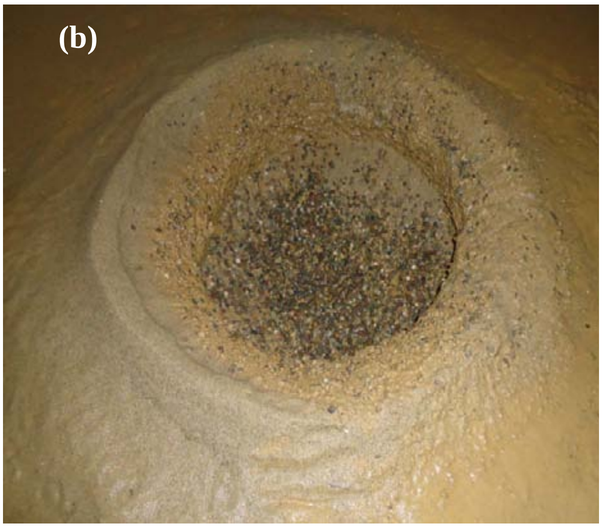

Run no. C10SG2, d_o = 12.5mm, h_j = 0.15 m, u_o = 7.19 m/s, d_a = 0.00132 m, P_c = 10%

Run no. C20SG2, d_o = 12.5mm, h_j = 0.15 m, u_o = 7.19 m/s, d_a = 0.00118 m, P_c = 20%

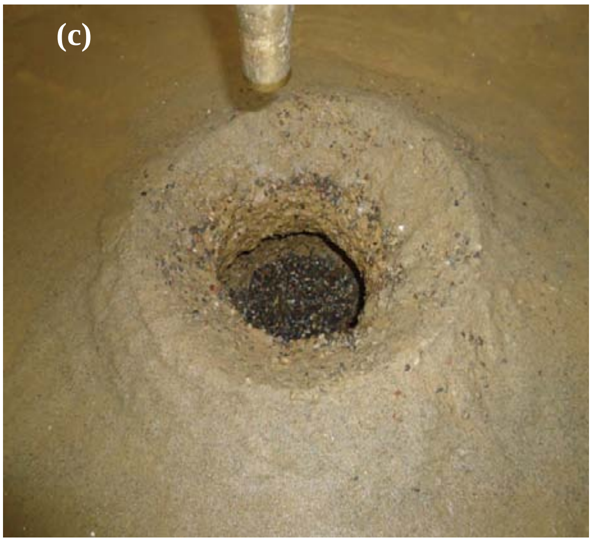

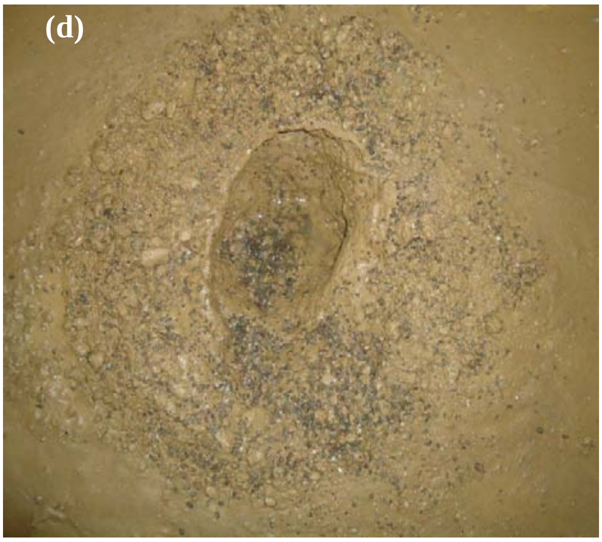

Run no. C30SG2, d_o = 12.5mm, h_j = 0.15 m, u_o = 7.19 m/s, d_a = 0.00103 m, P_c = 30%

Run no. C40SG2, d_o = 12.5mm, h_j = 0.15 m, u_o = 7.19 m/s, d_a = 0.00089 m, P_c = 40%

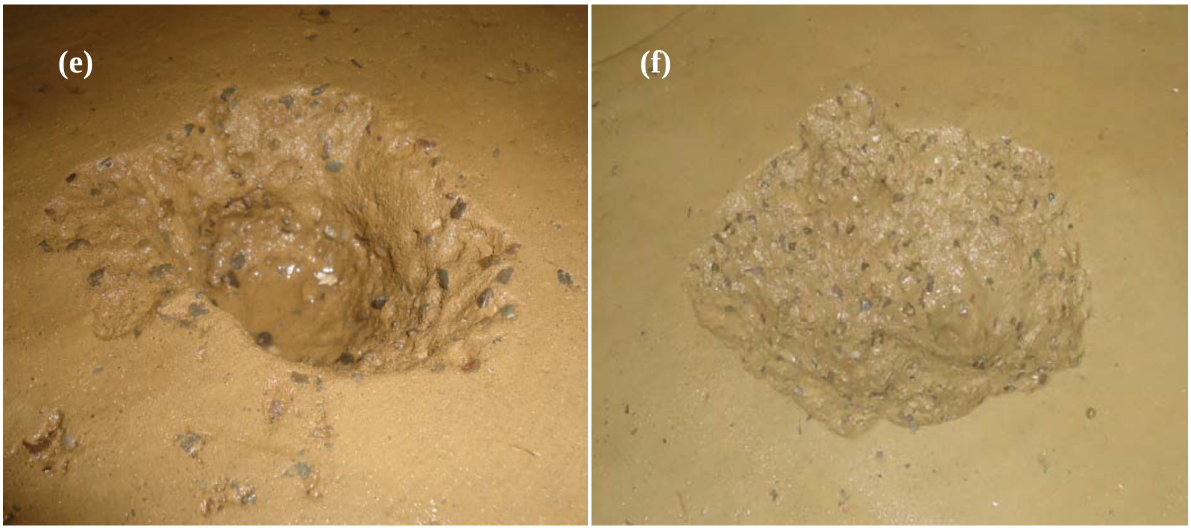

Run no. C50SG2, d_o = 12.5mm, h_j = 0.15 m, u_o = 7.19 m/s, d_a = 0.00074 m, P_c = 50%

Run no. C60SG2, d_o = 12.5mm, h_j = 0.15 m, u_o = 7.19 m/s, d_a = 0.00061 m, P_c = 60%

Fig. 5.23 Scour bed profiles under submerged vertical jets in different clay percent in the mixture

5.3.1 Temporal Variation of Scour Depth in Clay-Sand-Gravel Mixtures

5.3.1.1 Temporal variation of scour depth in 12.5 mm nozzle diameter

Experiments were conducted under submerged circular vertical impinging water jets in clay-sand-gravel mixtures. The temporal variation of scour depth are plotted to study the behavior scour in clay-sand-gravel cohesive sediment mixtures in different proportion of clay in the mixture varying from 10% to 60% using 12.5 mm nozzle diameter.

Figures 5.24 and 5.25 show the temporal variation of scour depth for various clay percentages, as illustration. Figure 5.24 shows that the scour has been observed up 50 percent clay with sand-gravel. However, higher percentage of clay with sand-gravel, the scour was not observed due to more cohesion influence in the case of maximum jet height i.e. 0.30 m. While Fig. 5.25 show the scour depth for all clay percent with sand-gravel due to minimum jet height i.e. 15 cm. The influence of cohesion was more apparent with clay percent more than 40% in the mixture. In such cases, the process of scour initiates after 15 to 35 minutes from start of the experimental run.

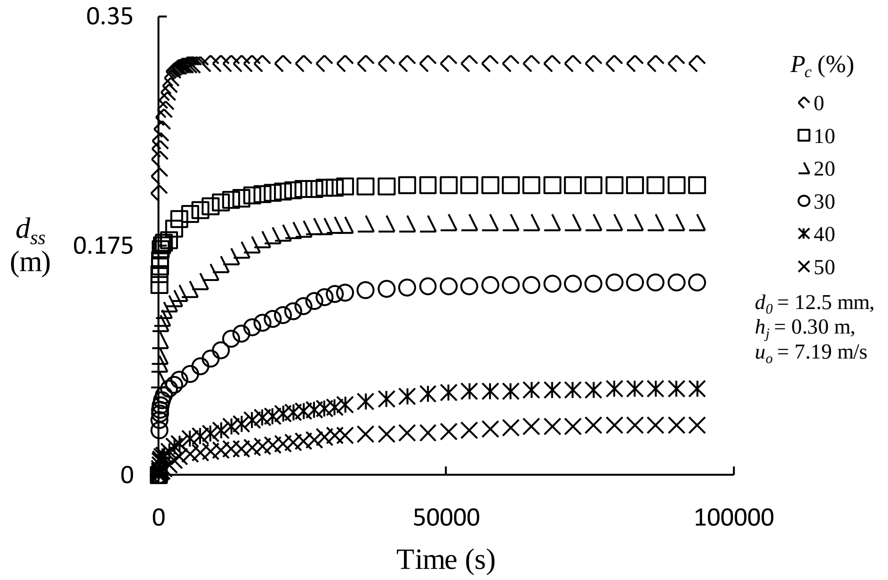

Fig. 5.24 Comparison of temporal variation of scour depth in clay-sand-gravel mixtures for d_0 = 12.5 mm, h_j = 0.30 m, u_o = 7.19 m/s

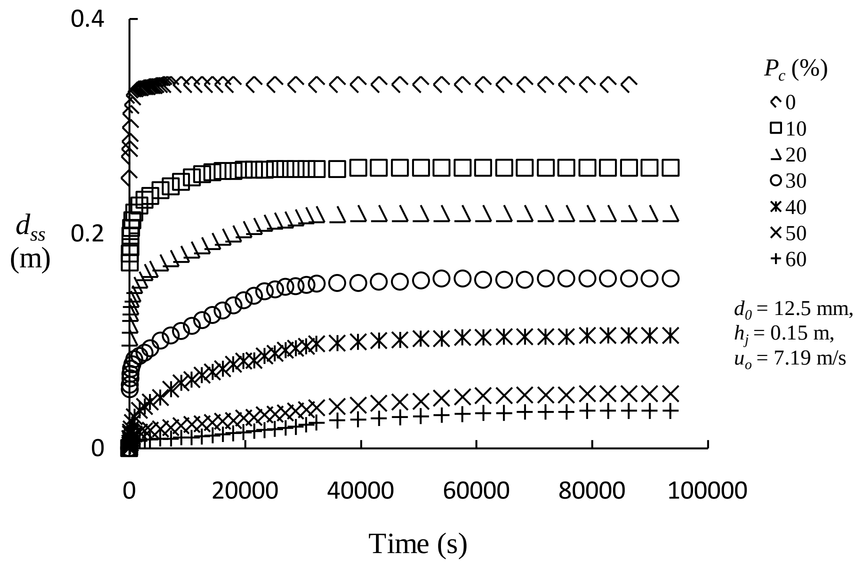

Fig. 5.25 Comparison of temporal variation of scour depth in clay-sand-gravel mixtures for d_0 = 12.5 mm, h_j = 0.15 m, u_o = 7.19 m/s

For higher jet height and low jet velocity, the dynamic scour depth was observed low as compared to lower jet height and high jet velocity as also noticed in case of clay-gravel mixtures. The static scour depth was observed low for low jet height and low jet velocity. This is may be due to jet off condition in which all the moving sediment particles get settled on the scour hole.

The difference in static and dynamic maximum scour was observed up to 30% clay with sand-gravel. Sand-gravel mixtures have high difference in dynamic and static maximum scours. Addition of 10% clay in the sand-gravel mixture results in insignificant change in the difference due to less clay percent in the mixture i.e. less cohesion influence. However, it was found that as percentage of clay in the mixtures increases, maximum dynamic and static scour depth reduces and the difference between these becomes almost negligible for higher percentage of clay. While, the saturation time increases with increase of clay percent in the mixtures.

Almost similar pattern has been observed for temporal variation of scour depth in clay-sand-gravel mixtures using 8 mm nozzle diameter. However, differences have been observed in static and dynamic scour depth. The temporal variation of scour depth in this case is not shown here due to similar pattern as noticed using 12.5 mm nozzle diameter.

Figures 5.26 and 5.27 shows the temporal variation of scour depth for 10% and 20% clay in the mixture as illustration for different flow and jet parameters. The behavior of temporal variation of scour depth in 10 % clay in the mixture, scour depth was almost similar to that observed in sand-gravel bed due to negligible effect of cohesion of clay. However, in case of 20 % clay in the mixture, the cohesion starts influencing, which results in reduction of scour depth. The time taken to reach in equilibrium state increases with increase of clay percent in the mixtures.

Similarly, variation of scour depth with time was also studied in case of 30%, 40%, 50% and 60% clay in present in clay-sand-gravel cohesive sediment mixtures. But these figures are not shown here due to space limitations.

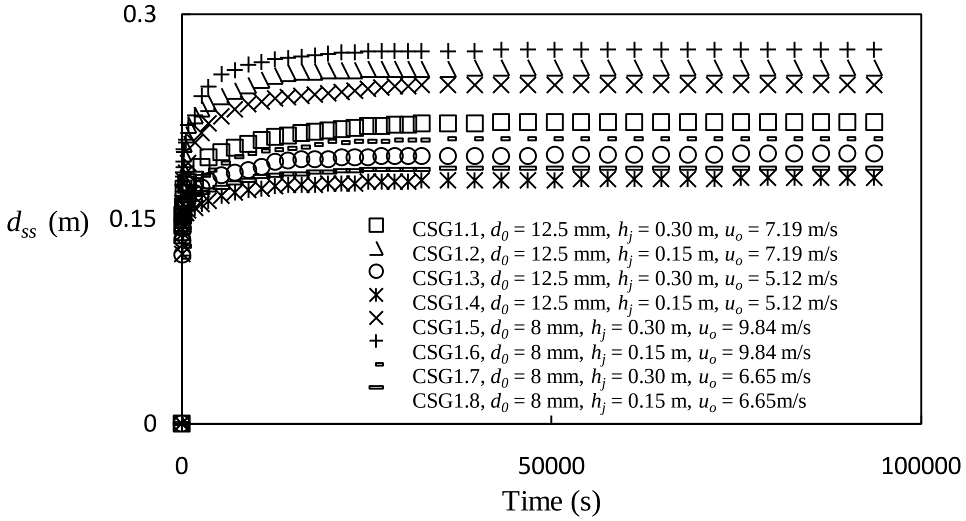

Fig. 5.26 Variation of scour depth with time in 10% clay in the mixture

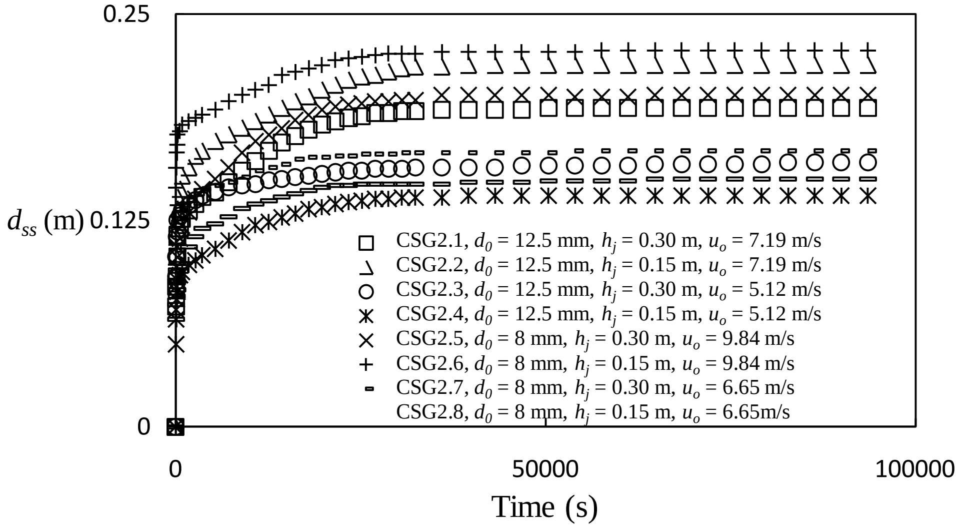

Fig. 5.27 Variation of scour depth with time in 20% clay in the mixture

5.3.1.2 Relationship for saturation time in clay-sand-gravel mixtures

The saturation time, T_s is defined as time required from start of the scour process to achieve 99% of the total scour. The value of T_s is analyzed and found that it is the function of dimensionless parameters d_a/h_j, d_o/h_j , $u_o\big/\sqrt{gh_j}$ and percentages of clay content, P_c. It is found that the saturation time increases with increase of sediment size, jet velocity, nozzle diameter and clay percent. The following relationship is proposed for the estimation of saturation time in clay-gravel cohesive sediment mixtures.

$$\frac{T_s}{(h_j/u_o)} = 6.79\left(\frac{d_a}{h_j}\right)^{0.26}\left(\frac{d_o}{h_j}\right)^{0.1}\left(\frac{u_o}{\sqrt{gh_j}}\right)^{0.84}(P_c)^{1.28} \quad (R^2 = 0.98) \qquad (5.12)$$

Equation (5.12) has been tested for the data collected in present study for clay-sand-gravel cohesive sediment mixtures. It is found that Eq. (5.12) predicts saturation time within error band of ± 10 % as shown in Fig. 5.28.

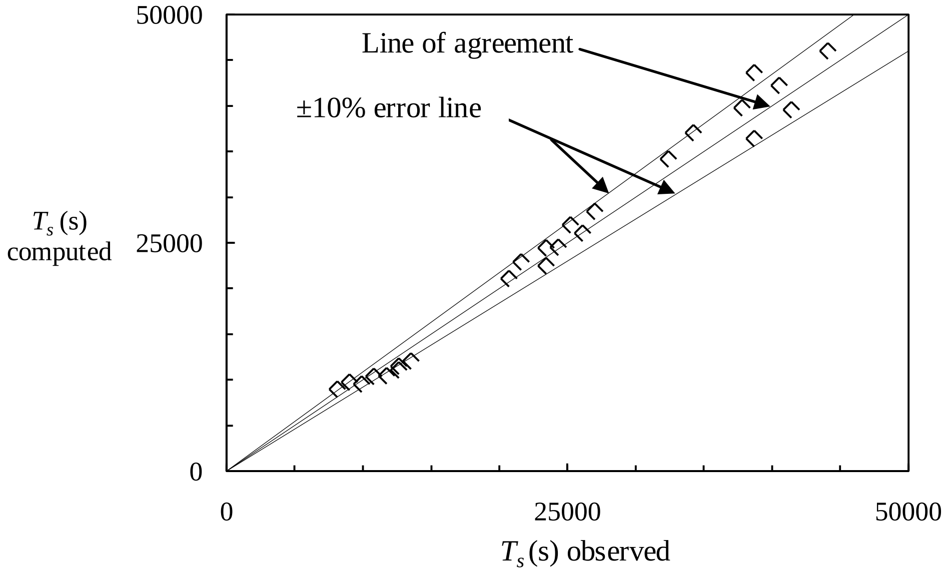

Fig. 5.28 Saturation time (T_s) for clay gravel sediment in observed and computed conditions

It may be mentioned here that various other functional forms of the relations viz. exponential, power, logarithmic etc. were also attempted for describing the temporal variation of scour depth under submerged circular vertical impinging water jets. The variation in saturation time was also studied with other hydraulic parameters such as $d_a/h_j, u_o/\sqrt{gd_o}$ or $d_o/h_j, u_o/\sqrt{gd_a}$ with P_c, however, it was found that their correlation was not satisfactory; therefore, the best results are reported herein.

5.3.1.3 Development of relationship for estimation of scour depth with time

The results obtained from previous investigations on scour due to submerged circular vertical jets such as, Moore and Masch (1962) and Hanson (1990) have suggested that the dimensional analysis can be used to developed parameters to describe the scour process. The temporal evaluation of the maximum scour depth using dimensional analysis for clay-sand-gravel mixtures was analyzed in similar manner as discussed in case of clay-gravel mixtures.

To develop a relationship for estimation of temporal variation of scour depth data have been analyzed in dimensionless form to show the variation of instantaneous depth of scour below the original bed level with respect to time.

The analysis of data has been plotted in dimensionless form to study the behavior of the temporal variation of scour depth in clay-sand-gravel cohesive sediment mixtures. The temporal variation of scour depth has been first plotted as dimensionless scour depth d_{ss}/d_{dms} with dimensionless time t/T_s as shown in Figs. 5.29 and 5.30 for 30% and 40 % clay in mixture, respectively.

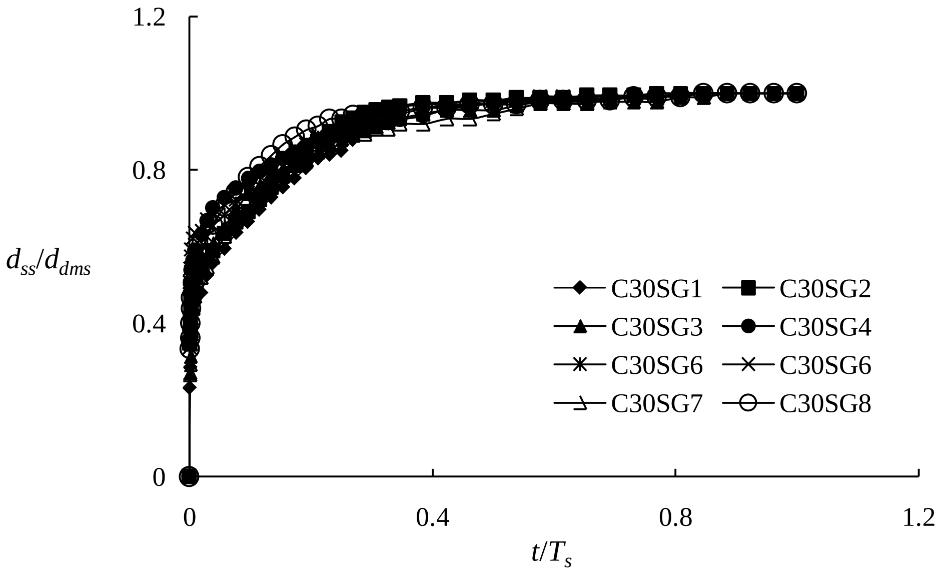

Fig. 5.29 Variation of d_{ss}/d_{dms} with t/T_s for 30 % clay in clay-sand-gravel mixtures

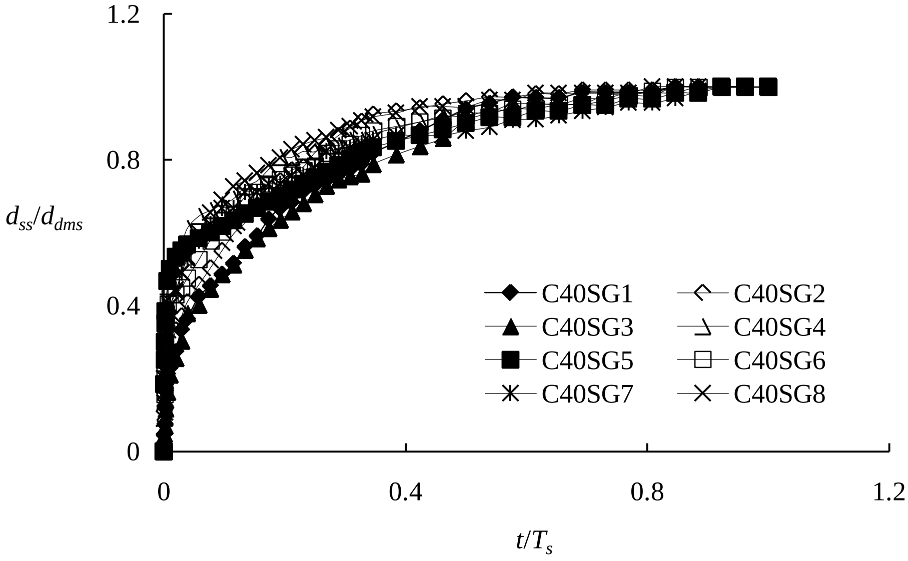

Fig. 5.30 Variation of d_{ss}/d_{dms} with t/T_s for 40 % clay in clay-sand-gravel mixtures

Form the above figures; it is found that the temporal variation of scour depth follows a sin curve for better indication of the variation in between these two parameters and can be understood by plotting dimensionless scour depth, d_{ss}/d_{dms} with dimensionless time, $\sin(\pi t/2T_s)$.

Figures 5.29 to 5.30 are re-plotted in dimensionless scour depth d_{ss}/d_{dms} with dimensionless time $\sin(\pi t/2T_s)$ for better representation of the variation between the two parameters which are shown in Figs. 5.31 and 5.32 for 30% and 40% clay in the clay-sand-gravel mixtures. From the above figures, it is apparent that the time required reaching in equilibrium state increases with increase in clay content in the mixture. Also these figures indicate that the clay has a significant effect on the rate of scour produced by water jets with respect to time.

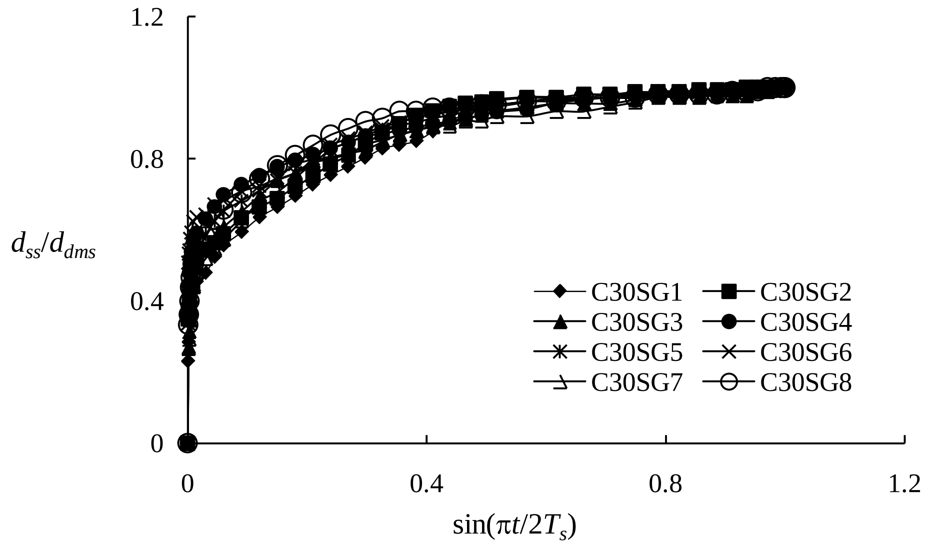

Fig. 5.31 Variation of d_{ss}/d_{dms} with $\sin(\pi t/2T_s)$ for 30 % clay in clay-sand-gravel mixtures

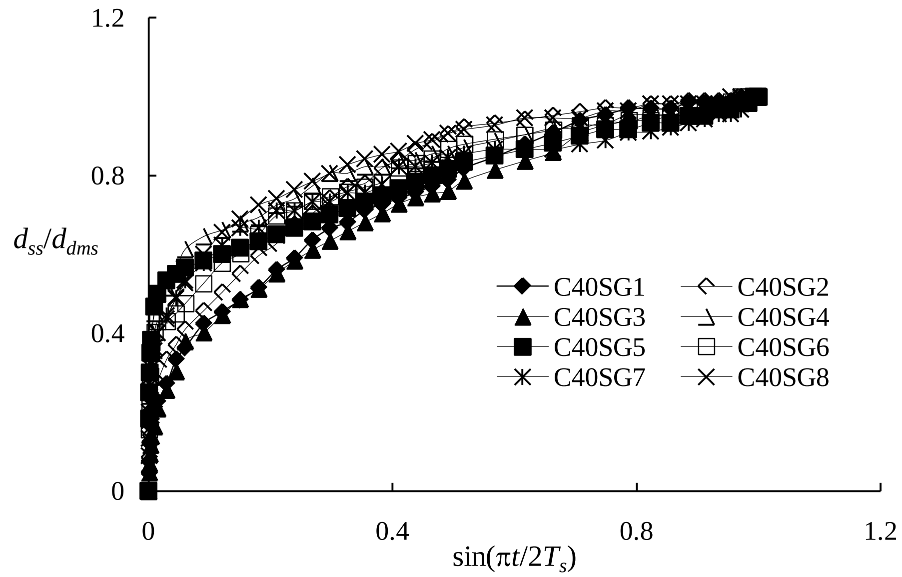

Fig. 5.32 Variation of d_{ss}/d_{dms} with $\sin(\pi t/2T_s)$ for 40 % clay in clay-sand-gravel mixture

Analysis of the data as plotted in Figs 5.31 and 5.32 reveal that the following functional relationship satisfactorily described the temporal variation of maximum scour depth under submerged circular vertical impinging water jets in case of cohesive mixtures;

$$\frac{d_{ss}}{d_{dms}} = \left[\sin\left(\frac{\pi t}{2T_s}\right)\right]^{m_s} \tag{4.5}$$

5.3.1.4 Relationship for the value exponent

In order to estimate the temporal variation of scour depth, the value of exponent which appears in the equation for temporal variation of scour depth is required a priori. The data collected in present study is analyzed and it is found that it is a function of dimensionless parameters d_a/h_j, d_o/h_j, $u_o/\sqrt{gh_j}$ and percentages of clay content, P_c. Analysis of data reveals that the value of exponent increases with increases of nozzle diameter, jet velocity and clay percent and reduces with sediment size. Accordingly, Eq. (5.13) is proposed to compute the value of exponent for clay-sand-gravel cohesive sediment mixtures.

$$m_s = 5.2\times10^{-5}\left(\frac{d_a}{h_j}\right)^{-1.098}\left(\frac{d_o}{h_j}\right)^{0.80}\left(\frac{u_o}{\sqrt{gh_j}}\right)^{0.49}(P_c)^{1.16} \qquad (R^2 = 0.95) \qquad \textbf{(5.13)}$$

The suitability of the proposed relationship is analyzed and found that Eq. (5.13) predicts the value of m_s within error band of ± 15 % as shown in Fig. 5.33.

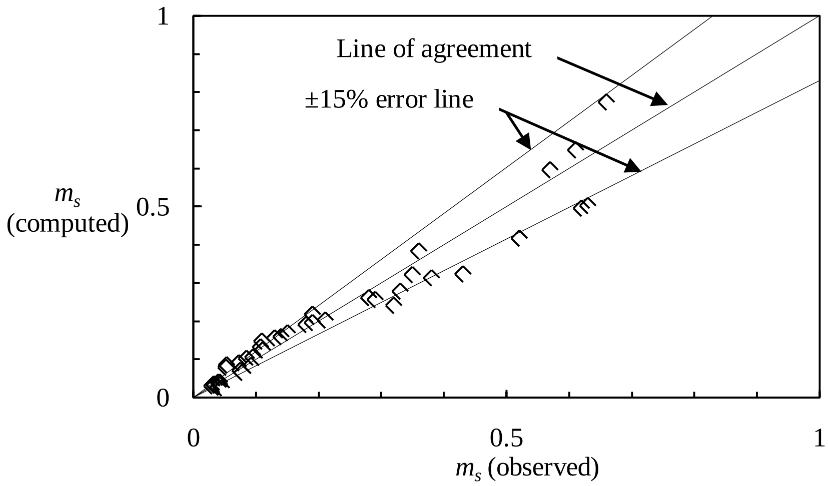

Fig. 5.33 Comparison of observed and computed value of exponent in clay-sand-gravel mixtures

The variation of m_s was also studied with other dimensionless groups viz; $d_a/h_j, u_o/\sqrt{gd_o}$, $d_o/h_j, u_o/\sqrt{gd_a}$ and P_c. However, a weak correlation was observed with these variables.

5.3.1.5 Validation of proposed relationship in clay-sand-gravel mixtures

The proposed Eqs. (4.5), (5.12) and (5.13) for estimation of scour depth with time have been validated using data of clay-sand-gravel mixtures collected in the preset study as shown in Figs. 5.34, 5.35 and 5.36 for clay 10%, 20% and 30%, respectively. It is apparent that the computation of temporal variation of scour depth in clay-sand-gravel mixtures using Eq. (4.5) is quite satisfactory.

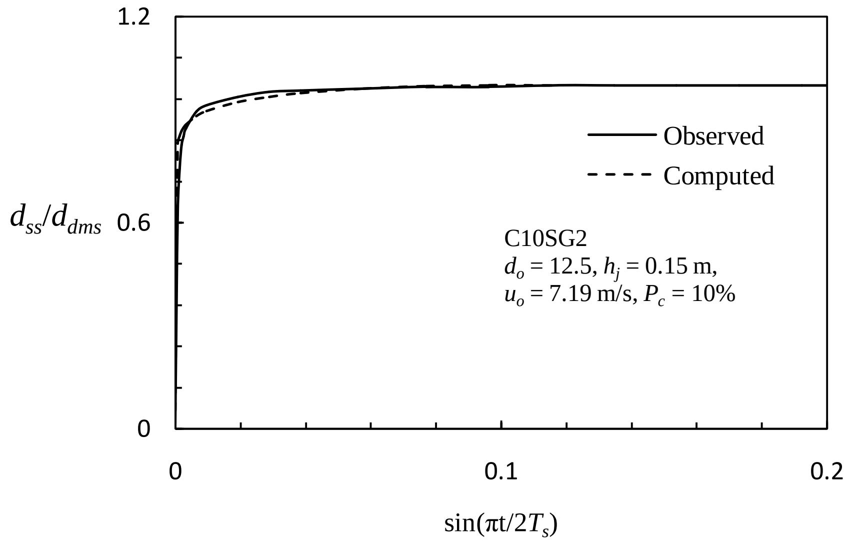

Fig. 5.34 Comparison of observed and computed saturation time (T_s) in clay-sand-gravel mixture having 10% clay

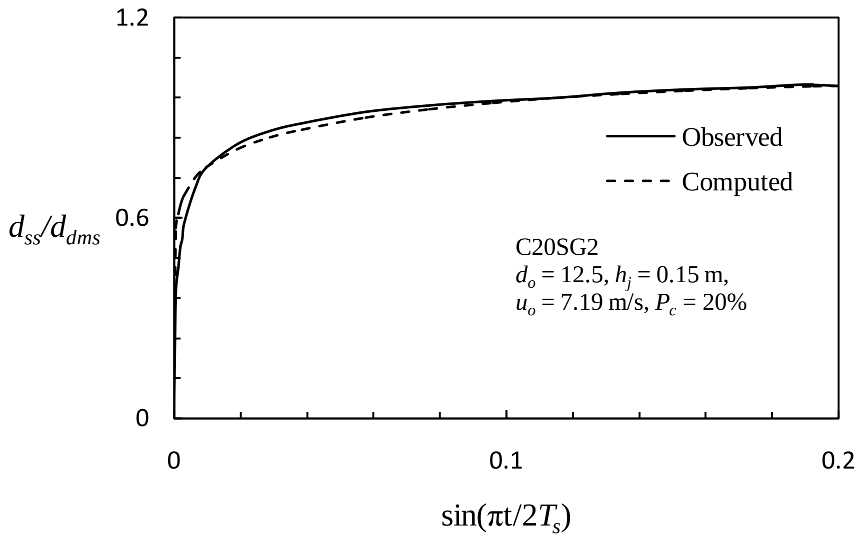

Fig. 5.35 Comparison of observed and computed saturation time, T_s in clay-sand-gravel mixture having 20% clay

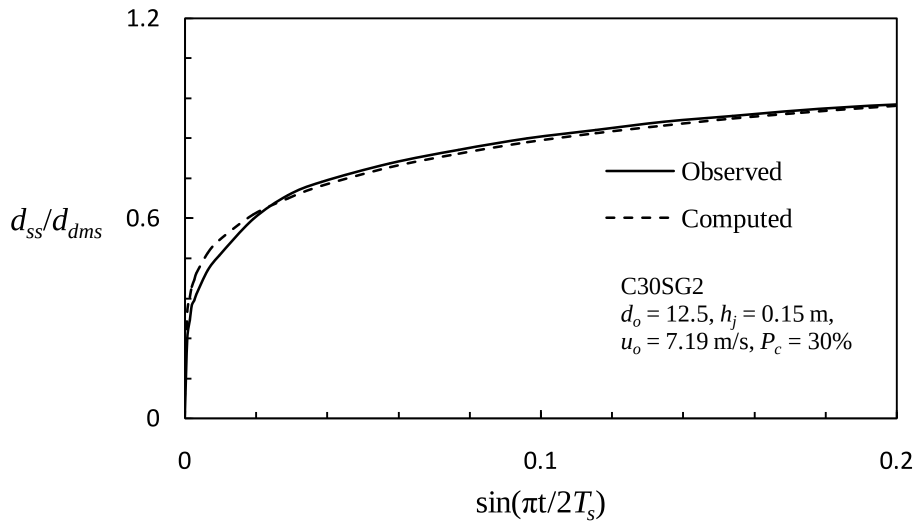

Fig. 5.36 Comparison of observed and computed saturation time (T_s) in clay-sand-gravel mixture having 30% clay

A similar comparison was also obtained in case of 40%, 50% and 60 % clay in clay-sand-gravel cohesive sediment mixtures. These figures are not shown here due to space limitation.

5.3.2 Estimation of Various Parameters in Clay-Sand-Gravel Mixture

The data collected in the present study have been used to develop relationships for various scour parameters like maximum static scour depth, maximum dynamic scour depth, radius of scour hole; height of dune and volume of scour hole.

(a) Maximum static scour depth

Sarma (1967), Westrich and Kobus (1973), Rajaratnam (1982), Aderibigbe and Rajaratnam (1996) and Ansari et al. (2003) identified non-dimensional parameter (E_c). It is used to describe the process of estimation of maximum static scour depth as described in Eq. (4.7) for different clay percent in clay-sand-gravel mixtures.

Maximum static scour depth has been analyzed with erosion parameter for various percentages of clay content, P_c i.e. 10 to 60% in clay-sand-gravel as shown in Fig. 5.37. It is apparent from Fig. 5.37 that the depth of scour reduces significantly with increase in clay percentage in the mixture which indicates that the depth of scour is a function of clay content and erosion parameter.

Equation (5.14) is proposed to estimate the maximum static scour depth in clay-sand-gravel mixtures which can be given as follows;

$$\frac{d_{sms}}{h_j} = 1.1(P_c)^{-0.557}(E_c)^{0.604} \qquad (R^2 = 0.73) \qquad (5.14)$$

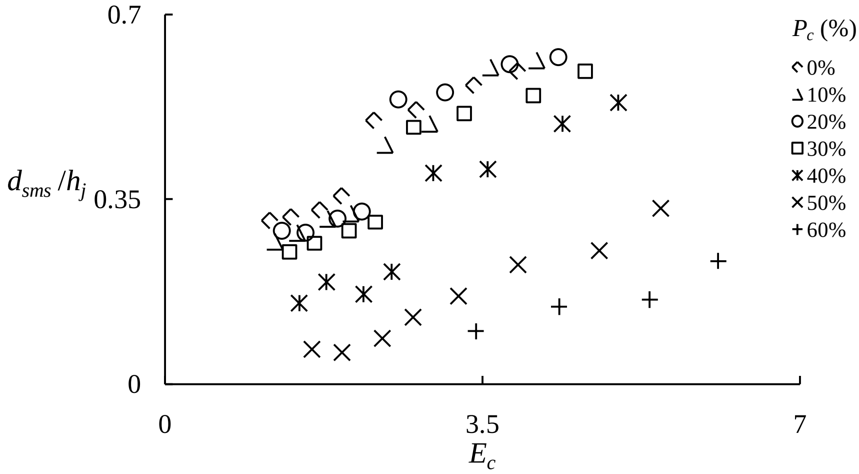

Fig. 5.37 Variation of static scour depth, d_{sms} with erosion parameter, E_c with different clay percent in clay-sand-gravel mixture

Equation (5.14) is proposed to estimate the maximum static scour depth in clay-sand-gravel mixtures which predicts the scour depth within ± 25% error as shown in Fig. 5.38.

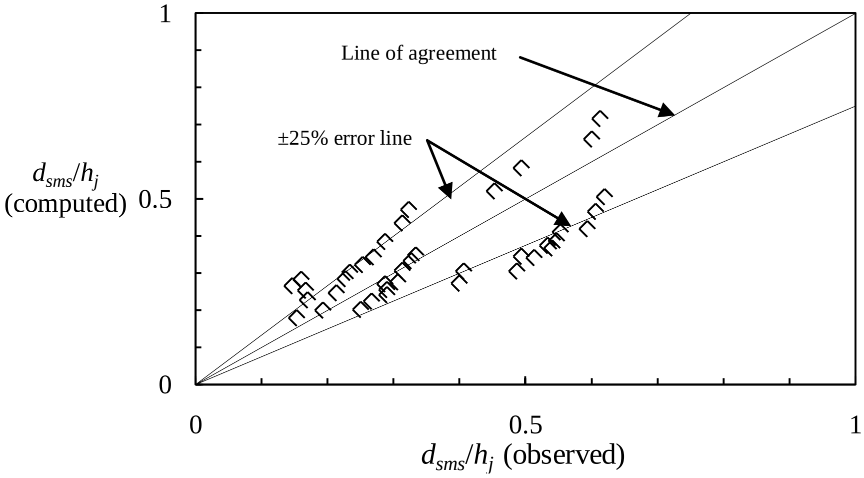

Fig. 5.38 Comparison of observed and computed maximum static scour depth using Eq. (5.14)

Further, the maximum static scour depth is analyzed with sediment size, nozzle diameter, jet velocity, and clay percentages. The variation of maximum static scour depth can be well explained with dimensionless parameters i.e., d_a / h_j, d_o / h_j, $u_o / \sqrt{gh_j}$ and clay content, P_c instead of erosion parameter. Analysis of data reveals that the static scour depth increases with increase of sediment size, jet velocity and decrease with nozzle diameter and clay percent. Eq. (5.15) is proposed to estimate the maximum static scour depth in clay-sand-gravel sediment mixtures.

$$d_{sms}/h_j = 80\left(\frac{d_a}{h_j}\right)^{1.02}\left(\frac{d_o}{h_j}\right)^{-0.064}\left(\frac{u_o}{\sqrt{gh_j}}\right)^{0.048}(P_c)^{-0.105} \quad (R^2=0.82) \qquad (5.15)$$

The positive exponent of d_a/h_j is due to fact that the sizes of all particles are not uniform and once scour started segregation occurs in material. In the case of segregation of the bed material, the fine particles washed away from scour hole in the form of suspension and only gravels stay in the scour hole due to its heavy weight. In that case, the scour is mainly in gravel. However, in the analysis of data of cohesive sediment i.e. clay-sand-gravel mixture, weighted arithmetic mean has been taken into account, which is smaller than the size of the boulder. Since in the calculation smaller size is being used, however, the maximum scour is mainly governed by gravel size, therefore, positive exponent of d_a/h_j has been obtained.

The proposed relationship for computation of maximum static scour depth check for the suitability of the equation which predicts the scour depth with ± 20% error band as shown in Fig. 5.39.

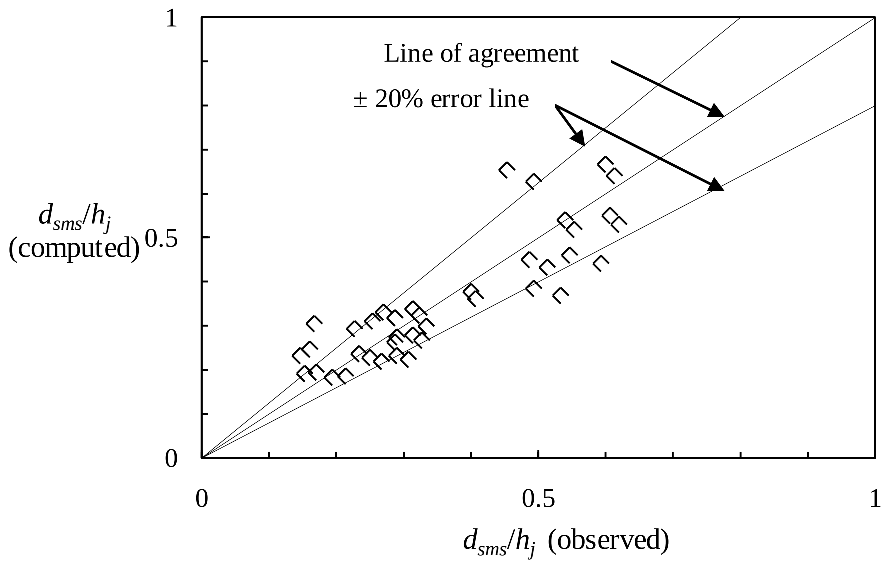

Fig. 5.39 Comparison of observed and computed maximum static scour depth using Eq. (5.15) in clay-sand-gravel mixtures

(b) Maximum dynamic scour depth

The variation of maximum dynamic scour depth is studied with the similar parameters as that for maximum static scour depth. It is found that the dynamic scour depth increases with increase of sediment size, nozzle diameter and jet velocity, and reduces with clay percent. A new relationship (Eq. 5.16) is proposed to estimate the maximum dynamic scour depth in clay-sand-gravel sediment mixtures.

$$d_{dms}/h_j = 213.6\left(\frac{d_a}{h_j}\right)^{0.567}\left(\frac{d_o}{h_j}\right)^{0.467}\left(\frac{u_o}{\sqrt{gh_j}}\right)^{0.545}(P_c)^{-0.76} \qquad (R^2=0.92) \qquad (5.16)$$

Positive exponent of d_a/h_j is due to segregation of bed material as explained earlier. The proposed relationship has been checked for its accuracy and found that Eq. (5.16) predicts the maximum dynamic scour depth within ± 15% error band as shown in Fig. 5.40.

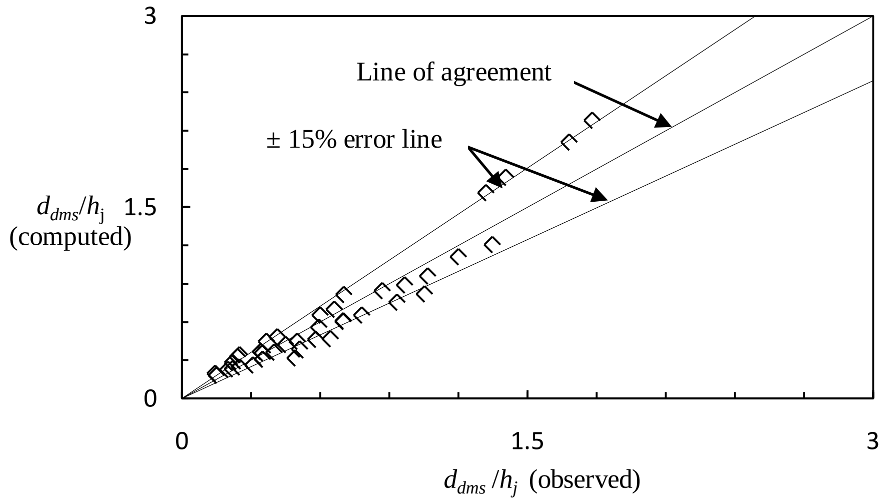

Fig. 5.40 Comparison of observed and computed maximum dynamic scour depth using Eq. (5.16) in clay-sand-gravel mixture

It is important to mention here that no data other than collected in the present study are available to the best of knowledge of writer, since no study has been conducted for the jet scour in cohesive sediment consisting of clay-sand-gravel mixtures.

Figure 5.41 presents the variation of ratio of maximum dynamic and maximum static scour depth with different percentages of clay content in the clay-sand-gravel mixtures. It is evident from Fig. 5.41 that the difference between the maximum dynamic and maximum static scour depth decreases with the increase in clay percentage in the mixtures. At higher percentage of clay viz P_c > 40%, both maximum dynamic and maximum static scour depth appear to be almost same.

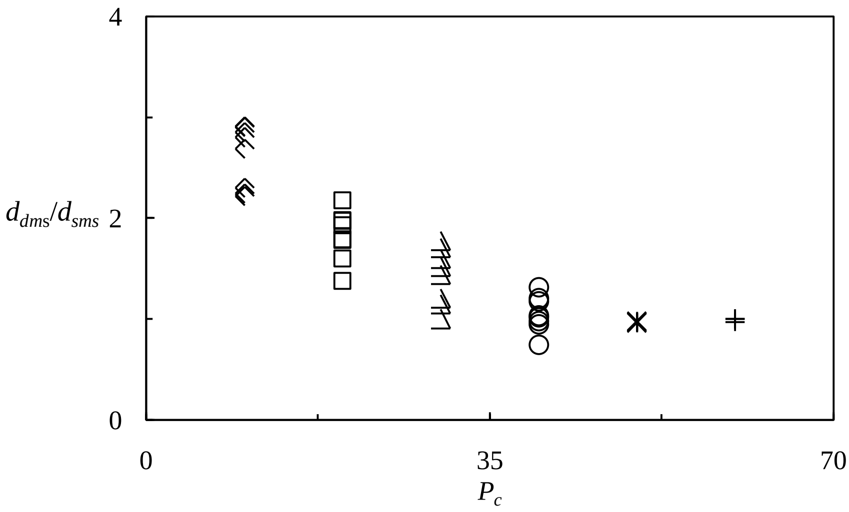

Fig. 5.41 Ratio of maximum dynamic and maximum static scour depths for different clay percentage in mixture

The variation of radius of scour hole, dune height, and volume of scour hole for presently collected data has been studied with various sediment and hydraulic parameters. After comprehensive analysis, it is found that these quantities are function of dimensionless parameters d_a/h_j, d_o/h_j, $u_o/\sqrt{gh_j}$ and percentages of clay content, P_c. Analysis of data reveals that the radius of scour and volume of scour increases with increase of sediment size, nozzle diameter and jet velocity, and reduces with increase of clay percent and sediment size. Following relationships have been developed using the data collected in the present study to predict radius of scour hole, dune height, and volume of scour hole in clay-sand-gravel mixtures as given.

$$r/h_j = 40.3\left(\frac{d_a}{h_j}\right)^{0.359}\left(\frac{d_o}{h_j}\right)^{0.403}\left(\frac{u_o}{\sqrt{gh_j}}\right)^{0.383}(P_c)^{-0..542} \qquad (R^2=0.78) \qquad (5.17)$$

$$\Delta/h_j = 0.654\left(\frac{d_a}{h_j}\right)^{-0.115}\left(\frac{d_o}{h_j}\right)^{0.928}\left(\frac{u_o}{\sqrt{gh_j}}\right)^{0.878}(P_c)^{-0.548} \qquad (R^2=0.94) \qquad (5.18)$$

$$\nabla/h_j^3 = 4.44\times10^9\left(\frac{d_a}{h_j}\right)^{3.01}\left(\frac{d_o}{h_j}\right)^{0.064}\left(\frac{u_o}{\sqrt{gh_j}}\right)^{-0.026}(P_c)^{-0.014} \qquad (R^2 = 0.92) \qquad (5.19)$$

It is found that the Eqs. (5.17 to 5.19) predict radius of scour hole with ± 15 % error band, volume of scour hole with ± 10 % error band and dune height with ± 15 % error band as shown in Figs. 5.42, 5.43 and 5.44 respectively.

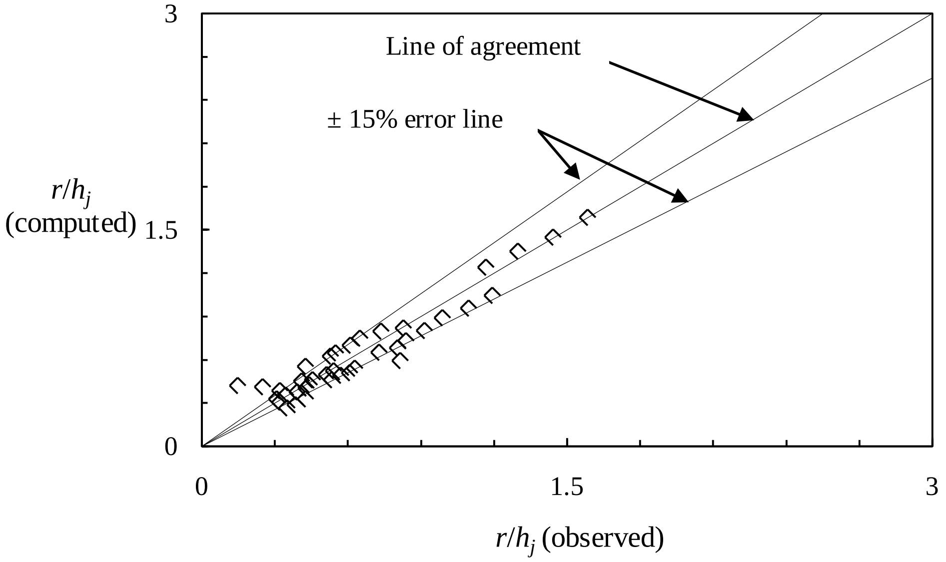

Fig. 5.42 Comparison of observed and computed radius of scour hole using Eq. (5.17) in clay-sand-gravel mixture

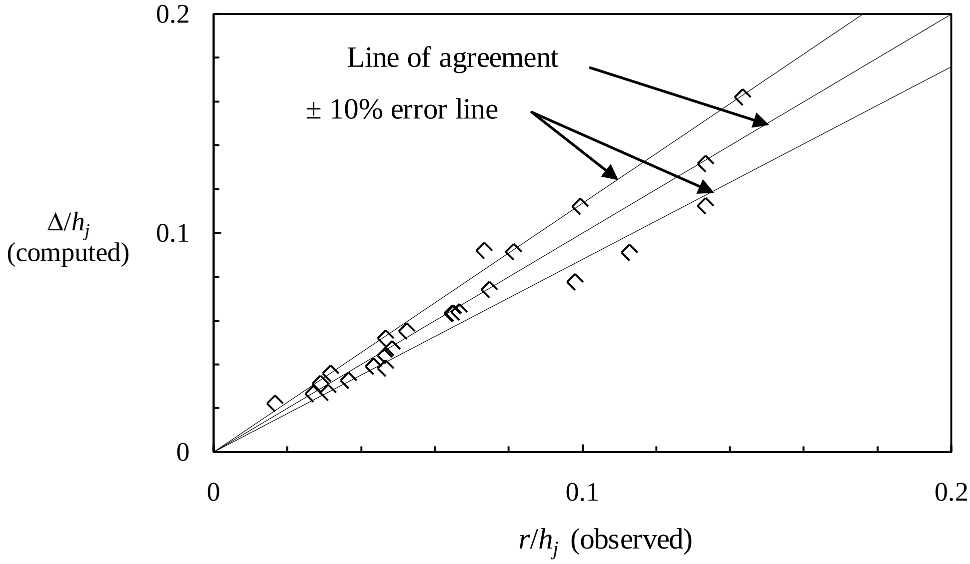

Fig. 5.43 Comparison of observed and computed height of dune using Eq. (5.18) in clay-sand-gravel mixture

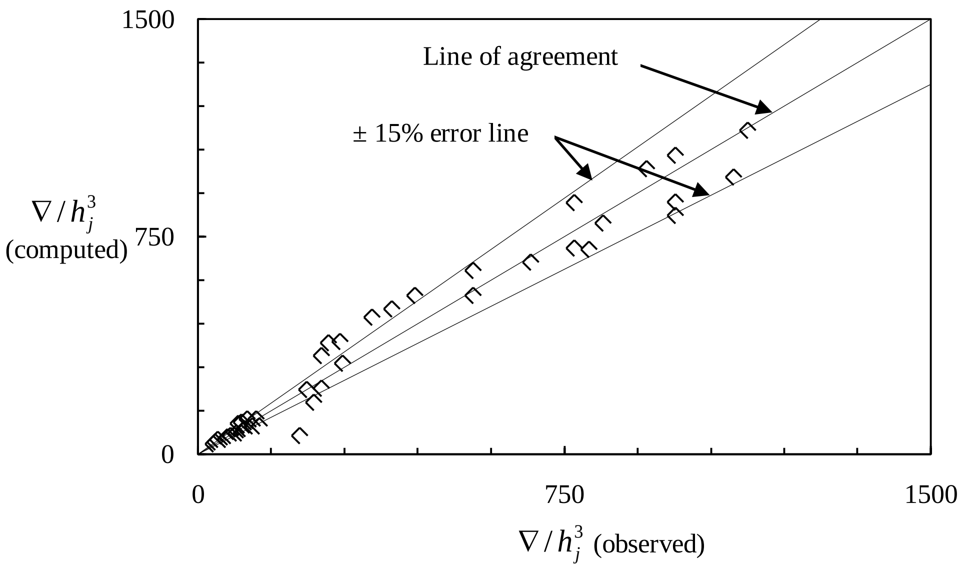

Fig. 5.44 Comparison of observed and computed volume of scour using Eq. (5.19) hole in clay-sand-gravel mixture

The variation in maximum dynamic scour depth, radius of scour hole, dune height, and volume of scour hole was also studied with erosion parameter but their correlation was not satisfactory. The variation of dynamic scour depth, radius of scour hole, dune height, and volume of scour hole was also studied with unconfined compressive strength, dry density, and antecedent moisture content. However, it is found that percentage of clay is more pronounced parameter to be used in formulation of relationships for various parameters under submerged circular vertical impinging water jets in cohesive sediment consisting of clay-sand-gravel mixtures.

5.8 CONCLUDING REMARKS

The collected data in the present study in the respect of scour in clay-gravel and clay-sand-gravel cohesive sediment mixtures under submerged circular vertical impinging water jets have been analyzed. The effects of various parameters on scour have been investigated under various permutations and combinations of the test conditions. Analysis regarding the temporal variation of scour depth has been presented using the data obtained in the present research work. Using the experimental data, working relationships have been established for computation of maximum static and maximum dynamic scour depth for clay-gravel and clay-sand-gravel cohesive sediment mixtures. Relationships have also been proposed for other length scale scour parameters like radius of scour hole, dune height and volume of scour hole.

CHAPTER 6

CONCLUSIONS

6.1 GENERAL

Several laboratory experiments were conducted to study the process of scour in cohesionless and cohesive sediment mixtures under submerged circular vertical jets for varying nozzle diameter, jet height and jet velocity. The characteristics of sediment mixtures like antecedent moisture content, clay content, dry density, void ratio, and unconfined compressive strength were also obtained. Three types of sediment mixtures were used for the experimentation, i.e., (a) Cohesionless sediment consisting of fine sand, gravel and sand-gravel mixture, (b) Gravel mixed with clay in proportions varying from 10% to 60% by weight and, (c) Gravel and sand in equal proportion by weight mixed with clay in proportions varying from 10% to 60% by weight.

A detailed parametric investigation were carried out to study the response of sediment materials i.e. sand, gravel, sand-gravel, clay-gravel and clay-sand-gravel mixture to the action of submerged circular vertical impinging water jets for various jet height, jet velocity, diameter of nozzle. The specific objectives of the present research work were to study the governing parameters of scour due to submerged circular vertical jets.

This laboratory research work extends the range of existing experimental data by using different jet diameters, jet velocity, jet heights from bed level and type of sediment mixtures. This resulted in much larger dynamic and static scour depths compared to the previous laboratory experiments. The temporal variation of scour depth under submerged circular vertical water jets in cohesive and non-cohesive sediment was modeled. Predictors for temporal variation of scour depth, maximum dynamic depth of scour, maximum static depth of scour, radius of scour hole, dune height, volume of scour hole were also developed. The main contribution of this research works are summarized as follows:

6.2 SCOUR DUE TO JET IN COHESIONLESS SEDIMENT

1. The laboratory research work includes probable one of the few or the first study as reported international literature on scour under submerged circular vertical jets consisting of gravel and sand-gravel mixtures in cohesionless sediment.
2. Visual examination of developed scour profile reveals that the scour parameters like maximum dynamic and maximum static scour depth increases with increases of jet velocity and nozzle size while scour depths reduces with increase of jet height and sediment size of the bed materials.
3. The experimental observations and analysis presented in this investigation established that the sediment size and sediment type have significant role on size of scour hole produced by water jets.
4. The geometries of scour hole in sand-gravel mixtures are found to be different than that of sand and gravel bed. Segregation of fine sand and gravel was observed in case of jet scour in sand-gravel mixtures. The sand material was deposited on the rim of scour hole while gravel was deposited in the core.
5. Different shapes of scour hole profiles in cohesionless sediment consisting of fine sand, gravel and sand-gravel mixture were observed. The side slope of the scour profile was steep in gravel and sand-gravel mixture compared to sand beds.
6. Radius of scour hole, dune height and volume of scour hole increase with increase of nozzle diameter, jet velocity while they decrease with increase of sediment size and jet height
7. The time required to reach in equilibrium state i.e. saturation time was found low in sand beds as compared to sand-gravel mixture and gravel beds.
8. Maximum dynamic scour is higher than the maximum static scour in all the experiments. The differences in maximum dynamic and static scour were higher in sand compared to gravel and sand-gravel mixtures. Relationships are proposed to compute the maximum static and dynamic scour depth.
9. The erosion parameter originally proposed by Aderibigbe and Rajaratnam (1996) and Ansari el al. (2003) describe satisfactorily the scour parameters like maximum static and maximum dynamic scour depths in cohesionless sediment. However better results were found using dimensionless parameters like d_a / h_j, d_o / h_j and $u_o / \sqrt{gh_j}$ in place of erosion parameter. The proposed relationship is based on the data that cover a wide range of the pertinent variables.

10. The temporal variation of scour depth is fitted to a sine function as mentioned in Eq. (4.5). It was found that the scaling parameters, m_s and T_s vary with sediment size, jet velocity, nozzle diameter and height of jet in fine sand, gravel and sand-gravel mixture. The computed temporal variation of scour depth using Eq. (4.5) is in good agreement with the observed values.
11. Radius of scour hole, dune height and volume of scour hole increase with increase of nozzle size, jet velocity while they decrease with increase of sediment size and jet height
12. Formation of dune is also important aspects which are influenced by sediment characteristics such as type, size and quantity of sediments. However, shape of scour holes depends on various flow and sediment characteristics.
13. Relationships are proposed, using present data available and previous study for the computation of various scour parameters like maximum static and maximum dynamic scour depths, radius of scour hole, dune height and volume of scour hole in sand, gravel and sand-gravel mixture. These relationships are able to predict the desired parameters within ± 20 percent error band.

6.3 SCOUR DUE TO JETS IN COHESIVE SEDIMENT

1. The laboratory research work includes the first study on scour under submerged circular vertical impinging water jets in cohesive sediment consisting of clay-gravel and clay-sand-gravel mixtures.
2. Visual examination of developed scour profile reveals that the scour parameters like maximum dynamic and maximum static scour depths increases with jet velocity and nozzle size while that reduce with increase of jet height, sediment size and percentage of clay content in clay-gravel and clay-sand-gravel mixtures.
3. The experiments revealed that the process of scour as well as scour depth, scour profile produced by water jets in cohesive sediment are significantly different from that of cohesionless sediments.
4. The time required to reach in equilibrium state i.e. saturation time was found minimum in low clay percentage and maximum for higher clay percentage in clay-gravel and clay-sand-gravel mixtures.
5. The experimental observations and analysis presented in this investigation has established that the percentage of clay content, P_c has significant effects on scour process in sediment mixtures consisting of clay.

6. It was found that when clay percentage exceeds 30% with gravel and sand-gravel mixture, there is no significant difference between maximum static and maximum dynamic scour depths due to more cohesion influences at higher clay percent.
7. The scour holes due to submerged circular vertical jets in cohesive sediments are found to have different geometries with their side slopes ranging from 30^o to 90^o. However, for 10% clay with gravel and with sand-gravel mixtures were found to be almost similar to that in case of gravel and sand-gravel beds. As clay percent increases; scour depth reduces and geometry of the scour profile was observed almost in vertical shapes for clay percentage higher than 30% in gravel and sand-gravel mixtures.
8. The formation of dune was very small in case of higher clay percentage in sediment bed and also the sediment was deposited far away from the scour hole profiles in the form of lumps and chunks of various size and shapes.
9. The time required to reach in equilibrium state i.e. saturation time was found minimum in low clay percent and maximum for higher clay percentage in clay-gravel and clay-sand–gravel mixtures.
10. The temporal variation of scour depth is fitted to a sine function as mentioned in Eq. (4.5). The parameters, m_s and T_s vary with sediment size, jet velocity, nozzle diameter, jet height and percentage of clay content in clay-gravel and clay-sand-gravel mixture. The computed temporal variation of scour depth using Eq. (4.5) is in good agreement with the observed values.
11. Relationships are proposed, using the available data for the computation of various scour parameters like maximum static, maximum dynamic scour depth, radius of scour hole, dune height and volume of scour hole in clay-gravel and clay-sand-gravel mixture. These relationships are able to predict the desired parameters within ± 20 percent error.

6.4 RECOMEMENDATION FOR FUTURE RESEARCH

The studies on scour under submerged circular vertical water jets are limited to the laboratory setup; also the flow characteristics do not truly represents the field conditions in view of large scale distortion of the models. However, such types of experimental studies are encouraged along with field investigations or large scale models. The theoretical or numerical approach may also be under taken for the validation of laboratory based experiments and field results with wide range of flow variations. It should also be remembered that the proposed equations likely do not apply to the sediment materials that are layered, inhomogeneous, fissured, disturbed. The equation proposed for cohesive sediment also may not apply to unsaturated sediment samples that can slake.

REFERENCES

Abt, S. R., and Ruff, J.F. (1982). "Estimating culvert scour in cohesive material." *Journal of Hydraulic Division, ASCE, Vol.* 108, pp 25-34.

Aderibigbe, O., and Rajaratnam, N. (1996) "Erosion of loose beds by submerged circular impinging vertical turbulent jets." *Journal of Hydraulic Research, Vol.* 34(1), 19–33.

Aderibigbe, O., and Rajaratnam, N. (1998). "Effects of sediment gradation on erosion by plane turbulent wall jets" *Journal of Hydraulic Engineering, ASCE, Vol.* 124(10), pp-1034–1042.

Adduce, C. and Mele, P. (2004). "Local scour by submerged turbulent jets." *Advances in Hydro-Science and Engineering, Vol. VI,* pp-1-7.

Ade, F. and Rajaratnam, N. (1998). "Generalized study of erosion by circular horizontal turbulent jets." *Journal of Hydraulic* Research, *Vol.* 36(4), pp 613-636.

Agostino, V. D. and Ferro, V. (2004). "Scour on alluvial bed downstream of grade-control structures". *Journal of Hydraulic Engineering, ASCE, Vol.* 130, No. 1, pp. 24-37.

Altinbilek, H., and Okyay, S. (1973). "Localized scour in a horizontal sand bed under vertical jets." *Proc., IAHR Conf., Istanbul, Vol.* (1), A14, pp- 1–8.

Ansari, S. A. (1999). "Influence of cohesion on local scour." Ph. D. Thesis, Department of Civil Engineering, Indian Institute of Technology, Roorkee (Formerly University of Roorkee, Roorkee), India.

Ansari, S.A., Kothyari, U.C., and Ranga Raju, K.G. (2003). "Influence of cohesion on scour under submerged circular vertical jet." *Journal of Hydraulic Engineering, ASCE, Vol.* 129(12), pp-1014–1019.

Ansari, S.A., Kothyari, U.C. and Ranga Raju, K.G. (2002). "Influence of cohesion on scour around bridge piers." *Journal of Hydraulic Research, IAHR, Vol.* 40, No. 6, pp-717-729.

Azamathulla, H., Aminuddin, A.G., Zakaria, N.A., Leow C.S. and Chang, C.K. (2009). "Prediction of scour around hydraulic structure using soft computing technique." *International Conference on Water Resources* (ICWR 2009), Langkawi, Kedah, Malaysia.

Azamathulla, H. and Zakaria, N.A. (2011). "Prediction of scour below submerged pipeline crossing a river using ANN." Water science and Technology, Vol. 63(10), pp 2225-2230.

Bagnold, R.A. (1966). “An approach to the sediment transport problem from general physics” *Physiographic and Hydraulic Studies of River, Geological, Survey Professional Paper* 422-I, pp-1-37.

Blaisdell, F.W., Anderson, C.L., Hebaus, G.G. (1981). “Ultimate dimensions of local scour.” *Journal of Hydraulic Division, ASCE, Vol*. 107(HY3), pp 327-337.

Beltaos, S. and Rajaratnam, N. (1974). “Impinging circular turbulent jets.” *Journal of Hydraulic Division, ASCE, Vol*. 100(10), pp-1313–1328.

Breusers, H.N.C., and Raudkivi, A.J. (1991). “Scouring.” *Hydraulic structure manual, I.A.H.R.,* Balkema, Rotterdam, Netherland.

Bormann, N.E. and Julien, P.Y. (1991). “Scour downstream of grade-control structures”. *Journal of Hydraulic Engineering, ASCE, Vol.* 117, No. 5, pp. 579-594.

Bowles. J.E. (1984). “Physical and geotechnical properties of soils.” *McGraw Hill Book Company,* 2nd Edition.

Chakravarti, A., Jain, R.K. and Kothyari, U.C. (2013). “Scour under submerged circular vertical jets in cohesionless sediments.” *ISH Journal of Hydraulic Engineering, Taylor & Francis Group, Vol*. 20(1), pp 32-37.

Chahar B.R. (2011). “Discussion of simplified accurate solution for design of erodible trapezoidal channels.” *Journal of Hydraulic Division, ASCE, Vol.* 16 (11), 960-965.

Chalov R.S. (1995). “Equilibrium longitudinal profile and directional vertical channel deformations.” *Geomorphology, No.*3, pp. 18–24.

Chalov R.S., Zavadskiy A. S., and Panin, A. V. (2004). “River Meanders.” *MSU Publ., Moscow,* pp. 371.

Clarke, F. R. W. (1962). “The action of submerged jets on movable material” *Ph.D thesis, Imperial College,* London.

Dargahi, B. (2003). “Scour development downstream of a spillway”. *J. Hydr. Res., Vol.* 41, No. 4, pp. 417-426.

Dehghani, A.A., Azamathulla, H.Md., Hashemi Najafi, S.A. and Ayyoubzadeh, S.A. (2013). “Local scouring around L-head groynes.” *Journal of Hydrology, Elsevier Science, Vol.* 504, pp-125–131.

Dehghani, A.A., Bashiri, H., and Meshkati Shahmirzadi, M.E. (2010). “Local scouring due to flow jet at downstream of rectangular sharp-crested weirs.” *Water and Geoscience Conf., Cambridge,* ISBN: 978-960-474-160-1.

Dey S. and Sarkar A. (2006).“Scour downstream of an apron due to submerged horizontal jets.” *Journal of Hydraulic Engineering, ASCE, Vol.*132(3), 146-257.

Dey, S. and Westrich, B. (2003). “Hydraulics of submerged jet subject to change in cohesive bed geometry”. *Journal of Hydraulic Engineering, ASCE, Vol.* 129, No. 1, pp. 44-53.

Doddiah, D., Albertson, M.L., and Thomas, R. (1953). “Scour from jets.” Proc., 5th Int. Assoc. for Hydraulic Research Congress, IAHR, Minneapoli, USA

Donoghue, T.O., Trajkovic, B., and Piggins J. (2001). “Sand bed response to submerged water jet.” *Proc., Eleventh Int. Offshore and Polar Engineering Conference, Stavanger*, Norvey, June 17–22.

Dunn, I.S. (1959). “Tractive resistance of cohesive channels.” *Journal of Soil Mechanics and Foundation Division, ASCE, Vol.* 85, No. SM-3, June, pp. 1-24.

Francis, J.R.D., and Mccreath, P. S. (1979). “bed load transport by submerged jets.” *Proc. Natl. Acad. Sci. U.S.A., Vol.* 76(9), pp-4159-4161.

Fukuoka, S. and Osada K. (2009). “Sediment transport mechanism and grain size distributions in stony bed rivers” *33rd IAHR Congress, Water Engineering for a Sustainable Environment,* ISBN 978-94-90365-01-1

Fukuoka, S., Sumi, T. and Horiuchi, S. (2013). “Sediment management on the arase dam removal project.” *Advances in River Sediment Research, Taylor & Francis Group, London,* ISBN 978-1-138-00062-9 pp-1201-1209.

Francis, J.R.D. and Mccreath, P.S. (1979). “Bed load transport by submerged jets.” *Applied Physical sciences, Proc. Natl, Acad. Sci. USA, Vol.* 76(9), pp-4159-4161.

George L.R. (1980). “Impinging jets” *Hydraulics Branch Division of Research, Engineering Centre, Denver, Colorado,* REC-ERC-80-8.

Grim, R.E. (1962). “Applied clay mineralogy” *McGraw Hill Book Company*, 1st Edition.

Goel, A. (2010). “Scour investigations behind a vertical sluice gate without apron.” *The Pacific Journal of Science and Technology,Vol.* 11 (2), pp-59-65.

Hanson, G. J. (1991). “Development of a jet index to characterize erosion resistance of soils in earthen spillways.” *Trans. ASAE,* 34(5), pp-2015–2020.

Hanson, G.J. (1992). “Erosion resistance of compacted soils.” *Transportation Research Record Number 1369, Advances in Geotechnical Engineering, National Academy Press,* Washington D.C., pp. 26-30.

Hanson, G.J., (1993) “Effect of consolidation on soil erodibility.” *A.S.A.E. Paper* 932091, *St. Joseph*, MI. ASCE.

Hanson, G. J., and Robinson, K. R. (1993). “The influence of soil moisture and compaction on spillway erosion.” *Trans. ASAE,* 36(5), pp-1349–1352.

Hanson, G.J., and Cook, K.R. (2004). “Apparatus, test procedures, and analytical methods to measure soil erodibility in-situ.” *Trans. ASAE*, 20(4), pp 455-462.

Hanson, G.J., and Cook, K.R. (1997). “Development of excess shear stress parameters for circular jet testing.” *Proc., 1997 ASAE Annual International Meeting, Minneapolis, Minnesota,* Paper 972227.

Hanson, G.J., Robinson, K.M., and Temple, D.M. (1990). “Pressure and stress distributions due to a submerged impinging jet.” *Hydr. Engineering, Proc.* 1990 *National Conference, ASCE, Reston*, VA, pp 525-530.

Hayter, E.J. (1983). "Prediction of Cohesive Sediment Movement in Estuarial Waters." *Ph. D. Thesis, the University of Florida at Gainesville*

Hrycak, P., Lee, D.T., Gauntner, J.W. and Livingood, J.N.B. (1970). “Experimental Flow Characteristics of a Single Turbulent Jet Impinging on a Flat Plate.” *National Aeronautics & Space Administration,* TND-5652, pp-32.

Hoffmans, G.J.C.M. (1998). “Jet scour in equilibrium phase.” *Journal of Hydraulic Engineering, ASCE, Vol.* 124, No. 4, pp. 430-437.

Hoffmans, G.J.C.M. (2009). “Closer problem to jet scour.” *Journal of Hydraulic Research, I.A.H.R., Vol.* 47(1), pp 100-109.

IS: 1498 (1970). “Classification of soils for general engineering purposes.”

IS: 2720 Part XXIX (1975). “Determination of in- place density by core-cutter method.”

IS: 2720 Part X (1991). “Determination of shear strength by unconfined compression method.”

Islam, M.N., Garde, R.J. and Ranga Raju, K.G. (1986). “Temporal variation of local scour.” *Proc. I.A.H.R., Symposium on scale effects in modeling sediment transport phenomenon, Toronto,* Canada, pp. 252-262.

Jain, R. K. (2008). “Influence of cohesion on detachment and transport of clay-sand-gravel mixtures.” *Ph.D. Thesis,* IIT Roorkee.

Jain, R.K. and Kothyari U.C. (2009a). “Cohesion influences on erosion and bed load transport.” *Water Resour. Res.,* 45, W06410.

Jain, R. K. and Kothyari U. C. (2009b). “Flow characteristics in degraded bed profile of clay-gravel mixtures.” Proceedings of 33rd IAHR Congress, Vancouver, British Columbia, August 9-14, 2009.

Jain, R. K. and Kothyari, U. C. (2010). “Influence of cohesion on suspended load transport of non-uniform sediments” *Journal of Hydraulic Research, I.A.H.R., Vol.* 48(1), pp. 33–43.

Johnston, A.J. (1990). “Scourhole developments in shallow tailwater” *Journal of Hydraulic Research, I.A.H.R., Vol.* 28(3), 341-354.

Kells, J. A., Balachandar, R. and Hagel, K. P. (2001). “Effect of grain size on local channel scour below a sluice gate”. *Can. J. Civ. Engrg., Vol*. 28, No. 3, pp. 440-451.

Kothyari, U. C., Garde, R. J. and Ranga Raju, K. G. (1992 a). “Temporal variation of scour around circular bridge piers.” J. Hydraul. Eng., ASCE, 118(8): 1091-1106.

Kothyari, U. C., Garde, R. J. and Ranga Raju, K. G. (1992 b). “Live bed scour- around cylindrical bridge piers.” *Journal of Hydraulic Research, I.A.H.R., Vol.* 30(5), 701-715.

Kothyari, U. C. (2007). “Indian practice on estimation of scour around bridge piers-A comment.” *Sadhana,* 32(3), pp-187–197.

Kothyari, U. C. and Jain, R. K. (2008). “Influence of cohesion on the incipient motion condition of sediment mixtures.” *Water Resour. Res.,* 44, W04410.

Kothyari, U.C. and Jain, R.K. (2010) “Erosion characteristics of cohesive sediment mixtures.” *River flow-Dittrich, Koll, Aberle and Geisenhainer,* ISBN978-3-939230-00-7.

Kumar A. (2011). “Scour around circular piers founded in clay-sand-gravel sediment mixtures.” *Ph.D. thesis*, IIT Roorkee-247667.

Kuti, E.O. and Yen, C. (1976). “Scouring of cohesive soils.” *Journal of Hydraulic Research, I.A.H.R., Vol.* 14, pp. 195-206.

Lambermont, J. and Lebon, G. (1978). “Erosion of cohesive soils.” *Journal of Hydraulic Research, I.A.H.R., Vol.* 16(1), pp 27-44.

Laursen, E.M, (1958). “Scour at bridge crossing.” *U.S. Geological Survey Open File Report,* pp-695-734.

Li, Y.T. (1987). “Initial study of the bed material gradation under deposition-erosion equilibrium.” *Journal of Sediment Research, Vol.* (1), pp 82-87.

Li, Y.T. (1987). “Bank failure mechanism and prevention in the middle and lower Yangtze River.” *Research Report,* Wuhan University, Wuhan, China.

Liu, H.K., Chang, F.M., and Skinner, M.M. (1961). “Effect of bridge construction on scour and backwater.” Res. No.CER-60-HKL-22, Deptt. Of Civil Engg., Colorado state university, USA.

Mason, P.J. and Arumugam, K. (1985). “Free jet scour below dams and flip buckets”. *Journal of Hydraulic Engineering, ASCE, Vol.* 111, No. 2, pp. 220-235.

Mazurek, K.A., Rajaratnam, N. and Sego D. C. (2001). "Scour of cohesive soil by submerged circular turbulent impinging jets." *Journal of Hydraulic Engineering, ASCE, Vol.* 127, pp-598–606.

Mazurek, K.A., Rajaratnam, N., and Sego, D. C. (2003). "Scour of a cohesive soil by submerged plane turbulent wall jets." *Journal of Hydraulic Research,I.A.H.R., Vol.* 41(2), 195–206.

Mazurek, K.A., Gautam, B. and Ahsan, Md. R. (2009). "Submergence effects on jets behavior and scour for plane wall jets in cohesionless materials." *33rd I.A.H.R. Congress,* ISBN:978-94-90365-01-1.

Mazurek, K.A., Christison K. and Rajaratnam, N. (2002). "Turbulent sand jets in water" *Journal of Hydraulic Research,I.A.H.R., Vol.* 40(4), pp-527-530.

Mazurek K.A. (2010). "Erodibility of a cohesive soil using a submerged circular turbulent impinging jet test." *2nd joint Fedral interagency Conference, Las Vegas, NV, June 27-July 1.*

Mazurek, K.A., and Hossain, Tanvir (2007). "Scour by jets in cohesionless and cohesive soils." *Can. J. Civil Eng., Vol.* 34, pp 744–751.

Mih, W.C., and Kabir, J. (1983). "Impingement of water jets on nonuniform streambed." *Journal of Hydraulic Engineering, ASCE, Vol.*109(4), pp 536–548.

Moore, W.L., and Masch, F.D. (1962). "Experiments on the scour resistance of cohesive sediments." *J. Geophys. Res., Vol.* 67(4), pp 1437–1446.

Pagliara, S., Hager, W.H. and Minor, H.E. (2006) "Hydraulics of plane plunge pool scour" *Journal of Hydraulic Engineering, ASCE, Vol.* 132(5), pp 450-461.

Pagliara, S. (2007). "Influence of sediment gradation on scour downstream of block ramps." *Journal of Hydraulic Engineering, ASCE, Vol.* 133(11), pp 1241–1248.

Pagliara, S., Hager, W.H. and Unger, J. (2008) "Temporal evolution of plunge pool scour" *Journal of Hydraulic Engineering, ASCE, Vol.* 134(11), pp 1630-1638.

Pagliara, S. and Michele, P. (2008). "Scour control and surface sediment distribution downstream of block ramps." *Journal of Hydraulic Research, IAHR, Vol.* 46, No. 3, pp. 334–343.

Partheniades, E. (1971). "Erosion and deposition of cohesive soils." *Chapter 25 in River Mechanics, Vol. II(Ed). H.W. Shen published by H.W. Shen, Fort Collins, USA.*

Patel, P.L. and Rangaraju, K.G. (1996). "Fractionwise calculation of bed load transport." *Journal of Hydraulic Research, I.A.H.R., Vol.* 34 (3), pp 363-379.

Patel, P.L. and Ranga Raju, K.G. (1999). "Critical tractive stress of nonuniform sediments." *Journal of Hydraulic Research, I.A.H.R., Vol.* 37(1), pp 39-58.

Poreh, M. and Cermak, J.E. (1959). “Flow characteristics of a circular submerged jet impinging normally on a flat boundary.” *Proceedings of the Sixth Midwestern Conference on Fluid Mechanics, University of Texas, Austin, TX,* pp-198–212.

Rajaratnam, N., and Beltaos, S. (1977). “Erosion by impinging circular turbulent jets.” *Journal of Hydraulic Division, ASCE, Vol.* 103(10), pp 1191–1205.

Rajaratnam, N. And Berry, S. (1977). “Erosion by circular turbulent wall jets”. Journal of Hydraulic Research, Vol. 15(3), pp-277-289.

Rajaratnam, N. (1981). “Erosion of plane turbulent jets.” *Journal of Hydraulic Research, I.A.H.R., Vol.* 19(4), pp 339–359.

Rajaratnam, N. (1982). “Erosion by submerged circular jets.” *Journal of Hydraulic Division*, ASCE, vol. 108(2), pp 262–267.

Rajaratnam, N., and Mazurek, K.A. (2003). “Erosion of sand by circular impinging water jets with small tail water.” *Journal of Hydraulic Engineering, ASCE, Vol..* 129(3), pp 225–229.

Rajaratnam, N., and Mazurek, K.A. (2005). “Impingement of circular turbulent jets on rough boundaries.” *Journal of Hydraulic Research, I.A.H.R., Vol.*43 (6), pp 688–694.

Rajaratnam, N., and Mazurek, K.A. (2006). “An experimental study of sand deposition from sediment laden water jets.” *Journal of Hydraulic Research, I.A.H.R., Vol.*44, pp 560–566.

Raudkivi, A. J. (1990). “Loose boundary hydraulics.” *3rd Edition, Pergamon Press, Chap*. 9, New York, USA.

Raudkivi, A.J. and Tan, S.K. (1984). “Erosion of cohesive soils.” *Journal of Hydraulic Research, I.A.H.R., Vol.* 22(4), pp 217-233.

Rouse, H. (1940). “Criteria for similarity in the transportation of sediment.” *Bulletin 20, University of Iowa, Iowa,* USA, 33–49.

Sarkar, A. and Dey, S. (2004). “Review on local scour due to jets.” *International Journal of Sediment Research*, Vol. 19, No. 3, pp-210-239.

Sarma, K.V.N. (1967). “Study of scour phenomenon and its functional form.” *Ph.D. thesis, Indian Institute of Sciences*, Banglore, India.

Sarma A. K., (2005). “Influence of bank line configuration on river bank erosion.” *Disaster Management Journal,* AASC, Vol.1 No.1, pp.1-7.

Srivastava, R. and Contractor, D. N. (1992.). “Bed-load and suspended load transport of nonuniform sediments.” *Journal of Hydraulic Engineering, ASCE, Vol.* 118, pp-948-949.

Smerdon, E.T., and Beasly, R.P. (1959). “The tractive force theory applied to stability of open channels in cohesive soils.” *Missouri University, Agr. Espt. Sta. Research Bull. Vol*. 715, pp-36.

Stain, O. R., Julien, P.Y., and Alonso, C. V. (1993). “Mechanics of jet scour downstream of a headcut.” *Journal of Hydraulic* Research, *I.A.H.R. Vol.* 31(6), pp-723-738.

Uyumaz A. (1988). “Scour downstream of vertical gate.” *Journal of Hydraulic Engineering, ASCE, Vol.* 114(7) pp 811-816.

Westrich, B., and Kobus, H. (1973). “Erosion of a uniform sand bed by continuous and pulsating jets.” *Proc., 15th IAHR Congress, Istanbul, Turkey, Vol.* 1, A13.1–A13.8.

Yalin, M.S. (1977) “Mechanics of sediment transport.” *2nd Edition, Pergamon Press*, New York, N.Y.

Yeh, P.H., Chang, K.A., Henriksen, J., Edge, B. and Chang, P. (2009). “Large-scale laboratory experiment on erosion of sand beds by moving circular vertical jets.” *Ocean Engineering*, Elsevier, Vol. 36, pp 248-255.

APPENDIX – A

HYDRAULIC AND SEDIMENT PARAMETERS UNDER SUBMERGED CIRCULAR VERTICAL JETS IN SAND BEDS

Run No	d_o (m)	u_o (m/s)	h_j (m)	d_{50} (m)
S1	0.0125	7.19	0.3	0.00024
S2	0.0125	7.19	0.15	0.00024
S3	0.0125	5.12	0.3	0.00024
S4	0.0125	5.12	0.15	0.00024
S5	0.008	9.84	0.3	0.00024
S6	0.008	9.84	0.15	0.00024
S7	0.008	6.65	0.3	0.00024
S8	0.008	6.65	0.15	0.00024

(Here the notation S1, stands for S = sand, 1 = run number)

APPENDIX – B

HYDRAULIC AND SEDIMENT PARAMETERS UNDER SUBMERGED CIRCULAR VERTICAL JETS IN SAND-GRAVEL MIXTURES BEDS

Run No	d_o (m)	u_o (m/s)	h_j (m)	d_a (m)
SG1	0.0125	7.19	0.3	0.00147
SG2	0.0125	7.19	0.15	0.00147
SG3	0.0125	5.12	0.3	0.00147
SG4	0.0125	5.12	0.15	0.00147
SG5	0.008	9.84	0.3	0.00147
SG6	0.008	9.84	0.15	0.00147
SG7	0.008	6.65	0.3	0.00147
SG8	0.008	6.65	0.3	0.00147

(Here the notation SG1, stands for S = sand, G = gravel, 1 = run number)

APPENDIX – C

HYDRAULIC AND SEDIMENT PARAMETERS UNDER SUBMERGED CIRCULAR VERTICAL JETS IN GRAVEL BEDS

Run No.	d_o (m)	u_o (m/s)	h_j (m)	d_{50} (m)
G1	0.0125	7.19	0.3	0.0027
G2	0.0125	7.19	0.15	0.0027
G3	0.0125	5.12	0.3	0.0027
G4	0.0125	5.12	0.15	0.0027
G5	0.008	9.84	0.3	0.0027
G6	0.008	9.84	0.15	0.0027
G7	0.008	6.65	0.3	0.0027
G8	0.008	6.65	0.15	0.0027

(Here the notation G1, stands for G = gravel, 1 = run number)

APPENDEX – D

HYDRAULIC AND SEDIMENT PARAMETERS UNDER SUBMERGED CIRCULAR VERTICAL JETS IN CLAY-GRAVEL COHESIVE SEDIMENT MIXTURES

Run No.	P_c	d_o (m)	u_o (m/s)	h_j (m)	d_a (m)	*W (%)*	γ (kN/m^2)	γ_d (kN/m^2)	e	*UCS* (kN/m^2)
C10G1	10	0.0125	7.19	0.3	0.00243	3.78	17.295	16.665	0.559	0
C10G2	10	0.0125	7.19	0.15	0.00243	5.22	17.063	16.216	0.603	0
C10G3	10	0.0125	5.12	0.3	0.00243	5.91	17.179	16.219	0.602	0
C10G4	10	0.0125	5.12	0.15	0.00243	5.43	17.011	16.128	0.611	0
C10G5	10	0.008	9.84	0.3	0.00243	3.63	17.237	16.632	0.563	0
C10G6	10	0.008	9.84	0.15	0.00243	5.91	17.237	16.276	0.597	0
C10G7	10	0.008	6.65	0.3	0.00243	5.18	16.982	16.145	0.610	0
C10G8	10	0.008	6.65	0.15	0.00243	4.01	16.924	16.598	0.598	0
C20G1	20	0.0125	7.19	0.3	0.00216	5.28	17.469	16.592	0.566	3.4603
C20G2	20	0.0125	7.19	0.15	0.00216	6.09	17.701	16.685	0.558	3.7847
C20G3	20	0.0125	5.12	0.3	0.00216	7.79	17.911	16.616	0.564	4.1091
C20G4	20	0.0125	5.12	0.15	0.00216	5.93	17.852	16.852	0.542	3.8904
C20G5	20	0.008	9.84	0.3	0.00216	6.31	17.585	16.541	0.571	4.0217
C20G6	20	0.008	9.84	0.15	0.00216	5.14	17.993	17.114	0.519	4.0151
C20G7	20	0.008	6.65	0.3	0.00216	6.42	17.817	16.742	0.552	3.9563
C20G8	20	0.008	6.65	0.15	0.00216	5.37	17.736	16.831	0.544	3.5688
C30G1	30	0.0125	7.19	0.3	0.00189	7.33	18.688	17.417	0.493	12.435
C30G2	30	0.0125	7.19	0.15	0.00189	9.69	17.572	16.935	0.535	12.216
C30G3	30	0.0125	5.12	0.3	0.00189	8.33	18.345	16.291	0.535	13.084

APPENDEX – D contd…

C30G4	30	0.0125	5.12	0.15	0.00189	8.14	18.572	17.17	0.51378	13.516
C30G5	30	0.008	9.84	0.3	0.00189	8.73	18.22	16.76	0.551	12.868
C30G6	30	0.008	9.84	0.15	0.00189	7.02	18.479	17.51	0.505	12.54
C30G7	30	0.008	6.65	0.3	0.00189	8.07	18.218	17.26	0.4975	13.841
C30G8	30	0.008	6.65	0.15	0.00189	7.38	18.398	17.132	0.5173	13.084
C40G1	40	0.0125	7.19	0.3	0.00163	11.34	19.1528	17.2	0.51123	19.139
C40G2	40	0.0125	7.19	0.15	0.00163	9.78	19.036	17.036	0.49924	19.772
C40G3	40	0.0125	5.12	0.3	0.00163	10.55	18.978	17.1666	0.5144	20.059
C40G4	40	0.0125	5.12	0.15	0.00163	11.2	18.804	16.91	0.5372	20.325
C40G5	40	0.008	9.84	0.3	0.00163	12.39	19.3269	17.195	0.5118	20.437
C40G6	40	0.008	9.84	0.15	0.00163	10.04	18.978	17.246	0.5073	20.113
C40G7	40	0.008	6.65	0.3	0.00163	11.37	18.861	16.935	0.535	20.221
C40G8	40	0.008	6.65	0.15	0.00163	10.4	19.094	17.351	0.4982	19.891
C50G2	50	0.0125	7.19	0.15	0.00136	12.57	19.849	17.631	0.4744	32.211
C50G4	50	0.0125	5.12	0.15	0.00136	13.5	19.675	17.332	0.4998	33.195
C50G6	50	0.008	9.84	0.15	0.00136	15.2	19.768	17.158	0.515	32.227
C50G8	50	0.008	6.65	0.15	0.00136	12.08	19.81	17.67	0.4704	33.391
C60G2	60	0.0125	7.19	0.15	0.00109	13.67	20.429	17.97	0.4464	41.199
C60G4	60	0.0125	5.12	0.15	0.00109	16.98	20.66	17.66	0.4718	41.524
C60G6	60	0.008	9.84	0.15	0.00109	13.76	20.48	18.009	0.4434	51.521
C60G8	60	0.008	6.65	0.15	0.00109	13.59	20.42	17.997	0.4441	41.639

APPENDEX – E

HYDRAULIC AND SEDIMENT PARAMETERS UNDER SUBMERGED CIRCULAR VERTICAL JETS IN CLAY-SAND-GRAVEL COHESIVE SEDIMENT MIXTURES

Run No	P_c	d_o m	u_o (m/s)	h_j (m)	d_a (m)	*W (%)*	γ (kN/m^2)	γ_d (kN/m^2)	e	*UCS* (kN/m^2)
C10SG1	10	0.0125	7.19	0.3	0.00132	4.37	18.978	18.182	0.4298	0
C10SG2	10	0.0125	7.19	0.15	0.00132	6.04	19.2689	18.17	0.4307	0
C10SG3	10	0.0125	5.12	0.3	0.00132	5	19.09	18.18	0.4295	0
C10SG4	10	0.0125	5.12	0.15	0.00132	6.4	18.86	17.727	0.4665	0
C10SG5	10	0.008	9.84	0.3	0.00132	5.29	18.74	17.8	0.46	0
C10SG6	10	0.008	9.84	0.15	0.00132	5.76	19.187	18.141	0.433	0
C10SG7	10	0.008	6.65	0.3	0.00132	5.5	18.36	17.65	0.472	0
C10SG8	10	0.008	6.65	0.15	0.00132	4	19.036	18.288	0.4214	0
C20SG1	20	0.0125	7.19	0.3	0.00118	9.3	19.385	17.72	0.436	8.751
C20SG2	20	0.0125	7.19	0.15	0.00118	8	19.84	18.36	0.4154	9.845
C20SG3	20	0.0125	5.12	0.3	0.00118	9	19.96	18.32	0.4195	10.05
C20SG4	20	0.0125	5.12	0.15	0.00118	8.6	19.73	18.16	0.432	10.05
C20SG5	20	0.008	9.84	0.3	0.00118	8.5	19.61	18.068	0.4388	9.191
C20SG6	20	0.008	9.84	0.15	0.00118	9.4	19.5	17.82	0.458	7.893
C20SG7	20	0.008	6.65	0.3	0.00118	9.2	19.79	18.1	0.4357	7.786
C20SG8	20	0.008	6.65	0.15	0.00118	8.6	19.9	18.32	0.4186	7.893
C30SG1	30	0.0125	7.19	0.3	0.00103	11.84	20.48	18.32	0.3985	29.85
C30SG2	30	0.0125	7.19	0.15	0.00103	12.28	20.32	18.0918	0.3866	27.03
C30SG3	30	0.0125	5.12	0.3	0.00103	11.11	20.25	18.23	0.40121	28.59

APPENDEX – E contd…

C30SG4	30	0.0125	5.12	0.15	0.00103	11.58	20.16	17.71	0.41523	30.58
C30SG5	30	0.008	9.84	0.3	0.00103	11.85	20.33	18.02	0.4426	29.11
C30SG6	30	0.008	9.84	0.15	0.00103	12.22	20.54	18.048	0.4324	29.65
C30SG7	30	0.008	6.65	0.3	0.00103	11.25	20.139	18.102	0.436	28.87
C30SG8	30	0.008	6.65	0.15	0.00103	10.68	20.37	18.404	0.4125	30.33
C40SG1	40	0.0125	7.19	0.3	0.00089	13.51	21.184	18.66	0.393	46.49
C40SG2	40	0.0125	7.19	0.15	0.00089	13.17	21.044	18.59	0.398	49.21
C40SG3	40	0.0125	5.12	0.3	0.00089	13	20.975	18.56	0.4	48.78
C40SG4	40	0.0125	5.12	0.15	0.00089	13.21	20.83	18.25	0.424	47.57
C40SG5	40	0.008	9.84	0.3	0.00089	13.3	21.1	18.62	0.396	47.03
C40SG6	40	0.008	9.84	0.15	0.00089	12.78	21.12	18.73	0.3879	48.66
C40SG7	40	0.008	6.65	0.3	0.00089	12.35	20.71	18.12	0.4021	49.74
C40SG8	40	0.008	6.65	0.15	0.00089	13.351	20.85	18.83	0.3803	49.56
C50SG1	50	0.0125	7.19	0.3	0.00074	14.59	21.7	18.94	0.372	53.37
C50SG2	50	0.0125	7.19	0.15	0.00074	14	21.83	19.14	0.358	52.81
C50SG3	50	0.0125	5.12	0.3	0.00074	14.6	21.76	18.98	0.369	55.14
C50SG4	50	0.0125	5.12	0.15	0.00074	15	21.64	18.823	0.381	54.6
C50SG5	50	0.008	9.84	0.3	0.00074	14.9	21.59	18.789	0.3836	55.68
C50SG6	50	0.008	9.84	0.15	0.00074	14.79	21.41	18.655	0.3935	54.85
C50SG7	50	0.008	6.65	0.3	0.00074	14.28	21.7	18.99	0.368	53.59
C50SG8	50	0.008	6.65	0.15	0.00074	14.79	21.47	18.7	0.389	54.39
C60SG2	60	0.0125	7.19	0.15	0.0006	15.78	21.93	18.947	0.3721	61.47
C60SG4	60	0.0125	5.12	0.15	0.0006	16.23	22.11	19.023	0.3665	61.63
C60SG6	60	0.008	9.84	0.15	0.0006	15.62	22.28	19.275	0.3487	60.53
C60SG8	60	0.008	6.65	0.15	0.0006	16.3	22.4	19.25	0.3503	62.56

APPENDIX – F

TEMPORAL VARIATION OF SCOUR DEPTH UNDER SUBMERGED CIRCULAR VERTICAL JETS IN COHESIONLESS SEDIMENTS

RUN NO. S1

t (s)	d_{ss} (m)
0	0
60	0.214
120	0.231
180	0.247
240	0.259
300	0.264
600	0.283
900	0.295
1200	0.306
1500	0.318
1800	0.325
2100	0.33
2400	0.333
2700	0.333
3000	0.333
3300	0.333
3600	0.334
3900	0.334
4200	0.334
4500	0.334
4800	0.335
5100	0.335
5400	0.335
5700	0.335
6000	0.336
6600	0.336
7200	0.336
9000	0.336
10800	0.336
12600	0.337
14400	0.337
16200	0.337
18000	0.337
21600	0.337
25200	0.337
28800	0.337

RUN NO. S2

t (s)	d_{ss} (m)
0	0
60	0.275
120	0.289
180	0.307
240	0.32
300	0.328
600	0.343
900	0.351
1200	0.357
1500	0.361
1800	0.363
2100	0.364
2400	0.364
2700	0.365
3000	0.365
3300	0.365
3600	0.366
3900	0.366
4200	0.367
4500	0.367
4800	0.368
5100	0.368
5400	0.368
5700	0.369
6000	0.369
6600	0.369
7200	0.37
9000	0.37
10800	0.37
12600	0.371
14400	0.371
16200	0.371
18000	0.371
21600	0.371
25200	0.371
28800	0.371

RUN NO. S3

t (s)	d_{ss} (m)
0	0
60	0.173
120	0.185
180	0.197
240	0.204
300	0.215
600	0.232
900	0.252
1200	0.259
1500	0.267
1800	0.274
2100	0.279
2400	0.283
2700	0.283
3000	0.284
3300	0.284
3600	0.285
3900	0.285
4200	0.285
4500	0.285
4800	0.286
5100	0.286
5400	0.286
5700	0.287
6000	0.287
6600	0.288
7200	0.288
9000	0.289
10800	0.289
12600	0.29
14400	0.29
16200	0.29
18000	0.29
21600	0.29
25200	0.29
28800	0.29

APPENDIX – F contd……

RUN NO. S4

t (s)	d_{ss} (m)
0	0
60	0.191
120	0.213
180	0.225
240	0.234
300	0.242
600	0.257
900	0.268
1200	0.278
1500	0.289
1800	0.298
2100	0.305
2400	0.309
2700	0.31
3000	0.31
3300	0.311
3600	0.311
3900	0.311
4200	0.312
4500	0.312
4800	0.313
5100	0.313
5400	0.313
5700	0.313
6000	0.313
6600	0.313
7200	0.314
9000	0.314
10800	0.314
12600	0.314
14400	0.314
16200	0.314
18000	0.314
21600	0.314
25200	0.314
28800	0.314

RUN NO. S5

t (s)	d_{ss} (m)
0	0
60	0.195
120	0.217
180	0.229
240	0.241
300	0.249
600	0.27
900	0.281
1200	0.289
1500	0.297
1800	0.304
2100	0.305
2400	0.305
2700	0.305
3000	0.305
3300	0.306
3600	0.306
3900	0.306
4200	0.306
4500	0.306
4800	0.307
5100	0.307
5400	0.307
5700	0.307
6000	0.308
6600	0.308
7200	0.308
9000	0.308
10800	0.308
12600	0.309
14400	0.309
16200	0.309
18000	0.309
21600	0.309
25200	0.309
28800	0.309

RUN NO. S6

t (s)	d_{ss} (m)
0	0
60	0.233
120	0.251
180	0.267
240	0.276
300	0.283
600	0.298
900	0.311
1200	0.322
1500	0.327
1800	0.328
2100	0.329
2400	0.33
2700	0.33
3000	0.33
3300	0.331
3600	0.331
3900	0.331
4200	0.332
4500	0.332
4800	0.332
5100	0.332
5400	0.333
5700	0.333
6000	0.333
6600	0.333
7200	0.333
9000	0.333
10800	0.334
12600	0.334
14400	0.334
16200	0.334
18000	0.334
21600	0.334
25200	0.334
28800	0.334

APPENDIX – F contd……

RUN NO. S7

t (s)	d_{ss} (m)
0	0
60	0.203
120	0.218
180	0.225
240	0.236
300	0.245
600	0.257
900	0.264
1200	0.268
1500	0.272
1800	0.275
2100	0.279
2400	0.28
2700	0.28
3000	0.281
3300	0.281
3600	0.281
3900	0.282
4200	0.282
4500	0.282
4800	0.283
5100	0.283
5400	0.283
5700	0.283
6000	0.284
6600	0.284
7200	0.284
9000	0.284
10800	0.284
12600	0.285
14400	0.285
16200	0.285
18000	0.285
21600	0.285
25200	0.285
28800	0.285

RUN NO. S8

t (s)	d_{ss} (m)
0	0
60	0.16
120	0.183
180	0.193
240	0.204
300	0.215
600	0.232
900	0.239
1200	0.245
1500	0.251
1800	0.252
2100	0.253
2400	0.253
2700	0.253
3000	0.253
3300	0.254
3600	0.254
3900	0.254
4200	0.255
4500	0.255
4800	0.255
5100	0.256
5400	0.256
5700	0.256
6000	0.257
6600	0.257
7200	0.257
9000	0.258
10800	0.258
12600	0.258
14400	0.259
16200	0.259
18000	0.259
21600	0.259
25200	0.259
28800	0.259

APPENDIX – F contd……

RUN NO. SG1

t (s)	d_{ss} (m)
0	0
60	0.215
120	0.228
180	0.241
240	0.249
300	0.255
600	0.264
900	0.273
1200	0.279
1500	0.286
1800	0.292
2100	0.297
2400	0.303
2700	0.305
3000	0.309
3300	0.31
3600	0.311
3900	0.311
4200	0.312
4500	0.312
4800	0.312
5100	0.313
5400	0.313
5700	0.313
6000	0.313
6600	0.313
7200	0.313
9000	0.314
10800	0.314
12600	0.314
14400	0.314
16200	0.314
18000	0.314
21600	0.314
25200	0.314
28800	0.314

RUN NO. SG2

t (s)	d_{ss} (m)
0	0
60	0.237
120	0.252
180	0.272
240	0.279
300	0.286
600	0.299
900	0.312
1200	0.32
1500	0.329
1800	0.332
2100	0.334
2400	0.335
2700	0.335
3000	0.335
3300	0.336
3600	0.336
3900	0.336
4200	0.337
4500	0.337
4800	0.337
5100	0.337
5400	0.338
5700	0.338
6000	0.338
6600	0.338
7200	0.339
9000	0.339
10800	0.339
12600	0.339
14400	0.339
16200	0.339
18000	0.339
21600	0.339
25200	0.339
28800	0.339

RUN NO. S3

t (s)	d_{ss} (m)
0	0
60	0.165
120	0.18
180	0.192
240	0.2
300	0.205
600	0.214
900	0.22
1200	0.223
1500	0.226
1800	0.228
2100	0.232
2400	0.235
2700	0.236
3000	0.238
3300	0.242
3600	0.243
3900	0.243
4200	0.244
4500	0.244
4800	0.244
5100	0.245
5400	0.245
5700	0.245
6000	0.246
6600	0.246
7200	0.246
9000	0.246
10800	0.247
12600	0.247
14400	0.247
16200	0.247
18000	0.247
21600	0.247
25200	0.247
28800	0.247

APPENDIX – F contd….

RUN NO. SG4

t (s)	d_{ss} (m)
0	0
60	0.191
120	0.203
180	0.216
240	0.222
300	0.227
600	0.242
900	0.253
1200	0.26
1500	0.263
1800	0.265
2100	0.268
2400	0.27
2700	0.272
3000	0.273
3300	0.274
3600	0.275
3900	0.276
4200	0.277
4500	0.277
4800	0.278
5100	0.278
5400	0.279
5700	0.28
6000	0.28
6600	0.28
7200	0.28
9000	0.28
10800	0.28
12600	0.28
14400	0.28
16200	0.28
18000	0.28
21600	0.28
25200	0.28
28800	0.28

RUN NO. SG5

t (s)	d_{ss} (m)
0	0
60	0.19
120	0.213
180	0.231
240	0.243
300	0.249
600	0.261
900	0.266
1200	0.271
1500	0.274
1800	0.277
2100	0.279
2400	0.282
2700	0.283
3000	0.284
3300	0.284
3600	0.284
3900	0.285
4200	0.285
4500	0.285
4800	0.286
5100	0.286
5400	0.286
5700	0.286
6000	0.287
6600	0.287
7200	0.287
9000	0.287
10800	0.288
12600	0.288
14400	0.288
16200	0.288
18000	0.288
21600	0.288
25200	0.288
28800	0.288

RUN NO. SG6

t (s)	d_{ss} (m)
0	0
60	0.21
120	0.229
180	0.241
240	0.253
300	0.262
600	0.278
900	0.287
1200	0.292
1500	0.299
1800	0.303
2100	0.304
2400	0.305
2700	0.305
3000	0.305
3300	0.306
3600	0.306
3900	0.306
4200	0.307
4500	0.307
4800	0.307
5100	0.307
5400	0.308
5700	0.308
6000	0.308
6600	0.308
7200	0.308
9000	0.309
10800	0.309
12600	0.309
14400	0.309
16200	0.309
18000	0.309
21600	0.309
25200	0.309
28800	0.309

APPENDIX – F contd……

RUN NO. SG7

t (s)	d_{ss} (m)
0	0
60	0.181
120	0.194
180	0.211
240	0.219
300	0.226
600	0.239
900	0.244
1200	0.249
1500	0.254
1800	0.255
2100	0.257
2400	0.259
2700	0.263
3000	0.264
3300	0.264
3600	0.265
3900	0.265
4200	0.265
4500	0.265
4800	0.266
5100	0.266
5400	0.266
5700	0.267
6000	0.267
6600	0.267
7200	0.268
9000	0.268
10800	0.268
12600	0.269
14400	0.269
16200	0.269
18000	0.27
21600	0.27
25200	0.27
28800	0.27

RUN NO. SG8

t (s)	d_{ss} (m)
0	0
60	0.175
120	0.187
180	0.196
240	0.204
300	0.211
600	0.222
900	0.226
1200	0.229
1500	0.234
1800	0.236
2100	0.241
2400	0.242
2700	0.242
3000	0.243
3300	0.243
3600	0.243
3900	0.243
4200	0.244
4500	0.244
4800	0.244
5100	0.244
5400	0.245
5700	0.245
6000	0.245
6600	0.245
7200	0.245
9000	0.245
10800	0.246
12600	0.246
14400	0.246
16200	0.246
18000	0.246
21600	0.246
25200	0.246
28800	0.246

APPENDIX – F contd……

RUN NO. G1

t (s)	d_{ss} (m)
0	0
60	0.172
120	0.195
180	0.211
240	0.223
300	0.229
600	0.238
900	0.242
1200	0.245
1500	0.248
1800	0.251
2100	0.253
2400	0.255
2700	0.257
3000	0.259
3300	0.261
3600	0.262
3900	0.263
4200	0.264
4500	0.264
4800	0.265
5100	0.265
5400	0.266
5700	0.266
6000	0.267
6600	0.267
7200	0.268
9000	0.268
10800	0.269
12600	0.269
14400	0.269
16200	0.27
18000	0.27
21600	0.27
25200	0.27
28800	0.27

RUN NO. G2

t (s)	d_{ss} (m)
0	0
60	0.195
120	0.217
180	0.241
240	0.254
300	0.262
600	0.276
900	0.283
1200	0.29
1500	0.292
1800	0.293
2100	0.294
2400	0.295
2700	0.296
3000	0.296
3300	0.296
3600	0.297
3900	0.297
4200	0.297
4500	0.298
4800	0.298
5100	0.298
5400	0.298
5700	0.299
6000	0.299
6600	0.299
7200	0.299
9000	0.299
10800	0.299
12600	0.3
14400	0.3
16200	0.3
18000	0.3
21600	0.3
25200	0.3
28800	0.3

RUN NO. G3

t (s)	d_{ss} (m)
0	0
60	0.142
120	0.155
180	0.168
240	0.174
300	0.18
600	0.192
900	0.196
1200	0.201
1500	0.204
1800	0.207
2100	0.209
2400	0.211
2700	0.213
3000	0.215
3300	0.216
3600	0.217
3900	0.218
4200	0.219
4500	0.219
4800	0.22
5100	0.22
5400	0.22
5700	0.221
6000	0.221
6600	0.221
7200	0.222
9000	0.222
10800	0.222
12600	0.222
14400	0.223
16200	0.223
18000	0.223
21600	0.223
25200	0.223
28800	0.223

APPENDIX – F contd……

RUN NO. G4

t (s)	d_{ss} (m)
0	0
60	0.171
120	0.185
180	0.192
240	0.198
300	0.205
600	0.216
900	0.225
1200	0.228
1500	0.232
1800	0.234
2100	0.236
2400	0.238
2700	0.239
3000	0.24
3300	0.241
3600	0.242
3900	0.242
4200	0.243
4500	0.243
4800	0.244
5100	0.244
5400	0.244
5700	0.245
6000	0.245
6600	0.245
7200	0.245
9000	0.246
10800	0.246
12600	0.246
14400	0.246
16200	0.247
18000	0.247
21600	0.247
25200	0.247
28800	0.247

RUN NO. G5

t (s)	d_{ss} (m)
0	0
60	0.172
120	0.187
180	0.199
240	0.206
300	0.211
600	0.22
900	0.226
1200	0.231
1500	0.235
1800	0.237
2100	0.239
2400	0.24
2700	0.241
3000	0.242
3300	0.24
3600	0.24
3900	0.241
4200	0.241
4500	0.241
4800	0.242
5100	0.242
5400	0.242
5700	0.243
6000	0.243
6600	0.243
7200	0.244
9000	0.244
10800	0.244
12600	0.244
14400	0.245
16200	0.245
18000	0.245
21600	0.245
25200	0.245
28800	0.245

RUN NO. G6

t (s)	d_{ss} (m)
0	0
60	0.198
120	0.206
180	0.219
240	0.223
300	0.23
600	0.241
900	0.247
1200	0.254
1500	0.259
1800	0.262
2100	0.263
2400	0.264
2700	0.262
3000	0.263
3300	0.263
3600	0.263
3900	0.264
4200	0.264
4500	0.264
4800	0.264
5100	0.265
5400	0.265
5700	0.265
6000	0.265
6600	0.266
7200	0.266
9000	0.266
10800	0.266
12600	0.266
14400	0.267
16200	0.267
18000	0.267
21600	0.267
25200	0.267
28800	0.267

APPENDIX – F contd……

RUN NO. G7

t (s)	d_{ss} (m)
0	0
60	0.151
120	0.165
180	0.174
240	0.182
300	0.189
600	0.203
900	0.211
1200	0.216
1500	0.222
1800	0.223
2100	0.223
2400	0.224
2700	0.224
3000	0.225
3300	0.225
3600	0.226
3900	0.226
4200	0.226
4500	0.226
4800	0.227
5100	0.227
5400	0.227
5700	0.228
6000	0.228
6600	0.228
7200	0.229
9000	0.229
10800	0.229
12600	0.229
14400	0.23
16200	0.23
18000	0.23
21600	0.23
25200	0.23
28800	0.23

RUN NO. G8

t (s)	d_{ss} (m)
0	0
60	0.132
120	0.145
180	0.155
240	0.165
300	0.171
600	0.179
900	0.182
1200	0.185
1500	0.187
1800	0.189
2100	0.191
2400	0.193
2700	0.194
3000	0.194
3300	0.195
3600	0.195
3900	0.195
4200	0.195
4500	0.196
4800	0.196
5100	0.196
5400	0.196
5700	0.196
6000	0.197
6600	0.197
7200	0.197
9000	0.197
10800	0.197
12600	0.197
14400	0.197
16200	0.197
18000	0.197
21600	0.197
25200	0.197
28800	0.197

APPENDEX – G

TEMPORAL VARIATION OF SCOUR DEPTH UNDER SUBMERGED CIRCULAR VERTICAL JETS IN CLAY-GRAVEL COHESIVE SEDIMENT MIXTURES

RUN NO. C10G1

t (s)	d_{ss} (m)
0	0
300	0.141
600	0.154
900	0.167
1800	0.178
2700	0.185
3600	0.191
7200	0.198
10800	0.206
14400	0.208
18000	0.209
21600	0.21
25200	0.211
28800	0.211
32400	0.212
36000	0.212
39600	0.213
43200	0.213
46800	0.213
50400	0.214
54000	0.214
57600	0.214
61200	0.214
64800	0.214
68400	0.214
72000	0.215
75600	0.215
79200	0.215
82800	0.215
86400	0.215
90000	0.215

RUN NO. C10G2

t (s)	d_{ss} (m)
0	0
300	0.162
600	0.174
900	0.183
1800	0.195
2700	0.204
3600	0.21
7200	0.217
10800	0.221
14400	0.225
18000	0.23
21600	0.231
25200	0.232
28800	0.233
32400	0.233
36000	0.234
39600	0.235
43200	0.235
46800	0.235
50400	0.236
54000	0.236
57600	0.237
61200	0.237
64800	0.238
68400	0.238
72000	0.238
75600	0.238
79200	0.238
82800	0.239
86400	0.239
90000	0.239

RUN NO. C10G3

t (s)	d_{ss} (m)
0	0
300	0.095
600	0.109
900	0.118
1800	0.126
2700	0.14
3600	0.15
7200	0.161
10800	0.167
14400	0.17
18000	0.171
21600	0.172
25200	0.173
28800	0.174
32400	0.174
36000	0.175
39600	0.175
43200	0.176
46800	0.176
50400	0.176
54000	0.177
57600	0.177
61200	0.177
64800	0.177
68400	0.178
72000	0.178
75600	0.178
79200	0.178
82800	0.178
86400	0.178
90000	0.178

APPENDEX – G contd…..

RUN NO. C10G4

t (s)	d_{ss} (m)
0	0
300	0.146
600	0.152
900	0.159
1800	0.164
2700	0.171
3600	0.175
7200	0.178
10800	0.182
14400	0.188
18000	0.189
21600	0.191
25200	0.191
28800	0.192
32400	0.192
36000	0.193
39600	0.193
43200	0.193
46800	0.194
50400	0.194
54000	0.194
57600	0.195
61200	0.195
64800	0.195
68400	0.195
72000	0.195
75600	0.195
79200	0.195
82800	0.195
86400	0.195
90000	0.195

RUN NO. C10G5

t (s)	d_{ss} (m)
0	0
300	0.125
600	0.133
900	0.14
1800	0.145
2700	0.15
3600	0.153
7200	0.159
10800	0.164
14400	0.167
18000	0.171
21600	0.172
25200	0.173
28800	0.173
32400	0.174
36000	0.174
39600	0.175
43200	0.175
46800	0.175
50400	0.176
54000	0.176
57600	0.176
61200	0.176
64800	0.176
68400	0.176
72000	0.176
75600	0.176
79200	0.177
82800	0.177
86400	0.177
90000	0.177

RUN NO. C10G6

t (s)	d_{ss} (m)
0	0
300	0.154
600	0.17
900	0.178
1800	0.186
2700	0.192
3600	0.199
7200	0.205
10800	0.209
14400	0.211
18000	0.213
21600	0.214
25200	0.215
28800	0.215
32400	0.216
36000	0.216
39600	0.217
43200	0.217
46800	0.218
50400	0.218
54000	0.218
57600	0.219
61200	0.219
64800	0.219
68400	0.219
72000	0.219
75600	0.219
79200	0.219
82800	0.219
86400	0.219
90000	0.219

APPENDEX – G contd…..

RUN NO. C10G7

t (s)	d_{ss} (m)
0	0
300	0.103
600	0.111
900	0.115
1800	0.121
2700	0.124
3600	0.128
7200	0.134
10800	0.138
14400	0.141
18000	0.145
21600	0.146
25200	0.147
28800	0.147
32400	0.148
36000	0.148
39600	0.148
43200	0.149
46800	0.149
50400	0.149
54000	0.15
57600	0.15
61200	0.15
64800	0.15
68400	0.151
72000	0.151
75600	0.151
79200	0.152
82800	0.152
86400	0.152
90000	0.152

RUN NO. C10G8

t (s)	d_{ss} (m)
0	0
300	0.102
600	0.115
900	0.131
1800	0.137
2700	0.142
3600	0.149
7200	0.154
10800	0.157
14400	0.161
18000	0.162
21600	0.164
25200	0.164
28800	0.165
32400	0.165
36000	0.165
39600	0.166
43200	0.166
46800	0.166
50400	0.167
54000	0.167
57600	0.167
61200	0.168
64800	0.168
68400	0.168
72000	0.168
75600	0.168
79200	0.168
82800	0.168
86400	0.168
90000	0.168

APPENDEX – G contd…..

RUN NO. C20G1

t (s)	d_{ss} (m)
0	0
300	0.065
600	0.074
900	0.082
1800	0.089
2700	0.106
3600	0.114
7200	0.131
10800	0.14
14400	0.146
18000	0.149
21600	0.151
25200	0.152
28800	0.152
32400	0.152
36000	0.153
39600	0.153
43200	0.154
46800	0.155
50400	0.155
54000	0.155
57600	0.156
61200	0.156
64800	0.156
68400	0.156
72000	0.157
75600	0.157
79200	0.157
82800	0.157
86400	0.157
90000	0.157

RUN NO. C20G2

t (s)	d_{ss} (m)
0	0
300	0.116
600	0.124
900	0.131
1800	0.136
2700	0.143
3600	0.148
7200	0.156
10800	0.163
14400	0.169
18000	0.172
21600	0.173
25200	0.174
28800	0.174
32400	0.175
36000	0.175
39600	0.176
43200	0.176
46800	0.177
50400	0.177
54000	0.177
57600	0.177
61200	0.177
64800	0.178
68400	0.178
72000	0.178
75600	0.178
79200	0.178
82800	0.178
86400	0.178
90000	0.178

RUN NO. C20G3

t (s)	d_{ss} (m)
0	0
300	0.063
600	0.071
900	0.075
1800	0.079
2700	0.084
3600	0.09
7200	0.097
10800	0.102
14400	0.109
18000	0.114
21600	0.118
25200	0.121
28800	0.121
32400	0.122
36000	0.122
39600	0.123
43200	0.123
46800	0.123
50400	0.124
54000	0.124
57600	0.124
61200	0.124
64800	0.125
68400	0.125
72000	0.125
75600	0.125
79200	0.125
82800	0.125
86400	0.125
90000	0.125

APPENDEX – G contd…..

RUN NO. C20G4

t (s)	d_{ss} (m)
0	0
300	0.097
600	0.102
900	0.106
1800	0.111
2700	0.113
3600	0.117
7200	0.123
10800	0.127
14400	0.132
18000	0.136
21600	0.137
25200	0.138
28800	0.139
32400	0.14
36000	0.141
39600	0.142
43200	0.142
46800	0.142
50400	0.142
54000	0.143
57600	0.143
61200	0.144
64800	0.144
68400	0.144
72000	0.145
75600	0.145
79200	0.145
82800	0.145
86400	0.145
90000	0.145

RUN NO. C20G5

t (s)	d_{ss} (m)
0	0
300	0.088
600	0.095
900	0.101
1800	0.106
2700	0.109
3600	0.113
7200	0.118
10800	0.122
14400	0.124
18000	0.128
21600	0.131
25200	0.131
28800	0.132
32400	0.132
36000	0.133
39600	0.133
43200	0.134
46800	0.134
50400	0.134
54000	0.134
57600	0.134
61200	0.135
64800	0.135
68400	0.135
72000	0.135
75600	0.135
79200	0.135
82800	0.135
86400	0.135
90000	0.135

RUN NO. C20G6

t (s)	d_{ss} (m)
0	0
300	0.088
600	0.095
900	0.105
1800	0.117
2700	0.124
3600	0.132
7200	0.137
10800	0.141
14400	0.145
18000	0.149
21600	0.157
25200	0.163
28800	0.164
32400	0.165
36000	0.166
39600	0.167
43200	0.167
46800	0.168
50400	0.169
54000	0.17
57600	0.17
61200	0.17
64800	0.171
68400	0.171
72000	0.171
75600	0.172
79200	0.172
82800	0.172
86400	0.172
90000	0.172

APPENDEX – G contd…..

RUN NO. C20G7

t (s)	d_{ss} (m)
0	0
300	0.055
600	0.062
900	0.069
1800	0.073
2700	0.077
3600	0.081
7200	0.084
10800	0.088
14400	0.091
18000	0.093
21600	0.096
25200	0.098
28800	0.1
32400	0.102
36000	0.102
39600	0.103
43200	0.103
46800	0.103
50400	0.104
54000	0.104
57600	0.104
61200	0.105
64800	0.105
68400	0.105
72000	0.105
75600	0.105
79200	0.106
82800	0.106
86400	0.106
90000	0.106

RUN NO. C20G8

t (s)	d_{ss} (m)
0	0
300	0.065
600	0.072
900	0.083
1800	0.086
2700	0.089
3600	0.094
7200	0.098
10800	0.102
14400	0.107
18000	0.111
21600	0.115
25200	0.121
28800	0.124
32400	0.127
36000	0.128
39600	0.128
43200	0.129
46800	0.129
50400	0.129
54000	0.13
57600	0.13
61200	0.13
64800	0.131
68400	0.131
72000	0.131
75600	0.131
79200	0.131
82800	0.131
86400	0.131
90000	0.131

APPENDEX – G contd…..

RUN NO. C30G1

t (s)	d_{ss} (m)
0	0
300	0.017
600	0.03
900	0.036
1800	0.043
2700	0.051
3600	0.058
7200	0.064
10800	0.073
14400	0.077
18000	0.082
21600	0.087
25200	0.091
28800	0.095
32400	0.099
36000	0.101
39600	0.102
43200	0.103
46800	0.104
50400	0.105
54000	0.105
57600	0.106
61200	0.106
64800	0.107
68400	0.107
72000	0.107
75600	0.108
79200	0.108
82800	0.108
86400	0.108
90000	0.108
93600	0.108
97200	0.108

RUN NO. C30G2

t (s)	d_{ss} (m)
0	0
300	0.051
600	0.066
900	0.073
1800	0.082
2700	0.093
3600	0.101
7200	0.11
10800	0.114
14400	0.121
18000	0.125
21600	0.128
25200	0.132
28800	0.135
32400	0.138
36000	0.139
39600	0.139
43200	0.14
46800	0.14
50400	0.141
54000	0.142
57600	0.142
61200	0.143
64800	0.143
68400	0.143
72000	0.143
75600	0.143
79200	0.143
82800	0.143
86400	0.143
90000	0.143
93600	0.143
97200	0.143

RUN NO. C30G3

t (s)	d_{ss} (m)
0	0
300	0.013
600	0.021
900	0.029
1800	0.035
2700	0.038
3600	0.043
7200	0.047
10800	0.052
14400	0.056
18000	0.059
21600	0.063
25200	0.067
28800	0.071
32400	0.074
36000	0.076
39600	0.077
43200	0.077
46800	0.078
50400	0.078
54000	0.079
57600	0.079
61200	0.079
64800	0.08
68400	0.08
72000	0.08
75600	0.08
79200	0.081
82800	0.081
86400	0.081
90000	0.081
93600	0.081
97200	0.081

APPENDEX – G contd…..

RUN NO. C30G4

t (s)	d_{ss} (m)
0	0
300	0.04
600	0.043
900	0.047
1800	0.051
2700	0.056
3600	0.063
7200	0.068
10800	0.078
14400	0.085
18000	0.089
21600	0.095
25200	0.098
28800	0.101
32400	0.106
36000	0.108
39600	0.11
43200	0.111
46800	0.112
50400	0.112
54000	0.113
57600	0.113
61200	0.114
64800	0.114
68400	0.114
72000	0.115
75600	0.115
79200	0.115
82800	0.115
86400	0.115
90000	0.115
93600	0.115
97200	0.115

RUN NO. C30G5

t (s)	d_{ss} (m)
0	0
300	0.031
600	0.033
900	0.036
1800	0.039
2700	0.044
3600	0.049
7200	0.056
10800	0.061
14400	0.065
18000	0.069
21600	0.074
25200	0.077
28800	0.081
32400	0.083
36000	0.084
39600	0.085
43200	0.086
46800	0.086
50400	0.087
54000	0.087
57600	0.088
61200	0.088
64800	0.088
68400	0.089
72000	0.089
75600	0.089
79200	0.09
82800	0.09
86400	0.09
90000	0.09
93600	0.09
97200	0.09

RUN NO. C30G6

t (s)	d_{ss} (m)
0	0
300	0.057
600	0.061
900	0.069
1800	0.076
2700	0.082
3600	0.087
7200	0.091
10800	0.094
14400	0.098
18000	0.104
21600	0.11
25200	0.113
28800	0.117
32400	0.119
36000	0.122
39600	0.126
43200	0.127
46800	0.128
50400	0.129
54000	0.13
57600	0.13
61200	0.13
64800	0.131
68400	0.131
72000	0.131
75600	0.131
79200	0.131
82800	0.132
86400	0.132
90000	0.132
93600	0.132
97200	0.132

APPENDEX – G contd…..

RUN NO. C30G7

t (s)	d_{ss} (m)
0	0
300	0.019
600	0.022
900	0.024
1800	0.026
2700	0.031
3600	0.033
7200	0.035
10800	0.039
14400	0.043
18000	0.046
21600	0.049
25200	0.053
28800	0.056
32400	0.059
36000	0.062
39600	0.064
43200	0.065
46800	0.065
50400	0.065
54000	0.066
57600	0.066
61200	0.066
64800	0.067
68400	0.067
72000	0.067
75600	0.067
79200	0.068
82800	0.068
86400	0.068
90000	0.068
93600	0.068
97200	0.068

RUN NO. C30G8

t (s)	d_{ss} (m)
0	0
300	0.025
600	0.029
900	0.033
1800	0.035
2700	0.04
3600	0.045
7200	0.051
10800	0.056
14400	0.063
18000	0.068
21600	0.072
25200	0.075
28800	0.08
32400	0.084
36000	0.088
39600	0.092
43200	0.092
46800	0.093
50400	0.093
54000	0.094
57600	0.094
61200	0.094
64800	0.095
68400	0.095
72000	0.095
75600	0.095
79200	0.095
82800	0.095
86400	0.096
90000	0.096
93600	0.096
97200	0.096

APPENDEX – G contd…..

RUN NO. C40G1

t (s)	d_{ss} (m)
0	0
300	0.004
600	0.007
900	0.009
1800	0.013
2700	0.015
3600	0.018
7200	0.022
10800	0.027
14400	0.032
18000	0.036
21600	0.038
25200	0.041
28800	0.043
32400	0.046
36000	0.048
39600	0.05
43200	0.051
46800	0.052
50400	0.053
54000	0.053
57600	0.054
61200	0.054
64800	0.054
68400	0.054
72000	0.055
75600	0.055
79200	0.055
82800	0.055
86400	0.055
90000	0.055
93600	0.055
97200	0.055
100800	0.055

RUN NO. C40G2

t (s)	d_{ss} (m)
0	0
300	0.004
600	0.007
900	0.009
1800	0.012
2700	0.015
3600	0.027
7200	0.034
10800	0.045
14400	0.052
18000	0.057
21600	0.061
25200	0.066
28800	0.069
32400	0.073
36000	0.076
39600	0.077
43200	0.078
46800	0.078
50400	0.079
54000	0.079
57600	0.079
61200	0.079
64800	0.08
68400	0.08
72000	0.08
75600	0.08
79200	0.08
82800	0.08
86400	0.08
90000	0.08
93600	0.08
97200	0.08
100800	0.08

RUN NO. C40G3

t (s)	d_{ss} (m)
0	0
300	0.004
600	0.007
900	0.011
1800	0.013
2700	0.015
3600	0.016
7200	0.017
10800	0.021
14400	0.024
18000	0.026
21600	0.029
25200	0.031
28800	0.032
32400	0.033
36000	0.034
39600	0.035
43200	0.036
46800	0.036
50400	0.037
54000	0.037
57600	0.037
61200	0.037
64800	0.038
68400	0.038
72000	0.038
75600	0.038
79200	0.039
82800	0.039
86400	0.039
90000	0.039
93600	0.039
97200	0.039
100800	0.039

APPENDEX – G contd…..

RUN NO. C40G4

t (s)	d_{ss} (m)
0	0
300	0.008
600	0.012
900	0.014
1800	0.016
2700	0.018
3600	0.02
7200	0.022
10800	0.024
14400	0.027
18000	0.029
21600	0.031
25200	0.032
28800	0.034
32400	0.037
36000	0.039
39600	0.042
43200	0.045
46800	0.046
50400	0.047
54000	0.048
57600	0.049
61200	0.05
64800	0.05
68400	0.051
72000	0.051
75600	0.052
79200	0.052
82800	0.052
86400	0.053
90000	0.053
93600	0.053
97200	0.053
100800	0.053

RUN NO. C40G5

t (s)	d_{ss} (m)
0	0
300	0.005
600	0.009
900	0.012
1800	0.014
2700	0.016
3600	0.017
7200	0.018
10800	0.021
14400	0.024
18000	0.026
21600	0.028
25200	0.031
28800	0.034
32400	0.036
36000	0.038
39600	0.04
43200	0.042
46800	0.045
50400	0.046
54000	0.046
57600	0.047
61200	0.047
64800	0.048
68400	0.048
72000	0.049
75600	0.049
79200	0.05
82800	0.05
86400	0.05
90000	0.05
93600	0.05
97200	0.05
100800	0.05

RUN NO. C40G6

t (s)	d_{ss} (m)
0	0
300	0.057
600	0.062
900	0.066
1800	0.069
2700	0.072
3600	0.075
7200	0.077
10800	0.079
14400	0.082
18000	0.084
21600	0.086
25200	0.088
28800	0.091
32400	0.094
36000	0.096
39600	0.099
43200	0.101
46800	0.104
50400	0.106
54000	0.107
57600	0.108
61200	0.108
64800	0.109
68400	0.109
72000	0.109
75600	0.111
79200	0.112
82800	0.112
86400	0.112
90000	0.113
93600	0.113
97200	0.113
100800	0.113

APPENDEX – G contd…..

RUN NO. C40G7

t (s)	d_{ss} (m)
0	0
300	0.005
600	0.009
900	0.012
1800	0.013
2700	0.015
3600	0.017
7200	0.019
10800	0.021
14400	0.023
18000	0.025
21600	0.027
25200	0.028
28800	0.03
32400	0.032
36000	0.033
39600	0.034
43200	0.035
46800	0.036
50400	0.036
54000	0.037
57600	0.037
61200	0.037
64800	0.037
68400	0.038
72000	0.038
75600	0.038
79200	0.038
82800	0.038
86400	0.039
90000	0.039
93600	0.039
97200	0.039
100800	0.039

RUN NO. C40G8

t (s)	d_{ss} (m)
0	0
300	0.008
600	0.013
900	0.016
1800	0.019
2700	0.023
3600	0.026
7200	0.028
10800	0.03
14400	0.033
18000	0.035
21600	0.038
25200	0.042
28800	0.046
32400	0.049
36000	0.052
39600	0.055
43200	0.058
46800	0.061
50400	0.061
54000	0.062
57600	0.062
61200	0.062
64800	0.063
68400	0.063
72000	0.063
75600	0.063
79200	0.064
82800	0.064
86400	0.064
90000	0.065
93600	0.065
97200	0.065
100800	0.065

APPENDEX – G contd…..

RUN NO. C50G2

t (s)	d_{ss} (m)
0	0
300	0.005
600	0.012
900	0.025
1800	0.032
2700	0.037
3600	0.041
7200	0.048
10800	0.055
14400	0.059
18000	0.064
21600	0.069
25200	0.075
28800	0.079
32400	0.082
36000	0.084
39600	0.085
43200	0.086
46800	0.088
50400	0.089
54000	0.089
57600	0.09
61200	0.09
64800	0.091
68400	0.092
72000	0.092
75600	0.093
79200	0.093
82800	0.093
86400	0.094
90000	0.094
93600	0.094
97200	0.094
100800	0.094

RUN NO. C50G4

t (s)	d_{ss} (m)
0	0
300	0.002
600	0.004
900	0.006
1800	0.008
2700	0.01
3600	0.012
7200	0.013
10800	0.014
14400	0.016
18000	0.018
21600	0.02
25200	0.022
28800	0.024
32400	0.026
36000	0.028
39600	0.032
43200	0.035
46800	0.037
50400	0.038
54000	0.039
57600	0.041
61200	0.042
64800	0.043
68400	0.044
72000	0.044
75600	0.044
79200	0.044
82800	0.045
86400	0.045
90000	0.045
93600	0.045
97200	0.045
100800	0.045

RUN NO. C50G6

t (s)	d_{ss} (m)
0	0
300	0.02
600	0.025
900	0.033
1800	0.039
2700	0.045
3600	0.048
7200	0.056
10800	0.062
14400	0.064
18000	0.067
21600	0.07
25200	0.074
28800	0.078
32400	0.082
36000	0.085
39600	0.087
43200	0.09
46800	0.092
50400	0.093
54000	0.094
57600	0.095
61200	0.096
64800	0.097
68400	0.098
72000	0.099
75600	0.101
79200	0.103
82800	0.104
86400	0.104
90000	0.104
93600	0.104
97200	0.104
100800	0.104

APPENDEX – G contd…..

RUN NO. C50G8

t (s)	d_{ss} (m)
0	0
300	0.004
600	0.009
900	0.012
1800	0.014
2700	0.016
3600	0.018
7200	0.02
10800	0.023
14400	0.024
18000	0.026
21600	0.028
25200	0.032
28800	0.034
32400	0.038
36000	0.043
39600	0.047
43200	0.051
46800	0.054
50400	0.057
54000	0.059
57600	0.063
61200	0.067
64800	0.069
68400	0.071
72000	0.072
75600	0.072
79200	0.073
82800	0.073
86400	0.073
90000	0.074
93600	0.074
97200	0.074
100800	0.074

RUN NO. C60G2

t (s)	d_{ss} (m)
0	0
300	0.007
600	0.012
900	0.015
1800	0.021
2700	0.033
3600	0.039
7200	0.044
10800	0.051
14400	0.055
18000	0.06
21600	0.065
25200	0.069
28800	0.074
32400	0.078
36000	0.082
39600	0.083
43200	0.089
46800	0.092
50400	0.093
54000	0.095
57600	0.097
61200	0.099
64800	0.1
68400	0.1
72000	0.102
75600	0.103
79200	0.104
82800	0.104
86400	0.104
90000	0.104
93600	0.104
97200	0.104
100800	0.104

RUN NO. C60G4

t (s)	d_{ss} (m)
0	0
300	0.002
600	0.004
900	0.007
1800	0.009
2700	0.011
3600	0.013
7200	0.016
10800	0.018
14400	0.022
18000	0.025
21600	0.029
25200	0.035
28800	0.039
32400	0.044
36000	0.047
39600	0.049
43200	0.051
46800	0.053
50400	0.056
54000	0.057
57600	0.058
61200	0.059
64800	0.06
68400	0.06
72000	0.061
75600	0.061
79200	0.062
82800	0.063
86400	0.064
90000	0.065
93600	0.065
97200	0.065
100800	0.065

APPENDEX – G contd…..

RUN NO. C60G6

t (s)	d_{ss} (m)
0	0
298.8	0.008
576	0.013
900	0.019
1800	0.025
2700	0.028
3600	0.032
5400	0.034
7200	0.041
9000	0.045
10800	0.048
14400	0.052
18000	0.055
21600	0.058
25200	0.062
28800	0.066
32400	0.072
36000	0.077
39600	0.083
43200	0.089
46800	0.095
50400	0.099
54000	0.102
57600	0.105
61200	0.11
64800	0.112
68400	0.113
72000	0.114
75600	0.115
79200	0.116
82800	0.116
86400	0.116
90000	0.116
93600	0.116
97200	0.116
100800	0.116

RUN NO. C60G8

t (s)	d_{ss} (m)
0	0
298.8	0.002
576	0.005
900	0.008
1800	0.012
2700	0.014
3600	0.015
5400	0.017
7200	0.019
9000	0.022
10800	0.023
14400	0.025
18000	0.026
21600	0.029
25200	0.031
28800	0.035
32400	0.039
36000	0.045
39600	0.049
43200	0.052
46800	0.055
50400	0.057
54000	0.059
57600	0.062
61200	0.064
64800	0.067
68400	0.069
72000	0.072
75600	0.074
79200	0.076
82800	0.077
86400	0.077
90000	0.077
93600	0.077
97200	0.077
100800	0.077

APPENDEX – H

TEMPORAL VARIATION OF SCOUR DEPTH UNDER SUBMERGED CIRCULAR VERTICAL JETS IN CLAY-SAND-GRAVEL COHESIVE SEDIMENT MIXTURES

RUN NO. C10SG1

t (s)	d_{ss} (m)
0	0
60	0.173
120	0.181
180	0.187
240	0.198
300	0.205
600	0.212
900	0.219
1800	0.226
2700	0.231
3600	0.235
5400	0.24
7200	0.244
9000	0.248
10800	0.252
12600	0.255
14400	0.257
16200	0.258
18000	0.258
19800	0.259
21600	0.259
23400	0.259
25200	0.26
27000	0.26
28800	0.26
30600	0.26
32400	0.26
36000	0.26
39600	0.261
43200	0.261
46800	0.261
50400	0.261
54000	0.261
57600	0.261

RUN NO. C10SG2

t (s)	d_{ss} (m)
0	0
60	0.155
120	0.171
180	0.179
240	0.187
300	0.198
600	0.206
900	0.215
1800	0.223
2700	0.235
3600	0.244
5400	0.25
7200	0.254
9000	0.258
10800	0.259
12600	0.26
14400	0.26
16200	0.261
18000	0.262
19800	0.262
21600	0.263
23400	0.263
25200	0.263
27000	0.264
28800	0.264
30600	0.264
32400	0.265
36000	0.265
39600	0.265
43200	0.267
46800	0.267
50400	0.267
54000	0.267
57600	0.267

RUN NO. C10SG3

t (s)	d_{ss} (m)
0	0
60	0.124
120	0.135
180	0.143
240	0.151
300	0.157
600	0.162
900	0.165
1800	0.169
2700	0.173
3600	0.178
5400	0.182
7200	0.184
9000	0.186
10800	0.188
12600	0.192
14400	0.193
16200	0.194
18000	0.194
19800	0.194
21600	0.195
23400	0.195
25200	0.195
27000	0.196
28800	0.196
30600	0.196
32400	0.196
36000	0.196
39600	0.196
43200	0.196
46800	0.196
50400	0.197
54000	0.197
57600	0.197

APPENDEX – H contd….

61200	0.261
64800	0.261
68400	0.261
72000	0.261
75600	0.261
79200	0.261
82800	0.261
86400	0.261
90000	0.261
93600	0.261

61200	0.266
64800	0.266
68400	0.266
72000	0.267
75600	0.267
79200	0.267
82800	0.267
86400	0.267
90000	0.267
93600	0.267

61200	0.197
64800	0.197
68400	0.197
72000	0.197
75600	0.198
79200	0.198
82800	0.198
86400	0.198
90000	0.198
93600	0.198

RUN NO. C10SG4

t (s)	d_{ss} (m)
0	0
60	0.145
120	0.153
180	0.159
240	0.164
300	0.172
600	0.178
900	0.182
1800	0.185
2700	0.191
3600	0.196
5400	0.198
7200	0.201
9000	0.203
10800	0.205
12600	0.206
14400	0.207
16200	0.207
18000	0.207
19800	0.208
21600	0.208
23400	0.208
25200	0.209
27000	0.209
28800	0.209

RUN NO. C10SG5

t (s)	d_{ss} (m)
0	0
60	0.122
120	0.13
180	0.15
240	0.156
300	0.161
600	0.17
900	0.174
1800	0.179
2700	0.182
3600	0.186
5400	0.191
7200	0.196
9000	0.198
10800	0.2
12600	0.201
14400	0.202
16200	0.203
18000	0.205
19800	0.207
21600	0.206
23400	0.207
25200	0.207
27000	0.207
28800	0.208

RUN NO. C10SG6

t (s)	d_{ss} (m)
0	0
60	0.172
120	0.185
180	0.194
240	0.207
300	0.213
600	0.218
900	0.222
1800	0.227
2700	0.234
3600	0.237
5400	0.241
7200	0.243
9000	0.245
10800	0.246
12600	0.247
14400	0.247
16200	0.248
18000	0.248
19800	0.249
21600	0.249
23400	0.249
25200	0.25
27000	0.25
28800	0.25

APPENDEX – H contd….

30600	0.209
32400	0.21
36000	0.21
39600	0.21
43200	0.21
46800	0.21
50400	0.21
54000	0.21
57600	0.21
61200	0.211
64800	0.211
68400	0.211
72000	0.211
75600	0.211
79200	0.211
82800	0.211
86400	0.211
90000	0.211
93600	0.211

30600	0.208
32400	0.208
36000	0.209
39600	0.209
43200	0.209
46800	0.209
50400	0.209
54000	0.209
57600	0.209
61200	0.209
64800	0.209
68400	0.209
72000	0.209
75600	0.209
79200	0.209
82800	0.209
86400	0.209
90000	0.209
93600	0.209

30600	0.25
32400	0.251
36000	0.251
39600	0.251
43200	0.251
46800	0.252
50400	0.252
54000	0.252
57600	0.252
61200	0.252
64800	0.252
68400	0.252
72000	0.252
75600	0.252
79200	0.252
82800	0.252
86400	0.252
90000	0.252
93600	0.252

RUN NO. C10SG7

t (s)	d_{ss} (m)
0	0
60	0.124
120	0.131
180	0.139
240	0.146
300	0.152
600	0.154
900	0.156
1800	0.158
2700	0.161
3600	0.163
5400	0.167
7200	0.169
9000	0.171
10800	0.172
12600	0.174

RUN NO. C10SG8

t (s)	d_{ss} (m)
0	0
60	0.133
120	0.145
180	0.152
240	0.159
300	0.165
600	0.169
900	0.173
1800	0.176
2700	0.178
3600	0.18
5400	0.182
7200	0.184
9000	0.186
10800	0.188
12600	0.19

APPENDEX – H contd….

14400	0.175
16200	0.175
18000	0.175
19800	0.176
21600	0.176
23400	0.176
25200	0.177
27000	0.177
28800	0.177
30600	0.177
32400	0.178
36000	0.178
39600	0.178
43200	0.178
46800	0.178
50400	0.178
54000	0.179
57600	0.179
61200	0.179
64800	0.179
68400	0.179
72000	0.179
75600	0.18
79200	0.18
82800	0.18
86400	0.18
90000	0.18
93600	0.18

14400	0.192
16200	0.193
18000	0.194
19800	0.194
21600	0.194
23400	0.194
25200	0.195
27000	0.195
28800	0.195
30600	0.195
32400	0.196
36000	0.196
39600	0.196
43200	0.196
46800	0.196
50400	0.197
54000	0.197
57600	0.197
61200	0.197
64800	0.197
68400	0.197
72000	0.198
75600	0.198
79200	0.198
82800	0.198
86400	0.198
90000	0.198
93600	0.198

RUN NO. C20SG1

t (s)	d_{ss} (m)
0	0
60	0.073
120	0.085
180	0.091
240	0.103
300	0.116
600	0.12

RUN NO. C20SG2

t (s)	d_{ss} (m)
0	0
60	0.103
120	0.115
180	0.121
240	0.126
300	0.131
600	0.137

RUN NO. C20SG3

t (s)	d_{ss} (m)
0	0
60	0.073
120	0.089
180	0.095
240	0.101
300	0.107
600	0.114

APPENDEX – H contd….

900	0.126
1800	0.131
2700	0.135
3600	0.139
5400	0.142
7200	0.148
9000	0.155
10800	0.161
12600	0.167
14400	0.172
16200	0.176
18000	0.18
19800	0.183
21600	0.185
23400	0.187
25200	0.188
27000	0.19
28800	0.19
30600	0.191
32400	0.191
36000	0.192
39600	0.192
43200	0.192
46800	0.192
50400	0.193
54000	0.193
57600	0.193
61200	0.193
64800	0.193
68400	0.193
72000	0.193
75600	0.193
79200	0.193
82800	0.193
86400	0.193
90000	0.193
93600	0.193

900	0.142
1800	0.148
2700	0.155
3600	0.161
5400	0.164
7200	0.169
9000	0.173
10800	0.175
12600	0.179
14400	0.182
16200	0.185
18000	0.188
19800	0.191
21600	0.195
23400	0.196
25200	0.196
27000	0.197
28800	0.197
30600	0.197
32400	0.198
36000	0.198
39600	0.198
43200	0.198
46800	0.202
50400	0.202
54000	0.202
57600	0.202
61200	0.2
64800	0.2
68400	0.201
72000	0.201
75600	0.201
79200	0.202
82800	0.202
86400	0.202
90000	0.202
93600	0.202

900	0.118
1800	0.122
2700	0.125
3600	0.129
5400	0.133
7200	0.136
9000	0.138
10800	0.139
12600	0.14
14400	0.142
16200	0.143
18000	0.144
19800	0.146
21600	0.147
23400	0.148
25200	0.148
27000	0.148
28800	0.149
30600	0.149
32400	0.149
36000	0.15
39600	0.15
43200	0.15
46800	0.151
50400	0.151
54000	0.151
57600	0.152
61200	0.152
64800	0.152
68400	0.152
72000	0.152
75600	0.153
79200	0.153
82800	0.153
86400	0.153
90000	0.153
93600	0.153

APPENDEX – H contd….

RUN NO. C20SG4

t (s)	d_{ss} (m)
0	0
60	0.091
120	0.103
180	0.115
240	0.118
300	0.125
600	0.128
900	0.131
1800	0.134
2700	0.137
3600	0.14
5400	0.142
7200	0.145
9000	0.146
10800	0.147
12600	0.149
14400	0.15
16200	0.151
18000	0.152
19800	0.153
21600	0.154
23400	0.155
25200	0.155
27000	0.156
28800	0.156
30600	0.156
32400	0.157
36000	0.157
39600	0.157
43200	0.157
46800	0.158
50400	0.158
54000	0.158
57600	0.158
61200	0.158
64800	0.159
68400	0.159

RUN NO. C20SG5

t (s)	d_{ss} (m)
0	0
60	0.064
120	0.071
180	0.075
240	0.079
300	0.084
600	0.089
900	0.094
1800	0.102
2700	0.106
3600	0.11
5400	0.113
7200	0.117
9000	0.121
10800	0.124
12600	0.129
14400	0.132
16200	0.135
18000	0.138
19800	0.141
21600	0.143
23400	0.145
25200	0.144
27000	0.145
28800	0.146
30600	0.146
32400	0.147
36000	0.15
39600	0.15
43200	0.15
46800	0.15
50400	0.15
54000	0.148
57600	0.149
61200	0.149
64800	0.149
68400	0.149

RUN NO. C20SG6

t (s)	d_{ss} (m)
0	0
60	0.125
120	0.129
180	0.134
240	0.138
300	0.143
600	0.146
900	0.147
1800	0.149
2700	0.151
3600	0.154
5400	0.158
7200	0.161
9000	0.163
10800	0.165
12600	0.168
14400	0.171
16200	0.172
18000	0.173
19800	0.174
21600	0.175
23400	0.175
25200	0.176
27000	0.176
28800	0.177
30600	0.177
32400	0.177
36000	0.177
39600	0.177
43200	0.177
46800	0.177
50400	0.177
54000	0.177
57600	0.177
61200	0.177
64800	0.18
68400	0.18

APPENDEX – H contd….

72000	0.159
75600	0.159
79200	0.159
82800	0.16
86400	0.16
90000	0.16
93600	0.16

72000	0.149
75600	0.15
79200	0.15
82800	0.15
86400	0.15
90000	0.15
93600	0.15

72000	0.18
75600	0.18
79200	0.18
82800	0.18
86400	0.18
90000	0.18
93600	0.18

RUN NO. C20SG7

t (s)	d_{ss} (m)
0	0
60	0.053
120	0.058
180	0.065
240	0.069
300	0.073
600	0.076
900	0.079
1800	0.084
2700	0.088
3600	0.092
5400	0.095
7200	0.101
9000	0.103
10800	0.105
12600	0.106
14400	0.107
16200	0.108
18000	0.109
19800	0.111
21600	0.112
23400	0.113
25200	0.114
27000	0.115
28800	0.115
30600	0.115
32400	0.116
36000	0.116

RUN NO. C20SG8

t (s)	d_{ss} (m)
0	0
60	0.065
120	0.074
180	0.079
240	0.083
300	0.088
600	0.094
900	0.099
1800	0.103
2700	0.107
3600	0.113
5400	0.117
7200	0.123
9000	0.127
10800	0.129
12600	0.131
14400	0.133
16200	0.135
18000	0.136
19800	0.137
21600	0.137
23400	0.138
25200	0.138
27000	0.139
28800	0.14
30600	0.14
32400	0.141
36000	0.141

APPENDEX – H contd….

39600	0.117
43200	0.117
46800	0.117
50400	0.117
54000	0.118
57600	0.118
61200	0.118
64800	0.119
68400	0.119
72000	0.119
75600	0.12
79200	0.12
82800	0.12
86400	0.12
90000	0.12
93600	0.12

39600	0.141
43200	0.142
46800	0.142
50400	0.142
54000	0.143
57600	0.143
61200	0.143
64800	0.144
68400	0.144
72000	0.144
75600	0.145
79200	0.145
82800	0.145
86400	0.145
90000	0.145
93600	0.145

RUN NO. C30SG1

t (s)	d_{ss} (m)
0	0
60	0.034
120	0.042
180	0.047
240	0.05
300	0.053
600	0.057
900	0.061
1800	0.066
2700	0.069
3600	0.073
5400	0.077
7200	0.083
9000	0.089
10800	0.095
12600	0.104
14400	0.108
16200	0.113
18000	0.116

RUN NO. C30SG2

t (s)	d_{ss} (m)
0	0
60	0.055
120	0.059
180	0.065
240	0.069
300	0.074
600	0.078
900	0.083
1800	0.086
2700	0.089
3600	0.093
5400	0.1
7200	0.105
9000	0.109
10800	0.114
12600	0.119
14400	0.124
16200	0.128
18000	0.133

RUN NO. C30SG3

t (s)	d_{ss} (m)
0	0
60	0.025
120	0.029
180	0.033
240	0.035
300	0.038
600	0.041
900	0.046
1800	0.05
2700	0.053
3600	0.056
5400	0.06
7200	0.064
9000	0.068
10800	0.07
12600	0.073
14400	0.074
16200	0.075
18000	0.076

APPENDEX – H contd….

19800	0.119		19800	0.138		19800	0.078
21600	0.122		21600	0.142		21600	0.08
23400	0.125		23400	0.146		23400	0.081
25200	0.129		25200	0.148		25200	0.082
27000	0.133		27000	0.15		27000	0.083
28800	0.136		28800	0.151		28800	0.084
30600	0.138		30600	0.152		30600	0.085
32400	0.139		32400	0.153		32400	0.086
36000	0.141		36000	0.154		36000	0.087
39600	0.142		39600	0.154		39600	0.088
43200	0.143		43200	0.155		43200	0.088
46800	0.144		46800	0.155		46800	0.088
50400	0.144		50400	0.156		50400	0.089
54000	0.144		54000	0.158		54000	0.09
57600	0.145		57600	0.158		57600	0.09
61200	0.145		61200	0.157		61200	0.09
64800	0.145		64800	0.157		64800	0.09
68400	0.146		68400	0.157		68400	0.09
72000	0.146		72000	0.158		72000	0.09
75600	0.146		75600	0.158		75600	0.091
79200	0.147		79200	0.158		79200	0.091
82800	0.147		82800	0.158		82800	0.092
86400	0.147		86400	0.158		86400	0.092
90000	0.147		90000	0.158		90000	0.092
93600	0.147		93600	0.158		93600	0.092

RUN NO. C30SG4

t (s)	d_{ss} (m)
0	0
60	0.045
120	0.052
180	0.056
240	0.059
300	0.063
600	0.066
900	0.069
1800	0.074
2700	0.078

RUN NO. C30SG5

t (s)	d_{ss} (m)
0	0
60	0.035
120	0.038
180	0.042
240	0.045
300	0.049
600	0.052
900	0.056
1800	0.061
2700	0.065

RUN NO. C30SG6

t (s)	d_{ss} (m)
0	0
60	0.071
120	0.083
180	0.087
240	0.091
300	0.094
600	0.097
900	0.103
1800	0.107
2700	0.113

APPENDEX – H contd….

3600	0.082
5400	0.085
7200	0.088
9000	0.091
10800	0.093
12600	0.095
14400	0.097
16200	0.099
18000	0.101
19800	0.102
21600	0.103
23400	0.104
25200	0.105
27000	0.106
28800	0.107
30600	0.108
32400	0.109
36000	0.11
39600	0.112
43200	0.113
46800	0.114
50400	0.115
54000	0.115
57600	0.115
61200	0.116
64800	0.116
68400	0.116
72000	0.116
75600	0.117
79200	0.117
82800	0.117
86400	0.117
90000	0.117
93600	0.117

3600	0.068
5400	0.071
7200	0.074
9000	0.077
10800	0.079
12600	0.082
14400	0.086
16200	0.088
18000	0.09
19800	0.092
21600	0.093
23400	0.094
25200	0.095
27000	0.096
28800	0.097
30600	0.098
32400	0.099
36000	0.1
39600	0.101
43200	0.102
46800	0.102
50400	0.102
54000	0.103
57600	0.103
61200	0.103
64800	0.103
68400	0.103
72000	0.103
75600	0.104
79200	0.104
82800	0.104
86400	0.104
90000	0.104
93600	0.104

3600	0.115
5400	0.116
7200	0.118
9000	0.12
10800	0.121
12600	0.122
14400	0.123
16200	0.124
18000	0.125
19800	0.127
21600	0.129
23400	0.13
25200	0.131
27000	0.132
28800	0.133
30600	0.134
32400	0.135
36000	0.136
39600	0.136
43200	0.136
46800	0.136
50400	0.137
54000	0.137
57600	0.137
61200	0.138
64800	0.138
68400	0.139
72000	0.139
75600	0.139
79200	0.14
82800	0.14
86400	0.14
90000	0.14
93600	0.14

APPENDEX – H contd….

RUN NO. C30SG7

t (s)	d_{ss} (m)
0	0
60	0.02
120	0.022
180	0.026
240	0.028
300	0.031
600	0.033
900	0.036
1800	0.039
2700	0.041
3600	0.043
5400	0.047
7200	0.051
9000	0.053
10800	0.056
12600	0.059
14400	0.06
16200	0.061
18000	0.063
19800	0.064
21600	0.065
23400	0.066
25200	0.067
27000	0.067
28800	0.068
30600	0.068
32400	0.069
36000	0.069
39600	0.07
43200	0.07
46800	0.071
50400	0.072
54000	0.073
57600	0.073
61200	0.073
64800	0.074
68400	0.074

RUN NO. C30SG8

t (s)	d_{ss} (m)
0	0
60	0.035
120	0.038
180	0.042
240	0.046
300	0.049
600	0.053
900	0.057
1800	0.061
2700	0.066
3600	0.069
5400	0.074
7200	0.078
9000	0.082
10800	0.085
12600	0.088
14400	0.091
16200	0.093
18000	0.095
19800	0.096
21600	0.098
23400	0.098
25200	0.099
27000	0.099
28800	0.099
30600	0.1
32400	0.1
36000	0.101
39600	0.101
43200	0.102
46800	0.105
50400	0.105
54000	0.103
57600	0.103
61200	0.103
64800	0.103
68400	0.104

APPENDEX – H contd….

72000	0.074
75600	0.075
79200	0.075
82800	0.075
86400	0.075
90000	0.075
93600	0.075

72000	0.104
75600	0.104
79200	0.105
82800	0.105
86400	0.105
90000	0.105
93600	0.105

RUN NO. C40SG1

t (s)	d_{ss} (m)
0	0
60	0.003
120	0.005
180	0.008
240	0.011
300	0.012
600	0.014
900	0.015
1800	0.018
2700	0.022
3600	0.024
5400	0.028
7200	0.03
9000	0.032
10800	0.034
12600	0.037
14400	0.039
16200	0.042
18000	0.044
19800	0.045
21600	0.047
23400	0.048
25200	0.049
27000	0.05
28800	0.051
30600	0.052
32400	0.054
36000	0.056

RUN NO. C40SG2

t (s)	d_{ss} (m)
0	0
60	0.005
120	0.009
180	0.013
240	0.015
300	0.018
600	0.024
900	0.029
1800	0.035
2700	0.039
3600	0.043
5400	0.047
7200	0.055
9000	0.061
10800	0.064
12600	0.068
14400	0.071
16200	0.074
18000	0.078
19800	0.081
21600	0.082
23400	0.086
25200	0.088
27000	0.091
28800	0.093
30600	0.095
32400	0.097
36000	0.098

RUN NO. C40SG3

t (s)	d_{ss} (m)
0	0
60	0.002
120	0.003
180	0.004
240	0.005
300	0.006
600	0.007
900	0.009
1800	0.011
2700	0.013
3600	0.015
5400	0.016
7200	0.017
9000	0.018
10800	0.019
12600	0.02
14400	0.021
16200	0.022
18000	0.023
19800	0.024
21600	0.025
23400	0.026
25200	0.027
27000	0.028
28800	0.029
30600	0.031
32400	0.033
36000	0.035

APPENDEX – H contd….

39600	0.058
43200	0.06
46800	0.062
50400	0.063
54000	0.064
57600	0.064
61200	0.064
64800	0.065
68400	0.065
72000	0.065
75600	0.065
79200	0.066
82800	0.066
86400	0.066
90000	0.066
93600	0.066

39600	0.099
43200	0.1
46800	0.101
50400	0.102
54000	0.102
57600	0.103
61200	0.103
64800	0.104
68400	0.104
72000	0.104
75600	0.104
79200	0.105
82800	0.105
86400	0.105
90000	0.105
93600	0.105

39600	0.036
43200	0.037
46800	0.039
50400	0.04
54000	0.041
57600	0.041
61200	0.041
64800	0.041
68400	0.042
72000	0.042
75600	0.042
79200	0.043
82800	0.043
86400	0.043
90000	0.043
93600	0.043

RUN NO. C40SG4

t (s)	d_{ss} (m)
0	0
60	0.015
120	0.018
180	0.02
240	0.022
300	0.025
600	0.028
900	0.031
1800	0.032
2700	0.035
3600	0.038
5400	0.04
7200	0.041
9000	0.042
10800	0.043
12600	0.045
14400	0.046
16200	0.048
18000	0.05

RUN NO. C40SG5

t (s)	d_{ss} (m)
0	0
60	0.011
120	0.015
180	0.018
240	0.021
300	0.023
600	0.028
900	0.03
1800	0.032
2700	0.033
3600	0.034
5400	0.035
7200	0.036
9000	0.037
10800	0.038
12600	0.039
14400	0.04
16200	0.041
18000	0.042

RUN NO. C40SG6

t (s)	d_{ss} (m)
0	0
60	0.013
120	0.018
180	0.024
240	0.029
300	0.033
600	0.036
900	0.039
1800	0.042
2700	0.044
3600	0.046
5400	0.047
7200	0.048
9000	0.05
10800	0.054
12600	0.058
14400	0.059
16200	0.061
18000	0.062

APPENDEX – H contd….

19800	0.05
21600	0.051
23400	0.051
25200	0.052
27000	0.052
28800	0.053
30600	0.053
32400	0.054
36000	0.055
39600	0.056
43200	0.057
46800	0.057
50400	0.058
54000	0.058
57600	0.059
61200	0.059
64800	0.06
68400	0.06
72000	0.061
75600	0.061
79200	0.061
82800	0.062
86400	0.062
90000	0.062
93600	0.062

19800	0.043
21600	0.044
23400	0.045
25200	0.046
27000	0.047
28800	0.048
30600	0.049
32400	0.05
36000	0.051
39600	0.052
43200	0.053
46800	0.054
50400	0.055
54000	0.055
57600	0.056
61200	0.056
64800	0.057
68400	0.057
72000	0.058
75600	0.058
79200	0.059
82800	0.059
86400	0.06
90000	0.06
93600	0.06

19800	0.063
21600	0.064
23400	0.065
25200	0.068
27000	0.069
28800	0.07
30600	0.072
32400	0.073
36000	0.074
39600	0.075
43200	0.076
46800	0.077
50400	0.077
54000	0.078
57600	0.078
61200	0.079
64800	0.079
68400	0.08
72000	0.081
75600	0.082
79200	0.083
82800	0.083
86400	0.083
90000	0.083
93600	0.083

RUN NO. C40SG7

t (s)	d_{ss} (m)
0	0
60	0.004
120	0.006
180	0.008
240	0.012
300	0.014
600	0.016
900	0.018
1800	0.02
2700	0.022

RUN NO. C40SG7

t (s)	d_{ss} (m)
0	0
60	0.011
120	0.012
180	0.014
240	0.016
300	0.018
600	0.02
900	0.022
1800	0.024
2700	0.027

APPENDEX – H contd….

3600	0.024
5400	0.026
7200	0.028
9000	0.03
10800	0.03
12600	0.032
14400	0.032
16200	0.033
18000	0.033
19800	0.034
21600	0.034
23400	0.035
25200	0.037
27000	0.037
28800	0.037
30600	0.038
32400	0.038
36000	0.039
39600	0.039
43200	0.039
46800	0.04
50400	0.04
54000	0.04
57600	0.041
61200	0.041
64800	0.042
68400	0.042
72000	0.043
75600	0.043
79200	0.044
82800	0.044
86400	0.045
90000	0.045
93600	0.045

3600	0.029
5400	0.033
7200	0.036
9000	0.039
10800	0.041
12600	0.043
14400	0.046
16200	0.047
18000	0.047
19800	0.048
21600	0.048
23400	0.048
25200	0.049
27000	0.05
28800	0.05
30600	0.051
32400	0.051
36000	0.051
39600	0.052
43200	0.052
46800	0.052
50400	0.053
54000	0.053
57600	0.054
61200	0.054
64800	0.054
68400	0.054
72000	0.054
75600	0.055
79200	0.055
82800	0.055
86400	0.055
90000	0.055
93600	0.055

APPENDEX – H contd….

RUN NO. C50SG1

t (s)	d_{ss} (m)
0	0
60	0.001
120	0.001
180	0.002
240	0.002
300	0.003
600	0.003
900	0.005
1800	0.008
2700	0.011
3600	0.014
5400	0.016
7200	0.017
9000	0.018
10800	0.019
12600	0.02
14400	0.02
16200	0.021
18000	0.022
19800	0.023
21600	0.024
23400	0.025
25200	0.026
27000	0.027
28800	0.029
30600	0.03
32400	0.03
36000	0.031
39600	0.031
43200	0.032
46800	0.032
50400	0.033
54000	0.034
57600	0.035
61200	0.036
64800	0.037
68400	0.037
72000	0.037
75600	0.038

RUN NO. C50SG2

t (s)	d_{ss} (m)
0	0
60	0.001
120	0.003
180	0.005
240	0.007
300	0.009
600	0.011
900	0.013
1800	0.015
2700	0.016
3600	0.017
5400	0.018
7200	0.019
9000	0.021
10800	0.022
12600	0.023
14400	0.024
16200	0.025
18000	0.026
19800	0.028
21600	0.029
23400	0.031
25200	0.032
27000	0.033
28800	0.035
30600	0.036
32400	0.038
36000	0.039
39600	0.04
43200	0.042
46800	0.043
50400	0.044
54000	0.047
57600	0.048
61200	0.049
64800	0.049
68400	0.05
72000	0.05
75600	0.05

RUN NO. C50SG3

t (s)	d_{ss} (m)
0	0
60	0.001
120	0.001
180	0.001
240	0.001
300	0.002
600	0.002
900	0.002
1800	0.002
2700	0.003
3600	0.003
5400	0.003
7200	0.003
9000	0.004
10800	0.004
12600	0.005
14400	0.007
16200	0.007
18000	0.007
19800	0.007
21600	0.008
23400	0.008
25200	0.009
27000	0.009
28800	0.01
30600	0.01
32400	0.011
36000	0.012
39600	0.013
43200	0.013
46800	0.013
50400	0.014
54000	0.014
57600	0.015
61200	0.015
64800	0.016
68400	0.016
72000	0.017
75600	0.017

APPENDEX – H contd….

79200	0.038	79200	0.051	79200	0.017
82800	0.038	82800	0.051	82800	0.018
86400	0.038	86400	0.051	86400	0.018
90000	0.038	90000	0.051	90000	0.018
93600	0.038	93600	0.051	93600	0.018

RUN NO. C50SG4

t (s)	d_{ss} (m)
0	0
60	0.001
120	0.002
180	0.003
240	0.004
300	0.005
600	0.007
900	0.009
1800	0.01
2700	0.012
3600	0.014
5400	0.015
7200	0.016
9000	0.017
10800	0.018
12600	0.019
14400	0.02
16200	0.02
18000	0.021
19800	0.022
21600	0.022
23400	0.023
25200	0.024
27000	0.024
28800	0.025
30600	0.025
32400	0.026
36000	0.027
39600	0.027
43200	0.028
46800	0.028
50400	0.029

RUN NO. C50SG5

t (s)	d_{ss} (m)
0	0
60	0.001
120	0.002
180	0.003
240	0.005
300	0.007
600	0.009
900	0.01
1800	0.012
2700	0.013
3600	0.014
5400	0.016
7200	0.017
9000	0.018
10800	0.018
12600	0.019
14400	0.021
16200	0.02
18000	0.021
19800	0.021
21600	0.022
23400	0.022
25200	0.022
27000	0.023
28800	0.023
30600	0.023
32400	0.023
36000	0.024
39600	0.024
43200	0.024
46800	0.024
50400	0.024

RUN NO. C50SG6

t (s)	d_{ss} (m)
0	0
60	0.004
120	0.006
180	0.008
240	0.01
300	0.012
600	0.013
900	0.014
1800	0.015
2700	0.016
3600	0.017
5400	0.018
7200	0.018
9000	0.019
10800	0.021
12600	0.023
14400	0.025
16200	0.029
18000	0.029
19800	0.031
21600	0.032
23400	0.033
25200	0.034
27000	0.035
28800	0.036
30600	0.037
32400	0.037
36000	0.037
39600	0.038
43200	0.038
46800	0.038
50400	0.038

APPENDEX – H contd….

54000	0.03
57600	0.031
61200	0.031
64800	0.032
68400	0.032
72000	0.032
75600	0.033
79200	0.033
82800	0.033
86400	0.034
90000	0.034
93600	0.034

54000	0.025
57600	0.025
61200	0.025
64800	0.025
68400	0.025
72000	0.025
75600	0.026
79200	0.026
82800	0.026
86400	0.026
90000	0.026
93600	0.026

54000	0.035
57600	0.035
61200	0.036
64800	0.036
68400	0.036
72000	0.037
75600	0.037
79200	0.037
82800	0.038
86400	0.038
90000	0.038
93600	0.038

RUN NO. C50SG7

t (s)	d_{ss} (m)
0	0
60	0.001
120	0.002
180	0.003
240	0.004
300	0.005
600	0.006
900	0.007
1800	0.008
2700	0.009
3600	0.011
5400	0.012
7200	0.013
9000	0.013
10800	0.014
12600	0.015
14400	0.016
16200	0.017
18000	0.018
19800	0.018
21600	0.018
23400	0.019
25200	0.019
27000	0.019

RUN NO. C50SG8

t (s)	d_{ss} (m)
0	0
60	0.001
120	0.002
180	0.003
240	0.004
300	0.005
600	0.006
900	0.007
1800	0.009
2700	0.011
3600	0.013
5400	0.014
7200	0.015
9000	0.016
10800	0.017
12600	0.018
14400	0.019
16200	0.02
18000	0.021
19800	0.022
21600	0.023
23400	0.024
25200	0.025
27000	0.025

APPENDEX – H contd….

28800	0.019
30600	0.019
32400	0.019
36000	0.019
39600	0.019
43200	0.019
46800	0.019
50400	0.019
54000	0.019
57600	0.019
61200	0.019
64800	0.019
68400	0.019
72000	0.02
75600	0.02
79200	0.02
82800	0.02
86400	0.02
90000	0.02
93600	0.02

28800	0.025
30600	0.025
32400	0.025
36000	0.025
39600	0.025
43200	0.025
46800	0.025
50400	0.023
54000	0.023
57600	0.023
61200	0.024
64800	0.024
68400	0.024
72000	0.024
75600	0.025
79200	0.025
82800	0.025
86400	0.025
90000	0.025
93600	0.025

RUN NO. C60SG2

t (s)	d_{ss} (m)
0	0
60	0.001
120	0.002
180	0.003
240	0.004
300	0.005
600	0.006
900	0.007
1800	0.007
2700	0.008
3600	0.008
5400	0.009
7200	0.009
9000	0.01
10800	0.01

RUN NO. C60SG4

t (s)	d_{ss} (m)
0	0
60	0.001
120	0.002
180	0.002
240	0.003
300	0.003
600	0.004
900	0.004
1800	0.005
2700	0.005
3600	0.007
5400	0.009
7200	0.009
9000	0.01
10800	0.01

RUN NO. C60SG6

t (s)	d_{ss} (m)
0	0
60	0.001
120	0.002
180	0.003
240	0.004
300	0.004
600	0.005
900	0.005
1800	0.006
2700	0.006
3600	0.007
5400	0.007
7200	0.008
9000	0.009
10800	0.009

APPENDEX – H contd….

12600	0.011
14400	0.012
16200	0.013
18000	0.014
19800	0.015
21600	0.016
23400	0.017
25200	0.018
27000	0.019
28800	0.02
30600	0.022
32400	0.024
36000	0.026
39600	0.027
43200	0.028
46800	0.029
50400	0.03
54000	0.031
57600	0.032
61200	0.033
64800	0.033
68400	0.034
72000	0.034
75600	0.034
79200	0.035
82800	0.035
86400	0.035
90000	0.035
93600	0.035

12600	0.011
14400	0.012
16200	0.013
18000	0.013
19800	0.014
21600	0.015
23400	0.015
25200	0.016
27000	0.017
28800	0.017
30600	0.018
32400	0.018
36000	0.018
39600	0.019
43200	0.019
46800	0.019
50400	0.02
54000	0.02
57600	0.02
61200	0.021
64800	0.021
68400	0.021
72000	0.022
75600	0.022
79200	0.022
82800	0.022
86400	0.022
90000	0.022
93600	0.022

12600	0.01
14400	0.011
16200	0.013
18000	0.014
19800	0.016
21600	0.018
23400	0.02
25200	0.02
27000	0.02
28800	0.02
30600	0.02
32400	0.02
36000	0.021
39600	0.021
43200	0.021
46800	0.021
50400	0.022
54000	0.022
57600	0.022
61200	0.022
64800	0.023
68400	0.023
72000	0.023
75600	0.023
79200	0.024
82800	0.024
86400	0.024
90000	0.024
93600	0.024